SEMMELWEIS EGYETEM

DOKTORI ISKOLA

Ph.D. értekezések

3045.

SAFAA MOHAMMED OMER MUSA

A gyógyszerészeti tudományok korszerű kutatási irányai
című program

Programvezető: Dr. Antal István, egyetemi tanár

Témavezető: Dr. Zelkó Romána, egyetemi tanár

Dr. Nochta-Kazsoki Adrienn Katalin,

egyetemi adjunktus

FORMULATION, DEVELOPMENT, AND EVALUATION OF INNOVATIVE ELECTROSPUN NANOFIBER-BASED OPHTHALMIC INSERTS

Ph.D. thesis

Safaa Mohammed Omer Musa

Semmelweis University Doctoral School

Pharmaceutical Sciences and Health Technologies Division

Supervisor: Romána Zelkó, PharmD, D.Sc.
                            Adrienn Katalin Nochta-Kazsoki, PharmD, Ph.D.
Official reviewers: Rita Ambrus, PharmD, Ph.D.
                            Krisztina Ludányi, PharmD, Ph.D.

Head of the Complex Examination Committee:
                            István Antal, PharmD, PhD

Members of the Complex Examination Committee:
                            Ildikó Bácskay, PharmD, Ph.D.
                            Imre Klebovich, PharmD, D.Sc.

Budapest
2024

TABLE OF CONTENTS

LIST OF ABBREVIATIONS

API	Active pharmaceutical ingredient
ASD	Amorphous solid dispersion
CD	Cyclodextrin
Cys	Cysteamine
CysH	Cysteamine hydrochloride
EDTA	Ethylenediaminetetraacetic acid
FTIR	Fourier transform infrared spectroscopy
HET-CAM	Hen's egg test on chorioallantoic membrane
HP-β-CD	Hydroxypropyl-beta-cyclodextrin
NEPA	Nepafenac
OI	Ophthalmic insert
PAMPA	Parallel artificial membrane permeability assay
PBS	Phosphate-buffered saline
PCL	Polycaprolactone
PO-407	Poloxamer 407
PS-80	Polysorbate 80
PSS	Physiological saline solution
PVA	Poly(vinyl alcohol)
SEM	Scanning electron microscopy
TEOS	Tetraetoxysilane
XRD	X-ray diffraction

1. INTRODUCTION

Efficient delivery of the drug to the eye faces a huge challenge as a result of different biological barriers that interfere with the drug before reaching the targeted site of action. Rapidly renewed precorneal tear film and blinking reflex shorten the residence time of the drugs in the precorneal area. Furthermore, conjunctival administration of the drug is accompanied by systemic drug absorption and adverse effects. Hence, topical administration via the cornea represents the main route for targeting the inner layers of the eye (1,2). For transcorneal delivery, a drug must cross multiple corneal layers and overcome the transmembrane efflux pumps. It is more complicated when targeting the posterior eye segment because of long diffusional distance, additional barriers, and dilution of the drug in the vitreous humor (3,4).

Diseases involving the posterior eye segment are an significant target with unmet therapeutic needs. Untreated diseases can lead to visual impairment or can develop into blindness. To reach the posterior segment of the eye, drugs must diffuse through vitreous humor, or alternatively, drugs diffuse through the trans-scleral route, leads to the choroids, and then the blood-retinal barrier (5).

The topical route is the preferred and most commonly used way for administering the drug through the eyes, but it has limited bioavailability, which makes the treatment of different eye diseases a challenging process (6). Intravitreal, periocular, and/or transscleral injections are used for treating diseases of the posterior eye segment, especially with newly emerged drugs, but efficient, safe drug carriers that ensure comfort for the patients are needed (7,8).

Because of these obstacles to drug permeation through the different eye barriers, there is a clear demand for smart drug delivery systems that are capable of delivering the drug to the targeted site of action while being safe, effective, and comfortable. Many alternatives have been tried in the last few decades; of them, nanocarriers have received a great deal of attention since they have the ability to interact with the ocular mucosa, thereby extending the duration that the drug remains in contact with the eye, consequently increasing its ability to pass through the corneal and conjunctival epithelium (9,10).

5

1.1. Anatomy of the ocular pathway

The human eye is a highly developed organ with special anatomy and physiology. It is a highly protected and isolated organ with slow blood circulation (2). The structure of the eye (**Figure 1**.) consists of the anterior and posterior segments. The anterior segment occupies one-third and the posterior segment occupies two-thirds (5). The anterior portion includes the cornea, conjunctiva, iris, ciliary body, tear film, and aqueous humor. The posterior part consists of the retina, sclera, macula, optic nerve, choroid, and vitreous humor (2,11). The cornea represents the first part of the eye's defense against foreign body invasion and drug penetration. It is a transparent avascular tissue consisting of epithelium, parenchyma and endothelium, approximately 0.5 mm thick and 11 mm in diameter (11). The stroma is rich in collagen and constitutes the majority of corneal tissue (12). The epithelium is lipophilic and has tight intercellular junctions, whereas the stroma is hydrophilic and highly organized to prevent penetration of large and/or hydrophobic molecules (7,11). Differences in corneal composition and varying degrees of hydrophilicity make drug penetration through the cornea a difficult process (12). In addition to the cornea, there are various physiological and biological barriers that affect drug absorption, including nasolacrimal drainage, tear dilution, conjunctival absorption, blood-retinal barrier, and blood-water barrier (3).
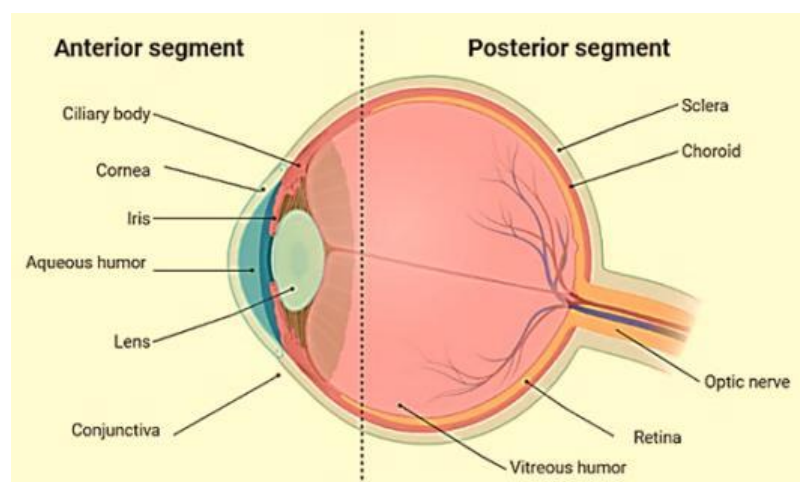
Figure 1. The anatomy of the human eye (anterior and posterior segments).

[Created with Biorender.com]

6

1.2. Ophthalmic disorders

Visual impairment can affect people's quality of life and lead to social, academic, and economic difficulties (13). An estimated 2.2 billion people worldwide suffer from visual impairments and eye diseases, and half of these diseases are treatable or preventable (14). The World Health Organization estimates that the number of cases of glaucoma and age-related macular degeneration will increase by 1.3 times and 1.2 times, respectively, between 2020 and 2030. In addition, industrial development can cause many environmental changes (air pollution, low humidity, wind, etc.), which can also increase the number of people with eye inflammation and dry eye symptoms. Visual impairment primarily results from a range of eye diseases, such as cataracts, glaucoma, and diabetic retinopathy, with increasing prevalence in recent years due to population growth and aging. The prevalence of eye diseases is highest in low-income countries compared to other countries (15).

Raising public awareness of eye diseases is important to reduce the burden of visual impairment, as many diseases are asymptomatic or have mild symptoms. Genetics is an important factor in developing eye diseases, but lifestyle plays an important role in many eye diseases. Eye diseases can be progressive, chronic, and incurable, and if not properly treated, can lead to vision impairment and blindness. The prevalent eye conditions include glaucoma, age-related macular degeneration, diabetic macular edema, and diabetic retinopathy. The primary aim of treatment is to manage the diseases, alleviating symptoms, and preventing their progression (16).

1.3. Formulation approaches for the treatment of different eye diseases

Administration of the drugs to different eye sites includes different ways including topical, systemic, periocular and intravitreal (7,17). Despite their ease of administration and being highly preferred by the patients, topical administration by conventional ocular delivery systems is accompanied by a number of problems, of which poor bioavailability being the most significant due to pre-corneal loss of the drug by physical and biological barriers, beside their poor suitability for hydrophobic drugs, or drugs that are unstable at pH level tolerable to the eye (18,19). Different ocular systems aim to improve resident time and bioavailability of the administered drugs have been investigated for example; mini-tablets, disposable lenses, biodegradable polymeric systems, collagen shields,

hydrogel, implants and inserts (18–20). Novel drug delivery systems aim to overcome the ocular barriers and to increase patient's compliance by focusing in two areas; increasing the contact time and slowing down the elimination (20). A very promising approach for ocular targeting is using nanotechnology for production of colloidal drug delivery systems with particle sizes in the range of 1–1000 nm (21). Nanotechnology-based Ocular administration of the drugs offers many advantages over other conventional systems. They include but are not limited to nanocapsules, liposomes, nano micelles and lipid nanoparticles, liposomes, dendrimers, nanosuspensions, nanoemulsions, and nanocrystals (22,23).

1.3.1. Conventional formulations

Many challenges are encountered in ophthalmic drug administration through conventional formulations, mainly eye drops, because of premature loss of the installed drug and poor permeation across different barriers (24). Topical administration via eye drops is mostly preferred and accounts for about 90% of ophthalmic formulations because of ease of administration, non-invasiveness, reduction of systematic adverse effects, and relative safety due to lack of surgical complications (25,26). However, when treating different eye diseases, especially diseases involving the posterior part, using conventional eye drops is limited by poor bioavailability as a result of anatomical and physiological barriers such as tear turnover, nasolachrymal drainage, reflex blinking, blood-retinal barrier and blood-aqueous barrier (27). Therefore, the delivery of the drug is mainly restricted to the precorneal anterior part of the eye, and less than 5% reaches the deeper structures (28). On the other hand, penetration of different drugs via corneal tissue is governed by many factors, with drug concentration in the precorneal region being the driving factor; that's why most alternative formulations focus on increasing the residence time in the corneal epithelia (29).

1.3.2. Alternative approaches

The presence of ophthalmic physical and physiological barriers leads to poor bioavailability of conventional eye drops, which makes it difficult to achieve therapeutic drug concentration, particularly on the posterior side of the eye. These obstacles pose a great challenge for ophthalmologists and researchers (30). Other ways that may be used to deliver the drug to the posterior segment of the eye include intravitreal injections,

periocular injections, and systemic administration (7,8). Systemic administration through oral or parenteral administration is retarded by blood -Aqueous Barriers and Blood-Retinal Barriers and is accompanied by unwanted effects because very high doses are administered (31,32). Moreover, the parenteral intravitreal injection, although it is an effective way for site-specific targeting, is associated with many complications like hemorrhage, cataracts, and retinal detachment (2,9). These problems of unwanted adverse effects, frequent dose administrations, and treatment failure can lead to patient nonadherence to the treatment (17).

Researchers are putting great efforts into developing highly effective treatments for diseases involving the posterior segment of the eye (17). Therefore, many alternative formulations have been investigated, for example, using permeation enhancers and increasing formulation viscosity through gelling agents and cyclodextrins (CD) (9,10,25). Other promising systems have been developed to eliminate the limitations of conventional systems and improve residence time to obtain controlled drug release and enhanced bioavailability, including pro-drug strategy, nano micelles, nanoparticles, long-term or permanent punctual inserts, corneal shields, nanosuspensions, microneedles, liposomes, thermosensitive gels, ophthalmic inserts, and contact lenses (25,33,34).

Novel drug carriers based on nanotechnology can deliver the drugs into various parts of the eye with significant advantages (5,35,36). They offer; enhancement of corneal residence time, enhancement of the bioavailability, controlled and targeted release, nanomedicines reduce the drug elimination, which is ultimately reflected in therapeutic efficacy, reduction of the adverse effects, and lower possibility for eye irritation. In addition, using these carriers enables reducing the dose frequency and enable rapid uptake to targeted site thereby increase patients adherence and tolerance to medications (11,37,38), surface engineering using different polymers for different purposes such as muco-adhesive are also possible (39,40). The proper modifications of surface properties allow continuous discharge and release of the drug along with clearance from the body (22,41).

1.4. Ophthalmic inserts

Ophthalmic inserts (OIs) are sterile solid or semi-solid dosage forms consisting of polymeric material with or without medicament, whose suitable size and shape designed to be placed into the conjunctival sac (42). They enable increasing the contact time, provide sustained and targeted drug release, reduce the frequency and the amount of the administered drug, reduce the side effects, eliminate the need for preservatives, and provide a wide range for drugs and polymers incorporation (18,43). In addition, certain types of OIs eliminate patients suffering from corticosteroid drug tapering, and others are easily softened and eliminated through nasolacrimal secretion (44). However, they cause unpleasant sensations, transient blurred vision, and unwanted migration around the eye (34,45).

Based on their solubility behavior, OIs are classified into soluble inserts, insoluble inserts, and bio-erodible inserts. The soluble and erodible inserts undergo slow and complete dissolution without needing removal, while the insoluble inserts should be removed from the eye when they are free of drugs. The drug release from ocular inserts takes part through diffusion, osmosis, and erosion (34).

Because the insert expulsion and patient discomfort are tightly connected to the shape and size of ocular inserts (46), the ranges of overall volumes, length, height, thickness, and shape have been determined as follows: the majority of inserts are oval or elliptical with lengths ranging (8 to 15 mm), heights (4.5 to 6 mm), and thicknesses (0.07 to 0.5 mm), few inserts were circular or spherical and rectangular film, many inserts were rods shaped ranging in length (3.5 to 10 mm) and having the same thickness of 1.25 mm, the volume was calculated from insert dimensions (0.7 to 28.1µL) (47).

1.4.1. Electrospinning as a novel technique for ophthalmic insert preparation

The OIs are prepared using the following methods: solvent casting method, glass substrate technique, melt extrusion technique (48), and electrospinning has been used as a simple, versatile technique for the production of nanofibrous film with unique properties (49). Along with their inherited advantages as nanocarriers, nanofibers offer unique advantages as drug delivery systems such as different natural and synthetic polymers can be fabricated, one or more drugs can be encapsulated, small and large drug molecules can be loaded, the process is suitable for thermolabile substances, provide high

surface to volume ratio, enable formation of controlled, sustained and targeted release (50,51). The products and fibers are homogenous and highly reproducible (52). Due to their characteristic size and texture, they can also provide a good candidate for tissue reconstitution (53). They are ideal scaffolds that promote cell migration and proliferation (54).

The electrospun nanofibers can be fabricated from different hydrophilic and lipophilic polymeric mixtures, allowing control of the release profile. They also allow formulation modification with different materials such as permeation enhancers and mucoadhesive agent (55). The above-mentioned advantages prove that well-developed nanofibers, along with the advantages of OIs, might be a good alternative to conventional eye drops (56).

Many works have been published demonstrating the utilization of electrospinning technology for the fabrication of nanofiber-based ocular inserts and other ocular formulations. For example, fluocinolone acetonide-loaded polycaprolactone (PCL) nanofibers were successfully prepared using the electrospinning method to target retinal delivery and increase bioavailability. Results showed extended drug release and therapeutic levels at the target site (49).

Electrospun formulations of acyclovir, ciprofloxacin, and cyanocobalamin were prepared to sustain the release and enhancement of bioavailability by utilizing polyvinylpyrrolidone and PCL as fibers forming polymers. The drug release was successfully extended (57). In the case of nanofibrous OIs containing azithromycin nanoparticles to be used as a controlled-release ocular insert for treating bacterial keratitis, results showed that the release could be extended up to 10 days (58).

A successful novel acetazolamide polymeric implants were prepared by using electrospinning method to obtain a sustained drug release to decrease side effects and increase patient compliance (59). Biodegradable PCL fibrous implants containing cyclosporine A loaded poly-lactide-co-glycolide were prepared to achieve sustained release using electrospinning. Cyclosporine A loaded fiber implant formulation resulted in faster recovery from dry eye syndrome (60).

The aforementioned studies confirm the suitability of drug-loaded polymeric nanofibers for targeting ocular delivery with good efficacy, safety, and patient compliance.

1.4.2. Polymers used in the formulation of ophthalmic inserts

A wide range of natural, semisynthetic, and synthetic polymers are used for the production of nanofibers for ocular uses (61). The final properties and quality of the fibers are determined by many factors, of which type and concentration of polymers are of paramount importance. Some of the suitable polymers for the electrospinning technique include polyesters (e.g., poly-glycolic acid-, poly-lactic acid-, and PCL (55). They are biocompatible and biodegradable polymers with sufficient mechanical strength for electrospinning (52,62). In some cases, blends of the polymers are used together to control the drug release or to impart certain superior properties, for instance, surface modification by coating with mucoadhesive polymers or complexation with solubility or permeability enhancers (55,61). Hydrophilic polymers are suitable to encapsulate hydrophilic drugs without sustaining the drug release, while hydrophobic polymers have the ability to modulate the release of the embedded drugs (61). Many bioadhesive polymers are used in ocular formulations to enhance the bioavailability. For example, polyvinyl alcohol (PVA), polyacrylic acid, polyvinylpyrrolidone, hyaluronic acid, chitosan, polyethylene oxide, polymethacrylate, cellulose derivates, polyacrylamide and carboxy vinyl polymers (35,63,64).

1.4.3. Evaluation of the ophthalmic inserts

Ocular drug delivery systems should be sterile, safe, non-irritant, and comfortable to assure patient compliance. The physicochemical properties of the formulated OIs (nanofibrous film as intermediate of the final product) should be evaluated in terms of size and morphology of electrospun nanofibers (scanning electron microscopy (SEM)), drug excipients interaction (Fourier transform infrared spectroscopy (FTIR)), in-vitro release and release kinetics, surface pH, stability, ocular tolerability, and in-vivo drug release study (43,62,65,66). According to the European pharmacopeia requirements, ensuring proper dissolution behavior of the OIs is important. They must also comply with uniformity of dosage units and uniformity of content, and the label should specify the total quantity of active substance per insert and the dose released per unit of time (67).

2. OBJECTIVES

General objective (ultimate goal)

The main objective of my work was to develop and formulate electrospun nanofiber-based ophthalmic inserts (OIs) using different model drugs and different polymeric matrixes in an attempt to find a drug delivery system that is as efficient as invasive ways in targeting different ophthalmic diseases while maintaining the relative safety and self-convenience of the conventional eye drops with the overall goal of increasing patients' comfortness, acceptability, and reducing diseases burden.

Specific objectives

The details necessary for the complete accomplishment of this work are as follows:

I. Comprehensive literature searching about the nanofiber-based OIs to justify the research and to conduct a theoretical study to collect the necessary information regarding the active ingredients (nepafenac (NEPA), cysteamine hydrochloride (CysH)), polymers (polyvinyl alcohol (PVA) and poloxamer 407 (PO-407)), and other excipients (tetraetoxysilane (TEOS), hydroxypropyl-β-cyclodextrin (HP-β-CD), and polysorbate 80 (PS-80)).

II. To conduct preliminary experiments to set the precursor solutions' suitable composition and define the optimal electrospinning parameters.

III. Evaluation of the effect of different PVA grades, the addition of PO-407, and PS-80 on the morphology and physicochemical properties of the fibers using scanning electron microscopy (SEM) and Fourier transform infrared spectroscopy (FTIR), respectively.

IV. To formulate nepafenac-loaded and cysteamine-loaded fibrous webs and to evaluate their morphological and physicochemical characteristics.

V. To study the *in vitro* drug release and *in vitro* and *ex vivo* permeability.

VI. To study the cytocompatibility with hen eggs' chorioallantoic membrane (HET-CAM) of fertilized chick embryos.

VII. To study the effect of applying elevated humidity and temperature levels on the morphological and physicochemical characteristics.

3. METHODS

3.1. Materials

Nepafenac (NEPA) and Ellman's reagent ((5,5′-dithio-(bis-2-nitrobenzoic) acid, DTNB for UV-Visible quantification of thiol compound) were obtained from TCI Ltd. (Tokyo, Japan)). Cysteamine hydrochloride (CysH) was obtained from Sigma-Aldrich Chemie GmbH (Schnelldorf, Germany). Polyvinyl alcohol (PVA, Mowiol® 8–88, Mowiol® 18–88, and Mowiol® 40–88 with an average molecular weight Mw~ 67 kDa, Mw~ 130 kDa, Mw~ 205 kDa respectively), poloxamer 407 (PO-407, average molecular weight, Mw~ 12.6 kDa), tetraetoxysilane (TEOS) were obtained from Merck Ltd. (Budapest, Hungary), chloroform (anhydrous, ≥ 99%), hexane (anhydrous, 95%), dodecane (anhydrous, ≥ 99%) and methanol (anhydrous, 99.8%) were obtained from Merck Ltd. (Budapest, Hungary). L-α-phosphatidylcholine was purchased from Merck KGaA (Darmstadt, Germany). Hydroxypropyl-β-cyclodextrin (HP-β-CD) (average degree of substitution (n): 4.5, average molecular weight: $1135.0 + n \times 58.1$ g mol−1) was purchased from Cyclolab Ltd. (Budapest, Hungary). Polysorbate 80, potassium dihydrogen orthophosphate, sodium hydroxide, ethanol (EtOH, anhydrous, 96%), and Ethylenediaminetetraacetic acid (EDTA), sodium chloride, sodium hydrogen carbonate, and calcium chloride hexahydrate were purchased from Molar Chemicals Ltd (Budapest, Hungary). Pharmacopeial-grade distilled water (H_2O, was used as solvent for precursor solution preparation. For the permeation experiments, distilled water was purified by the Millipore Milli-Q® 140 Gradient Water Purification System. For the *ex vivo* experiments, porcine eyes were obtained from a local slaughterhouse (Porció-ÉK Ltd., Albertirsa, Hungary). Physiological salt solution (PSS) contained 0.9% w/v NaCl (Hungaropharma Plc., Budapest, Hungary). All materials were used without further purification.

3.2. Methods

3.2.1. Literature searching

A comprehensive literature search was conducted by following Preferred Reporting Items for Systematic Reviews and Meta-Analyses (PRISMA 2020) guidelines to search for relevant studies and report construction. A systematic search was performed in PubMed, Ovid Medline, Web of Science, ScienceDirect, Scopus, Reaxys, Google Scholar, and Google Patents/Espacenet taking (Drug-loaded) AND (electrospinning) AND (Nanofibers OR nanofibrous) AND (ocular inserts OR ophthalmic inserts) as search queries. The search was limited to original and peer-reviewed studies published in 2011–2021 in the English language. Search results from all databases were exported to the Mendeley reference manager, and the articles underwent two successive screening processes. The relevant articles were double-checked by the reviewers based on the inclusion criteria, and the required information was extracted and tabulated into the following variables: polymer base, loaded drug/concentration, dimensions of inserts used in the study, diameter of nanofibers, *in vivo* animal model, and effects/properties of presented system.

3.3. Preparation of electrospinning solutions

3.3.1. Preparation of polyvinyl alcohol (PVA)/poloxamer 407 (PO-407) solutions

Three different grades of PVA and PO-407 were used to prepare the precursor solutions of neat PVA and PVA/PO-407 fibers. Each individual solution of PVA was prepared by using the appropriate amount of polymer and distilled water ((15%, 17.5%, and 20% w/w in case of low molecular weight PVA), (13%, 14%, and 15% w/w in case of intermediate molecular weight PVA), and (5%, 7.5%, and 10% w/w in case of high molecular weight PVA)). The PVA solutions (P) were prepared by dispersing the polymers in the distilled water, followed by stirring under heating until clear solutions were obtained. PO-407 solutions were prepared by dissolving the required amount in cold water. PVA/PO-407 solutions (PP) were prepared by mixing the definite amount of each individual solution, followed by stirring at room temperature for 2 hours to prepare mass ratios of 85:15, 80:20, and 75:25 of PVA: PO-407 using the middle concentration from each PVA grade. Other solutions (PPP) were also prepared by adding PS-80 (0.5%(w/w) and 1%(w/w)) to the PVA/PO-407 solutions.

3.3.2. Preparation of tetraetoxysilane (TEOS)/ polyvinyl alcohol (PVA) solutions

For the preparation of TEOS/PVA precursor solutions, a solution of TEOS:EtOH:H_2O:HCl 1:3:8:0.04 molar was prepared firstly in a tightly sealed glass container at 60 $^{\circ}$C, to which, after 3 hours (h) of hydrolysis, solutions of 10, 12 and14 % (w/w) of PVA in water: ethanol 8:2 (m:m) were added in 4 different ratios (mass ratio of the TEOS: PVA solutions were 1:4, 2:3, 3:2, and 4:1) and stirred for 1 h at 60 $^{\circ}$C. The effect of the PVA concentration on the morphology of the fibers was investigated on three levels (10, 12, and 14 % (w/w)). For each of the concentrations, four TEOS/ PVA mass ratios (1:4, 2:3, 3:2, and 4:1 m:m) were examined.

3.3.3. Preparation of nepafenac (NEPA)/ Hydroxypropyl-β-cyclodextrin (HP-β-CD) solution in water

The solubility of NEPA in water in the presence of HP-β-CD was conducted according to the published method (68). 1 mg of NEPA powder was added to 50 mM HP-β-CD aqueous solutions and heated in sealed vials at 60 $^{\circ}$C for 1 hour. The dissolved amount was determined by determining the concentrations of the resultant solutions. The absorbance of the solutions was measured at λ_{max} 238 nm by Jasco 530 UV-VIS spectrophotometer coupled with inline probe. The measurements were performed in triplicate and the average amounts were determined based on the previously constructed calibration curve. The method of analysis was validated according to the reported work (69,70).

3.3.4. Preparation of nepafenac-loaded (NEPA-loaded) solutions

Variable amounts of HP-β-CD and PVA/PO-407 were used to prepare nine different precursor solutions of NEPA (Table 1). The HP-β-CD was added to solubilize and stabilize NEPA, PVA was used as fiber forming polymer, and PO-407 was added to impart the thermoreversible and bio-adhesive effects. The solutions were prepared using the required amounts of polymers and distilled water. PVA solutions were prepared by dispersing the polymers in the distilled water and stirred under heating until clear solutions were obtained. PO-407 solutions were prepared by dissolving the required amounts in cold water. PVA/PO-407 solutions were prepared by mixing PO-407 and PVA solutions then stirred at room temperature until complete homogenization. NEPA/HP-β-CD was added either to the PVA or PVA/PO-407 solutions and subjected

to stirring at 60 °C for 1 h followed by stirring at room temperature for 2 h until complete solubility of NEPA.

Table 1. Composition of nepafenac (NEPA)/ hydroxypropyl-beta-cyclodextrin (HP-β-CD), loaded in different ratios of polyvinyl alcohol (PVA): poloxamer 407 (PO-407)

Formulation Code	NEPA % (w/w)	HP-β-CD (mM)	PVA: PO-407 (m:m)
F1	0.1	50	100:00
F2	0.1	50	85:15
F3	0.1	50	80:20
F4	0.1	100	100:00
F5	0.1	100	85:15
F6	0.1	100	80:20
F7	0.1	150	100:00
F8	0.1	150	85:15
F9	0.1	150	80:20

3.3.5. Preparation of cysteamine-loaded (Cys-loaded) solutions

To prepare Cys-loaded solutions, 5.5 mg and 11 mg of CysH were added to 1g of plain PVA/PO-407 and TEOS/PVA viscous solutions to get the final solution concentration of 0.55% (w/w) and 1.1% (w/w). The drug-loaded solutions were then stirred at room temperature for 2 h until complete homogenization (**Tables 2 and 3**).

Table 2. Composition and the respective amount of cysteamine hydrochloride (CysH)/ polyvinyl alcohol (PVA)/Poloxamer 407 (PO-407)/ Ethylenediaminetetraacetic acid (EDTA)/polysorbate 80 (PS-80) samples

PVA: PO-407 (80:20) (m:m)	CysH concentration (% (w/w))	Formulation Code	
		CysH/PVA/PO-407	CysH/PVA/PO-407/EDTA/PS-80
Mowiol® 8–88 17.5% (w/w)	0.55	F1	F2
	1.1	F3	F4
Mowiol® 18–88 14% (w/w)	0.55	F5	F6
	1.1	F7	F8
Mowiol® 40–88 10% (w/w)	0.55	F9	F10
	1.1	F11	F12

Table 3. *Composition and respective amount of cysteamine hydrochloride (CysH)/ tetraetoxysilane (TEOS)/ polyvinyl alcohol (PVA) samples*

Polymer composition	Formulation code				
	PVA-Grade	PVA concentration (% (w/w))	CysH concentration (% (w/w))		
			0	0.55	1.1
TEOS: PVA 4:1 (m:m)	Mw~67 kDa	15	FT1	FT2	FT3
		17.5	FT4	FT5	FT6
		20	FT7	FT8	FT9
	Mw ~130 kDa	12	FT10	FT11	FT12
		14	FT13	FT14	FT15
		16	FT16	FT17	FT18
	Mw ~205 kDa	5	FT19	FT20	FT21
		7.5	FT22	FT23	FT24
		10	FT25	FT26	FT27

3.4. Electrospinning of the solutions

A laboratory-scale electrospinning equipment (SpinSplit Ltd., Budapest, Hungary) was used to prepare the fibers. A plastic syringe (Luer lock syringe, Merck Ltd., Budapest, Hungary) of 1mL volume was filled with either plain or drug-loaded viscous solutions and connected to a 22G conventional needle through a Teflon tube. The syringe was then connected to the pump to control the solution flow. After carrying out many preliminary experiments, the electrospinning process was set at 0.08-0.1 µL/sec flow rate, 10-20 kV applied voltage, and the effective distances between the needle and the grounded collector were kept at 10, 12.5, and 15 cm. The samples were collected on an aluminum foil wrapped on the surface of the grounded plate collector. The samples were then stored in a desiccator until further analysis. The process was conducted at ambient conditions of 22 ± 1 °C room temperature and 40 ± 5 % relative humidity.

3.5. Morphological characterization

A JEOL JSM-6380LA scanning electron microscope (SEM) was used to study the morphological characteristics of the prepared samples. The samples were fixed on copper ingots with the aid of a double-sided carbon adhesive. The samples were then coated with gold under vacuum. Images were taken at 3500 and 5000 magnifications at 10 mm distance and 10 kV. All images were then evaluated in terms of fibrous, nonfibrous, and

beads containing samples. The diameters of the fibrous samples were studied by measuring randomly selected 100 individual fibers (n =100) from 2 different images using ImageJ software (US National Institutes of Health, 138 Bethesda, MD, USA). The average fiber diameters ± the standard deviation for each sample measurement were calculated using Excel 2010. The histograms and fitting to Gaussian (normal) distribution were carried out using OriginPro 2018 software (v9.5.1., OriginLab Corporation, Northampton, MA, USA). The normality of fiber diameter distribution, skewness, and kurtosis were also calculated by using Microsoft Excel 2010 functions according to the **Equations 1 and 2**:

$$Skew = \frac{n}{(n-1)(n-2)} \Sigma (\frac{xi-\bar{x}}{s})^2 \tag{1}$$

$$Curtosis = \frac{n}{(n-1)(n-2)(n-3)} \Sigma \left(\frac{xi-\bar{x}}{s}\right)^4 \bigg\} - \frac{3(n-1)^2}{(n-2)(n-3)} \tag{2}$$

Where n is the number of data points, x_i is the mean, and s is the standard deviation.

3.6. Solid state characterization

3.6.1. Fourier Transform Infrared Spectroscopy (FTIR)

The physicochemical properties, compatibility, and interactions between polymers and other excipients were studied using FTIR (Jasco FT/IR-4200 spectrophotometer (Jasco Inc., Easton, MD, USA)). The study was performed for individual components and their fibrous mixtures for plain and drug-loaded samples. The measurement parameters were set as 400-4000 cm^{-1}, 4 cm^{-1} resolution, and ambient temperature in an average of 100 scans.

3.6.2. X-ray diffraction (XRD)

Diffraction patterns were measured on PANalytical X'Pert3 Powder diffractometer (Malvern Panalytical B.V., The Netherlands) using Cu Kα radiation with 45 kV accelerating voltage and 40 mA anode current over the range of 4–38 ° 2 θ with 0.0080 ° step size and 99.695 s times per step in reflection mode, spinning the sample holder by 1 s^{-1}. Incident beam optics were as following: programmable divergence slit with 15 mm constant irradiated length, anti-scatter slit at fixed 2 °. Diffracted beam optics consisted of X'Celerator Scientific ultra-fast line detector with 0.02 soller slit and programmable anti-scatter slit with 15 mm constant observed length. Data were collected

by PANalytical Data Collector Application, version 5.5.0.505 (Malvern Panalytical B.V., The Netherlands).

3.7. *In vitro* release study and release kinetics

The *in vitro* releases of NEPA and Cys from the fibrous samples were studied according to a modified method analogy to the basket method reported by Pharmacopoeia Hungarica (Ph. Hg. VIII) (71). The method was developed to fit small-volume dissolution media to accommodate the drugs that target small physiological compartments such as the buccal cavity and ophthalmic sac. Samples containing 10 µM of the API (NEPA and CysH) were weighed, folded in a dry magnetic bar, and inserted inside the 25 mL beaker. The beaker was placed on a magnetic stirrer adjusted to provide 100 rpm at a temperature of 35 ± 0.5 °C. An in-line probe of a Jasco-V-750 UV-VIS spectrophotometer was immersed in the beaker to detect the absorbance of the released drugs. A pre-warmed dissolution media (10 mL phosphate buffer pH 7.4 in case of NEPA) or (10 mL phosphate buffer pH 7.4 containing 30 µL of Ellman's reagent at 35°C in case of Cys) were added to the 25 mL beaker containing the sample and the absorbances were measured at a predetermined time interval (5 seconds) at λ_{max} 238 nm and λ_{max} 412 nm for NEPA and Cys respectively. The concentrations were determined from the measured absorbance. The measurements were performed in triplicate and the release curves were constructed from the average values of the measurements. A Weibull model was used to evaluate the kinetics of the drug release according to **Equation 3**:

$$M_t = M_\infty \left(1 - e^{-\frac{(t-t_0)^\beta}{\tau_d}} \right) \tag{3}$$

where M_t is the NEPA and Cys release at (t) time, while M_∞ is the maximum amount of the released NEPA and Cys. The parameters t_0 and τ_d are the lag and average dissolution times, respectively. The shape of the release curve is specified by the β parameter ($\beta = 1$ denotes first-order kinetics, $\beta > 1$ indicates a slow onset followed by an accelerated release, and $\beta < 1$ indicates a fast onset followed by a slow release) (72,73).

3.8. Permeability studies of nepafenac-loaded (NEPA-loaded) fibers

3.8.1. *In vitro* corneal parallel artificial membrane permeability assay (PAMPA)

The electrospun samples were dissolved in phosphate-buffered saline (PBS) to create solutions with 1 mg/ml nepafenac concentration, followed by a 20-fold dilution to simulate the tear effect on the applied formulations. In the case of the test formulations, each matching well of the acceptor plate (Multiscreen Acceptor Plate, MSSACCEPTOR; Millipore) was filled with HP-β-CD solution to reduce the reverse sink effect (containing 10% HP-β-CD of the diluted electrospun-samples) whereas in the case of Nevanac® the acceptor wells were filled with PBS. Samples were measured in six replicates. To prepare the artificial membrane, 16 mg phosphatidylcholine was in a 600 μL solvent mixture of dodecane, hexane, and chloroform (25:70:5 v/v) and used for coating the well of the donor plate (MultiscreenTM-IP, MAIPN4510, pore size 0.45 μm; Millipore) with 5 μL of the lipid solution (74)**.** Following that, the donor plate was filled with 150 μL sample solutions. Finally, the sandwich plate was assembled and covered with a wet sheet of paper and a plate lid to avoid evaporation. The system was incubated for 4 hours at 35°C (Heidolph Titramax 1000, Heidolph Instruments, Swabach, Germany). A parallel experiment was conducted using the same method while omitting the sink effect of 10% w/w of HP-β-CD. After that, initial donor and acceptor samples were collected and analyzed by HPLC-DAD (75). Effective permeability (P_e) and membrane retention (MR) were calculated using the Equation 4 and 5:

$$P_e = \frac{-2.303}{A \cdot (t-\tau_{ss})} \cdot \left(\frac{1}{1+r_v}\right) \cdot \lg\left[-r_v + \left(\frac{1+r_v}{1-MR}\right) \cdot \frac{c_D(t)}{c_D(0)}\right] \qquad (4)$$

$$MR = 1 - \frac{c_D(t)}{c_D(0)} - \frac{V_A c_A(t)}{V_D c_D(0)} \qquad (5)$$

where A is the filter area (0.3 cm^2), V_D and V_A are the volumes in the donor (0.15 cm^3) and acceptor phase (0.3 cm^3), t is the incubation time (s), τ_{SS} is the time to reach steady-state (s), $c_D(t)$ is the concentration of the compound in the donor phase at time point t (mol/cm^3), $c_D(0)$ is the concentration of the compound in the donor phase at time point zero (mol/cm^3), $c_A(t)$ is the concentration of the compound in the acceptor phase at time point t (mol/cm^3), r_v is the aqueous compartment volume ratio (V_D/V_A). For the comparison, the same experiment was repeated with omitting the effect of HP-β-CD.

3.8.2. *Ex vivo* corneal permeability studies on porcine eyes

Porcine eyes obtained freshly from the slaughterhouse were placed on a sterile cotton wool bed moistened with physiological saline solution and kept in a refrigerator box during transportation. Right before the experiment, the electrospun samples were dissolved in a physiological saline solution (PSS). The porcine eyes were first placed into Poly(tetrafluoroethene) (PTFE) inserts, where the cornea was uncovered and surrounded by a PTFE ring to prevent the flow of eye drops (75). The orifice above the corneal surface was first washed with PSS, and then the devices were pre-incubated at 35 $^{\circ}$C in a water bath for 5 minutes (min). After that, PSS was removed from the corneal surface, and 100 µL of the undiluted formulations were pipetted on each cornea using 3 eyes for each formulation, then the devices were incubated for 1 min. After that, the samples on the eye surface were diluted by adding PSS to the device's orifice to reach a 20-fold diluted concentration (~0.05 mg/mL) of the original dose, and the eyes were incubated with these diluted formulations for another 14, 29, or 59 min. At these endpoints, diluted formulations were removed from the precorneal area, the devices were disassembled, then aqueous humor was drained using a 26G needle, and finally the cornea was excised and NEPA was extracted with 2 mL of acetonitrile:water 50:50 (v/v) using an orbital shaker (Heidolph Titramax 100, Heidolph Instruments, Swabach, Germany) for 60 min at 450 rpm. Samples of precorneal fluid, aqueous humor, and corneal extract were analyzed by HPLC-DAD, and the NEPA concentration was calculated using a calibration curve (75). The corneal retention (CR) of NEPA, the apparent permeability (P_{app}C) of NEPA into the cornea, and the apparent permeability (P_{app}Aq) of NEPA into the aqueous humor were calculated using **Equations 6–8,** respectively.

$$CR = 1 - \frac{c_{CS}(t)}{c_{CS}(0)} - \frac{V_{AC}c_C(t)}{V_{CS}c_{CS}(0)} \qquad (6)$$

$$P_{app}C(cm/s) = \frac{\Delta[C]_C \times V_{AC}}{A \times [C]_{CS} \times \Delta t} \qquad (7)$$

$$P_{app}Aq(cm/s) = \frac{\Delta[C]_{Aq} \times V_{AC}}{A \times [C]_{CS} \times \Delta t} \qquad (8)$$

where $c_{CS}(t)$ is the concentration of the compound on the corneal surface at time point t (mol/cm^3), $c_{CS}(0)$ is the concentration of the compound on the corneal surface at time point zero (mol/cm^3), $c_C(t)$ is the concentration of the compound in the cornea at

time point t (mol/cm^3), and V_{AC} and V_{CS} are the volumes in the anterior chamber (0.25 cm^3) and on the corneal surface (0.75 cm^3).

$P_{app}C$ was calculated from the concentration difference of NEPA in the aqueous humor ($\Delta[C]_C$) after treatment, the initial concentration of the compound on the corneal surface at time point zero ($c_{CS}(0)$), the volume on the corneal surface V_{CS} (0.75 cm^3), A is the surface area available for permeability (1.77 cm^2), and t is the incubation time (s). $P_{app}Aq$ was calculated from the concentration difference of NEPA in the cornea ($\Delta[C]_{Aq}$) after treatment, the initial concentration of the compound on the corneal surface at time point zero ($c_{CS}(0)$), the volume on the corneal surface V_{CS} (0.75 cm^3), A is the surface area available for permeability (1.77 cm^2), and t is the incubation time (s).

3.8.3. *Ex vivo* cornea Raman mapping

Parallel with the corneal permeability, the distribution of NEPA in the excised cornea was investigated using Raman mapping after 15-, 30-, and 60-min treatment. The cornea was frozen after the treatment and divided into cross sections (15 μm thick) with a Leica CM1950 Cryostat (Leica Biosystems GmbH, Wetzlar, Germany). The selected specimens were mounted on aluminum-coated slides before the experiment. Raman spectroscopic analysis was performed with a Thermo Fisher DXR Dispersive Raman Spectrometer (Thermo Fisher Scientific Inc., Waltham, MA, USA) equipped with a Charge-coupled Device (CCD) camera and a diode laser with a wavelength of 780 nm. For marking the corneal area for investigation, an objective with 50x magnification was used. For the measurements, a laser power of 24 mW was used, and a slit aperture with a 50 μm size was applied. Raman maps were captured from an area of 150×1000 μm, with a step size of 50 μm vertically and horizontally. The OMNIC for Dispersive Raman 8.2 software (Thermo Fisher Scientific) was used for chemical evaluation. The individual spectrum of unformulated NEPA was used as a reference when profiling the chemical map.

3.9. Cytocompatibility Study

The Hen's egg test on chorioallantoic membrane (HET-CAM) test was used to examine the possibility of ophthalmic irritation of the developed NEPA-loaded and Cys-loaded nanofibers. The test is based on observing whether hyperemia, hemorrhage, and coagulation will occur upon exposing the CAM of 9-day-old chicken embryos to the

developed formulations. Fertilized White Leghorn chicken (*Gallus gallus domesticus*) eggs obtained from commercial breeders (Prophyl-BIOVO Hungary Ltd., Mohacs) were used for the study. The eggs were maintained at a temperature of 37.5 $^\circ$C $\pm$ 0.5 $^\circ$C in a humidified HEKA 1+ egg incubator (Rietberg, Germany). After the development of CAM on the 9th day of incubation, a small hole was made in the hard shell and expanded to about 2 cm with ophthalmic surgical scissors at the blunt end of the eggs. The inner membrane was carefully removed to expose the vascularized CAM. The plain, NEPA-loaded, and Cys-loaded nanofibers were placed on the surface of the vascularized CAM and evaluated against PBS (pH 7.4) and 0.1N NaOH solution as negative and positive controls, respectively. After 20 seconds of applying the tested materials, the vascular CAM was rinsed with 5 mL of PBS and evaluated for irritation effects. Images were captured at 0.5, 2, and 5 min using a Nikon SMZ25 stereomicroscope (Unicam Ltd., Hungary). Image processing was conducted using Nikon's proprietary software, QCapture Pro. Each sample was given a score based on the numerical time-dependent scores for hyperemia, hemorrhage, and coagulation (76,77).

3.10. Accelerated stability study

To carry out the accelerated stability study under stressful conditions, both samples (NEPA-loaded and Cys-loaded) electrospun samples were collected in aluminum foils and packed into hermetic bags with zip closures. A stability chamber (Sanyo type 022, Leicestershire, UK) was used to store the samples for four weeks under controlled conditions (40$\pm$2 $^\circ$C, 75$\pm$5% relative humidity (RH)). In predetermined time periods of 0, 1, 2, 3, and 4 weeks, the morphological and physicochemical characters of the NEPA-loaded and Cys-loaded electrospun samples were evaluated by SEM and FTIR, respectively, after applying elevated levels of temperature, humidity, and pressure.

3.11. Statistical analysis

The statistical analysis and figures were prepared using OriginPro 2018 software (v9.5.1., OriginLab Corporation, Northampton, MA, USA). ANOVA tests were used to assess the difference between the data. A p-value of less than 0.05 was considered statistically significant. To assess the normality of fiber diameter distribution, skewness and kurtosis have been calculated using Microsoft Excel 2010 functions.

4. RESULTS

4.1. Results of literature analysis and systematic review

A total of 795 articles and 197 patents were obtained from all database searches and search engines, among which 594 were from Science Direct, 47 from PubMed, 42 from Web of Science, 39 from Scopus, 31 from Reaxys, 24 from Google Scholar, and 18 from Ovid Medline. Considering the patents, 118 were from Google Patents, 34 from Espacenet, and 45 from Reaxys. After the screening and extraction processes, only 13 articles and 15 patents were included in the review, and they were selected based on the specified inclusion criteria. The process of identification and screening is presented in **Figure 2.**
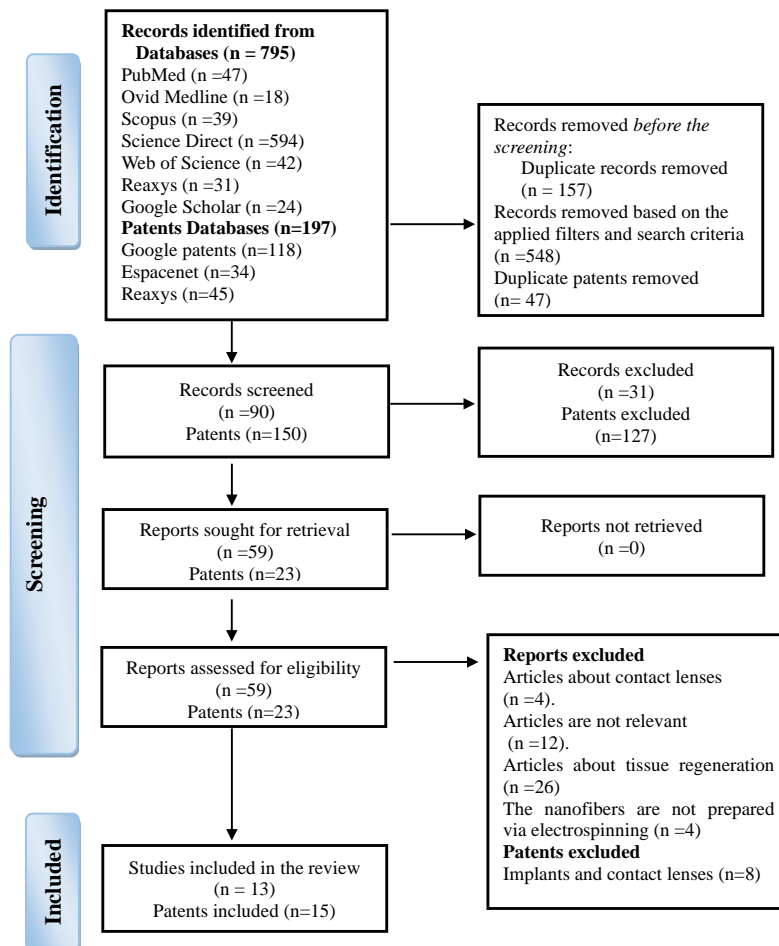
Figure 2. *PRISMA-2020 flow diagram displays the included relevant articles and patents. [II]*

4.2. Solution of nepafenac (NEPA)/hydroxypropyl-beta-cyclodextrin (HP-β-CD) in water

The solution of NEPA in water was successfully obtained by adding HP-β-CD and the result is consistent with the published work (68). Accordingly, each 1mg/mL (3.9 mM) of NEPA can be dissolved by adding approximately 0.069g (50 mM) of HP-β-CD to produce a clear yellow solution. The amount of the dissolved NEPA was successfully determined and confirmed according to a previously constructed calibration curve.

4.3. Morphological evaluation

4.3.1. Polyvinyl alcohol (PVA)/poloxamer 407 (PO-407)/polysorbate 80 (PS-80) samples

The SEM images for morphological characterization of electrospun PVA/PO-407/PS-80 samples are displayed in **Figure 3**. The presence of PS-80 in a concentration of 0.5-1% (w/w) slightly liquified the highly viscous PVA/PO-407 precursor solutions. The overall effect was random fiber deposition with most solution compositions. Nevertheless, a high amount of PS-80 (1% w/w) induced some bead formation and thinner fibers. This effect was more observable with low molecular weight PVA (Mw~67 kDa).
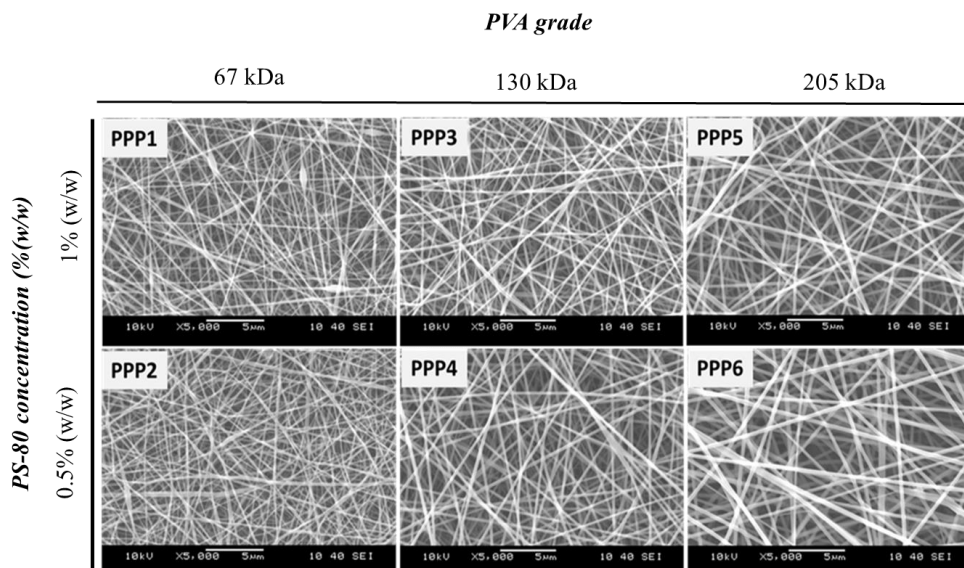
Figure 3. *Scanning Electron Microscope (SEM) images of electrospun samples of polyvinyl alcohol (PVA)/poloxamer 407(PO-407) blends with polysorbate 80 (PS-80) (0.5-1% (w/w)), (magnification: 5000×). [IV]*

The average fiber diameters of electrospun PVA/PO-407/PS-80 samples are presented in **Table 4.** The average fiber diameter was much lower than that of neat PVA and PVA/PO-407 blends.

Table 4. *Average fiber diameters of polyvinyl alcohol (PVA)/poloxamer 407 (PO-407)/polysorbate 80 (PS-80) nanofibers with respective skewness and kurtosis*

Formulation code	Total polymer Concentration (%(w/w)) PVA: PO-407 80:20 (m:m)	PS-80 %(w/w)	Average fiber diameter (nm) ± SD (nm)	Skewness	Kurtosis
PPP1		1%	85 ± 20	0.2109	-0.2370
	17.5				
PPP2	(Mw~67 kDa)	0.5%	109 ± 13	0.1132	-0.8671
PPP3		1%	105 ± 21	0.2307	-0.0149
	14				
PPP4	(Mw~130 kDa)	0.5%	131 ± 23	-0.0601	-0.2567
PPP5		1%	127 ± 13	-0.0275	-1.1673
	7.5				
PPP6	(Mw~205 kDa)	0.5%	141 ± 14	-0.2954	-0.6619

The fiber diameter distributions of electrospun PVA/PO-407/PS-80 are presented in **Figure 4**. The different solutions' compositions resulted in different distribution curves. Homogenous normal distribution and compound distribution were all observed. The higher concentration of PS-80 (1% (w/w)) led to shifting the fiber's distribution into lower nanometer scales.
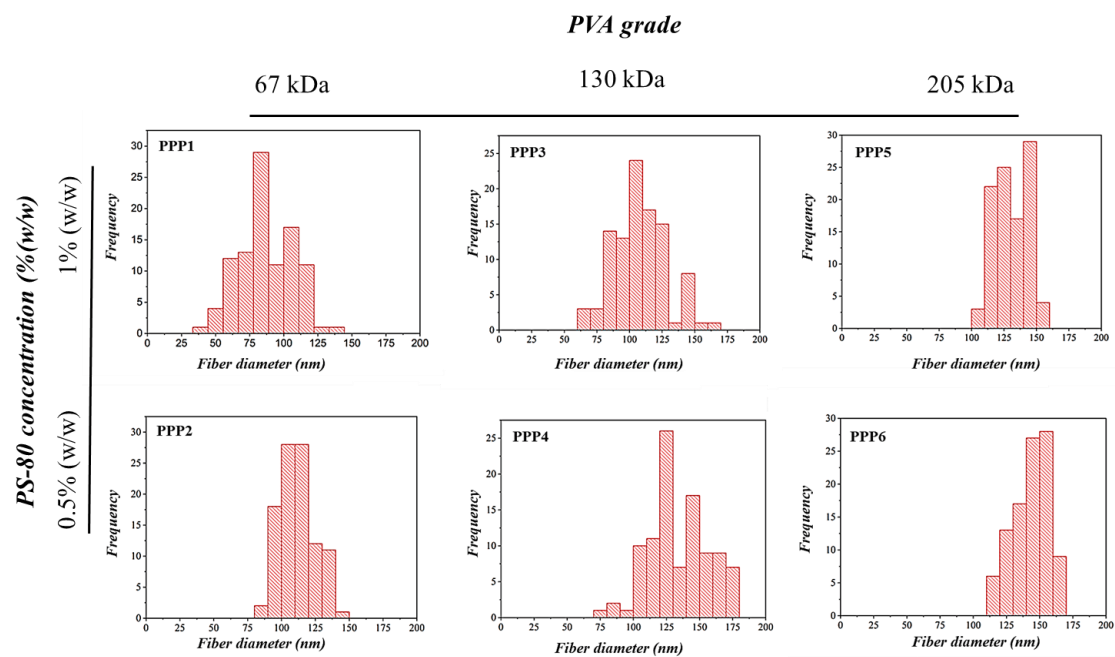
Figure 4. *Fiber diameter distributions of electrospun polyvinyl alcohol (PVAs)/poloxamer 407 (PO-407)/polysorbate 80 (PS-80) samples. [IV]*

4.3.2. Tetraetoxysilane (TEOS)/ polyvinyl alcohol (PVA) samples

The morphological features of the electrospun samples prepared from the different compositions of TEOS/PVA precursor solutions were studied using SEM (**Figure 5**.).
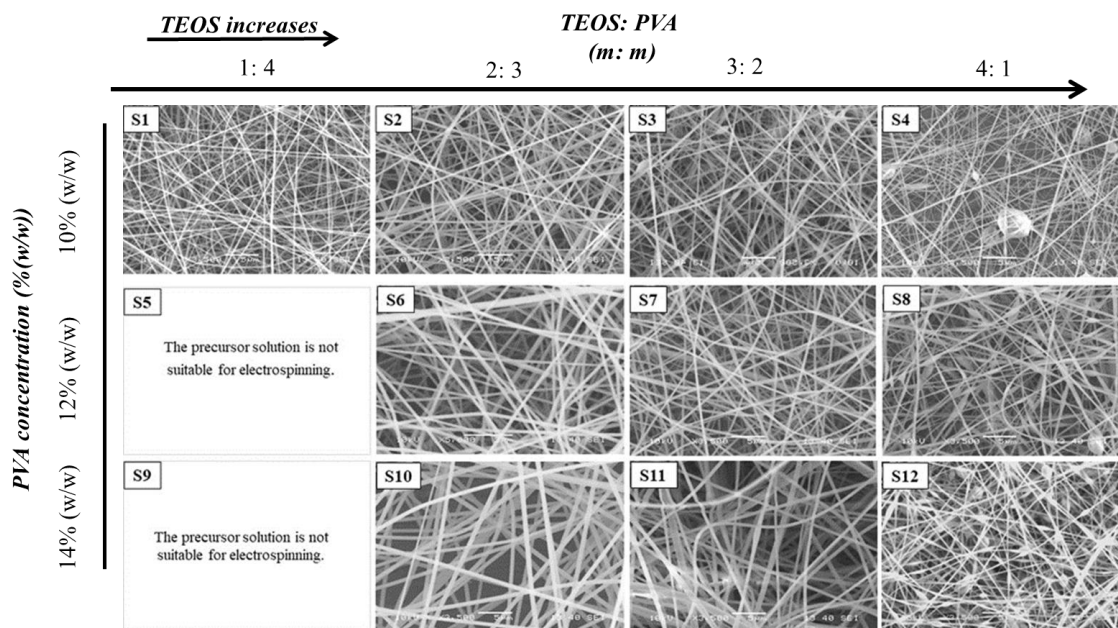
Figure 5. *Scanning Electron Microscope (SEM) images of electrospun samples prepared from different composition Tetraethoxysilane (TEOS)/ polyvinyl alcohol (PVA) precursor solutions by electrospinning (Magnification: 3500x). [IV]*

The fiber formation ability of the precursor solutions of different compositions and the morphology of the electrospun samples showed wide variability. For the same polymer ratio, increasing PVA concentration favored the formation of a fibrous structure, whereas increasing TEOS concentration, beady fibrous structures were observed. In the case of S5 and S9 solutions, due to interaction between PVA and TEOS gels were formed instead of highly viscous solutions. This resulted in increased resistance to the flow and failure of fiber's formation. There were significant differences in average fiber diameters. At the same TEOS: PVA ratio, the fiber diameter increased with increasing polymer concentration (**Table 5**).

Table 5. *The average fiber diameter values of the Tetraethoxysilane (TEOS)/ polyvinyl alcohol (PVA) samples*

Fiber diameter average (nm) ± SD (nm)		TEOS: PVA (m:m)			
		1:4	2:3	3:2	4:1
c PVA (% (w/w))	10%	183 ± 33	282 ± 57	235 ± 51	129 ± 30
	12%	-	386 ± 48	298 ± 52	217 ± 58
	14%	-	572 ± 79	549 ± 83	244 ± 63

There is no monotonic trend with increasing TEOS ratio for the same polymer concentration. The highest values are always obtained for the TEOS:PVA of 3:2 mass ratio. The fiber diameter distributions of the electrospun fibrous samples are shown in **Figure 6**.
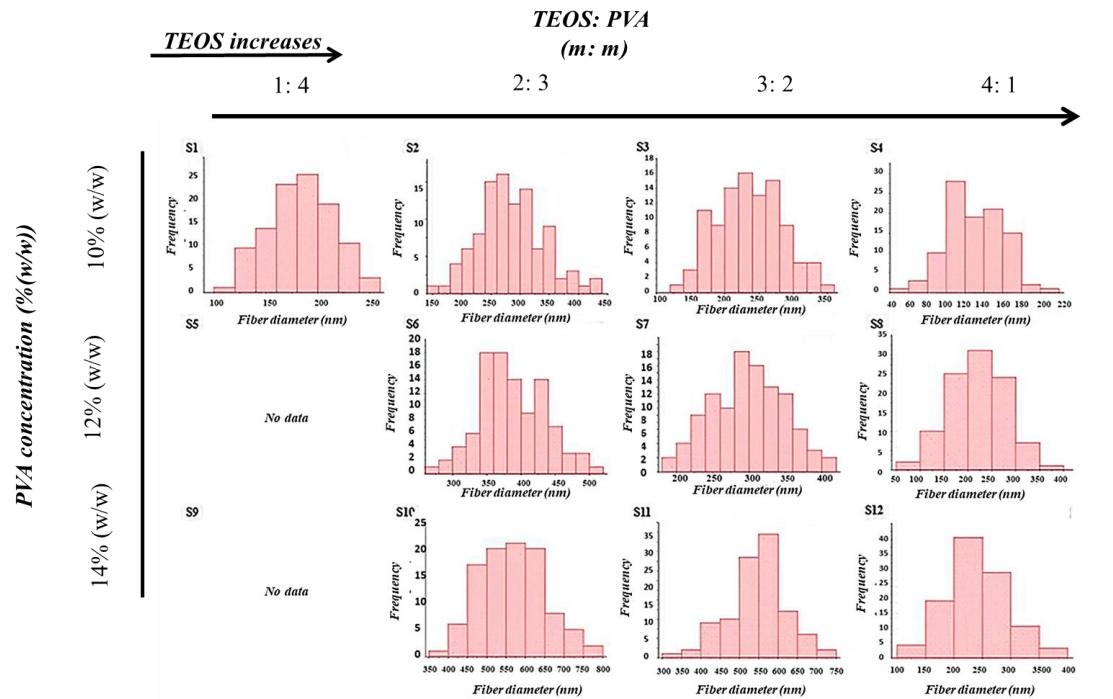
Figure 6. *Fiber diameter distribution of the electrospun samples prepare from different tetraethoxysilane (TEOS)/ polyvinyl alcohol (PVA). [IV]*

4.3.3. Nepafenac-loaded (NEPA-loaded) fibers

The SEM images for the fibrous samples for the different NEPA/HP-β-CD/PVA and NEPA/ HP-β-CD/PVA/PO-407 are displayed in **Figures 7**. The images show bead-free, randomly oriented fiber depositions and no gel droplets on the fibers' surfaces. It

has been observed that increasing the HP-β-CD amount results in a better fiber's surface with more clear, smoother, and more uniform fibers.
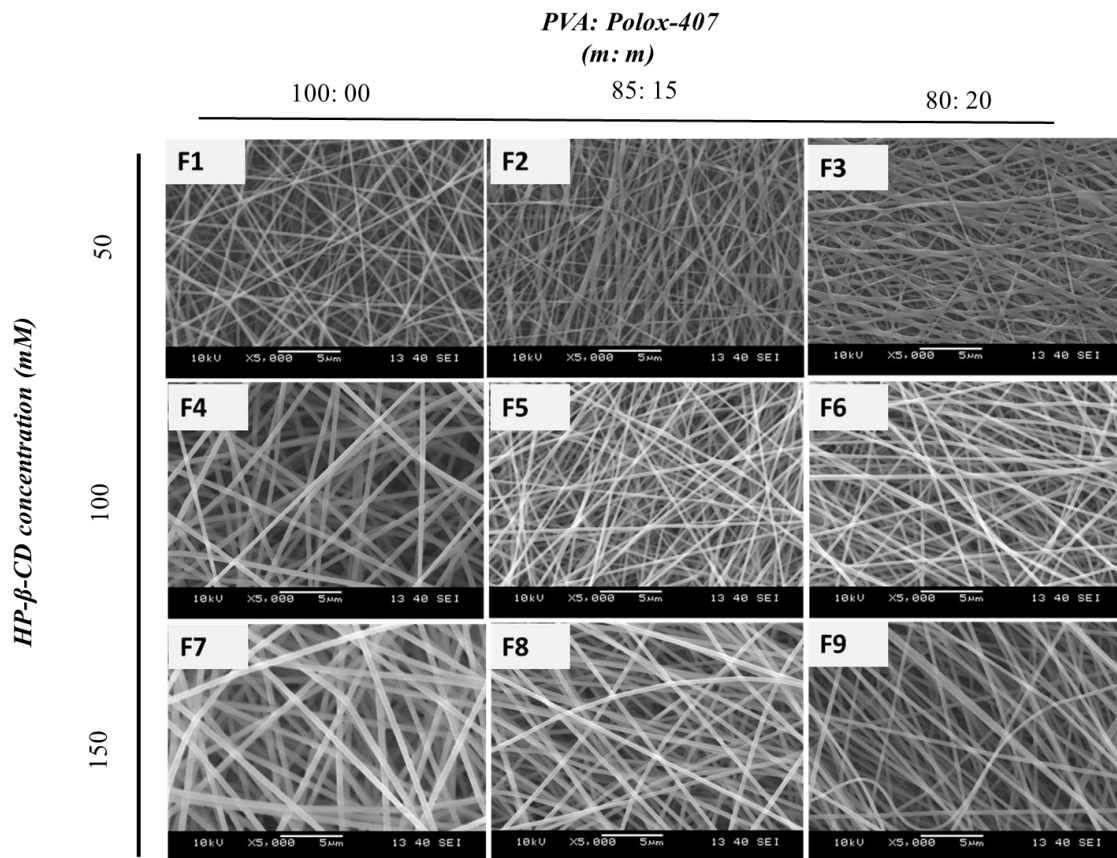
Figure 7. Scanning Electron Microscope (SEM) images of Nepafenac (NEPA)-loaded electrospun samples prepared from nepafenac/ hydroxypropyl-beta-cyclodextrin /polyvinyl alcohol (NEPA/HP-β-CD/PVA)(F1, F4, and F7); and NEPA/ HP-β-CD/PVA/Poloxamer 407 (F2, F3, F5, F6, F8, and F9) (magnification: 5000×). [III]

The fiber diameters ranging from 124 ± 20 nm to 464 ± 49 nm. It has been observed that increasing the HP-β-CD amount results in a better fiber's surface with more clear, smoother, and more uniform fibers. The presence of HP-β-CD in low amounts (F2 and F3) resulted in a lower average fiber diameter when compared to the double and the triple amount in the formulations (F5 and F6) and (F8 and F9), respectively (**Table 6**).

Table 6. *Average fiber diameters of nepafenac (NEPA)/ hydroxypropyl-beta-cyclodextrin complex (HPβCD), loaded in different ratios of polyvinyl alcohol (PVA): Poloxamer 407 9PO-407) with respective skewness and kurtosis*

Formulation Code	NEPA % (w/w)	HPβCD (mM)	PVA: PO-407 (m:m)	Average fiber diameter (nm) ± SD (nm)	Skewness	Kurtosis
F1	0.1	50	100:00	200 ± 27	0.6225	0.2188
F2	0.1	50	85:15	132 ± 25	0.5961	-0.5848
F3	0.1	50	80:20	124 ± 20	0.3360	-0.6292
F4	0.1	100	100:00	384 ± 39	-0.1411	-1.0768
F5	0.1	100	85:15	202 ± 33	0.3729	0.1127
F6	0.1	100	80:20	182 ± 30	-0.4320	-0.5959
F7	0.1	150	100:00	464 ± 49	0.2625	-0.3389
F8	0.1	150	85:15	301 ± 32	0.2308	-0.6104
F9	0.1	150	80:20	245 ± 30	-0.1361	-0.5533

Although there was no significant difference between average fiber diameters at p-value < 0.05 ($p=0.16921$), the histograms showed different diameter distributions (**Figure 8**).

Figure 8. *Fiber diameter distributions of Nepafenac-loaded electrospun samples prepared from nepafenac/ hydroxypropyl-beta-cyclodextrin/polyvinyl alcohol (NEPA/HPβCD/PVA) (F1, F4, and F7); and NEPA/ HPβCD/PVA/Poloxamer 407 (PO-407) (F2, F3, F5, F6, F8, and F9). [III]*

4.3.4. Cysteamine-loaded (Cys-loaded) fibers

SEM images of the Cys-loaded electrospun samples of both PVA/PO-407-based and TEOS/PVA-based polymer systems showed randomly oriented fibers with no remarkable beads or gel droplets on the fiber's surfaces. Regarding the PVA/PO-407-based samples, the images of fibers and the corresponding histograms diameter distribution are displayed in **Figure 9.**

Figure 9. *Scanning Electron Microscope (SEM) images and corresponding histograms of cysteamine-loaded (Cys-loaded) electrospun samples prepared from polyvinyl alcohol (PVA)/poloxamer 407 (PO-407) blends, ethylenediaminetetraacetic acid (EDTA) 0.05% (w/w), polysorbate 80 (PS-80) (0.5% (w/w)); cysteamine hydrochloride (CysH) 0.55% (w/w) (F2, F6, and F10); and CysH 1.1% (w/w) (F4, F8, and F12) (magnification: 5000×). [IV]*

Addition of CysH to the PVA/PO-407 slightly lower the average fiber diameter and the effect was concentration dependent; formulations loaded with 1.1% w/w (F4, F8, and F12) showed lower fibers diameter comparing to formulations with 0.55% w/w (F2, F6 and F10). The average diameter of fibers for Cys-loaded formulations are summarized in **Table 7**. It has also been observed that the presence of EDTA and 0.5 to 1% PS-80 in the polymeric matrix improved the appearance of fibers.

Table 7. *Average fiber diameters, skewness, and kurtosis of cysteamine-loaded (Cys-loaded) electrospun samples based on polyvinyl alcohol (PVA)/poloxamer 407 (PO-407)/polysorbate 80 (PS-80) polymeric blends*

Formulation code	Total polymer Concentration (%(w/w)) PVA: PO-407 80:20 (m:m)	CysH %(w/w)	Average fiber diameter (nm) ± SD (nm)	Skewness	Kurtosis
F2		0.55%	148±35	-0.1560	0.4718
	17.5				
F4	(Mw~67 kDa)	1.1%	127±25	-0.8385	-0.2784
F6		0.55%	197±35	-1.2019	0.1521
	14				
F8	(Mw~130 kDa)	1.1%	175±37	-0.8892	0.4554
F10		0.55%	167±41	-0.2257	0.5083
	7.5				
F12	(Mw~205 kDa)	1.1%	126±24	-1.0068	-0.0758

Considering TEOS/PVA-based samples, clearly fibrous bead-free structures were formed regardless of the TEOS:PVA ratio of the precursor solutions used for the fiber formation. Images of fibers and the corresponding histograms diameter distribution for the formulations provided best morphology are displayed in **Figure 10**. The addition of the active substance (CysH) reduced beads and improved the fiber formation ability when compared to the neat fibers. Moreover, the higher CysH concentration (1.1% w/w), the better fibers morphology was obtained.
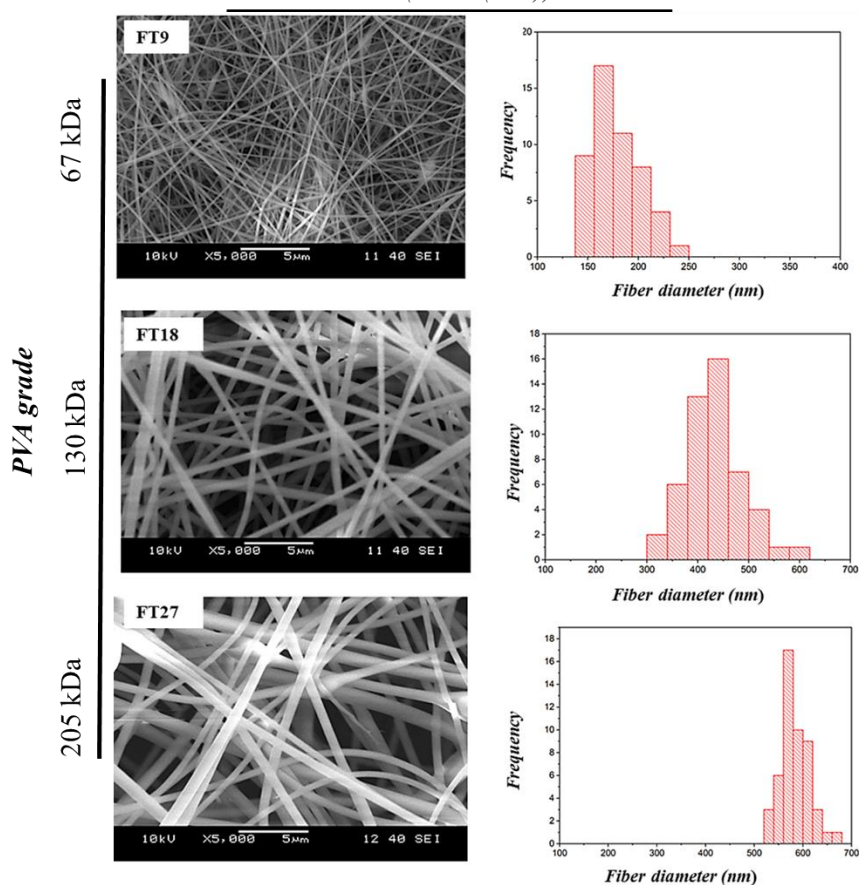
Figure 10. *Scanning Electron Microscope (SEM) images and corresponding histograms of cysteamine-loaded (Cys-loaded) electrospun samples prepared from polyvinyl alcohol (PVA) / Tetraethoxysilane (TEOS) and cysteamine hydrochloride 1.1%w/w. Where FT9, FT18, and FT27 prepared from Mw~67 kDa, Mw~130 kDa, and Mw~205 kDa of PVA respectively (magnification: 5000×). [IV]*

The average diameter of fibers for Cys-loaded TEOS/PVA-based formulations are summarized in **Table 8**. It has been observed that the fiber diameter increases with increasing the PVA molecular weight. The effect might be attributed to the increases in the solution viscosity as a result of increasing the concentration of the solution.

Table 8. *Average fiber diameters, skewness, and kurtosis of cysteamine-loaded (Cys-loaded) electrospun samples based on tetraetoxysilane (TEOS)/ polyvinyl alcohol (PVA) polymeric blend, TEOS: PVA (4:1=m:m)*

Formulation code	Formulation composition			Average fiber diameter (nm) ± SD (nm)	Skewness	Kurtosis
	PVA grade	PVA %(w/w)	CysH % (w/w)			
FT9	Mw~67 kDa	20	1.1	178 ± 25	-1.7038	-0.1651
FT18	Mw~130 kDa	16	1.1	434 ± 56	-2.0620	0.6001
FT27	Mw~205 kDa	10	1.1	584 ±29	-5.9067	0.2114

4.4. Fourier Transform Infrared Spectroscopy (FTIR)

FTIR analysis was conducted to study the structural changes in the components of NEPA-loaded and Cys-loaded electrospun nanofibers **Figure 11** and **Figure 12, respectively**. The spectra suggested formation of amorphous solid dispersion in both cases (CysH/PVA/PO-407 and CysH/TEOS/PVA samples). The spectra of all individual components, including NEPA, CysH, EDTA, PS-80, PVA, PO-407, TEOS, and HP-β-CD, and electrospun fibrous samples' spectra have been detected.

The PVA spectra in the 3 formulations showed the following important peaks: a broad band at 3282 cm^{-1}–3300 cm^{-1} characteristic for O-H stretching arising from the intermolecular and intra-molecular hydrogen bonds; the band at 2910 cm^{-1}–2920cm^{-1} is related to C-H stretching from alkyl group; the band at 1710 cm^{-1}–1750 cm^{-1} is attributed to carbonyl (C=O stretching); the band at 1400 cm^{-1}–1420 cm^{-1} is due to bending stretching of CH$_2$; the band at 1345 cm^{-1}–1370 cm^{-1} resulting from C-H vibration; the band at 1080 cm^{-1}–1090 cm^{-1} is related to C-O stretching of acetyl groups; and the band at 830 cm^{-1}–840 cm^{-1} is attributed to C-C stretching vibration (78–81).

Regarding PO-407 spectra (in NEPA-loaded and PVA/PO-407 based Cys-loaded), the absorption peak at 2939 cm^{-1} is related to CH$_3$ stretching; the peak at 2872 cm^{-1} is

due to CH$_2$ stretching; absorption bands at 1095 cm^{-1} and 1340 cm^{-1} are attributed to C-O stretching and O-H bending, respectively (82–84).

The spectra of NEPA powder showed the following distinctive peaks: medium absorption bands at 3317.92 cm^{-1} and 3326.6 cm^{-1} confirmed N-H$_2$ stretching; a peak appeared at 1676 cm^{-1} is attributed to C=C stretching; N-H bending appeared at 1554 cm^{-1}; a peak at1283 cm^{-1} is attributed to stretching of aromatic amine; an absorption peak at 1236 cm^{-1} is due to stretching of aliphatic amine (68,85,86).

The spectra of HP-β-CD showed the most important peaks as follows: a broad band at 3200 cm^{-1}–3485 cm^{-1} characteristic of O-H stretching arising from the intermolecular and intra-molecular hydrogen bonds; an absorption band at 2912 cm^{-1}–2986 cm^{-1} characteristic of C-H stretching; a peak at 1670 cm^{-1} is attributed to C=C stretching; a strong, sharp peak at 1024.9 cm^{-1} is related to C-O stretching (85,87).

The spectra of the nanofiber blends (PVA/PO-407/NEPA/HP-β-CD) display the presence of the main distinctive peaks of PVA, PO-407, and HP-β-CD: An overlapped absorption band ranging at 3118.3 cm^{-1}–3598.5 cm^{-1} (overlapped band of N-H$_2$ stretching from NEPA and O-H stretching from PVA and HP-β-CD); an overlapped absorption peak at 2823.2 cm^{-1}–2995.8 cm^{-1} (overlapped band of C-H stretching from PVA, PO-407 and HP-β-CD); absorption band at 1704 cm^{-1}–1744 cm^{-1} related to carbonyl (C=O stretching of PVA); an overlapped absorption band appeared at 1670 cm^{-1}–1674 cm^{-1} (is attributed to C=C stretching); absorption peak at 1360 cm^{-1}–1370 cm^{-1} indicating overlapped CH$_2$ bending stretching from PVA and O-H bending from PO-407; a strong sharp peak at 1024.9 cm^{-1} is related to that arising from C-O stretching of HP-β-CD; absorption peak at 1081 cm^{-1}–1100 cm^{-1} indicating overlapped peak due to C–O stretching from (PVA, PO-407); and peak at 828 cm^{-1}– 840 cm^{-1} is related to C-C stretching vibration of PVA.

The O-H absorption of nanofibers blends (PVA/PO-407/NEPA/HP-β-CD) was lower than that of individual PVA and HP-β-CD. This may be due to the incorporation of NEPA into HP-β-CD via inclusion complex and interaction of the resulting complex with O-H of the PVA.
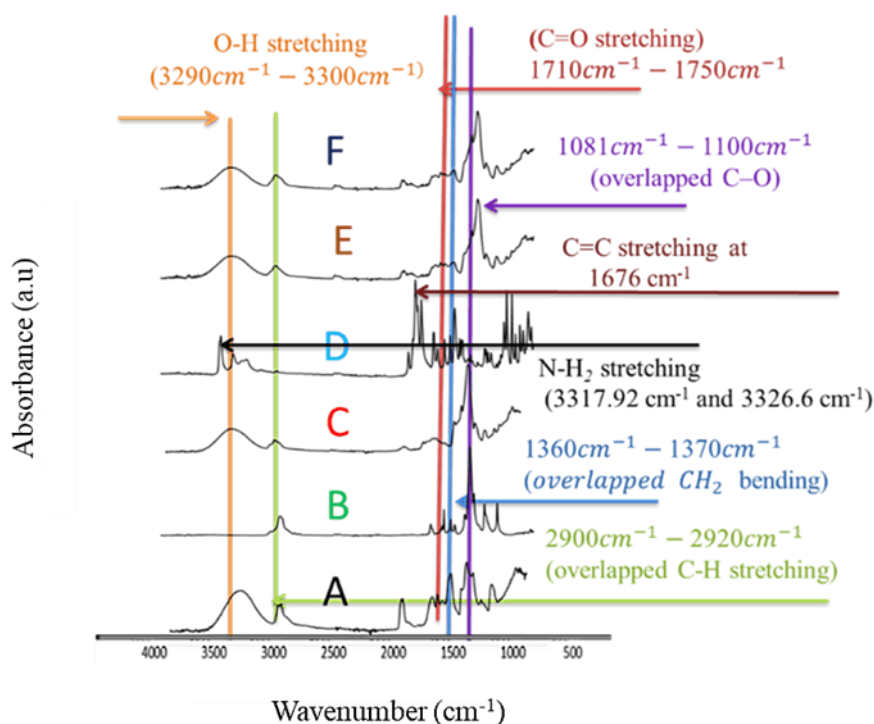
Figure 11. *Fourier transform infrared (FTIR) spectra of:* ***(A):*** *polyvinyl alcohol (PVA);* ***(B):*** *Poloxamer 407 (PO-407);* ***(C):*** *Hydroxypropyl-β-cyclodextrin (HP-β-CD);* ***(D):*** *Nepafenac (NEPA);* ***(E):*** *Electrospun nanofibers of NEPA/HP-β-CD/PVA (F1, F4, and F7); and* ***(F):*** *Electrospun nanofibers of NEPA/ HP-β-CD/PVA/PO-407 (F2, F3, F5, F6, F8, and F9). The PVA used was Mowiol® 18–88 (Mw~130 kDa). [III]*

In the case of PVA/PO-407-based samples **(Figure 12/I)**, the spectra of the mixtures display the presence of the main distinctive peaks of CysH, PVA, PO-407, EDTA, and PS-80. An overlapped absorption peak that appeared at 3296 cm^{-1}–3400 cm^{-1} is related to O-H stretching from PVA and the amino group of CysH and EDTA. The overlapped band at 2900 cm^{-1}–2920 cm^{-1} is due to C-H stretching from CysH, PVA, and PO-407. The presence of thiol group S-H of CH is confirmed by the appearance of an absorption band at 2550 cm^{-1}–2670 cm^{-1}. The absorption band at 1700 cm^{-1}–1730 cm^{-1} is attributed to carbonyl (C=O stretching of PVA, PS-80 and EDTA); band at 1360 cm^{-1}–1370 cm^{-1} indicates overlapped CH$_2$ bending stretching of PVA and O-H bending of PO-407; an overlapped peak at 1081cm^{-1}–1100 cm^{-1} is due to C–O stretching from PVA, PO-407 and PS-80; and C-C stretching vibration related to PVA at 828 cm^{-1}–840 cm^{-1}.

Considering TEOS/PVA-based samples (**Figure 12/II**), the silica shows characteristic peaks between 1100 and 500 cm^{-1}, which are related to the asymmetric and symmetric stretching and bending vibrations of Si-O-Si bonds. For the fibrous samples, two characteristic PVA peaks appear at 1700 cm^{-1}, which are specific to the C=O groups. These peaks cannot be observed in the spectrum of starting materials. The intensity of these peaks is proportional to the PVA content of the hybrid fibers (88). The spectra clearly show an increase in cross-linking as the TEOS ratio increases.
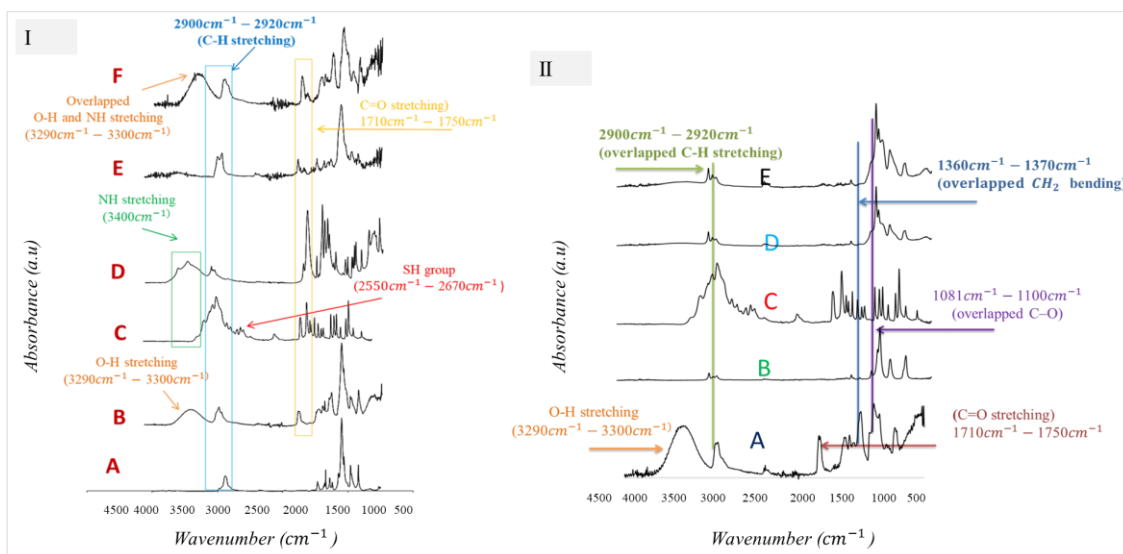
Figure 12. *Fourier transform infrared (FTIR) spectra of (**I**) cysteamine-loaded (Cys-loaded) samples based on polyvinyl alcohol (PVA)/ poloxamer 407 (PO-407) and (**II**) cysteamine-loaded samples based on tetraethoxysilane (TEOS)/ PVA. Where (**A**): PO-407; (**B**): PVA (Mw~130 kDa); (**C**): CysH; (**D**): Ethylenediaminetetraacetic acid (EDTA, 0.05(% w/w)); (**E**): Polysorbate 80 (PS-80); (**F**): Mixture of the former component. For II, (**A**): PVA (Mw~130 kDa); (**B**): TEOS; (**C**): CysH; (**D**): TEOS/PVA; and (**E**): CysH/TEOS/PVA. [IV]*

4.5. X-ray diffraction (XRD) for Nepafenac-loaded (NEPA-loaded) fibers

The XRD patterns of the NEPA, physical mixture, F3, F6, and F9 are displayed in **Figure 13.** The presence of sharp peaks confirmed the crystallinity of the NEPA in its pure state. The intensities of the peaks have decreased upon mixing the NEPA with HP-β-CD, PVA, or PO-407. The complete disappearance of these peaks from the nanofibers (F3, F6, and F9) confirms the formation of Amorphous solid dispersions (ASD) from crystalline NEPA through electrospinning of NEPA, HP-β-CD, PVA, and PO-407.
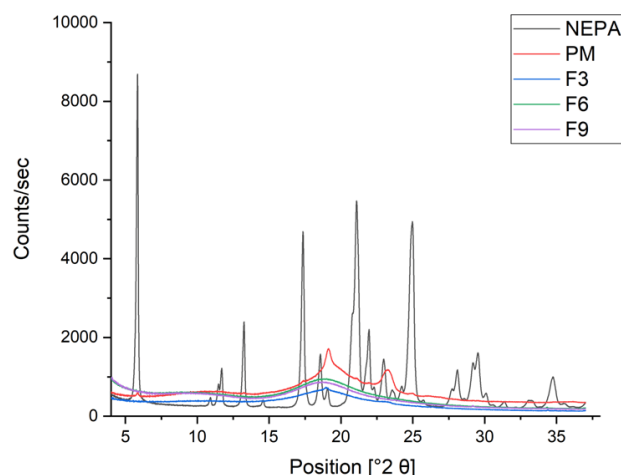
Figure 13. X-Ray Diffraction (XRD) patterns of the Nepafenac (NEPA), physical mixture of NEPA/ hydroxypropyl-β-cyclodextrin (HP-β-CD) / polyvinyl alcohol (PVA)/ Poloxamer 407 (PO-407); (PM), and Electrospun nanofibers of NEPA/ HP-β-CD/PVA/PO-407 (F3, F6, and F9). [III]

4.6. Determination of the drug content

The drug content of all formulations (F1–F9) of NEPA-loaded nanofibers ranged from 100.01 (% w/w) ± 0.03 to 101.05 (% w/w) ± 0.02. All formulations of Cys-loaded showed drug content of 99.74 ± 0.04 (% (w/w)) to 100.5 ± 0.05 (% (w/w)). This reflects the complete dissolution of the NEPA through complexation with HP-β-CD during the solution preparation. The results from both experiments show uniform drug content throughout the PVA/PO-407 fiber structure. During electrospinning, a homogenous precipitation of the drug/polymer blend occurred after solvent evaporation. Therefore, any deviation from the theoretically stated amounts might be attributed to errors that can occur during solution preparation or during fibers' weighing.

4.7. *In vitro* drug release and release kinetics

4.7.1. Nepafenac-loaded (NEPA-loaded) fibers

In vitro dissolution profiles of the NEPA/HP-β-CD-loaded nanofibers (0.1% w/w) conducted in PBS (pH 7.4) at 37 °C are displayed in **Figure 14**. All formulations (F1-F9) showed complete release of NEPA in less than 60 min (16.5- 40 min). All formulations completely dissolved within 5 seconds, forming a viscous gel when placed on the surface of filter paper wetted with a PBS (pH 7.4), which agrees with the

previously published work (89). Regardless of HP-β-CD amount, all formulations containing PO-407 (F2, F3, F5, F6, F8, and F9) released the NEPA at a faster rate compared to the formulations without PO-407. Some variations were observed in the dissolution profiles with varying the HP-β-CD and PO-407 amounts. Higher HP-β-CD levels resulted in a relatively longer drug release, while higher PO-407 levels resulted in a faster release ($p= 0.0325$ at p-value < 0.05). In a conclusion, there was no significant difference in the overall release of the nine formulations.
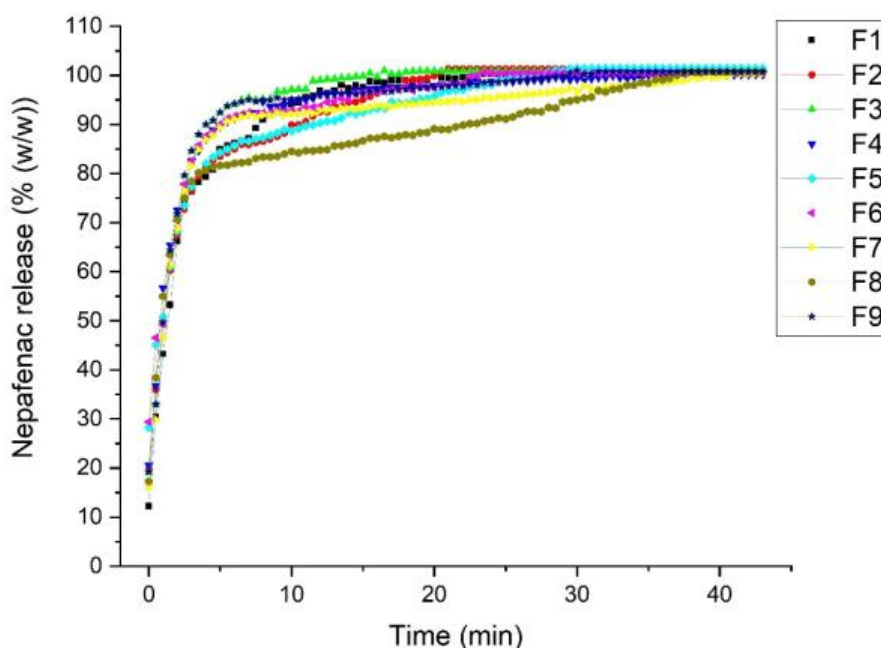
Figure 14. *In vitro dissolution profiles of Nepafenac (NEPA)/ Hydroxypropyl-β-cyclodextrin (HP-β-CD) (0.1%(w/w)) loaded in polyvinyl alcohol (PVA)/poloxamer 407 (PO-407) nanofibers. The dissolution was conducted in phosphate buffered solution (pH 7.4) at 37 ± 0.5 °C. [III]*

The release kinetics of NEPA from the nanofibrous matrix were studied using Weibull distribution due to the model's flexibility in dealing with diverse release patterns. The release parameters including M_∞, β, τ_d and R^2 are summarized in **Table 9**. All formulations (F1-F9) were successfully fitted to the Weibull model, and R^2 values were greater than 0.9, indicating linear regression. For most formulations, β values were < 0.75, indicating Fickian diffusion, while two formulations were $0.75 < \beta < 1$, which means a combined release mechanism. For instance, it could represent both diffusion and swelling-controlled release.

Table 9. *Dissolution kinetic parameters of Nepafenac (NEPA) (0.1%(w/w))/ Hydroxypropyl-β-cyclodextrin (HP-β-CD) loaded in polyvinyl alcohol (PVA) /poloxamer 407 (PO-407) nanofibers.*

Formulation code	M_∞ (min)	β Parameter	τ_d (min)	Correlation coefficient (R^2)
F1	100.3	0.6838	128.7	0.9929
F2	102.3	0.5154	121.4	0.9858
F3	100.4	0.8466	105.7	0.9909
F4	99.0	0.6501	88.4	0.9896
F5	103.5	0.4222	110.3	0.9824
F6	100.1	0.5807	92.7	0.9751
F7	96.2	0.8506	103.3	0.9681
F8	119.2	0.2479	259.1	0.9397
F9	98.6	0.9268	104.9	0.9812

4.7.2. Cysteamine-loaded (Cys-loaded) fibers

The *in vitro* releases of Cys based on PVA/PO-407 and TEOS/PVA are displayed in **Figure 15**. Regardless of the base type, whether soluble (PVA/PO-407) or insoluble (TEOS/PVA), the release of Cys from the matrices was complete and fast in less than 10 min. This observation suggests that the primary rate-limiting step in drug release is the immediate dissolution of the active pharmaceutical ingredient rather than its diffusion from the matrix base. The latter offers higher drug payloads, potentially improving drug delivery by sustaining optimal drug concentrations to overcome obstacles like vitreous humor and achieve therapeutic levels in the eye. Human pharmacokinetic studies also confirm that immediate-release Cys is effective in depleting cystine levels, with no statistically significant difference in effectiveness compared to delayed-release formulations (64).
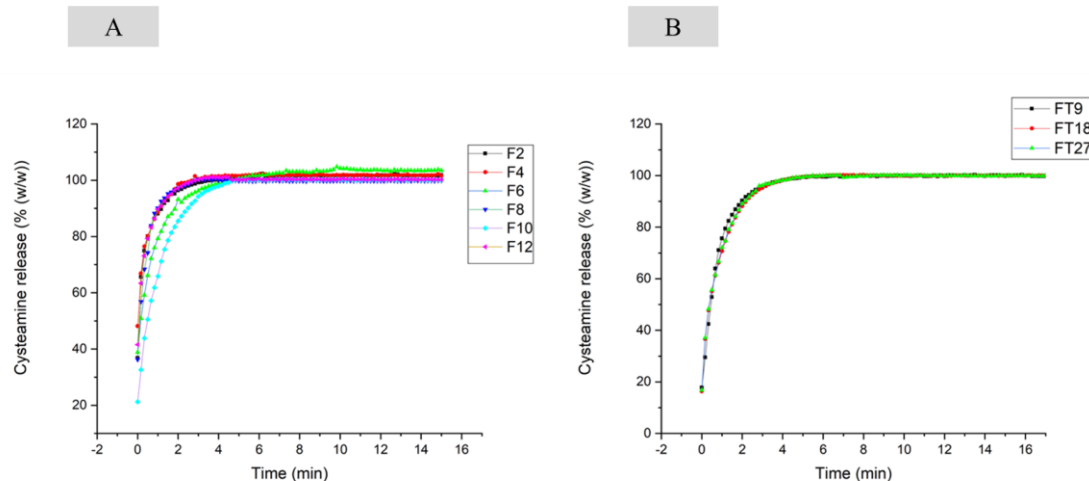
Figure 15. *In vitro dissolution profiles of cysteamine HCl loaded in (**A**): polyvinyl alcohol (PVA)/poloxamer 407 (PO-407) nanofibers using low molecular weight (PVA, Mw~67kDa) (F2 and F4); intermediate molecular weight (PVA, Mw~130,000 g mol^{-1}) (F6 and F8); and high molecular weight (PVA, Mw~205kDa) (F10 and F12) and (**B**): tetraetoxysilane (TEOS)/polyvinyl alcohol (PVA, Mw~130 kDa) (4:1). The dissolution was conducted in phosphate buffered solution (pH 7.4) at 35 ± 0.5 °C. [IV]*

Weibull distribution was used to study the Cys release kinetics from the two polymeric bases since it can be applied to different release behaviors. The release parameters including M_∞, β, τ_d and R^2 are summarized in **Table 10**. All formulations from the various bases were successfully fitted to the Weibull model ($R^2 > 0.9$), indicating linear regression. In the case of the TEOS/PVA system, the values were $0.75 < \beta < 1$, indicating a Case II transport, which is a specific mechanism of drug release from polymeric systems, characterized by non-Fickian diffusion where the rate of drug release is predominantly controlled by the relaxation of the polymer matrix rather than by the concentration gradient of the drug. In this transport, the polymer undergoes significant swelling or glass transition, leading to a sharp front of drug release that moves through the matrix. For instance, it could represent both diffusion and swelling-controlled release, which seems logical since the release occurred from the insoluble matrix.

For the PVA/PO-407 matrix, most values were < 0.75, indicating Fickian diffusion, and additional kinetic models may be useful for further interpretation.

Table 10. *Dissolution kinetic parameters of Cysteamine-HCl (CysH) loaded in polyvinyl alcohol (PVA)/poloxamer 407 (PO-407) and tetraetoxysilane (TEOS)/PVA*

Formulation code	M_∞	β Parameter	τ_d	Correlation coefficient (R^2)
F2	102.06	0.4548	12.37	0.9979
F4	101.99	0.5843	18.48	0.9939
F6	103.81	0.6201	39.87	0.9987
F8	99.90	0.8063	24.52	0.9977
F10	100.39	0.9751	69.25	0.9990
F12	100.49	0.6357	18.53	0.99583
FT9	99.80	0.9007	48.03	0.99785
FT18	100.14	0.8141	50.00	0.99821
FT27	100.08	0.8228	49.21	0.99806

4.8. Permeability studies of nepafenac-loaded fibers

4.2.1. *In vitro* corneal parallel artificial membrane permeability assay (PAMPA)

PAMPA permeability assay results are presented in **Figure 16**. Results from the experiment showed no significant difference between the 3 formulations (F3, F6, and F9) regardless of the HP-β-CD content per formulation (50 mM, 100 mM, and 150 mM for F3, F6, and F9, respectively). However, their permeability values were significantly lower than those measured for Nevanac® (p < 0.05). In this case, a 10% w/w of the donor's HP-β-CD content was added to the acceptor wells to create a more desirable environment for the poorly soluble nepafenac molecules. Unfortunately, corneal-PAMPA could not make a difference between the three formulations.

When the experiment was conducted using PBS acceptor media, omitting the sink effect of 10% w/w of HP-β-CD resulted in different tendencies within the samples containing various amounts of HP-β-CD. Results show that the increase in HP-β-CD amount among the 3 formulations resulted in an increased flux of NEPA to the acceptor compartment. The average permeabilities ± SD (10^{-6}cm/s) for the F3, F6, and F9 formulations were 11.9 ± 2.21, 13.8 ± 1.59, and 21.6 ± 2.968 respectively.
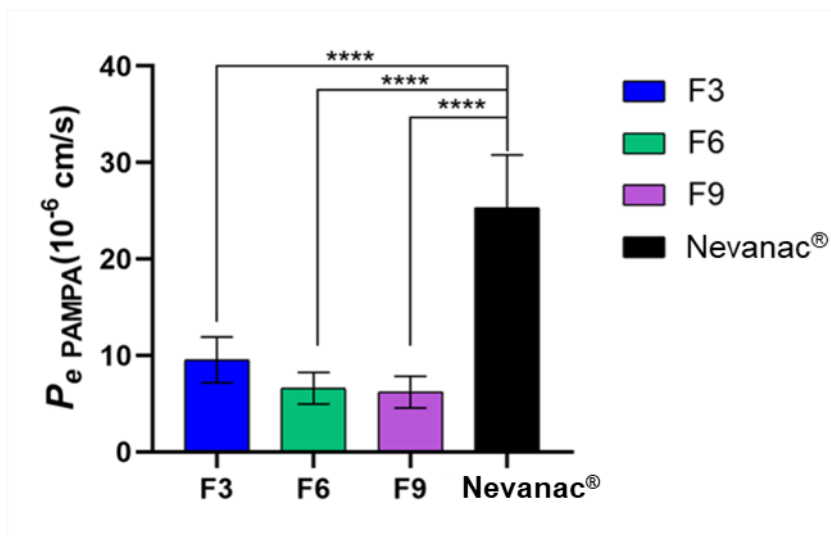
Figure 16. In vitro Corneal-parallel artificial membrane permeability (PAMPA) studies for the formulation F3, F6 and F9. Using nepafenac containing commercial product Nevanac®). Experiment conducted by adding 10% w/v of the donor's HP-β-CD content to the acceptor wells to create a more desirable environment for the poorly soluble nepafenac molecules. [III]

4.2.2. *Ex vivo* corneal permeability studies on porcine eyes

The concentration of the NEPA for the F3 in precorneal area, cornea, and aqueous humor has been determined at 15, 30, and 60 min. The results of **Figure 17** show that F3 has a significantly higher concentration than Nevanac® in precorneal area, as shown in **Figure 17A**. The values for the concentrations of NEPA in precorneal fluid for F3 and commercial Nevanac® at 15, 30 and 60 min were found to be 0.0269, 0.0013 and <0.0001 respectively. The highest dissolution was attained at 60 min. Regarding the cornea, although there is a slight increase in the Nevanac® compared to F3 formulation, it is only a numerical difference without statistical significance (**Figure 17B**). The NEPA concentrations in the aqueous humor were not significantly different at 15 and 30 min (**Figure 17C**). At 60 min Nevanac® had a significantly higher concentration than F3 formulation, with p value at 0.05 level of confidence being 0.0242.
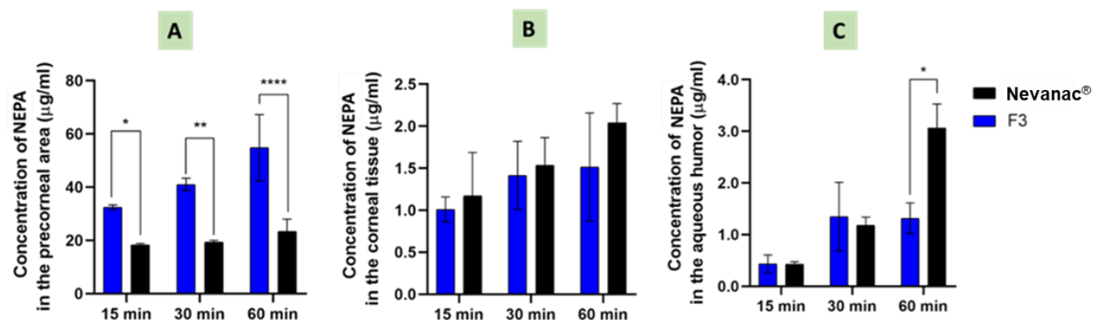
Figure 17. Nepafenac (NEPA) concentration of F3 for ex vivo experiment on porcine eye measured at (A): precorneal area; (B): cornea; and (C): aqueous humor, using Nevanac® as reference. [III]

4.2.3. *Ex vivo* cornea Raman mapping

The NEPA distribution within corneal tissues has been studied using Raman mapping. The F3 exposed porcine corneal tissues are presented in **Figure 18.** Based on the intensity scale, the high concentration of NEPA is reflected by the red color, the green color reflects lower concentration, whereas the blue color represents the area of the map where spectral resolution specify the untreated corneal tissue. The results show that in both cases NEPA distribution at 15 min was restricted to outer layers of the cornea, but it distributed to the inner most layer (stroma) at 30 and 60 min with more homogenous feature. In conclusion, there results support our finding that F3 could be bioequivalent to Nevanac® *in vivo*.
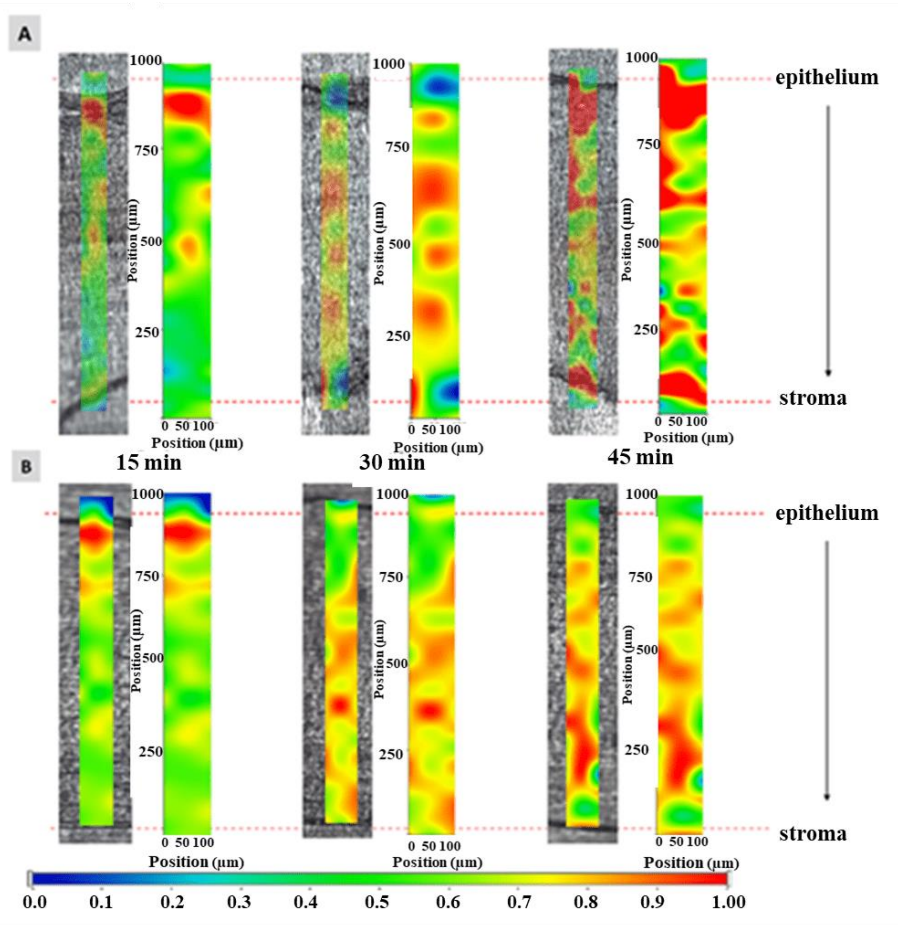
Figure 18. The Raman mapping of the distribution nepafenac (NEPA) in the excised porcine cornea for F3 formulation (A) and Nevanac® (B). [III]

4.3. Cytocompatibility Study

The applied samples, including NEPA-loaded, Cys-loaded nanofibers of different bases, the empty polymeric nanofibers, and the negative control (Phosphate buffer), resulted in no noticeable redness, coagulation, or bleeding, which indicates the tolerability and cytocompatibility of the formulation components when compared to a positive control (0.1 N NaOH). The later induced a strong hemorrhage on the surface of a chick CAM at embryonic day 9. The HET-CAM results are displayed in **Figure 19 and Figure 20**.
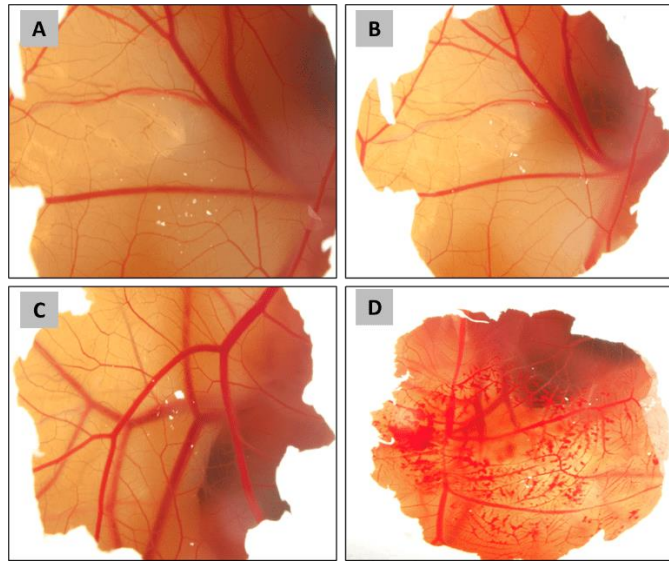
Figure 19. *Representative images of Hen's Egg Test on Chorioallantoic Membrane (HET-CAM); The test was conducted on the vascular structure of the CAM at day 9 of chicken development for a period of 5 min for electrospun nepafenac-loaded (NEPA-loaded) nanofibers. (A): Phosphate Buffered Saline (PBS) (negative control); (B): Empty fibers polyvinyl alcohol (PVA)/ Hydroxypropyl-β-cyclodextrin (HP-β-CD)/poloxamer 407 (PO-407); (C): Nepafenac-loaded fibers; (D): 0.1N NaOH (positive control). [III]*
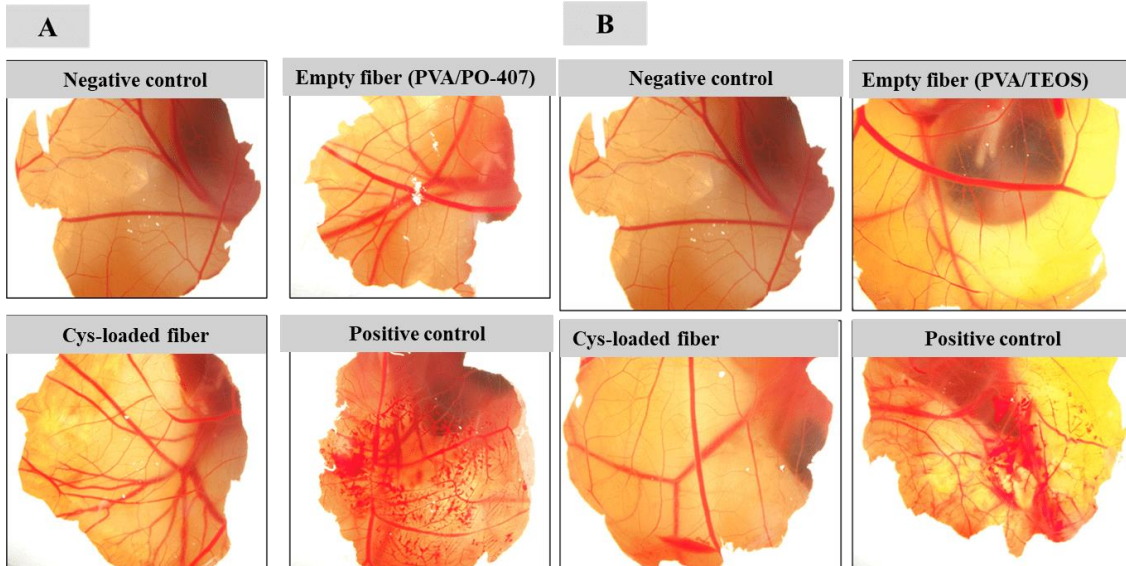
Figure 20. *Representative images of Hen's Egg Test on Chorioallantoic Membrane (HET-CAM); The test was conducted on the vascular structure of the CAM at day 9 of chicken development for a period of 5 min for electrospun cysteamine-loaded (Cys-loaded) based on (A):polyvinyl alcohol (PVA)/poloxamer 407 (PO-407) and (B) tetraetoxysilane (TEOS)/polyvinyl alcohol using Phosphate Buffered Saline (PBS) as negative control and 0.1 N NaOH as positive control. A strong hemorrhage induced by 0.1 N NaOH placed on the surface of a chick CAM at embryonic day 9. [IV]*

4.4. Accelerated stability study

The SEM images of the NEPA-loaded and Cys-loaded electrospun nanofibers for the freshly prepared samples and samples stored under stressful conditions are illustrated in **Figure 21** and **Figure 22**, respectively. The results suggest stable formulations of NEPA and Cys with PVA/PO-407 and TEOS/PVA polymeric bases. All formulations maintained their fibrous morphology over the period of study (4 weeks)
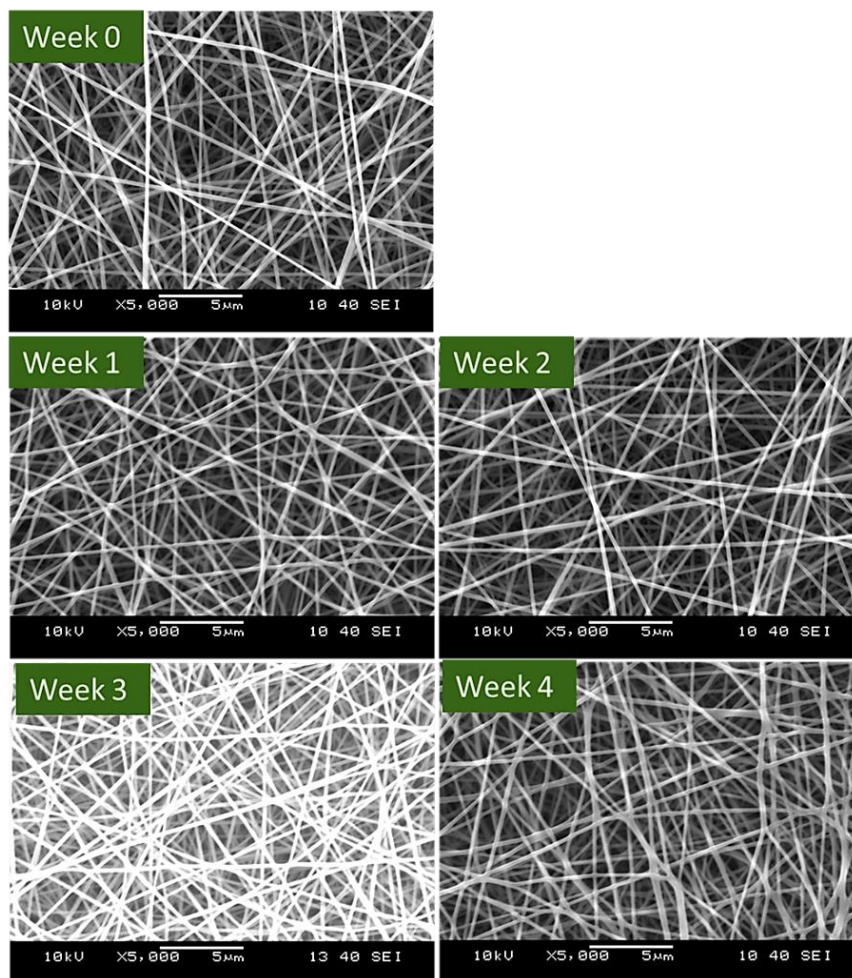
Figure 21. *Scanning electron microscopic (SEM) images of the Nepafenac-loaded (NEPA-loaded) fibers at 0, 1-, 2-, 3-, and 4- weeks storage under stress conditions (40 ± 2 °C, 75 ± 5% relative humidity (RH)). (magnification: 5000×). [III]*
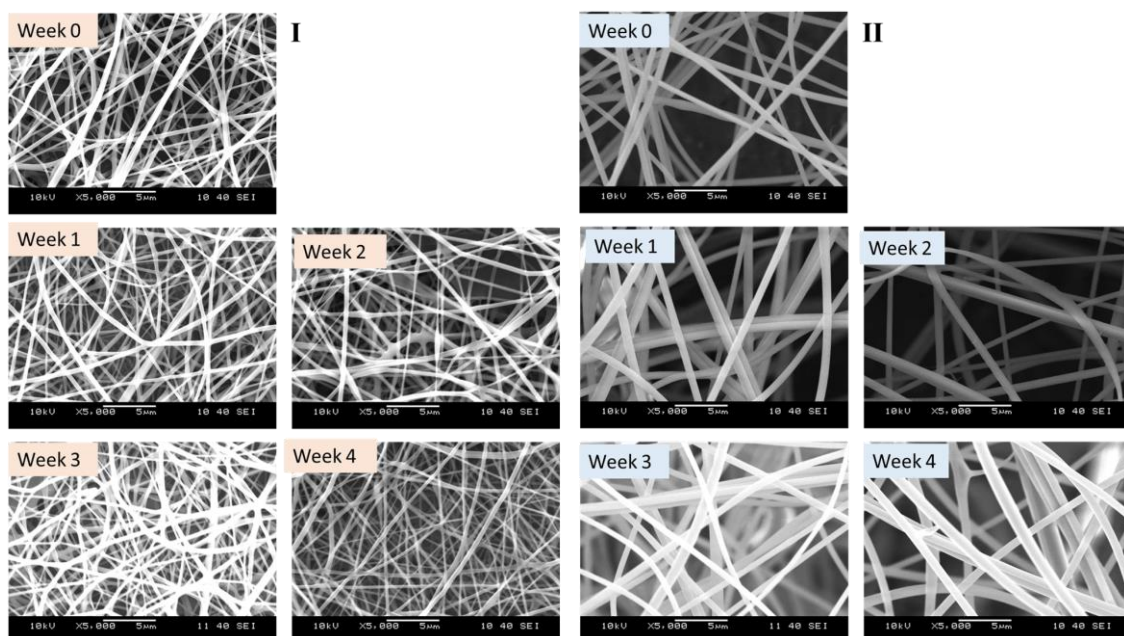
Figure 22. *Scanning electron microscopic (SEM) images of the cysteamine-loaded (Cys-loaded) fibers at 0, 1-, 2-, 3-, and 4-weeks storage under stress conditions (40 ± 2 °C, 75 ± 5% relative humidity (RH)). (I): polyvinyl alcohol (PVA) /poloxamer 407 (PO-407) and (II) tetraetoxysilane (TEOS)/polyvinyl alcohol (PVA) polymeric blends . (magnification: 5000×). [IV]*

The time dependent changes in physicochemical characteristics of the NEPA-loaded and Cys-loaded nanofibers exposed to stressful conditions have been displayed in **Figure 23** and **Figure 24**, respectively. The results of FTIR analysis come along with morphological results as applying elevated temperature and humidity have no substantial effects on the essential functional groups of the fibrous samples during the period of study. In conclusion, this short-term stability test under stressful conditions suggests that a stable, solid nanofibrous formulation could be successfully obtained using preservative-free components.
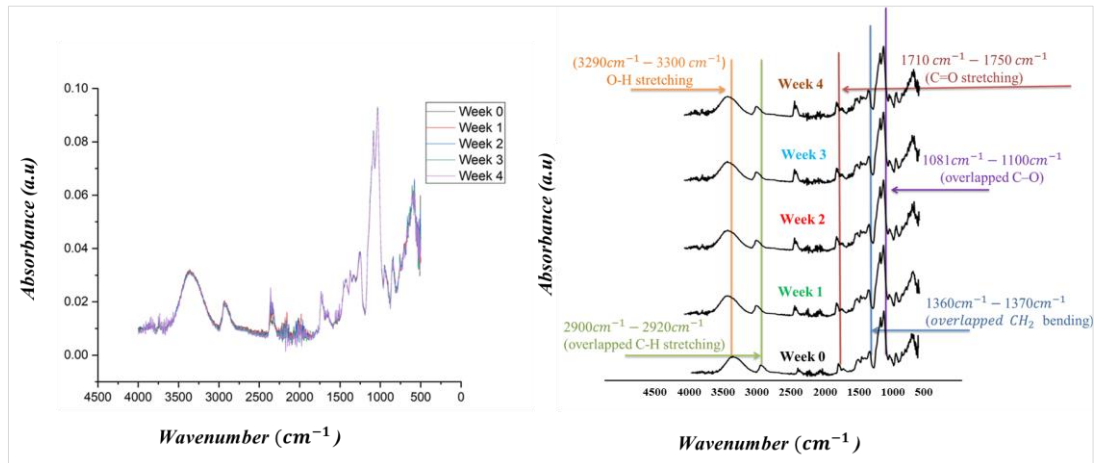
Figure 23. *Fourier transform infrared (FTIR) spectra of the Nepafenac-loaded (NEPA-loaded) fibers at 0, 1-, 2-, 3-, and 4-weeks storage under stress conditions (40 ± 2 °C, 75 ± 5% relative humidity (RH)). [III]*
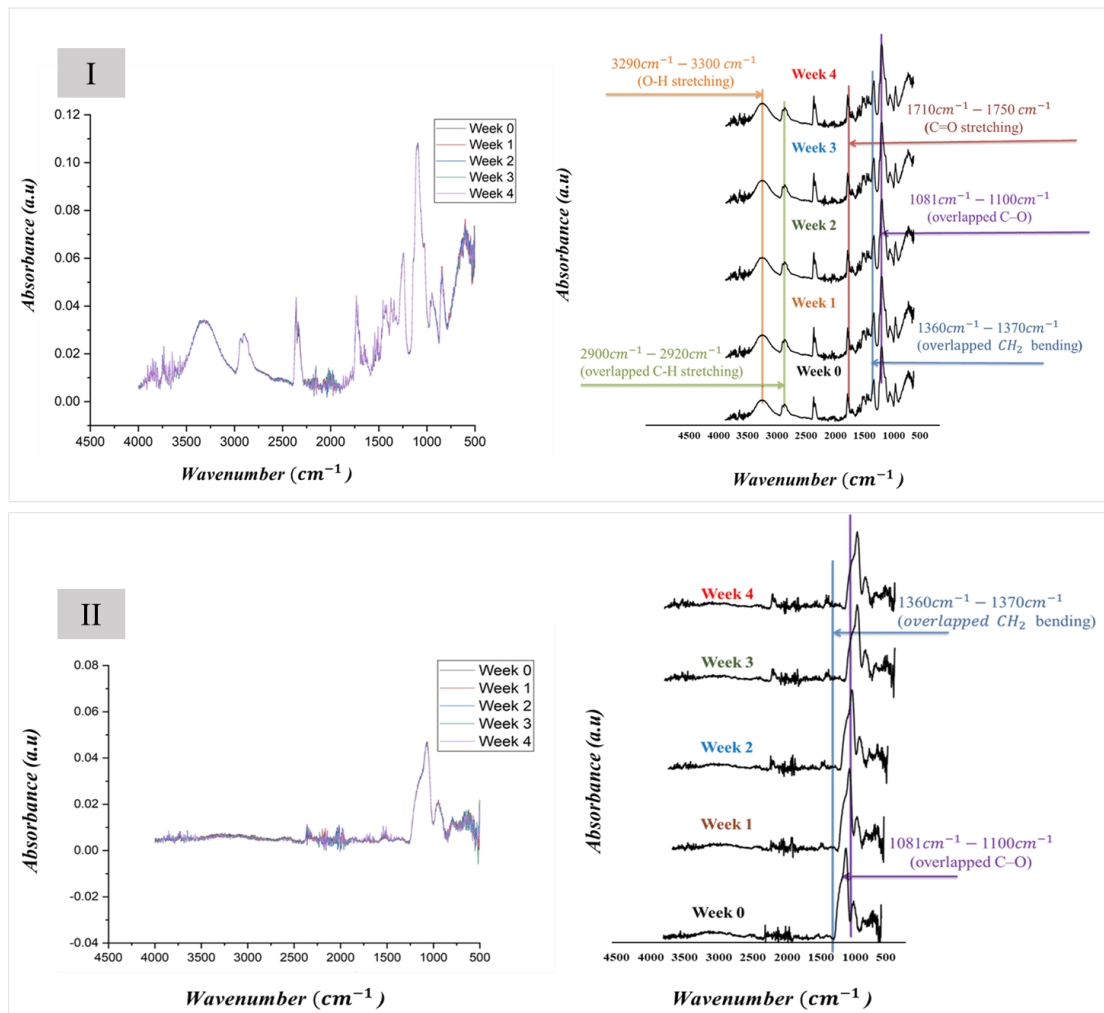
Figure 24. *Fourier transform infrared (FTIR) spectra of the cysteamine-loaded (Cys-loaded) fibers at 0, 1-, 2-, 3-, and 4-weeks storage under stress conditions (40 ± 2 °C, 75±5% relative humidity (RH)). (I): polyvinyl alcohol (PVA)/poloxamer 407 (PO-407) and (II) tetraetoxysilane (TEOS)/PVA polymeric blends. [IV]*

5. DISCUSSION

5.1. Results of literature analysis and systematic review

Scientists performed a lot of studies demonstrating eye diseases in an attempt to find an ideal ophthalmic formulation. This systematic review analyzed the possibility of utilizing nanotechnology-based formulations particularly the nanofibrous webs as a promising alternative to conventional way regarding site targeting and bioavailability improvement in targeting different eye diseases using different drug models. It has been demonstrated that nanocarriers have potential technological and therapeutic advantages for ophthalmic delivery. They are used to deliver the drug for local or systemic effect by localization in specific site of the eye and release the required drug concentration through diffusion or as a response to external stimuli (5,36).

In summary, the studies showed that numerous advantages encounter by nanofiber-based ophthalmic formulations. For instance, the surface of nanocarriers can be modified using different polymers for different purposes such as mucoadhesive, permeation enhancers, and release modulators, as a consequence, the bioavailability will be enhanced leading to the required patients' adherence to medications (11,37–40,90). The performed toxicity studies proofed their safety in animal models as well as *in vitro* alternative models. The pharmacokinetic studies showed sustained drug release through different models such as zero-order and Higuchi models. That means the possibility for single-dose administration even for up to 30 days (91).

Studies also demonstrate the possibility of encapsulation of different classes of drugs such as antimicrobial, nonsteroidal anti-inflammatory drugs, anti-glucoma, macromolecules, and different combinations. From a technical point of view, nanofibers can be used directly as films (92) or after further processing into suitable ocular inserts or other surface modifications (93). In addition it can be scaled up for large-scale production to meet the requirements and sustainability of pharmaceutical companies (94).

Combining the advantages of nanofibers together with the advantages of ocular inserts will result in a synergistic effect. In summary, the critical analysis of literature lies on two points: we were the first to shed light on mass production of nanofibers in drug delivery and pharmaceutical industries because only few studies highlight the

applications, parameter optimization, and characterization of electrospinning in this fields.

Considering these factors, our literature review clarifies the developed technologies for mass production, the challenges encountered, and light touches on products and devices that have been or are near to being released to the markets. The second systematic review is among the few published studies that describe nanofiber-based OIs as a promising, non-invasive method for targeting the posterior segment of the eye and improving drug's bioavailability.

5.2. Solution of nepafenac (NEPA)/hydroxypropyl-β-cyclodextrin (HP-β-CD) in water

The solubility of NEPA in water was successfully obtained by preparation of electrospun nanofiber of NEPA/HP-β-CD complex. There are many factors that act together and lead to fast dissolution of the NEPA; the electrospun nanofibers can be used to develop an amorphous system from a crystalline substance, which will have an impact on the drug's solubility. ASDs are well known for their effects on enhancing the solubility of poorly soluble water compounds. Electrospinning is one of the technologies used to produce ASDs.

The presence of PO-407 (a surfactant) in the system increases its solubility through surface-active properties. An interesting utilization of amphiphile compounds in enhancing the solubility of sparingly water-soluble compounds by the ability to form self-assemblies' aggregates. The addition of HP-β-CD to the system has a profound effect on the drug solubility by forming an inclusion complex. CDs have been widely used to enhance the aqueous solubility of poorly soluble compounds.

The morphological analysis of the developed nanofibers proved the formation of a nanoscale system, which means a large surface area and the possibility of rapid molecular diffusion and rapid dissolution. Nanofibers are nanocarriers with fiber diameters of a few nanometers to 1000 nm. They are considered good and promising candidates, providing fast drug release. In our work we focused on solubilizing and stabilizing the Biopharmaceutical Classification System (BCS class IV) drug by utilizing HP-β-CD.

5.3. Morphological evaluation

SEM images revealed random fiber deposition with all samples (PVA/PO-407, TEOS/PVA, NEPA-loaded, and Cys-loaded) regardless of the used excipient. Although some variations with the quality of the produced fibers have been noticed. In case of PVA/PO-407-based samples, addition of PS-80 in low concentration improved the spinnability and fibers morphology, while high concentration of it induced beads formation due to excessive liquification of the solution as a result of surface active effect. Moreover, the average fiber diameter was much lower than that of neat PVA and PVA/PO-407 blend. This can be explained by the additive effect of two non-ionic surfactants (PO-407 and PS-80).

Although there was a noticeable reduction in the average fiber diameters, the reduction was concentration-dependent. PS-80 concentration (1% (w/w)) reduced the average diameters to lower than 100 nm with low molecular weight PVA (Mw~67 kDa). Therefore, the addition of any kind of surfactants should be carefully controlled during the electrospinning process to avoid unnecessary negative effects on fiber formation. In case of TEOS/PVA samples, the fiber formation ability of the precursor solutions of different compositions and the morphology of the electrospun samples showed wide variability. For the same polymer ratio, increasing PVA concentration favored the formation of a fibrous structure, whereas increasing TEOS concentration, beady fibrous structures were observed. In the case of S5 and S9 solutions, due to interaction between PVA and TEOS gels were formed instead of highly viscous solutions. This resulted in increased resistance to the flow and failure of fiber's formation.

For the NEPA-loaded samples, it has been observed that increasing the HP-β-CD amount results in a better fiber's surface with more clear, smoother, and more uniform fibers. This enhancement in the fiber structure might be attributed to the unique physicochemical properties of HP-β-CD and its ability to form self-assembling aggregates that enhance the intermolecular interactions of the components of the electrospinning solution (95).

Comparing to PVA/PO-407 neat fibers, formulations containing Cys also showed good fibers morphology with non-remarkable defects. Addition of CysH to the PVA/PO-407 slightly lower the average fiber diameter and the effect was concentration dependent. It has also been observed that the presence of EDTA in the polymeric matrix improved

55

the appearance of fibers. This phenomenon could be attributed to the chelating effect of EDTA and thus the reduction of free salt concentration of the solution. The reduced conductivity due to the complex formation of EDTA and the free hydrochloride salts might inversely affect the morphology of the fibers.

In summary, these results indicate that not only polymer grades or concentrations should be considered during fibers preparation, but other electrospinning parameters should also be adjusted. These results confirm that electrospinning depends on multiple factors rather than individual parameters. Choosing the appropriate polymer concentration is critical regarding the quality of fibers, but it does not necessarily mean the formation of fibers of a normal distribution curve.

5.4. Interpretation of the diameter distribution from a mathematical point of view

Based on the morphological results, there is great diversity among different formulations of the neat PVA/PO-407 and drug-loaded formulations. Based on the calculated average fiber diameters, skewness, and kurtosis displayed in the results section, Samples prepared solely from PVA of different grades favor fiber formation, and the calculated skewness values reflect normal fiber distribution (Coefficients of skewness 22range from 0.090873 to 0.472034). For the samples prepared from PVA/PO-407, although adding PO-407 to the PVA improved the spinnability of the precursor solution, noticeable changes were observed in the fiber distributions of all PVA: PO-407 ratios. This effect can be explained by the fact that the addition of insufficient or too high surfactant concentration can result in noncontinuous or improper jet flow, reflected by compound distribution rather than homogenous normal fiber distribution (96,97).

Despite the diversity of fiber distribution, most formulations containing PO-407 have skewness values within an acceptable range from a mathematical point of view. The distribution curves are approximately symmetric (The absolute skewness values were between -0.5 and +0.5). The addition of PS-80 (0.5-1% w/w) to the PVA/PO-407 blend has further resulted in different fiber distributions. The presence of two surfactants in the formulation improved the spinnability of the solution. Nevertheless, the lower concentration of PS-80 (0.5% w/w) resulted in better morphology than the higher concentration (1% w/w). The increased surfactant concentration may increase the solution conductivity beyond the critical value, which will consequently interfere with

jet formation and fiber deposition (98). The absolute values of skewness indicate symmetric to moderately skewed distribution curves (The absolute skewness values were between -0.5 and +0.5).

In the case of NEPA-loaded samples, most formulations containing HP-β-CD have skewness values within an acceptable range, and the distribution curves are symmetric (the absolute skewness values lie between -0.5 and +0.5). This ununified behavior can be justified by the fact that electrospun nanofibers are not only evaluated by the SEM images but further analyses are to be conducted to evaluate and characterize normally distributed curves from compound distribution curves. This fiber's behavior proves that many factors overlap during electrospinning, including, for instance, the precursor solution composition and the process parameters.

The kurtosis values for the fiber distribution showed no very sharp peak or too flat curve (k values between +1 and -1). Some formulations showed a good fit ($R^2 \geq 0.95$) to the normal distribution, while the rest did not fit. These results are in accordance with skewness calculations (distribution curves are of symmetric and moderately skewness types). The calculated kurtosis values, on the other hand, confirmed the diversity among different formulations; the majority of the formulations showed kurtosis values (k values between +1 and −1), which means the majority of these curves are not too sharp or too flat, with few exceptions. Some formulations showed good fitting ($R^2 \geq 0.95$) to the Gaussian (normal) distribution, while the rest did not fit (99).

These mathematical results confirmed that electrospinning is a multifactorial process, and to obtain a good fibrous sample, all parameters must be considered. In addition, the morphological characterization of electrospun samples is not only about fiber diameter; instead, further analysis is needed to differentiate between normal and compound distribution curves (96,100).

The particle size distributions have different impacts on the drug release, and some drug delivery systems are intentionally fabricated in the form of multiunit particulate systems to modulate and tailor the drug release from immediate to controlled or modified release pattern. Therefore, from a pharmaceutical point of view, the fibers' distributions might also have a great impact on the release rate and pattern from electrospun nanofibers prepared for different pharmaceutical applications. A related work has been published demonstrating the effect of different size distributions on the release of the drug: A study

demonstrated the impact of size distribution on the diffusional drug release from numerous particle geometrics (spheres, fibers, and membranes). The results revealed that the size distribution affected the release profiles of spherical particles, followed by fibers, and had no effect on the release from the membrane (101). This study confirms the concept of considering fiber distribution in the formulation of nanofibers for pharmaceutical applications, particularly when the release is substantially important.

5.5. Solid-state characterization of the electrospun samples

The FTIR spectra of the prepared fibrous samples indicated the compatibility between the individual components of the formulations as well as the cross-linking between the fiber polymers (PVA/PO-407, PVA/PO-407/ HP-β-CD, and TEOS/PVA). The appearance of the major peaks of the components confirmed the absence of unwanted new functional groups, which confirmed physical interaction and compatibility. The FTIR spectra suggested the formation of amorphous solid dispersion in all formulations (PVA/PO-407, TEOS/PVA polymeric blends, and NEPA/ PVA/PO-407/ HP-β-CD).

The presence of sharp peaks in the XRD pattern confirmed the crystallinity of the NEPA in its pure state (Figure 13.). The intensities of the peaks decreased upon mixing the NEPA with HP-β-CD, PVA, or PO-407. The complete disappearance of these peaks from the nanofibers (F3, F6, and F9) confirms the formation of amorphous solid dispersion from crystalline NEPA through electrospinning of NEPA, HP-β-CD, PVA, and PO-407.

5.6. *In vitro* UV-VIS spectroscopic studies (drug content, drug release and release kinetics)

The results of the drug content of NEPA-loaded and Cys-loaded reflects the complete dissolution of the NEPA through complexation with HP-β-CD during the solution preparation as well as homogenous precipitation of the drug/polymer blend as nanofibers after solvent evaporation and total incorporation of the drug (NEPA and CysH) into the fibers. *In vitro* dissolution profiles of the NEPA-loaded and Cys-loaded nanofibers showed complete and fast release of NEPA. The fast release of the drug from nanofibers can be explained by the formation of amorphous solid dispersion, complete and fast wetting of the matrix, and high surface area to volume ratio of nanofibers.

Moreover, PO-407 act as surface-active agent, resulting in faster disintegration and dissolution of the formulations. It has been noticed that all formulations release the drug with no differences among them. Since each drug-loaded fiber formulation is within the nanometer scale, it is straightforward that there is no great difference in the surface and the consequent release among the different formulations. Based on the Weibull distribution, all formulations from the different bases were successfully fitted (R^2>0.9) which indicate linear regression. The release curves follow first-order (β values for all formulation were<1 kinetics).

5.7. Permeability studies

Based on *in vitro* PAMPA permeability assay results (**Figure 16**.), the results showed no significant difference between the 3 formulations (F3, F6 and F9) regardless of the HP-β-CD content per formulation. This can be explained by the fact that in the case of the PAMPA system where only passive diffusion occurs through the artificially fabricated lipid membrane, a reverse sink is created as the donor compartment contains HP-β-CD in high amount. Therefore, for further *ex vivo* studies, F3 is a good choice as it contains the least amount of HP-β-CD and shows similar average permeability values independently the applied models. The lower amount of HP-β-CD can be physiologically favorable for the penetration process (102).

Regarding *ex vivo* experiment, the concentration of the NEPA in F3 in precorneal area was significantly higher than Nevanac®, and this can be attributed to the complete dissolution of the NEPA-loaded nanofibers. The highest dissolution was attained at 60 min, which means the F3 had sufficient time to release more NEPA from the formulation. Regarding the cornea and aqueous humor, the NEPA concentration were less than Nevanac®. Nevertheless, it is only a numerical difference without statistical significance. It can be concluded that bioequivalent drug concentrations might be obtained if the study is conducted *in vivo*. From the Raman mapping, it can be concluded that in both formulations (F3 and Nevanac®), the NEPA distribution at 15 min was restricted to outer layers of the cornea, but it distributed to the inner most layer (stroma) at 30 and 60 min with more homogenous feature. In conclusion, there results support our finding that F3 could be bioequivalent to Nevanac® *in vivo*.

5.8. Cytocompatibility Study

All applied samples, including plain fibers and drug loaded samples have not resulted in any noticeable irritation on the CAM surface when compared to the positive control (0.1 N NaOH). The results suggest the cytocompatibility of the formulation components. These results confirm that the ingredients of the formulation are well tolerated. The reasons behind choosing this test are because of its simplicity, the increasing research in ocular formulations dictates less animal-intensive experimental methods; therefore, a method that mimics the *in vivo* Draize test should be used to minimize the animal suffering. Moreover, it is simpler with valid screening results particularly when testing a toxic compound. So that our studies confirmed the possibility of using a simple *in vitro* test and following the world regarding 3R's concept (Reduction, refinement, and replacement).

5.9. Stability investigation (accelerated stability study)

The SEM images and FTIR spectra of the freshly prepared samples and samples stored under stressful conditions reveal that samples retained their morphological features despite exposure to elevated levels of temperature, humidity, and pressure. For the NEPA-loaded fibers this can be attributed to the complexation and stabilizing effect of HP-β-CD. Stability under these stressful conditions could be taken to indicate the long-term stability under ambient conditions. These results suggest that it can be possible to formulate preservative-free, stable solid Cys-containing products that can be used to overcome the stability problem of liquid formulations. Therefore, it can be possible to formulate preservative-free, stable solid Cys- and NEPA loaded products that can be used to overcome the stability problem of liquid formulations. We focused to understand how to increase the long-term stability based on the applied stressful conditions and this can help in the possibility of shifting from liquid to solid formulations.

6. CONCLUSIONS

Targeting eye diseases, particularly the posterior part, is challenging due to the eye's unique anatomy and physiology. Unfortunately, eye diseases are increasing daily, and the untreated cases can lead to visual impairment or can develop into blindness. Conventional eye drops have limited bioavailability (approximately 5%) and systemic administration results in various toxicity problems. The most successful way used for posterior targeting is intravitreal routes which might be accompanied by severe complications such as retinal hemorrhage and detachment. Because of these challenges, there is a clear demand for smart drug delivery systems that are capable of delivering the drug to the targeted site of action while being safe, effective and comfortable.

Consequently, this project aimed to develop and formulate electrospun nanofiber-based OIs using Cys and NEPA as model drugs to find a stable, solid preservative-free formulation that can be used as potential alternatives to conventional eye drops in order to overcome premature drainage while maintaining the safety, comforts and patients' acceptability. The novelty of the work is based on added-value NEPA-loaded and Cys-loaded nanofibrous OIs were formulated to avoid the disadvantageous properties of conventional eyedrops by improving the ocular bioavailability and stability of both drugs.

The study was started by conducting a comprehensive literature review, and it has been concluded that the electrospinning process can be transferred from lab to production scale in pharmaceutical industries, which can be considered as techno-economic feasibility study. Extended literature searching in the form of a systematic review showed the feasibility of the electrospinning technique in the fabrication of OIs. Many promising results have been published, which revealed that by changing the polymeric composition of the precursor solution, there is a possibility of improving the solubility and stability as well as tailoring the release from few minutes up to month. As a result, the concept of nanotechnology was employed to develop patient-centric formulation.

In the second part of the project, the polymeric composition and the electrospinning parameters suitable for preparation of fibrous samples were selected. In this step, two neat polymeric systems were examined; the first consisted of studying the effect of PO-407 and PS-80 in the morphological and physicochemical characters of PVA of different grades and concentrations (Low, intermediate, and high molecular

weight) and the second was a modification of PVA solubility by addition of TEOS. Smooth nanofibrous mats comprising PVA/PO-407 blends have been successfully developed with an average fiber diameter of a hundred to a few hundred nanometers using 15 – 20% w/w of low molecular weight PVA, 13 – 15% w/w of intermediate molecular weight and 5 – 10% w/w of high molecular weight PVA. PO-407 appeared to have slight effects on the morphology of nanofibers, although it slightly decreased the nanofibers' diameters. There were no remarkable differences between the mean diameters.

Various diameter distribution curves were obtained, ranging from normal to moderately skewed (skewness values of -0.5 to +0.5). The spinnability was enhanced by adding nonionic surfactants (PS-80) without any observed negative effects. Based on the literature, PO-407 is widely used as a thermoreversible system. The FTIR spectra showed that all the major peaks of both polymers were intact, and no characteristic changes were observed in major peaks, indicating compatibility and no interactions between the selected polymers. The developed nanofibrous web can be a promising candidate for different pharmaceutical applications such as ophthalmic, topical, mucoadhesive, and thermoreversible systems.

Considering the TEOS/PVA system, the PVA concentration's effect on the fibers' morphology was investigated on three levels (10, 12, and 14 % (w/w)). Four TEOS/PVA mass ratios (1:4, 2:3, 3:2, and 4:1 m:m) were examined for each concentration. For the same polymer ratio, increasing PVA concentration favored the formation of a fibrous structure, whereas increasing TEOS concentration, beady fibrous structures were observed. The fiber diameter increased with increasing PVA concentration at the same TEOS: PVA ratio. There is no monotonic trend with increasing TEOS ratio for the same polymer concentration.

The third phase in the project was focused on the formulation of nanofibrous webs based on the selected polymers with different APIs; the first part was NEPA 0.1% (w/w) using HP-β-CD as solubilizer, stabilizer, and permeation enhancer. The second part consists of the formulation of CysH 0.55% (w/w) and 1.1% (w/w) utilizing two different polymeric matrixes (PVA/PO-407 and TEOS/PVA). All different formulations were prepared by electrospinning and investigated for morphology, physicochemical properties, drug release, cytocompatibility, and *in vitro* and *ex vivo* permeability.

The SEM images showed fibrous samples. FTIR spectroscopy and X-ray diffraction confirmed the polymer cross-linking and the formation of amorphous solid dispersion.

All formulations showed complete and fast release of Cys and NEPA ($\leq$15 min and $\leq$60 min respectively), and the release followed first-order kinetics (β values for all formulations were < 1). In case of NEPA, the formulations (F3, F6, and F9 which differ in the HP-β-CD amount) showed considerable *in vitro* and *ex vivo* permeability. The Raman studies revealed comparable corneal distributions of F3 and the commercial Nevanac® suspension at 60 min (p value = 0.6433).

The fibrous composition of NEPA-loaded and Cys-loaded samples remains stable under stress conditions (40 $\pm$2°C, 75$\pm$5% RH) in term of morphology and physicochemical characters. The formulation composition showed good cytocompatibility with hen eggs tested on the CAM of chick embryos.

In light of these results presented based on different polymer combinations and different model drugs; it can be concluded that the electrospun nanofiber webs could be promising carriers for various APIs for ophthalmic delivery.

7. SUMMARY

Despite the emergent development in pharmaceutical technologies, ocular drug delivery remains challenging due to the complex eye structure that interferes with drug permeation and leads to poor bioavailability. For successful disease targeting, especially posterior segment, invasive intravitreal injections are the most successful. Nevertheless, the method might lead to severe complications such as eye bleeding, retinal detachment, and endophthalmitis.

Therefore, we developed and formulated electrospun nanofiber-based OIs using different model drugs as an attempt to formulate a drug delivery system that is as efficient as an invasive way of treating different diseases in different eye sites while maintaining the relative safety and convenience of conventional eye drops with the overall goal of increasing patients' acceptability and reducing diseases burden.

Different studies were carried out to develop and formulate NEPA and Cys-loaded electrospun nanofibers as potential candidates for OIs using different ratios of PVA/PO-407/HP-β-CD and either PVA/PO-407 or TEOS/PVA polymeric blends, respectively.

The results revealed the formation of stable, nanofibrous, and ASDs that resulted in fast drug release regardless of the polymeric base type while maintaining compatibility between the components. For all polymeric blends, the results revealed randomly oriented fibers with diameter distribution on a nanometer scale. The PAMPA permeability assay and *ex vivo* study results showed remarkable drug permeation, as confirmed by the Raman mapping within corneal tissues.

The developed cytocompatible nanofibrous webs can be considered promising candidates as OIs, which can be used as an alternative to conventional systems for NEPA and Cys ocular delivery or any drugs with similar physicochemical properties with reasonable corneal permeation and better stability.

The developed cytocompatible NEPA and Cys-loaded nanofibers-based OIs could be a promising alternative to conventional systems with reasonable corneal permeation and better stability.

8. REFERENCES

1. Mehta P, Al-Kinani AA, Arshad MS, Chang MW, Alany RG, Ahmad Z. Development and characterisation of electrospun timolol maleate-loaded polymeric contact lens coatings containing various permeation enhancers. Int J Pharm. 2017;532(1):408–420. Doi: 10.1016/j.ijpharm.2017.09.029

2. Tsai CH, Wang PY, Lin IC, Huang H, Liu GS, Tseng CL. Ocular drug delivery: Role of degradable polymeric nanocarriers for ophthalmic application. Int J Mol Sci. 2018;19(9):2830. Doi: 10.3390/ijms19092830

3. Maharjan P, Cho KH, Maharjan A, Shin MC, Moon C, Min KA. Pharmaceutical challenges and perspectives in developing ophthalmic drug formulations. J Pharm Investig. 2019;49(2):215–228. Doi: 10.1007/s40005-018-0404-6

4. Lynch CR, Kondiah PPD, Choonara YE, du Toit LC, Ally N, Pillay V. Hydrogel Biomaterials for Application in Ocular Drug Delivery. Front Bioeng Biotechnol. 2020;8:1–18. Doi: 10.3389/fbioe.2020.00228

5. Barar J, Aghanejad A, Fathi M, Omidi Y. Advanced drug delivery and targeting technologies for the ocular diseases. BioImpacts. 2016;6(1):49–67. Doi: 10.15171/bi.2016.07

6. Mudgil M, Pawar PK. Preparation and in Vitro/Ex Vivo evaluation of moxifloxacin-loaded PLGA nanosuspensions for ophthalmic application. Sci Pharm. 2013;81(2):591–606. Doi: 10.3797/scipharm.1204-16

7. Kim YC, Chiang B, Wu X, Prausnitz MR. Ocular delivery of macromolecules. J Control Release. 2014;190:172–181. Doi: 10.1016/j.jconrel.2014.06.043

8. Shen J, Lu GW, Hughes P. Targeted Ocular Drug Delivery with Pharmacokinetic/Pharmacodynamic Considerations. Pharm Res. 2018;35(11):217. Doi: 10.1007/s11095-018-2498-y

9. Tundisi LL, Mostaço GB, Carricondo PC, Petri DFS. Hydroxypropyl methylcellulose: Physicochemical properties and ocular drug delivery formulations. Eur J Pharm Sci. 2021;159(2020):105736. Doi: 10.1016/j.ejps.2021.105736

10. Asim MH, Ijaz M, Mahmood A, Knoll P, Jalil A, Arshad S, Bernkop-Schnürch A. Thiolated cyclodextrins: Mucoadhesive and permeation enhancing excipients for ocular drug delivery. Int J Pharm. 2021;599:120451. Doi:

10.1016/j.ijpharm.2021.120451

11. Chen H, Jin Y, Sun L, Li X, Nan K, Liu H, Zheng Q, Wang B. Recent Developments in Ophthalmic Drug Delivery Systems for Therapy of Both Anterior and Posterior Segment Diseases. Colloids Interface Sci Commun. 2018;24:54–61. Doi: 10.1016/j.colcom.2018.03.008

12. Mehta P, Al-Kinani AA, Arshad MS, Chang MW, Alany RG, Ahmad Z. Development and characterisation of electrospun timolol maleate-loaded polymeric contact lens coatings containing various permeation enhancers. Int J Pharm. 2017;532(1):408–420. Doi: 10.1016/j.ijpharm.2017.09.029

13. Gedar Totuk ÖM, Kabadayi K, Ekizoğlu N, Arici T. Prevalence of childhood eye diseases. Turkiye Klin Pediatr. 2018;27(3):111–117. Doi: 10.5336/pediatr.2018-62285

14. Assi L, Chamseddine F, Ibrahim P, Sabbagh H, Rosman L, Congdon N, Evans J, Ramke J, Kuper H, Burton MJ, Ehrlich JR, Swenor BK. A global assessment of eye health and quality of life a systematic review of systematic reviews. JAMA Ophthalmol. 2021;139(5):526–541. Doi: 10.1001/jamaophthalmol.2021.0146

15. Trott M, Smith L, Veronese N, Pizzol D, Barnett Y, Gorely T, Pardhan S. Eye disease and mortality, cognition, disease, and modifiable risk factors: an umbrella review of meta-analyses of observational studies. Eye. 2022;36(2):369–378. Doi: 10.1038/s41433-021-01684-x

16. Kamińska A, Pinkas J, Wrześniewska-Wal I, Ostrowski J, Jankowski M. Awareness of Common Eye Diseases and Their Risk Factors—A Nationwide Cross-Sectional Survey among Adults in Poland. Int J Environ Res Public Health. 2023;20(4):3594. Doi: 10.3390/ijerph20043594

17. Biswas A, Choudhury AD, Bisen AC, Agrawal S, Sanap SN, Verma SK, Mishra A, Kumar S, Bhatta RS. Trends in Formulation Approaches for Sustained Drug Delivery to the Posterior Segment of the Eye. AAPS PharmSciTech. 2023;24(8):217. Doi: 10.1208/s12249-023-02673-x

18. Thakur R, Swami G, Rahman M. Development and Optimization of Controlled Release Bioerodable Anti Infective Ophthalmic Insert. Curr Drug Deliv. 2014;11(1):2–10. Doi: 10.2174/15672018113106660060

19. Park CG, Kim YK, Kim SN, Lee SH, Huh BK, Park MA, Won H, Park KH, Choy YB. Enhanced ocular efficacy of topically-delivered dorzolamide with nanostructured mucoadhesive microparticles. Int J Pharm. 2017;522(1–2):66–73. Doi: 10.1016/j.ijpharm.2017.02.035

20. Rahić O, Tucak A, Omerović N, Sirbubalo M, Hindija L, Hadžiabdić J, Vranić E. Novel drug delivery systems fighting glaucoma: Formulation obstacles and solutions. Pharmaceutics. 2021;13(1):28. Doi: 10.3390/pharmaceutics13010028

21. Khames A, Khaleel MA, El-Badawy MF, El-Nezhawy AOH. Natamycin solid lipid nanoparticles - sustained ocular delivery system of higher corneal penetration against deep fungal keratitis: Preparation and optimization. Int J Nanomedicine. 2019;14:2515–2531. Doi: 10.2147/IJN.S190502

22. Omerovi N, Vrani E. Application of nanoparticles in ocular drug delivery systems. Heal Technol. 2020;10:61–78. Doi: 10.1007/s12553-019-00381-w

23. Chetoni P, Burgalassi S, Monti D, Tampucci S, Tullio V, Cuffini AM, Muntoni E, Spagnolo R, Zara GP, Cavalli R. Solid lipid nanoparticles as promising tool for intraocular tobramycin delivery: Pharmacokinetic studies on rabbits. Eur J Pharm Biopharm. 2016;109:214–223. Doi: 10.1016/j.ejpb.2016.10.006

24. Agarwal P, Craig JP, Rupenthal ID. Formulation considerations for the management of dry eye disease. Pharmaceutics. 2021;13(2):207. Doi: 10.3390/pharmaceutics13020207

25. Souto EB, Dias-Ferreira J, López-Machado A, Ettcheto M, Cano A, Camins Espuny A, Espina M, Garcia ML, Sánchez-López E. Advanced formulation approaches for ocular drug delivery: State-of-the-art and recent patents. Pharmaceutics. 2019;11(9):460. Doi: 10.3390/pharmaceutics11090460

26. Del Amo EM, Urtti A. Current and future ophthalmic drug delivery systems. A shift to the posterior segment. Drug Discov Today. 2008;13(3–4):135–143. Doi: 10.1016/j.drudis.2007.11.002

27. Reimondez-Troitiño S, Csaba N, Alonso MJ, De La Fuente M. Nanotherapies for the treatment of ocular diseases. Eur J Pharm Biopharm. 2015;95:279–293. Doi:10.1016/j.ejpb.2015.02.019

28. Ahmed S, Amin MM, Sayed S. Ocular Drug Delivery: a Comprehensive Review. AAPS PharmSciTech. 2023;24(2):66. Doi: 10.1208/s12249-023-02516-9

29. Ibrahim MM, Maria DN, Di Wang X, Simpson RN, Hollingsworth TJ, Jablonski MM. Enhanced corneal penetration of a poorly permeable drug using bioadhesive multiple microemulsion technology. Pharmaceutics. 2020;12(8):704. Doi: 10.3390/pharmaceutics12080704

30. Patel A, Cholkar K, Agrahari V, Mitra AK. Ocular drug delivery systems: An overview. World J Pharmacol. 2013;2(2):47-64. Doi: 10.5497/wjp.v2.i2.47

31. Jervis LP. A Summary of Recent Advances in Ocular Inserts and Implants. J Bioequiv Availab. 2016;09(01):320–323. Doi: 10.4172/jbb.1000318

32. Gorantla S, Rapalli VK, Waghule T, Singh PP, Dubey SK, Saha RN, Singhvi G. Nanocarriers for ocular drug delivery: Current status and translational opportunity. RSC Adv. 2020;10(46):27835–27855. Doi: 10.1039/d0ra04971a

33. Xie J, Wang C, Ning Q, Gao Q, Gao C, Gou Z, Ye J. A new strategy to sustained release of ocular drugs by one-step drug-loaded microcapsule manufacturing in hydrogel punctal plugs. Graefe's Arch Clin Exp Ophthalmol. 2017;255(11):2173–2184. Doi: 10.1007/s00417-017-3755-1

34. Rozi MF, Mohmad Sabere AS. Review on Conventional and Novel Topical Ocular Drug Delivery System. J Pharm. 2021;1(1):19–26. Doi: 10.31436/jop.v1i1.32

35. Taghe S, Mirzaeei S. Preparation and Characterization of Novel, Mucoadhesive Ofloxacin Nanoparticles for Ocular Drug Delivery. Brazilian J Pharm Sci. 2019;55:1–12. Doi: 10.1590/s2175-97902019000117105

36. Fang G, Yang X, Wang Q, Zhang A, Tang B. Hydrogels-based ophthalmic drug delivery systems for treatment of ocular diseases. Mater Sci Eng C. 2021;127(April):112212. Doi: 10.1016/j.msec.2021.112212

37. B, Choudhary M, Kumar S, Bhatia M, Budhwar V. Formulation and in-Vitro Evaluation of Sustained Release Tropicamide Loaded Chitosan Nanoparticles for Ocular Drug Delivery. Int Res J Pharm. 2016;7(10):27–35. Doi: 10.7897/2230-8407.0710118

38. Bachu RD, Chowdhury P, Al-Saedi ZHF, Karla PK, Boddu SHS. Ocular drug delivery barriers—role of nanocarriers in the treatment of anterior segment ocular diseases. Pharmaceutics. 2018;10(1):28. Doi: 10.3390/pharmaceutics10010028

39. El Hoffy NM, Abdel Azim EA, Hathout RM, Fouly MA, Elkheshen SA.

Glaucoma: Management and Future Perspectives for Nanotechnology-Based Treatment Modalities. Eur J Pharm Sci. 2021;158:105648. Doi: 10.1016/j.ejps.2020.105648

40. Mahaling B, Katti DS. Physicochemical properties of core-shell type nanoparticles govern their spatiotemporal biodistribution in the eye. Nanomedicine. 2016;12(7):2149–2160. Doi: 10.1016/j.nano.2016.05.017

41. Da Silva GR, Lima TH, Oréfice RL, Fernandes-Cunha GM, Silva-Cunha A, Zhao M, Behar-Cohen F. In vitro and in vivo ocular biocompatibility of electrospun poly(ε-caprolactone) nanofibers. Eur J Pharm Sci. 2015;73:9–19. Doi: 10.1016/j.ejps.2015.03.003

42. Kaul S, Kumar G, Kothiyal P. An insight into ocular insert. Int J Pharm Sci Res. 2012;3(07):1905–1912.

43. Shadambikar G, Marathe S, Patil A, Joshi R, Bandari S, Majumdar S, Repka M. Novel Application of Hot Melt Extrusion Technology for Preparation and Evaluation of Valacyclovir Hydrochloride Ocular Inserts. AAPS PharmSciTech. 2021;22(1):48. Doi: 10.1208/s12249-020-01916-5

44. Tyson SL, Bafna S, Gira JP, Goldberg DF, Jones JJ, Jones MP, Kim JK, Martel JM, Nordlund ML, Piovanetti-Perez IK, Singh IP, Metzinger JL, Mulani D, Sane S, Talamo JH, Goldstein MH. Multicenter randomized phase 3 study of a sustained-release intracanalicular dexamethasone insert for treatment of ocular inflammation and pain after cataract surgery. J Cataract Refract Surg. 2019;45(2):204–212. Doi: 10.1016/j.jcrs.2018.09.023

45. Shi H, Wang Y, Bao Z, Lin D, Liu H, Yu A, Lei L, Li X, Xu X. Thermosensitive glycol chitosan-based hydrogel as a topical ocular drug delivery system for enhanced ocular bioavailability. Int J Pharm. 2019;570:118688. Doi: 10.1016/j.ijpharm.2019.118688

46. Bertens CJF, Gijs M, van den Biggelaar FJHM, Nuijts RMMA. Topical drug delivery devices: A review. Exp Eye Res. 2018;168:149-160. Doi: 10.1016/j.exer.2018.01.010

47. Land DL, Benjamin WJ. Review Sizes and Shapes of Conjunctival Inserts. International Contact Lens Clinic. 1994;21(11-12):212-217. Doi: 10.1016/0892-8967(94)90053-1

48. Dabral K, Uniyal Y. Ocular inserts: Novel approach for drug delivery into eyes. GSC Biol Pharm Sci. 2019;7(3):1–7. Doi: 10.30574/gscbps.2019.7.3.0087

49. Singla J, Bajaj T, Goyal AK, Rath G. Development of Nanofibrous Ocular Insert for Retinal Delivery of Fluocinolone Acetonide. Curr Eye Res. 2019;44(5):541–550. Doi: 10.1080/02713683.2018.1563196

50. Arthanari S, Mani G, Jang JH, Choi JO, Cho YH, Lee JH, Cha SE, Oh HS, Kwon DH, Jang HT. Preparation and characterization of gatifloxacin-loaded alginate/poly (vinyl alcohol) electrospun nanofibers. Artif Cells, Nanomedicine Biotechnol. 2016;44(3):847–852. Doi: 10.3109/21691401.2014.986676

51. Dadashi S, Boddohi S, Soleimani N. Preparation, characterization, and antibacterial effect of doxycycline loaded kefiran nanofibers. J Drug Deliv Sci Technol. 2019;52:979–985. Doi: 10.1016/j.jddst.2019.06.012

52. Di Prima G, Licciardi M, Carfì Pavia F, Lo Monte AI, Cavallaro G, Giammona G. Microfibrillar polymeric ocular inserts for triamcinolone acetonide delivery. Int J Pharm. 2019;567:118459. Doi: 10.1016/j.ijpharm.2019.118459

53. Chou SF, Luo LJ, Lai JY, Ma DHK. Role of solvent-mediated carbodiimide cross-linking in fabrication of electrospun gelatin nanofibrous membranes as ophthalmic biomaterials. Mater Sci Eng C. 2017;71:1145–1155. Doi: 10.1016/j.msec.2016.11.105

54. Tawfik EA, Craig DQM, Barker SA. Dual drug-loaded coaxial nanofibers for the treatment of corneal abrasion. Int J Pharm. 2020;581:119296. Doi: 10.1016/j.ijpharm.2020.119296

55. Polat HK, Bozdağ Pehlivan S, Özkul C, Çalamak S, Öztürk N, Aytekin E, Fırat A, Ulubayram K, Kocabeyoğlu S, İrkeç M, Çalış S. Development of besifloxacin HCl loaded nanofibrous ocular inserts for the treatment of bacterial keratitis: In vitro, ex vivo and in vivo evaluation. Int J Pharm. 2020;585:119552. Doi: 10.1016/j.ijpharm.2020.119552

56. Göttel B, De Souza e Silva JM, Santos de Oliveira C, Syrowatka F, Fiorentzis M, Viestenz A, Mäder K. Electrospun nanofibers – A promising solid in-situ gelling alternative for ocular drug delivery. Eur J Pharm Biopharm. 2020;146:125–132. Doi: 10.1016/j.ejpb.2019.11.012

57. Baskakova A, Awwad S, Jiménez JQ, Gill H, Novikov O, Khaw PT, Brocchini S,

Zhilyakova E, Williams GR. Electrospun formulations of acyclovir, ciprofloxacin and cyanocobalamin for ocular drug delivery. Int J Pharm. 2016;502(1–2):208–218. Doi: 10.1016/j.ijpharm.2016.02.015

58. Khalil IA, Ali IH, El-sherbiny IM. Noninvasive biodegradable nanoparticles-in-nanofibers single-dose ocular insert: in vitro, ex vivo and in vivo evaluation. Nanomedicine (Lond). 2018;14:33–55. Doi: 10.2217/nnm-2018-0297

59. Morais M, Coimbra P, Pina ME. Comparative analysis of morphological and release profiles in ocular implants of acetazolamide prepared by electrospinning. Pharmaceutics. 2021;13(2):260. Doi: 10.3390/pharmaceutics13020260

60. Yavuz B, Bozdağ Pehlivan S, Kaffashi A, Çalamak S, Ulubayram K, Palaska E, Çakmak HB, Ünlü N. In vivo tissue distribution and efficacy studies for cyclosporin A loaded nano-decorated subconjunctival implants. Drug Deliv. 2016;23(9):3279–3284. Doi: 10.3109/10717544.2016.1172368

61. Imperiale JC, Acosta GB, Sosnik A. Polymer-based carriers for ophthalmic drug delivery. J Control Release. 2018;285:106–141. Doi: 10.1016/j.jconrel.2018.06.031

62. Mirzaeei S, Berenjian K, Khazaei R. Preparation of the potential ocular inserts by electrospinning method to achieve the prolong release profile of triamcinolone acetonide. Adv Pharm Bull. 2018;8(1):21–27. Doi: 10.15171/apb.2018.003

63. Almeida H, Amaral MH, Lobão P, Lobo JMS. In situ gelling systems: A strategy to improve the bioavailability of ophthalmic pharmaceutical formulations. Drug Discov Today. 2014;19(4):400–412. Doi: 10.1016/j.drudis.2013.10.001

64. Singla J, Bajaj T, Goyal AK, Rath G. Development of Nanofibrous Ocular Insert for Retinal Delivery of Fluocinolone Acetonide. Curr Eye Res. 2019;44(5):541–550. Doi: 10.1080/02713683.2018.1563196

65. Shah SNH, Nawaz A, Javed H, Rafiq M, Riaz R, Sadaquat H, Akhtar M. Preparation and In Vitro/In Vivo Evaluation of Antihistaminic Ocular Inserts. Pharm Chem J. 2018;52(7):615–622. Doi: 10.1007/s11094-018-1870-x

66. Agarwal P, Scherer D, Günther B, Rupenthal ID. Semifluorinated alkane based systems for enhanced corneal penetration of poorly soluble drugs. Int J Pharm. 2018;538(1–2):119–129. Doi: 10.1016/j.ijpharm.2018.01.019

67. O'Malley B. European Pharmacopoeia (Tenth Edition). Vol. I, British Medical

Journal. 1971:4730 .

68. Lorenzo-Veiga B, Sigurdsson HH, Loftsson T. Nepafenac-loaded cyclodextrin/polymer nanoaggregates: A new approach to eye drop formulation. Materials (Basel). 2019;12(2):229. Doi: 10.3390/ma12020229

69. Rajput S, Shrimali C, Baghel M. Development and validation of UV and RP-HPLC method for estimation of Nepafenac in bulk drug and opthalmic formulation. J Adv Pharm Educ Res. 2015;5(1):15–19.

70. Wagh D, Shahi SR, Dabir PD, Deore W. Spectrophotometric Method for the Determination of Nepafenac in Opthalmic Formulation. World J Pharm Res. 2017;6(6):623–630. Doi: 10.20959/wjpr20176-8410

71. Kazsoki A, Palcsó B, Alpár A, Snoeck R, Andrei G, Zelk R. Formulation of acyclovir (core)-dexpanthenol (sheath) nanofibrous patches for the treatment of herpes labialis. Int J Pharm. 2021;611. Doi: 10.1016/j.ijpharm.2021.121354

72. Pourtalebi Jahromi L, Ghazali M, Ashrafi H, Azadi A. A comparison of models for the analysis of the kinetics of drug release from PLGA-based nanoparticles. Heliyon. 2020;6(2). Doi: 10.1016/j.heliyon.2020.e03451

73. Kazsoki A, Palcsó B, Omer SM, Kovacs Z, Zelk R. Formulation of Levocetirizine-Loaded Core – Shell Type Nanofibrous Orally Dissolving Webs as a Potential Alternative for Immediate Release Dosage Forms. Pharmaceutics. 2022; 14(7):1442. Doi: 10.3390/pharmaceutics14071442

74. Dargó G, Vincze A, Müller J, Kiss HJ, Nagy ZZ. Corneal-PAMPA : A novel , non-cell-based assay for prediction of corneal drug permeability. Eur J Pharm Sci. 2019;128:232–239. Doi: 10.1016/j.ejps.2018.12.012

75. Vincze A, Facskó R, Budai-Szűcs M, Katona G, Gyarmati B, Csorba A, Zelkó R, Nagy ZZ, Szente L, Balogh GT. Cyclodextrin-enabled nepafenac eye drops with improved absorption open a new therapeutic window. Carbohydr Polym. 2023;310:120717. Doi: 10.1016/j.carbpol.2023.120717

76. Luepke NP. Hen's egg chorioallantoic membrane test for irritation potential. Food Chem Toxicol. 1985;23(2):287–291. Doi: 10.1016/0278-6915(85)90030-4

77. Andreadis II, Karavasili C, Thomas A, Komnenou A, Tzimtzimis M, Tzetzis D, Andreadis D, Bouropoulos N, Fatouros DG. In Situ Gelling Electrospun Ocular Films Sustain the Intraocular Pressure-Lowering Effect of Timolol Maleate: In

Vitro, Ex Vivo, and Pharmacodynamic Assessment. Mol Pharm. 2022;19(1):274–286. Doi: 10.1021/acs.molpharmaceut.1c00766

78. Kharazmi A, Faraji N, Hussin RM, Saion E, Yunus WMM, Behzad K. Structural, optical, opto-thermal and thermal properties of ZnS-PVA nanofluids synthesized through a radiolytic approach. Beilstein J Nanotechnol. 2015;6(1):529–536. Doi: 10.3762/bjnano.6.55

79. Bhat N V., Nate MM, Kurup MB, Bambole VA, Sabharwal S. Effect of γ-radiation on the structure and morphology of polyvinyl alcohol films. Nucl Instruments Methods Phys Res Sect B Beam Interact with Mater Atoms. 2005;237(3–4):585–592. Doi: 10.1016/j.nimb.2005.04.058

80. Mansur HS, Sadahira CM, Souza AN, Mansur AAP. FTIR spectroscopy characterization of poly (vinyl alcohol) hydrogel with different hydrolysis degree and chemically crosslinked with glutaraldehyde. Mater Sci Eng C. 2008;28(4):539–548. Doi: 10.1016/j.msec.2007.10.088

81. García-Millán E, Quintáns-Carballo M, Otero-Espinar FJ. Solid-state characterization of triamcinolone acetonide nanosuspensiones by X-ray spectroscopy, ATR Fourier transforms infrared spectroscopy and differential scanning calorimetry analysis. Data Brief. 2017;15:133–137. Doi: 10.1016/j.dib.2017.09.002

82. Yasser M, Teaima M, El-Nabarawi M, El-Monem RA. Cubosomal based oral tablet for controlled drug delivery of telmisartan: formulation, in-vitro evaluation and in-vivo comparative pharmacokinetic study in rabbits. Drug Dev Ind Pharm. 2019;45(6):981–994. Doi: 10.1080/03639045.2019.1590392

83. Laurano R, Abrami M, Grassi M, Ciardelli G, Boffito M, Chiono V. Using Poloxamer® 407 as Building Block of Amphiphilic Poly(ether urethane)s: Effect of its Molecular Weight Distribution on Thermo-Sensitive Hydrogel Performances in the Perspective of Their Biomedical Application. Front Mater. 2020;7:1–15. Doi: 10.3389/fmats.2020.594515

84. Ellakwa TE, Fahmy A, Ellakwa DE. Influence of poloxmer on the dissolution properties of mosapride and its pharmaceutical tablet formulation. Egypt J Chem. 2017;60(3):443–451. Doi:10.21608/EJCHEM.2017.3685

85. Mecozzi M, Sturchio E. Computer assisted examination of infrared and near

infrared spectra to assess structural and molecular changes in biological samples exposed to pollutants: A case of study. J Imaging. 2017;3(1):11. Doi: 10.3390/jimaging3010011

86. Shelley H, Grant M, Smith FT, Abarca EM, Jayachandra Babu R. Improved Ocular Delivery of Nepafenac by Cyclodextrin Complexation. AAPS PharmSciTech. 2018;19(6):2554–2563. Doi: 10.1208/s12249-018-1094-0

87. Topal B, Çetin Altindal D, Gümüsderelioglu M. Melatonin/HPβCD complex: Microwave synthesis, integration with chitosan scaffolds and inhibitory effects on MG-63CELLS. Int J Pharm. 2015;496(2):801–811. Doi: 10.1016/j.ijpharm.2015.11.028

88. Pirzada T, Arvidson SA, Saquing CD, Shah SS, Khan SA. Hybrid Silica − PVA Nanofibers via Sol − Gel Electrospinning. 2012;28(13):5834-5844. Doi: 10.1021/la300049j

89. Pandit J, Chaudhary N, Emad NA, Ahmad S, Solanki P, Aqil M, Sultana Y, Solanki P. Fenofibrate loaded nanofibers based thermo-responsive gel for ocular delivery: Formulation development, characterization and in vitro toxicity study. J Drug Deliv Sci Technol. 2023;89:104935. Doi: 10.1016/j.jddst.2023.104935

90. Luraghi A, Peri F, Moroni L. Electrospinning for drug delivery applications: A review. J Control Release. 2021;334:463–484. Doi: 10.1016/j.jconrel.2021.03.033

91. Arribada RG, Behar-Cohen F, de Barros ALB, Silva-Cunha A. The Use of Polymer Blends in the Treatment of Ocular Diseases. Pharmaceutics. 2022;14(7):1431. Doi: 10.3390/pharmaceutics14071431

92. Mirzaeei S, Taghe S, Asare-Addo K, Nokhodchi A. Polyvinyl Alcohol/Chitosan Single-Layered and Polyvinyl Alcohol/Chitosan/Eudragit RL100 Multi-layered Electrospun Nanofibers as an Ocular Matrix for the Controlled Release of Ofloxacin: an In Vitro and In Vivo Evaluation. AAPS PharmSciTech. 2021;22(5):170. Doi: 10.1208/s12249-021-02051-5

93. Yan D, Yao Q, Yu F, Chen L, Zhang S, Sun H, Lin H, Fu Y. Surface modified electrospun poly(lactic acid) fibrous scaffold with cellulose nanofibrils and Ag nanoparticles for ocular cell proliferation and antimicrobial application. Mater Sci Eng C. 2020;111:110767. Doi: 10.1016/j.msec.2020.110767

94. Omer S, Forgách L, Zelkó R, Sebe I. Scale-up of Electrospinning: Market Overview of Products and Devices for Pharmaceutical and Biomedical Purposes. Pharmaceutics. 2021;13(2):286. Doi: 10.3390/pharmaceutics13020286

95. Dodero A, Schlatter G, Hébraud A, Vicini S, Castellano M. Polymer-free cyclodextrin and natural polymer-cyclodextrin electrospun nanofibers: A comprehensive review on current applications and future perspectives. Carbohydr Polym. 2021;264:118042. Doi: 10.1016/j.carbpol.2021.118042

96. Malašauskiene J, Milašius R. Mathematical analysis of the diameter distribution of Electrospun nanofibres. Fibres Text East Eur. 2010;83(6):45–58.

97. Kriegel C, Kit KM, McClements DJ, Weiss J. Influence of surfactant type and concentration on electrospinning of chitosan-poly(ethylene oxide) blend nanofibers. Food Biophys. 2009;4(3):213–228. Doi: 10.1007/s11483-009-9119-6

98. Haider A, Haider S, Kang IK. A comprehensive review summarizing the effect of electrospinning parameters and potential applications of nanofibers in biomedical and biotechnology. Arab J Chem. 2018;11(8):1165–1188. Doi: 10.1016/j.arabjc.2015.11.015

99. George D, Mallery P. IBM SPSS Statistics 26 Step by Step: A Simple Guide and Reference. 2019. Doi: 10.4324/9780429056765

100. Malašauskienė J, Milašius R, Kuchanauskaitė E. Possibilities for the estimation of electrospun nanofibre diameter distribution by normal (Gaussian) distribution. Fibres Text East Eur. 2016;24(2):23–28. Doi: 10.5604/12303666.1191423

101. Spiridonova TI, Tverdokhlebov SI, Anissimov YG. Investigation of the Size Distribution for Diffusion-Controlled Drug Release From Drug Delivery Systems of Various Geometries. J Pharm Sci. 2019;108(8):2690–2697. Doi: 10.1016/j.xphs.2019.03.036

102. Loftsson T, Vogensen SB, Brewster ME. Effects of Cyclodextrins on Drug Delivery Through Biological Membranes. J Pharm Sci. 2007;96(10):2532–2546. Doi: 10.1002/jps.20992. PMID: 17630644

9. BIBLIOGRAPHY OF THE CANDIDATE'S PUBLICATIONS

9.1. Publications related to the thesis

I. **Omer, S.,** Forgách, L., Zelkó, R., & Sebe, I. (2021). Scale-up of electrospinning: Market overview of products and devices for pharmaceutical and biomedical purposes. *Pharmaceutics*, 13(2), 1–21. https://doi.org/10.3390/pharmaceutics13020286.

    Q1, IF (2021): 6.625, **Citations:123** (independent citations:121)

II. **Omer, S.,** & Zelkó, R. (2021). A Systematic Review of Drug-Loaded Electrospun Nanofiber-Based Ophthalmic Inserts. *Pharmaceutics*, 13(10), 1637. https://doi.org/10.3390/pharmaceutics13101637.

    Q1, IF (2021): 6.625, **Citations: 22** (independent citations:22)

III. **Omer, S.,** Nagy, N., Szőcs, E., Kádár, S., Völgyi, G., Pinke, B., Mészáros, L., Katona, G., Vincze, A., Dormán, P., Zs. Nagy, Z., Balogh, G. T., Kazsoki, A., & Zelkó, R. (2023). Development of innovative electrospun nepafenac-loaded nanofibers-based ophthalmic inserts. *International Journal of Pharmaceutics*, 647(October).
    https://doi.org/10.1016/j.ijpharm.2023.123554.

    D1, IF (2023): 5.8, **Citations:1** (independent citations:1)

9.2. Other related publications

I. Romeo, A., Kazsoki, A., **Omer, S**., Pinke, B., Mészáros, L., Musumeci, T., & Zelkó, R. (2023). Formulation and Characterization of Electrospun Nanofibers for Melatonin Ocular Delivery. *Pharmaceutics*, 15(4). https://doi.org/10.3390/pharmaceutics15041296.

    Q1, IF (2023): 5.4, **Citations:3** (independent citations:3)

9.3. Publications not related to the thesis

I. Kazsoki, A., Palcsó, B., **Omer, S. M**., & Kovacs, Z. (2022). Formulation of Levocetirizine-Loaded Core-Shell Type Nanofibrous Orally Dissolving Webs as a Potential Alternative for Immediate Release Dosage Forms. *Pharmaceutics*.
    https://www.mdpi.com/1999-4923/14/7/1442.

    Q1, IF (2022): 5.4, **Citations:9** (independent citations: 7).

10. ACKNOWLEDGEMENTS

Review

Scale-up of Electrospinning: Market Overview of Products and Devices for Pharmaceutical and Biomedical Purposes

Safaa Omer [1], **László Forgách** [2]🆔, **Romána Zelkó** [1,*]🆔 and **István Sebe** [1,*]

[1] University Pharmacy Department of Pharmacy Administration, Semmelweis University, Hőgyes Endre Street 7-9, 1092 Budapest, Hungary; safaa.omer@phd.semmelweis.hu

[2] Department of Biophysics and Radiation Biology, Semmelweis University, Tűzoltó Street 37-47, 1094 Budapest, Hungary; forgach.laszlo@med.semmelweis-univ.hu

[*] Correspondence: zelko.romana@pharma.semmelweis-univ.hu (R.Z.); sebe.istvan@pharma.semmelweis-univ.hu (I.S.); Tel.:+36-208-259-621 (R.Z.); +36-203-396-399 (I.S.)

Abstract: Recently, the electrospinning (ES) process has been extensively studied due to its potential applications in various fields, particularly pharmaceutical and biomedical purposes. The production rate using typical ES technology is usually around 0.01–1 g/h, which is lower than pharmaceutical industry production requirements. Therefore, different companies have worked to develop electrospinning equipment, technological solutions, and electrospun materials into large-scale production. Different approaches have been explored to scale-up the production mainly by increasing the nanofiber jet through multiple needles, free-surface technologies, and hybrid methods that use an additional energy source. Among them, needleless and centrifugal methods have gained the most attention and applications. Besides, the production rate reached (450 g/h in some cases) makes these methods feasible in the pharmaceutical industry. The present study overviews and compares the most recent ES approaches successfully developed for nanofibers' large-scale production and accompanying challenges with some examples of applied approaches in drug delivery systems. Besides, various types of commercial products and devices released to the markets have been mentioned.

Keywords: electrospinning (ES); nanofibers (NFs); scale-up; pharmaceutical industry

1. Introduction

Ideal drug delivery systems have been developed to achieve the best therapeutic effects and lowest toxicity problems [1]. The rapid progress in the field of nanotechnology has led to the development of many techniques for the production of numerous nano-scale composites [2,3], of which nanofibers have received considerable attention [4] due to diversity in the fabrication technologies and applications [5,6], especially in the fields of pharmaceutical drug delivery [7–9], biomedical applications including wound dressing [10–13], and tissue engineering [14,15]. Electrospinning (ES) has been considered one of the most efficient techniques used for the synthesis of nanomaterials since the 20th century [16], and great works have been done in the late 1990s and early part of the 21st century [17,18]. ES is a simple, highly efficient and reproducible process [19]. It depends on the application of a high electrical field between a metallic needle (containing the polymeric solution or melt) [20] and a grounded collector [21,22]. Above a certain critical value [23], the liquid jet is ejected from the tip of a needle, forming a Taylor cone [24], followed by subsequent elongation, thinning, and deposition of sub-micron fibers on the collector [2,25]. Various polymers have been used in the production of nanofibers (NFs) [26,27] with unique properties [28–30], which make NFs a suitable candidate for many pharmaceutical applications, such as solubility improvement [31–36], oral delivery of biopharmaceutical [37], controlling the drug release [38–40], as well as one-step co-encapsulation of one or more drugs [41,42]. Various spinnerets and collecting-electrode devices and accessories are used [43] to produce different fiber mats, including non-woven fiber mats, aligned fiber

mats, patterned fiber mats, random three-dimensional structures, and sub-micron spring and convoluted fibers [44,45]. Sometimes multi-axial capillaries are exploited to produce NF mats that serve different application purposes [46–48], or to enable the fabrication of nanofibers from "unspinnable" liquids [49], or to enhance the quality of resulting nanofiber structures [50]. This means that the final quality of NFs is governed by solution properties, process used, and environmental conditions [51]. Since ES has become a novel, versatile, and applicable technology in the pharmaceutical research and drug development process, switching to industrial manipulation is of critical importance through scaling-up the production, because the laboratory-scale electrospinning device with a single needle has a rather low (0.01–2 g/h) productivity [52]. Even though the ES technique is relatively simple and easy to handle, it faces many challenges that need to be managed in order to have fibers of a high quality [53], such as the inconsistent properties between different batches when using natural polymers such as silk fibroin [54], the toxicity problem resulting from a residual organic solvent, and the stability of active agents with thermal treatment [55]. Moreover, it is a relatively slow and time-consuming process, the quality of the final NFs is affected by the electrical field interference when using multiple needles to increase the production, the improper optimization of parameters will adversely affect or even interfere with fiber formation [56], and difficulty in the NF fabrication of native materials of plant origin, such as starch, necessitates some modifications that adversely interfere with the properties of native materials [57]. Different attempts to use needle-free technologies have been carried out to overcome the limitations, but further studies are needed to formulate NFs with improved quality that fit the pharmaceutical industry [56]. Although the reviews that demonstrate the scale-up of ES technology have been rapidly growing recently, the majority of studies and reviews available mainly focused on the principle of ES, its applications, parameter optimization, and characterization; therefore, light must be shed on the different approaches that have been proved or exploited for massive NF production, particularly for pharmaceutical drug delivery. This review aims to give an overview of the ES technologies developed for the fiber mass production, the challenges encountered, and light touches to products and devices that have been or are near to being released to the markets, emphasizing pharmaceutical-industry-relevant examples.

2. Up-Scaling of Nanofiber Production

Many approaches have been described in the literature for increasing nanofiber productivity. They focus on increasing jet numbers through single-needle modification, using multiple needles, and needleless electrospinning [58–61]. Force-spinning, as a newly developed method which utilizes either centrifugal forces instead of electrostatic force [42] or a combination of both forces, has been found to give a profound effect [43]. Up to date, free-surface and centrifugal methods have been explored for their potential production volume up-scaling [62].

2.1. Challenges Facing the Scaling-up Process

Although it is easy to produce NFs in the lab, when it comes to industrial-scale production, mass productivity always remains a significant concern together with a collection and downstream processes, and there are many challenges which act as an obstacle for nanofiber production in the pharmaceutical industry [63]. The large-volume processing is a time-consuming process that will not fit the pharmaceutical industry capacity. Furthermore, safety and environmental attributes arise from organic solvent for scaled-up electrospinning [62]. The difficulty of process optimization is that only some of the electrospinning process parameters can be easily varied [63,64], which is still a significant challenge. Needleless technology suffers the fast evaporation of volatile solvents used for the solubilization of poorly water-soluble drugs; therefore, the concentration will change and make the process harder to handle, although many attempts have been made to overcome this problem. It is still a challenge, especially with highly concentrated solutions and highly volatile solvents, which leads to decreasing accuracy and reproducibility in

all fabrication stages [14]. When using multi-needle spinnerets, needles clogging and the interference of close by needles will inversely impact the jet formation and final quality of the fiber mats. The improper configuration of collectors and downwards spinning of the jets result in beads or even interfere with fiber formation [56]. It is well known that natural polymers have gained increasing interest in pharmacy, but, unfortunately, it is challenging to fabricate NFs from starch and similar natural polymer from pure materials because they have no sufficient mechanical strength beside their relatively low thermostability; this means that without modification it will be impossible, taking into consideration that the modification processes may negatively impact the function of natural polymers [57]. Inconsistent properties between different batches when using natural polymers such as silk fibroin may occur. Besides, silk fibroin plays a role in stabilizing the pharmaceutical agents, and it needs special treatment with organic solvents to increase its stability. However, using organic and caustic solvents might damage the structure and bio-activity of the bio-molecules and susceptible drugs [54].

2.2. Increasing Jet Production from a Single Needle

Multi-jet electrospinning was first accomplished using a single nozzle with a grooved tip, from which branches of multi-jets were formed, which in turn increases productivity from a single needle. Beadless membranes of poly-butadiene (PB) were successfully prepared by this method. Nevertheless, there was no clear cut about nanofibers' mass production of a single needle. The theory behind this method was based on the fact that increasing jet production might be attributed to the increased voltage, which causes inconsistent current distribution, and clogging of the passage-way of the polymer solution [65]. Jet splitting has been actually observed when fluid jets interact with electric fields, so it is not a just postulation [66]. Different cross-sectional shapes have been observed from a polymeric solution for fiber fabrication by electrospinning from which fibers that were split longitudinally from larger fibers were observed [67]. Only a few studies have been carried out because it is not as efficient as other methods.

2.3. Increasing Jet Production through Multi-Needle Electrospinning

A straightforward and easy way of mass producing nanofibers is by utilizing a multiple-needle instead of a single needle called "multi-needle electrospinning." [17,68–70]. Blended biodegradable nanofiber mats with different weight ratios of poly-vinyl alcohol (PVA) and cellulose acetate (CA) were successfully fabricated via multi-jet electrospinning; the results showed that the blended nanofiber mats have good dispersibility [54]. The process increases the output and enables simultaneous electrospinning of different materials along with the possibility of controlling and maintaining the NFs properties [71]. Nevertheless, this technique faces two main problems: electrostatic field interaction between needles and needles clogging [58,72], which will adversely impact the quality of the produced nanofibers. Therefore, a process modification and developments are of paramount importance. No notable increase in production rate has been observed [14]. Many attempts to overcome these problems have been carried out, including: using a large operating space and careful design of needles to address the problem of charge repulsion and uneven fiber deposition [73]. Therefore, different arrangements may be applied to the needles such as one-dimensional linear configuration or two-dimensional configurations such as elliptical, circular, triangular, square and hexagonal [65,74]. An arced multi-nozzle spinneret was designed to increase the production efficiency of electrospinning, resulting in relatively uniform electrical fields which in turn decreases the electrical interference of the needles and subsequently improves nanofiber quality [75]. The following are some examples for applying this technology for drug delivery and the pharmaceutical industry: an electro-spun formulation containing galactosidase as a model biopharmaceutical drug has been successfully developed through using scaled-up electrospinning experiments of a lab-scale, high-speed electrostatic spinning (HSES) setup consisting of a circular-shaped, stainless steel spinneret, equipped with eight orifices, and connected to a high-speed motor.

The feeding rate was increased to approximately 30 times higher than the usual feeding rate for single-needle electrospinning. The results showed that the content and the added excipients enabled appropriate grinding of the fibrous sample without secondary drying, and subsequently the preparation of pharmaceutical tablets. According to the obtained results, high-speed electrospinning is a viable alternative to traditional biopharmaceutical drying methods, especially for heat-sensitive molecules, and tablet formulation is achievable from the electrospun material prepared in this way [52].

Another interesting example is the formulation of a new intravenous (i.v.) bolus dosage form of doxycycline (DOX) by using a high-speed electrospinning (HSES) setup consisting of a stainless-steel spinneret equipped with 36 orifices and connected to a high-speed motor. The produced fibrous material was collected by a cyclone with a high (~80 g/h) productivity rate. The freeze-dried product was also prepared from the same precursor solution of HSES for comparison. The technology produced an amorphous, uniformly distributed DOX fibrous powder. The result of dissolution showed that the produced fibrous powder has a seven times higher dissolution rate than that of the marketed formulation, which confirmed that the reconstitution solution could be applied as an i.v. bolus dosage form. Subsequently, this work confirmed that the continuous high-speed electrospinning process could be a viable high productivity alternative to batch freeze-drying process [34]. In light of the aforementioned examples, it can be concluded that scaled-up multiple nozzle electrospinning technologies can be successfully used in the pharmaceutical industry after adjusting the process parameters, modification of spinneret by utilizing orifices or holes instead of needles, and through increasing the speed of spinning as shown in the two examples; thus, these configurations fulfil the requirements of the pharmaceutical industry.

2.4. Nozzleless (Free-Surface) Technologies

In this technology, the NF production is directly from an open surface instead of needles. The basic principle behind the formation of multi-jet from this system is as follows: the wave of an electrically conductive liquid is self-organized, followed by simultaneous multiple-jet formation when the applied voltage is above the critical value [65]. In contrast to multiple needles-based electrospinning, free-surface electrospinning requires a very high voltage to overcome the liquid's surface tension, which depends on the type of spinneret used. It is also difficult to maintain consistent solution viscosity owing to solvent evaporation from the surface [76]. However, the technology can be used successfully to address the clogging problem associated with the multiple-needle technique because the fiber formation is obtained without the need for needles [14]. Spinnerets for needleless electrospinning are classified into two categories: rotating and stationary spinnerets. The rotating spinnerets are capable of generating a mechanical rotation to the polymeric solution, while the stationary spinnerets require an auxiliary force to initiate the process (e.g., magnetic field, gravity, and gas bubble) [69].

2.4.1. Electrospinning Method Utilizing Rotating Spinneret

Many rotating spinnerets are available, from which cylinder, disc, ball, and wire are mostly reported [56]. The spinnerets are connected with a high voltage power supply and immersed in the spinning solution. The disc spinneret needs a relatively lower applied voltage than the cylindrical spinneret to initiate fiber formation, and the fibers were mainly formed on the top disc. Both electrospinning systems (disc and cylinder) could produce uniform nanofibers, but the fibers will be thinner with the disc than with the cylinder at the same process conditions [56]. The electrospun NFs are collected from an upward direction, which ensures drop-free fibers [69]. These types of spinnerets have superior advantages over needle-based electrospinning. They have production rates of 8.6 g/h with a cylinder, 6.2 g/h with a disk and 3.1 g/h with a ball as the spinneret for polyvinyl alcohol (PVA) fibers under the same working conditions [69,77]. The formation of multiple jets utilizing a charged cylindrical electrode from the surface of the polymeric solution was the

first patent regarding this technology [78], followed by the development of the world's first industrial free-surface electrospinning setup (Nanospider®) by the Elmarco Company (Liberec, Czech Republic) with nanofibrous non-woven membranes obtained with a 50–500 nm diameter at a production rate of 1.5 g/min per meter of roller length [71,79]. The technology is widely used to manufacture NFs for pharmaceutical applications; a notable example of this is the investigation of electrospun fibers containing antiretroviral drugs tenofovir (TFV) as a new antiviral topical formulation against HIV-1. Manufacturing scalability of drug-eluting fibers was assessed using a NanospiderTM NS-1WS500U large-scale production instrument (Elmarco, Inc., Liberec, Czech Republic). NS-1WS500U (wire instrument) and the parameters were optimized for the best fibers production. The TFV loading in fibers increased with increasing the TFV per cent in solution, and encapsulation efficiency was improved. The study results have specified the important parameters for the scale-up production of TFV drug-eluting fibers by wire electrospinning and support the possibility of the scale-up and transferability of TFV-loaded electrospun fibers to the pharmaceutical industry [80].

2.4.2. Electrospinning Method Utilizing a Stationary Spinneret

In contrast to rotating spinnerets when using stationary spinnerets, an external source of force is required for jet initiation such as a magnetic force [81], high-pressure gas flow [65,82], gravity and ultrasound radiation [83]. Again, similar to rotating spinnerets, this method produces nanofibers with higher production rates than multiple-needle ES. The process setup is more complicated, and the produced nanofibers are relatively coarse [69]. The first study produced nanofibers from dextran utilizing a steel rod and collector as a needleless electrospinning setup to spin solutions directly from the surface. After parameter optimization, the rod diameter is an important parameter for the Taylor cone numbers and electrospinning productivity. The results showed a spinning performance of 0.67 g/min per meter and an average diameter of 162 nm. This study set the parameters necessary for high-quality NFs of dextran fabrication using needleless technology to be used for drug delivery [83]. Another example is a fabrication of antimicrobial polycaprolactone (PCL) NFs using uncommon needleless and collectorless alternating current (AC) electrospinning. The morphological evaluation of resultant fibers showed smooth beadless NFs [84].

Recently, many theoretical and practical studies have been carried out to develop the free-surface method for large-scale production [85]. A novel modified spinneret based on needleless technology called mushroom has been developed to increase the quality and yield of NF production by generating stable pre-Taylor cones with high curvature, resulting in the production rate of 13.7 g/h [86]. To increase the electric current, an auxiliary electrode can be introduced [17,87]. For instance, a modified spinneret consisting of a narrow, long gutter bounded by a metal electrode having a sharp edge has been developed for a continuous high production rate of NFs. The concept behind mass production is explained by the highest electrical charge density that forms along the sharp edge, which will lead to many self-assembled Taylor cones. The technology was assessed using polyacrylonitrile/dimethyl-formamide and polyvinylpyrrolidone/ethanol solutions. The small size of the prototype made possible a 20–50 times increase in productivity compared to the single capillary method [88].

2.5. Other Approaches

Significant improvement in production was obtained by introducing the polymer melt differential electrospinning (PMDES) method, which enables the production of multiple jets with the smallest inter-jet distance of an umbrella-shaped spinneret addition. Suction wind and multistage electric field were proposed to refine the fibers [70]. A centrifuge spinning method that utilizes centrifugal force, rather than the electrostatic force can be successfully used for solution and melt electrospinning. The device consists of a multiple orifice spinneret, thermal system, collecting devices, environmental chamber, control system, motor, and brake. Some researchers have utilized centrifuge spinning to fabricate

nanofibers from several ordinary materials [59], other setups based on utilizing air-sealed centrifugal spinning [89]. Alternating current electrospinning (ACES) was also compared to direct current electrospinning. The results showed comparable nanofiber properties with the capability of ACES to increase the productivity of the mat by approximately six-folds [90]. Hybrid electrospinning methods that used secondary assistant force for the mass production of NFs have also been studied [59]. A new approach for the mass production of NFs is based on the combination of magnetic and electric fields acting on a two-layer system [81].

Another technology has been proven for the production of co-axial NFs on a large scale. The technology is based on the formation of bilayer liquid on the surface of needleless weir spinneret, which eventually supports co-axial nanofibers' formation. The results demonstrated an increased production rate of uniform core/shell NFs compared to needle coaxial spinneret [91]. A comparative study of traditional electrospinning (TES) with ultrasound enhanced electrospinning (USES) has been conducted for the formulation of a nanofiber drug delivery system using polyethylene oxide (PEO) and chitosan as carrier polymers and theophylline anhydrate as a water-soluble model drug. The results showed that NFs produced by USES were amorphous compared to those produced by TES [92]. A very promising novel application of the free-surface method has been manipulated by combining the alternating current electrospinning (ACES)—instead of using direct current— with centrifugal force, and a higher throughput has been obtained [93]. Another study involves utilizing centrifugal and electrostatic forces simultaneously for the fabrication of NFs from poly-acrylonitrile (PAN) and poly-L-lactic acid (PLLA) [94]. Modified free-surface electrospinning (MFSE) using a cone-shaped air, and added sodium dodecylbenzene sulfonates (SDBS) to generate bubbles on the liquid surface. The results revealed that the quality and production rate were increased [95]. A very promising study, compatible with the pharmaceutical industry has been developed for the fabrication of a poorly water-soluble drug itraconazole utilizing scalable, high-speed electrospinning setup. The scaled-up experiment was carried out using a stainless steel spinneret with sharp edges and spherical cap geometry connected to a high-speed motor. In addition to high production output (75-fold productivity improvement, i.e., 450 g/h), the obtained morphology and quality were similar to that produced by single-needle electrospinning. Therefore, it could be possible to have a continuous, efficient, and scaled-up method that meets the pharmaceutical industry's requirements [33].

3. Impact of Scaling Condition on the Nanofibers' Functionality-Related Properties

The morphology of nanofibers is controlled by electrospinning process parameters (flow rate, viscosity, the distance between tip and collector, solvent conductivity, temperature, and humidity); so far, it is not an easy process to have nanofibers with desired properties and architecture, because it is still challenging even for conventional electrospinning [96]. Increasing the flow rate to increase the throughput will affect the morphology of electrospun fibers and leads to the formation of beads due to incomplete drying results in increased pore size and fiber diameters [2]. The collector types and configurations have also been demonstrated to affect the final NF properties, for example, polycaprolactone (PCL) fibers were produced by electrospinning using three collectors: rotating drum static copper wires, and a rotating mandrel and the effect on morphology was evaluated. The best fiber alignment and lowest average fiber diameter were obtained using parallel copper wires with a 1 cm gap [97]. There are many published works comparing the properties of nanofibers fabricated through scaled-up and conventional needle electrospinning methods. Free-surface electrospinning (wire electrode) for the high-throughput fabrication of fibers delivering tenofovir (TFV) was compared to the conventional needle electrospinning method (needle electrode), polyvinyl alcohol (PVA) fibers containing up to 60% TFV were fabricated, and all electrospinning solutions were in the same conditions with regard to solution conductivity, viscosity, surface tension, or pH. The resultant fibers were evaluated for physicochemical parameters such as fiber morphology, drug crystallinity, drug loading and

release kinetics. The results showed that electrospinning using needle and wire instruments produced materials with similar mesh and fiber properties, and fiber diameter decreased with increasing drug loading for both the needle and wire instruments, except for formulations used to fabricate 60% TFV fibers, in which the wire instrument produced fibers with slightly smaller diameters compared to the needle instrument, which was attributed to greater solution conductivity with increasing drug loading and the greater overall electric field strength of the wire. Additionally, the electrospinning of both instruments showed that the finished fibers have a generally smooth and cylindrical morphology. The actual drug loading and encapsulation efficiency of TFV was comparable between the needle and wire electrospinning; the only significant difference observed between actual drug loading and encapsulation efficiency values was for the 60% TFV fibers in which the fibers produced by the wire instrument had a 10% decrease in absolute actual drug loading compared with the fibers produced by the needle instrument. This difference was attributed to the settling of drug precipitate in the carriage tube during electrospinning with the wire instrument. To overcome the problem, a more uniform micronization of the drug before electrospinning was suggested or actively mixing the polymer solution in the reservoir during electrospinning. It can be concluded that the TFV–PVA fibers were successfully transferred from a laboratory-scale to a production-scale instrument [80]. Another study utilizing high-speed electrospinning (HSES) that fit the pharmaceutical requirements was used to prove that a higher production rate will be obtained than that of a single-needle electrospinning (SNES) setup. Itraconazole (ITRA) electrosspun nanofibrous material was formulated using HSES, SNES, spray drying (SD), and film casting (FC). The nanofiber products were evaluated in terms of the dissolution, morphology, and amorphous dispersion. The results showed fast dissolution with both scaled-up and single-needle electrospun fibers. The obtained morphological properties were the same for both lab-scale SNES and the scaled-up HSES method with a diameter range of 0.5–2 mm. Further studies are expected to explain the reason behind some beads' micrometer size in the case of HSES nanofibers [33].

4. Development of Electrospinning Machines from Laboratory to Industrial Scale

The continuous increase in passion and research in electrospinning has led to increased competition among laboratory-scale equipment's suppliers. The market movement was revived with various spinning and collecting-electrode devices and accessories. For example, 4Spin Company (Dolní Dobrouč, Czech Republic) offers highly modular systems and polysaccharides such as hyaluronic acid, chitosan, or cellulose can spin, resulting in a fiber diameter of 300–500 nm [98]. E-Spintronic equipment (Gernlinden, Germany) is characterized by being easy to clean and capable of forming 3D spinning movement with a speed of 1–600 mm/min [99]; information on the fiber diameter range is not available on their website. HOLMARC Opto-Mechatronics (Kerala, India) designed equipment suitable for the production of protein NFs, carbon nanotubes, and inorganic NFs of diameter size 50–5000 nm. They provide systems for research in various fields, such as thin films, biotechnology, nanotechnology, life sciences [100]. NEU KatoTech Co. Ltd. device (Kyoto, Japan) uses electrospinning techniques to safely and easily produce NFs with diameters of 50 to 800 nm. This device is widely used in the automotive industry to research and develop filters and fuel cells [101]. Nadetech Innovations (Navarra, Spain) produce completely automatized ES systems, with completely controllable ES parameters with high accuracy and reproducibility. Their system uses single, coaxial, tri-axial or multi-nozzle spinnerets [102]. Physics Equipments (Chennai, India)—similar to the E-Spintronic equipment—offers devices with a spinning chamber constructed of aluminium strut frames, two polycarbonate clear doors, a window and a fiberglass panel with a voltage sensor, emergency stop and multiple safety features (a core-shell nozzle spinneret is also available); fiber diameter data are not available [103]. A spinbox instrument by Bioinicia (Valencia, Spain) designed for the lab-scale fabrication of micro- or nano-structured fibers and particles for use in a wide variety of applications including regenerative medicine, drug delivery, micro-encapsulation (of food and skin-care ingredients), functional textiles,

and filtration [104]. Besides, various basic, intermediate and advanced kits are available, engineered by Bioinicia and Fluidnatek systems, for research purposes; their large-volume solution feeding system for extended production batches is remarkable. Their product line offers models with easy-to-clean construction, which are dedicated to Cleanroom-ES in the biomedical and pharmaceutical field [105]. Spraybase Company (Kildare, Ireland) supplies different types of spinnerets, including coaxial and tri-axial. Extraordinarily, a melt ES device is available in their line-up [106].

Therefore, a wide range of laboratory-scale equipment is available in the market. The majority is based on needle-type electrospinning, with a low production rate, but is compatible with research capacity. In recent years, many companies have attempted to address low productivity by developing new methods adapted from conventional electrospinning to increase production. Thereafter, the potential for the use of NFs in industrial applications has become feasible [107]. Many companies have released electrospinning equipment for industrial production to the markets, which could be used for pharmaceutical applications (Table 1). Many of them use nozzle-based technologies to control the NF properties, particularly when they are exploited as drug delivery products, while others are based on needleless electrospinning (NLES). Unfortunately, no large number of devices applicable to pharmaceutical industries have been released to date. Nevertheless, the research works are increasing daily based on NLES technology in an attempt to find novel techniques and instruments compatible with the pharmaceutical industry [56], for example, Bioinicia (Valencia, Spain) [105], Elmarco [108], and Fnm Co. (Fanavaran Nano-Meghyas) (Baghestan, Iran) [109]. The first patent in nanofiber scale-up production is based on the possibility to create Taylor cones and the subsequent flow of material not only from the tip of a capillary, but also from a thin film of a polymer solution [78], which led to the development of the world's first industrial free-surface electrospinning setup (Nanospider®) by the Elmarco Company (Liberec, Czech Republic). It is based on needle-free electrospinning technology and designed for the effective production of the highest-quality nanofibers with low solvent consumption, continuous production, and a wide range of solvent for polymer solubility. Furthermore, it is a versatile technology and is easily adapted to various process parameters to optimize the specific properties. The Nanospider™ NS 8S1600U is the base unit for industrial production. It is characterized by being scalable to up to four units and designed for 24 h/7 days operation. Throughput depends on the polymer, substrate, process and fiber diameter, for example: 20,000,000 m^2/year for PA6 on cellulose, nanofiber layer width: 1.6 m, basis weight: 0.03 g/m^2, fiber diameter: 150 nm +/− 30% [108].

Table 1. Summary of electrospinning setups by the technology used instrument scale and manufacturer.

Manufacturer (Country of Origin)	Setup Scales Available	Operation Capacities	Way of Properties	References
Electroblowing				
4Spin (Dolní Dobrouč, Czech Republic)	Laboratory	Unit type/Project system	Highly modular systems; Polysaccharides like Hyaluronic acid, Chitosan or Cellulose can be electrospun Fiber diameter: (>100) 300–500 nm	[98,119]
Needle/Nozzleless electrospinning				
Elmarco (Liberec, Czech Republic)	Laboratory and Industrial (Nanospider production line)	Unit type/Project system Mass production system Continuous system	Lab-based units: high throughput compared to needle-based systems; Industrial unit: low solvent consumption (minimalised usage and evaporation); Maximum effective nanofiber width: 1.6 m Fiber diameter: ● Industrial unit: ~150 nm +/− 30% SD; ● Mass production unit: 80–700 nm +/− 30% SD	[108,120,121]
SKE (Research Equipment) (Bollate, Italy) (by Elmarco) (Czech Republic)	Laboratory and Pilot and Industrial	Unit type/Project system Batch type systems	Also needle-based units available (laboratory scale); Pilot- and industrial-scale units are needleless Co- and triaxial needles available	[116,122]

Table 1. *Cont.*

Manufacturer (Country of Origin)	Setup Scales Available	Operation Capacities	Way of Properties	References
Needle/Nozzle-based electrospinning				
Electrospinning (Tong Li Tech)/NaBond (Hong Kong)	Laboratory and Pilot and Industrial	Unit type/Project system Batch type systems Mass production systems	Needle-based electrospinning; Near-field electrospinning; Coaxial electrospinning; 3D print electrospinning; Melt electrospinning; Continuous electrospinning; For Scale-up units: 0.5–1–1.6–2 m width machines available; Basic, Professional, Scale-up, Robotic, All-in-one, Bio-medical, Portable instruments; Accessories: Multi-needle spinneret, tubeless spinneret, rotating and magnetic electrode collector, x-y moving stage, syringe and continuous pump;	[110,123]
Spraybase (Kildare, Ireland)	Laboratory	Unit type/Project system Batch type systems	Needle/Nozzle-based electrospinning; Melt electrospinning *; 5–40 um * (melt electrospinning); Coaxial/traixial kits available; 25–250 °C—PCL, PLA, PLGA, PP, PE, PMMA can be used (melt electrospinning)	[106,124]
Bioinicia (Valencia, Spain)	Industrial *	Mass production system Continuous system	* Electrospinning contractor; GMP and ISO validated for pharma and biomedical products.	[105,125]
E-Spin NanoTech Pvt. Ltd. (Uttar Pradesh, India)	Laboratory and Pilot	Unit type/Project system Batch type systems	Vertical, Horizontal, Inert Gas Spinning, Under solvent spinning; Ultra compact spinning chamber for low vacuum and inert gas spinning	[126,127]
Erich Huber GmbH (Gernlinden, Germany)	Laboratory	Unit type/Project system	Programmable spinning nozzle; Rotating collector/x-y-plate; 3D spinning possible Insulated, easy-to-clean system hood; 3D spinning movement speed: 1–600 mm/min	[99,128]
Fnm Co. (Fanavaran Nano-Meghyas) (Baghestan, Iran)	Laboratory and Pilot and Industrial	Unit type/Project system Batch type systems Mass production systems Continuous system	Lab-scale unit: Dual Pump Electrospinning Machine (Side by Side Electroris®) For polymeric/carbon/ceramic nanofibers with diameter range of 50 nm to a few micron core-shell nanofibers. One–eight spinning units for industrial unit, all parameters can be set separately Fiber diameter: 60–500 nm	[109,129]
Fluidnatek (by Bioinicia) (Valencia, Spain)	Laboratory and Pilot	Unit type/Project system Batch type systems	Large-volume solution feeding system for extended production batches (single-phase or coaxial)* Multihead emitter system with larger-volume solution reservoirs; Solvent resistant housing; Easy-to-clean contruction for most models—ideal for cleanrooms; Package for GMP validation available (or ISO13485)	[105,125]
HOLMARC Opto-Mechatronics (Kerala, India)	Laboratory	Unit type/Project system Batch type systems	Protein nanofibers, carbon nanotubbes, inorganic nanofibers; UV curing lamp (254 nm) can be added on the top of the rotating collector to cure the spun fibers; Holmarc's model (HO-NFES-SYS): Nano Fiber Double Spinning and Yarning system Fiber diameter: 50–5000 nm	[100,130]
INOVENSO (İstanbul, Turkey)	Laboratory and Pilot and Industrial	Unit type/Project system Batch type systems Mass production systems Continuous system	Single- and multi-nozzle systems for lab-scale workflow available; Maximum number of nozzles: 204 (industrial-scale machine); 180–5000 m²/day, 5000 g nanofiber/day. 50–400 nm diameter; 49,350 m²/day (23.5 h/day) Fiber diameter: 50–400 nm diameter	[111,131]

Table 1. *Cont.*

Manufacturer (Country of Origin)	Setup Scales Available	Operation Capacities	Way of Properties	References
KatoTech Co. Ltd. (Kyoto, Japan)	Laboratory	Unit type/Project system	This device is widely used in the automotive industry for research and development of filters and fuel cells. Fiber diameter: 50–800 nm	[65,101]
LINARI NanoTech (Pisa, Italy)	Laboratory and Industrial	Unit type/Project system Batch type systems	Coaxial needle/multineedle systems; Up to eight independently controlled syringe pumps; Automatic cleaning of needles. Internal temp. and humidity control.	[112,132]
MECC Co. Ltd. (Fukuoka, Japan)	Laboratory and Pilot	Unit type/Project system Batch type systems	Dedicated device for healthcare/medical application; Production of nonwoven nanofiber (effective width: 0.4–1 m); Fiber diameter: 10 nm- several micrometers	[133,134]
Nadetech Innovations (Navarra, Spain)	Laboratory	Unit type/Project system	Spinnerets: single/coaxial/traixial/multi-nozzle	[102,135]
Nanoflux (Singapore)	Laboratory and Pilot and Industrial	Unit type/Project system Batch type systems Continuous system	Multi-nozzle system for the continuous production of the nanofiber fabric products; Up to 135 needles; High-temperature unit (up to 280 °C available)	[113,136]
NanoNC (Seoul, Korea)	Laboratory and Pilot and Industrial	Unit type/Project system Batch type systems Mass production systems Continuous system	Dual/multi-channel syringe pumps available; Coaxial/triaxial/precision/multi/heating /micro nozzle options; (Rotary jet and wet spinning machines available)	[114,137]
Physics Equipment (Chennai, India)	Laboratory	Unit type/Project system Batch type systems	Spinning Chamber: Constructed with Aluminium Strut Frames. • Two Polycarbonate- Clear doors • Window on one side • Fiberglass Panel on other sides • With Sensor to switch of H.V.Power Supply	[103,138]
Progene Link Sdn Bhd (Selangor, Malaysia)	Laboratory and Pilot and Industrial	Unit type/Project system Batch type systems Mass production systems Continuous system	Industrial unit: In each unit, there is a rotating drum dipped in the polymeric solution, and a plate/rotating drum collector placed on the top of each unit.	[115,139]
Spinbox (by Bioinicia) (Valencia, Spain)	Laboratory	Unit type/Project system Batch type systems	Basic/Intermediate/Advanced kits available; Spare parts available; Engineered by Bioinicia and Fluidnatek systems, for research purposes	[105,125]
SPINBOW (San Giorgio di Piano Italy)	Laboratory and Pilot	Unit type/Project system	Feeding unit with infusion pump (up to four syringes); Linear sliding system with a reciprocating motion housing (up to four needles) spinneret Rotating interchangeable drum collector	[140,141]
Yflow (Málaga, Spain)	Laboratory and Pilot and Industrial	Unit type/Project system Batch type systems Mass production systems Continuous system	Upgrade: additional syringe pump for coaxial spinning; coaxial nozzle injector, Taylor cone visualization system. (From Professional system upwards upgrades are included)	[117,142]

* refers to the industrial electrospinning contractor indicated in the second coloumn.

Bioinicia (Valencia, Spain) is the first company to have overcome the up-scaling issues related to the electro-hydrodynamic-spinning and electro-spraying technology with a large scale; it has reached a unique positioning in the pharmaceutical industry, being the only company fully capable of developing and producing drugs with optimized performance. The instrument is versatile with continuous ISO and GMP-certified production of pharmaceutical products: one can use any solvent, excipient or API (even live cells) at solutions, suspensions, and emulsions; no stress is applied to the API at the highest product stability and quality; dry product in a single step (easy downstream process); minimal moisture content and excellent processability of the final product with high reproducibility and dose uniformity; narrow and controllable particle size distribution (50 nm–10 μm) [105]. Similarly, electrospinning (Tong Li Tech)/NaBond (Hong Kong) has developed laboratory-, pilot-, and industrial-scale equipment; a wide range of instrumental selection is available, including a dedicated bio-medical instrument, and various techniques can be applied, such

as needle-based electrospinning, near-field electrospinning, coaxial electrospinning, 3D print electrospinning, melt electrospinning, and continuous electrospinning [110]. Another commercialized instrument that can be used in the pharmaceutical industry is PE3550 from INOVENSO (İstanbul, Turkey); initially conceived for the production of air filtration nanofiber-based products (N95/N99 filtration media), it enables high-throughput NF production based on needles and core-shell electrospinning. PE3550 is equipped with 168 electrospinning nozzles, allowing the surface to be uniform with a fiber diameter of 50–400 nm, and it also enables continuous production at the required quality even under changing environmental conditions [111]. Other companies that supply electrospinning equipment for both laboratory- and large-scale production include LINARI NanoTech (Pisa, Italy), offering coaxial needle/multi-needle systems, which use up to eight independently controlled syringe pumps and have an automatic cleaning system in addition to internal temperature and humidity control [112]. Nanoflux (Singapore) is a multi-nozzle system for the continuous production of the Nanofiber fabric products, containing up to 135 needles [113]. NanoNC (Seoul, Korea) needle-based electrospinning, 3D electrospinning, and near-field electrospinning, with dual- or multi-channel syringe pumps, are available, and coaxial or tri-axial could be applicable [114]. Progene Link Sdn Bhd (Selangor, Malaysia) is widely used for producing nanofiber-based filters and face masks [115]. SKE (Research Equipment) (Bollate, Italy) systems offer various technological solutions to accurately control each process, guaranteeing batch-to-batch reproducibility and precise control of nanofiber parameters such as diameter, orientation and texture, co- and triaxial needles are also available [116]. Yflow® fiber roller supplies more than one type of machine characterized by the following features: designed and optimized to work with electrospinning and electrospraying technologies; works with any polymer solution reported in the scientific literature with the continuous and non-stop operation. The machines are used in a wide variety of applications in diverse sectors, including the pharmaceutical industry [117]. Another example is ANSTCO (NF-LINE IV) (Tehran, Iran). The flexibility in design, ease of use, range of accessories provided, and high precision control and the wide range of variations considered for the main electrospinning parameters are the main outstanding features of ANSTCO electrospinning machinery. Hence, one can easily apply various electrospinning strategies and operational and environmental conditions to produce various nanofibrous products, especially nanofibrous air filters and wound dressing [118].

5. Electrospun Products for Commercial Purposes

The progress in electrospinning involves not only the machines and their accessories but also the electrospun products, so many companies have emerged in the last few years, offering electrospun commercial products that could be used for different applications (Table 2). Commercial usage of electrospun fibers across various fields is now possible.

5.1. Non-Medical Device (Non-MD) Products

Revolution Fibers Ltd. is New Zealand's premier advanced materials company and a global leader in nanofiber production. Revolution Fibers Ltd. has commercialized products with various clients in the areas of filtration, skin health, composites, acoustics, biotech and anti-allergy bedding [143]. According to the data released by "Research and Markets", the nanofibers' global market can reach USD 1 billion by the end of 2021 [17].

Neotherix nanofiber scaffolds for tissue regeneration are bioresorbable scaffolds that possess a non-woven three-dimensional architecture, comprising nano/micro-scale synthetic bioresorbable polymer fibers. The highly porous scaffold structure supports the migration and proliferation of fibroblast cells from surrounding healthy skin tissue to facilitate wound healing [144]. Bio-Spun™: BioSurfaces' patented electrospinning process allows for the incorporation of drugs, growth factors, radiopaque agents, or other bioactives directly into the fibers of both degradable and non-degradable materials with multiple advantages, such as high bioavailability, no extraneous binding agents are necessary, the

ultra-high surface area provides a complete release of loaded drugs, and release rate can be tailored [145].

The Smart Mask filters out over 99%; it also offers virus trapping and bacteria killing and is highly comfortable due to its high breathability [146]. Reusable nanofiber-filtered masks use a nanofilter that maintains excellent filtering efficiency even after handwashing through the development of proprietary technology that aligns nanofibers with a diameter of 100~500 nm in orthogonal or unidirectional directions. This reusable nanofiltered face mask could relieve the challenges arising from the supply shortage of face masks [147]. The SETA nanofiber layer is a revolutionary approach to air filtration using electrospun nanofibers infused with antibacterial additives to trap even the smallest airborne parts, such as spores, allergens, and bacteria [148].

5.2. Medical Devices (MD) and Drug Delivery Systems (DDS)

ReBOSSIS is an innovative-type synthetic cotton-like bone-void/defect-filling material consisting of β-TCP (β-Tricalcium Phosphate), Bioabsorbable Polymer and SiV (Silicone-containing Calcium Carbonate that promotes the bone formation). Its cottony-type property makes it easier to handle at the time of operations compared to existing artificial bones. To give an example, unlike block-type solid artificial bone, processing can be done in advance to make ReBOSSIS fit into the shape or condition of different bone defects. Also, unlike granular-type artificial bone, ReBOSSIS does not fall from a bone-defect/void after filling. In addition to its good handling property, ReBOSSIS is featured with good elasticity and resilient capability, which is a great difference from the existing types of artificial bones. Being elastic and resilient, ReBOSSIS is designed to perfectly fill a bone void of any part of a patient's body and in any size in a shorter time. Furthermore, ReBOSSIS can stay in a void firmly without any risk of falling from the void. Thereafter, ReBOSSIS replaces itself with the patient's bone after healing [149]. Bioweb™ composites electrospun composites offer novel alternatives to traditional stent graft materials thanks to their microporous structure and increased surface area promoting cellular in-growth. Its high surface-to-weight ratio makes it suitable for tissue scaffolding. As a stent covering, the composites allow for the safe and non-inflammatory implantation of these devices [150]. HealSmart™ personalized wound care dressings are made from two types of microfiber polymers: hydrophilic (absorbing) and hydrophobic (moisture repelling). HealSmart™ is a patented microfiber technology that adapts to create dressings that are absorbent or hydrating, as specified. It contains polyhexamethylene biguanide (PHMB), an antimicrobial agent that protects healing cells from a bacterial proliferation in the dressing, and hyaluronic acid (HA), a naturally occurring glycosaminoglycan distributed widely throughout connective, epithelial, and neural tissues known to assist in wound healing. These dressing are FDA approved and have been clinically evaluated in over 12000 placements with a 96% satisfaction rate due to personalized treatment. Several clinical studies have demonstrated improvements in wound area reduction. Furthermore, the dressing composition is adjusted based on the wound's functional needs. It eliminates variability and saves time, and the frequency of dressing changes can remain in place for up to 7 days [151]. In 2018, the Spain-based Bioinicia SL announced the approval for nanofiber-based drug delivery products, the Rivelin® patch. The product is manufactured at Bioinicia's industrial-scale nanofiber production facilities. It is a multi-component electrospun product designed for the unidirectional delivery of a pharmaceutical drug to a mucosal surface. Their controllable fiber diameter results in a large active-surface area and highly efficient drug release in the sub-micrometre range. Bioactive compounds are dissolved in the fiber matrix, effectively forming a uniform solid molecular solution that ensures high bioavailability even for poorly water-soluble substances. The wide range of materials that can be processed, including food- and pharmaceutical-grade biopolymers, synthetic polymers, and inorganic materials, allows for various drug release profiles, which can be tailored to a specific application [105]. The SWASA Surgical Mask is a three-layer membrane technology that protects from bacteria and other pollutions, UV sterile and anti-germ packing comfort-

able breathing [152]. AVflo™ is a superior alternative when considering vascular access for hemodialysis. Rapid hemostasis occurs in less than three minutes, no bleeding from the suture line, no weeping, rapid tissue integration, and no hematoma, seroma or pseudoaneurysm formation [153]. The PK Papyrus® covered coronary stent system achieves greater bending flexibility and a smaller crossing profile than the traditional sandwich design stent. Electrospun polyurethane fibers on the stent surface create a thin and highly elastic membrane to seal perforations with high confidence [154]. The SurgiCLOT® fibrin sealant patch is the first and only fibrin sealant designed specifically for bone bleeding, utilizing the dextran nanofibers to deliver a bolus of human fibrinogen and thrombin, augmenting the clotting cascade to promote a fast, strong and natural fibrin clot to aid the bone healing process [155].

Table 2. Summary of electrospun products by product grade. MD = Medical Device, DDS = Drug Delivery System

Product Type (e.g., Technology, Device, Filter, Mask, etc.)	Brand Name *(Type)*	Product Grade	Manufacturer	Detailed Specification (Availability, Key Features, etc.)	References
			Publicly available products		
Face mask *(nanofiber for mask or filter technology)*	SWASA® face mask (odorless, plus) N95/N99 Face mask technology	MD *(recommended for medical doctors)*	E-SPin NanoTech Pvt. Ltd. (Uttar Pradesh, India)	Patented face mask technology	[152]
	SWASA® Surgical mask	MD		Surgical face mask	
Surgical implants and wound treating products/wound dressings	AVflo™	MD	Nicast (Lod, HaMerkaz, Israel)	Unique Nanofibrous Vascular Access Graft	[153]
	PK Papyrus®		Biotronic (Berlin, Germany)	Electrospun polyurethane fibers on stent surface; thin and highly elastic membrane	[154]
	Surgiclot®		St. Theresa Medical Inc. (Eagan, USA)	Dextran nanofibers; fibrin sealant designed specifically for bone bleeding;	[155]
	NanoCare®		Nanofiber Solutions™ (Ohio, USA)	Veterinary product; ECM-like fiber structure	[160]
	Phoenix Wound Matrix RenovoDerm®			Treatment of both partial- and full-thickness wounds	[161]
	Zeus Bioweb™		Zeus Industrial Products, Inc. (Orangeburg SC, USA)	Ultrasmall PTFE polymeric fibers with low chemical reactivity	[150]
	ReBOSSIS®		Ortho ReBirth (Yokohama-shi Kanagawa pref., Japan)	Bone-void/defect-filling material; Components: TCP (β-Tricalcium Phosphate), Bioabsorbable Polymer and SiV (Silicone-containing Calcium Carbonate that promotes the bone formation).	[149]
	ReDura™		MEDPRIN (Guangzhou, China)	FDA approved degradable material poly-L-lactic acid (PLA) Similar to native extracellular matrix (ECM), rapid repair and regeneration.	[162]
	HealSmart™	DDS	PolyRemedy®, Inc. (Concord, MA, USA)	Antimicrobial Dressings with the addition of Hyaluronic Acid (HA)	[151]
	3D Insert™-PCL	DDS	3D Biotek (New Jersey, USA)	Biodegradable polyester material that has been used in many FDA approved implants, drug delivery devices, suture, adhesion barrier.	[163]
			Products under development		
Patches	Pathon	other	N/A	N/A nitric oxide releasing patch	[164]
	Rivelin® patch	DDS	Bioinicia (Valencia, Spain)	Designed for unidirectional drug delivery to a mucosal surface.	[165]

5.3. D Cell Culture for Drug Development and Sensitivity Screening

It has been clear that three-dimensional (3D) cell culture offers a more realistic one step similar to the in vivo cell growth environment for the manipulation of cell properties than animals, and provides an alternative system to investigate the drug screening in the pre-clinical study phase [156] or to investigate the sensitivity of cancer cells to anticancer drugs [157]; therefore, the design and fabrication of a suitable 3D cell culture platform became an integral and indispensable part of the drug development process. As in other fields, some companies have succeeded in making excellent models for cell culture using the electrospinning process and have been incorporated with other commercial products, for example, Dipole Materials launched BioPaper^TM Technology to help researchers improve pharmaceutical drug screening capabilities. The novel BioPaper technology is a 3D fibrous scaffold that easily fits all of the needs for 3D cell culture; it is biological-derived materials (including gelatin and collagen) with controlled properties and is easily handled for applications in high-throughput drug screening [158]. Another example of 3D cell culture is: nanofiber solution products (plates, chamber slides, dishes, and plate inserts from Nanofiber solutions). Nanofiber Solutions' products are true 3D cell culture surfaces, optically transparent, compatible with light/visible microscopy, the physical dimensions are compatible with high-throughput and standard lab equipment, the fibers are made of polycaprolactone (PCL), the diameter of the nanofiber polymers is 700 nm, no special media or reagents are needed, and they are characterized by batch to batch consistency [159].

6. Future Perspective of Electrospinning and the Scale-up Production

Despite the revolution concerning scaling up instruments and products, it is documented that Nanospider is the only commercialized instrument used in pharmaceutical applications. Nevertheless, the research covering scaled-up ES technologies showed promising results and is expected to help the pharmaceutical industry's field flourish. Therefore, industrial translation requires further developments and support from companies since most released studies are of academic origin. Based on nanofibrous systems' morphological and physicochemical properties, it may become part of real pharmaceutical preparations in the future by increasing the solubility and dissolution rate of poorly soluble drugs [166], reducing the appropriate dose or repositioning existing chemical entities. It may be possible to use the fibrous structure for wound healing, absorbable dressings and topical preparations, grafts, stents, sclerotherapy balloons and diagnostic sensors, taking advantage of its stimulating effect on tissue regeneration [167]. There is also an example in the literature that preclinical-level, specific cell culture-based screening of drugs via nanofibers has been implemented [168,169]. According to the research considerations, the nanofibers can be used directly (e.g., buccal inserts or topical formulations) or with further processing as an intermediate to the final dosage form (e.g., tablets, capsules). In the drug-polymer nanofiber matrix, the drug remains in a higher energy amorphous state. It forms a well or improved soluble amorphous solid dispersion with the excipients used for formulation [170,171]. Although we find examples of extrusion-based formulations on the market [172], a fiber-based pharmaceutical formulation is not yet commercially available, since their thermodynamic stability and the prediction of amorphous–solid conversion needs more in-depth tracking. In both laboratory-scale and scale-up production, it is an essential criterion that the active substance is homogeneously distributed after incorporation into the fiber, remains stable in the preparation and meets strict regulatory requirements. The percentage of active ingredient incorporated into the fibers is low, up to ~10–20%. If the desired dosage form is a tablet, for a 200 mg API dose, the amount of fibrous phase product would be 1 g, which would result in a tablet of a size that is difficult for the patient to swallow. As noted above, nanofiber drug delivery systems in tablets or capsules may only be relevant for low-dose (1–1–10 mg) drugs, which leads to homogeneity. A promising alternative to the pharmaceutical application could be electrospinning for the gentle drying of bioactive substances [36]. A further limitation of the introduction of electrospinning into the pharmaceutical industry and its use in the preparation of a classical dosage form

may be that the fibrous phase product cannot be subjected to further solution processes to preserve any amorphous solid dispersion so that the final dosage form can be formed for dry operations (e.g., compaction and homogenization), or limited to wet suspension operations. In the case of poorly soluble active ingredients, solvents may not be acceptable from official and patient safety. The production of medical or pharmaceutical medical devices and in-vitro diagnostics are promising areas of application for nanofiber systems where the thickness and orientation [173], chemical quality, and biodegradability [174] of the fibers can be finely tuned [175]. An example is a group of implants that help tissue regeneration, where nanometer-diameter, extremely long, individual fibers can help the fibroblast cells of a similar size range grow and adhere [176,177]. No study is available to discuss the effects of the scale-up of electrospinning for pharmaceutical purposes from various points of physical, physicochemical parameters, drug homogeneity, formulation stability, and manufacturing conditions, and robust manufacturing technology. In view of the successful achievements of the Bioinicia Company in the pharmaceutical industry, there is no longer an obstacle for the scaling-up of electrospinning, and it is only a time factor for further developments in the field of the pharmaceutical industry.

7. Conclusions

Electrospinning has been one of the innovative and potential methods for nanofiber (NF) production, especially for drug delivery systems. It is evident that nanofibers have great advantages and unique properties that enable the utilization of NF mats in a different area of drug delivery; for instance, the NFs produced by this method result in amorphous solid for poorly water-soluble drugs, making it a viable alternative to freeze drying and suitable for sensitive biopharmaceuticals. Furthermore, the proven possibilities for the downstream process of the fibers to prepare suitable dosage form necessitate mass production. The majority of the developed methods are based on increasing the jet numbers through: using multiple needles, needleless electrospinning, centrifugal spinning, hybrid electrospinning, and alternating current electrospinning. It has been demonstrated that free-surface, particularly spider spinning, and centrifugal methods exhibit high potential for high-throughput production rates, and centrifugal spinning has developed to be an efficient alternative to ordinary electrostatic-force-based spinning. Several companies offer specialized electrospinning equipment as well as nanofiber-based products for different applications, but the fewer are for the pharmaceutical industry. Electrospinning will remain a popular nanotechnology in laboratories, and the market of electrospinning equipment, both for laboratory research and for industrial production, is expected to grow significantly.

References

1. Pant, B.; Park, M.; Park, S.-J. Drug Delivery Applications of Core-Sheath Nanofibers Prepared by Coaxial Electrospinning: A Review. *Pharmaceutics* **2019**, *11*, 305. [CrossRef]
2. Haider, A.; Haider, S.; Kang, I.-K. A comprehensive review summarizing the effect of electrospinning parameters and potential applications of nanofibers in biomedical and biotechnology. *Arab. J. Chem.* **2018**, *11*, 1165–1188. [CrossRef]
3. Huang, Y.; Song, J.; Yang, C.; Long, Y.; Wu, H. Scalable manufacturing and applications of nanofibers. *Mater. Today* **2019**, *28*, 98–113. [CrossRef]

4.　　Zandi, N.; Lotfi, R.; Tamjid, E.; Shokrgozar, M.A.; Simchi, A. Materials Science & Engineering C Core-sheath gelatin based electrospun nanofibers for dual delivery release of biomolecules and therapeutics. *Mater. Sci. Eng. C* **2020**, *108*, 110432. [CrossRef]

5.　　Ibrahim, Y.S.; Hussein, E.A.; Zagho, M.M.; Abdo, G.G.; Elzatahry, A.A. Melt Electrospinning Designs for Nanofiber Fabrication for Different Applications. *Int. J. Mol. Sci.* **2019**, *20*, 2455. [CrossRef]

6.　　Zupančič, Š.; Škrlec, K.; Kocbek, P.; Kristl, J.; Berlec, A. Effects of Electrospinning on the Viability of Ten Species of Lactic Acid Bacteria in Poly(Ethylene Oxide) Nanofibers. *Pharmaceutics* **2019**, *11*, 483. [CrossRef] [PubMed]

7.　　Kim, K.; Luu, Y.K.; Chang, C.; Fang, D.; Hsiao, B.S.; Chu, B.; Hadjiargyrou, M. Incorporation and controlled release of a hydrophilic antibiotic using poly(lactide-co-glycolide)-based electrospun nanofibrous scaffolds. *J. Control. Release* **2004**, *98*, 47–56. [CrossRef] [PubMed]

8.　　Nguyen, K.V.; Laidmäe, I.; Kogermann, K.; Lust, A.; Meos, A.; Ho, D.V.; Raal, A.; Heinämäki, J.; Nguyen, H.T. Preformulation Study of Electrospun Haemanthamine-Loaded Amphiphilic Nanofibers Intended for a Solid Template for Self-Assembled Liposomes. *Pharmaceutics* **2019**, *11*, 499. [CrossRef] [PubMed]

9.　　Domokos, A.; Balogh, A.; Dénes, D.; Nyerges, G.; Ződi, L.; Farkas, B.; Marosi, G.; Nagy, Z.K. Continuous manufacturing of orally dissolving webs containing a poorly soluble drug via electrospinning. *Eur. J. Pharm. Sci.* **2019**, *130*, 91–99. [CrossRef] [PubMed]

10.　　Unalan, I.; Endlein, S.J.; Slavik, B.; Buettner, A.; Goldmann, W.H.; Detsch, R.; Boccaccini, A.R. Evaluation of Electrospun Poly(ε-Caprolactone)/Gelatin Nanofiber Mats Containing Clove Essential Oil for Antibacterial Wound Dressing. *Pharmaceutics* **2019**, *11*, 570. [CrossRef] [PubMed]

11.　　Dwivedi, C.; Pandey, H.; Pandey, A.C.; Patil, S.; Ramteke, P.W.; Laux, P.; Luch, A.; Singh, A.V. In Vivo Biocompatibility of Electrospun Biodegradable Dual Carrier (Antibiotic + Growth Factor) in a Mouse Model—Implications for Rapid Wound Healing. *Pharmaceutics* **2019**, *11*, 180. [CrossRef] [PubMed]

12.　　Sebe, I.; Kállai-Szabó, B.; Nagy, Z.K.; Szabó, D.; Zsidai, L.; Kocsis, B.; Zelkó, R. Polymer structure and antimicrobial activity of polyvinylpyrrolidone-based iodine nanofibers prepared with high-speed rotary spinning technique. *Int. J. Pharm.* **2013**, *458*, 99–103. [CrossRef] [PubMed]

13.　　Palo, M.; Rönkönharju, S.; Tiirik, K.; Viidik, L.; Sandler, N.; Kogermann, K. Bi-Layered Polymer Carriers with Surface Modification by Electrospinning for Potential Wound Care Applications. *Pharmaceutics* **2019**, *11*, 678. [CrossRef]

14.　　Vass, P.; Szabó, E.; Domokos, A.; Hirsch, E.; Galata, D.; Farkas, B.; Démuth, B.; Andersen, S.K.; Vigh, T.; Verreck, G.; et al. Scale-up of electrospinning technology: Applications in the pharmaceutical industry. *Wiley Interdiscip. Rev. Nanomed. Nanobiotechnol.* **2020**, *12*, e1611. [CrossRef] [PubMed]

15.　　Son, Y.J.; Kim, W.J.; Yoo, H.S. Therapeutic applications of electrospun nanofibers for drug delivery systems. *Arch. Pharmacol. Res.* **2014**, *37*, 69–78. [CrossRef] [PubMed]

16.　　Ghosal, K.; Agatemor, C.; Tucker, N.; Kny, E. Electrical Spinning to Electrospinning: A Brief History: *From Basic Research to Commercialization*. *R. Soc. Chem.* **2018**, *7*, 1–23. [CrossRef]

17.　　Xue, J.; Wu, T.; Dai, Y.; Xia, Y. Electrospinning and Electrospun Nanofibers: Methods, Materials, and Applications. *Chem. Rev.* **2019**, *119*, 5298–5415. [CrossRef] [PubMed]

18.　　Wang, Y.; Guo, Z.; Qian, Y.; Zhang, Z.; Lyu, L.; Wang, Y.; Ye, F. Study on the Electrospinning of Gelatin/Pullulan Composite Nanofibers. *Polymers* **2019**, *11*, 1424. [CrossRef] [PubMed]

19.　　Shi, X.; Zhou, W.; Ma, D.; Ma, Q.; Bridges, D.; Ma, Y.; Hu, A. Electrospinning of Nanofibers and Their Applications for Energy Devices. *J. Nanomater.* **2015**, *2015*, 1–20. [CrossRef]

20.　　Kalra, V.; Lee, J.H.; Park, J.H.; Marquez, M.; Joo, Y.L. Confined Assembly of Asymmetric Block-Copolymer Nanofibers via Multiaxial Jet Electrospinning. *Small* **2009**, *5*, 2323–2332. [CrossRef] [PubMed]

21.　　Luginina, M.; Schuhladen, K.; Orrú, R.; Cao, G.; Boccaccini, A.R.; Liverani, L. Electrospun PCL/PGS Composite Fibers Incorporating Bioactive Glass Particles for Soft Tissue Engineering Applications. *Nanomaterials* **2020**, *10*, 978. [CrossRef] [PubMed]

22.　　Dodero, A.; Brunengo, E.; Castellano, M.; Vicini, S. Investigation of the Mechanical and Dynamic-Mechanical Properties of Electrospun Polyvinylpyrrolidone Membranes: A Design of Experiment Approach. *Polymers* **2020**, *12*, 1524. [CrossRef]

23.　　Lukas, D.; Sarkar, A.; Pokorny, P. Self-organization of jets in electrospinning from free liquid surface: A generalized approach. *J. Appl. Phys.* **2008**, *103*, 084309. [CrossRef]

24.　　Taylor, G.I. Disintegration of water drops in an electric field. *Proc. R. Soc. Lond. Ser. A Math. Phys. Sci.* **1964**, *280*, 383–397. [CrossRef]

25.　　Rogina, A. Electrospinning process: Versatile preparation method for biodegradable and natural polymers and biocomposite systems applied in tissue engineering and drug delivery. *Appl. Surf. Sci.* **2014**, *296*, 221–230. [CrossRef]

26.　　Khalf, A.; Madihally, S.V. Recent advances in multiaxial electrospinning for drug delivery. *Eur. J. Pharm. Biopharm.* **2017**, *112*, 1–17. [CrossRef]

27.　　Zupančič, Š.; Sinha-Ray, S.; Sinha-Ray, S.; Kristl, J.; Yarin, A.L. Controlled Release of Ciprofloxacin from Core–Shell Nanofibers with Monolithic or Blended Core. *Mol. Pharm.* **2016**, *13*, 1393–1404. [CrossRef] [PubMed]

28.　　Kai, D.; Liow, S.S.; Loh, X.J. Biodegradable polymers for electrospinning: Towards biomedical applications. *Mater. Sci. Eng. C* **2014**, *45*, 659–670. [CrossRef] [PubMed]

29.　　Contreras-Cáceres, R.; Cabeza, L.; Perazzoli, G.; Díaz, A.; López-Romero, J.M.; Melguizo, C.; Prados, J. Electrospun Nanofibers: Recent Applications in Drug Delivery and Cancer Therapy. *Nanomaterials* **2019**, *9*, 656. [CrossRef]

30. Balogh, A.; Drávavölgyi, G.; Faragó, K.; Farkas, A.; Vigh, T.; Sóti, P.L.; Wagner, I.; Madarász, J.; Pataki, H.; Marosi, G.; et al. Plasticized Drug-Loaded Melt Electrospun Polymer Mats: Characterization, Thermal Degradation, and Release Kinetics. *J. Pharm. Sci.* **2014**, *103*, 1278–1287. [CrossRef]

31. Ignatious, F.; Sun, L.; Lee, C.-P.; Baldoni, J. Electrospun Nanofibers in Oral Drug Delivery. *Pharm. Res.* **2010**, *27*, 576–588. [CrossRef]

32. Sipos, E.; Kósa, N.; Kazsoki, A.; Szabó, Z.-I.; Zelkó, R. Formulation and Characterization of Aceclofenac-Loaded Nanofiber Based Orally Dissolving Webs. *Pharmaceutics* **2019**, *11*, 417. [CrossRef]

33. Nagy, Z.K.; Balogh, A.; Démuth, B.; Pataki, H.; Vigh, T.; Szabó, B.; Molnár, K.; Schmidt, B.T.; Horák, P.; Marosi, G.; et al. High speed electrospinning for scaled-up production of amorphous solid dispersion of itraconazole. *Int. J. Pharm.* **2015**, *480*, 137–142. [CrossRef]

34. Kiss, K.; Vass, P.; Farkas, A.; Hirsch, E.; Szabó, E.; Mező, G.; Nagy, Z.K.; Marosi, G. A solid doxycycline HP-β-CD formulation for reconstitution (i.v. bolus) prepared by scaled-up electrospinning. *Int. J. Pharm.* **2020**, *586*, 119539. [CrossRef]

35. Balogh, A.; Horváthová, T.; Fülöp, Z.; Loftsson, T.; Harasztos, A.H.; Marosi, G.; Nagy, Z.K. Electroblowing and electrospinning of fibrous diclofenac sodium-cyclodextrin complex-based reconstitution injection. *J. Drug Deliv. Sci. Technol.* **2015**, *26*, 28–34. [CrossRef]

36. Vass, P.; Démuth, B.; Farkas, A.; Hirsch, E.; Szabó, E.; Nagy, B.; Andersen, S.K.; Vigh, T.; Verreck, G.; Csontos, I.; et al. Continuous alternative to freeze drying: Manufacturing of cyclodextrin-based reconstitution powder from aqueous solution using scaled-up electrospinning. *J. Control. Release* **2019**, *298*, 120–127. [CrossRef]

37. Domján, J.; Vass, P.; Hirsch, E.; Szabó, E.; Pantea, E.; Andersen, S.K.; Vigh, T.; Verreck, G.; Marosi, G.; Nagy, Z.K. Monoclonal antibody formulation manufactured by high-speed electrospinning. *Int. J. Pharm.* **2020**, *591*, 120042. [CrossRef]

38. Li, H.; Sang, Q.; Wu, J.; Williams, G.R.; Wang, H.; Niu, S.; Wu, J.; Zhu, L.-M. Dual-responsive drug delivery systems prepared by blend electrospinning. *Int. J. Pharm.* **2018**, *543*, 1–7. [CrossRef] [PubMed]

39. Loscertales, I.G.; Barrero, A.; Guerrero, I.; Cortijo, R.; Marquez, M.; Gañán-Calvo, A.M. Micro/Nano Encapsulation via Electrified Coaxial Liquid Jets. *Science* **2002**, *295*, 1695–1698. [CrossRef]

40. Lv, Y.; Pan, Q.; Bligh, S.A.; Li, H.; Wu, H.; Sang, Q.; Zhu, L.-M. Core-Sheath Nanofibers as Drug Delivery System for Thermoresponsive Controlled Release. *J. Pharm. Sci.* **2017**, *106*, 1258–1265. [CrossRef]

41. Jiang, H.; Wang, L.; Zhu, K. Coaxial electrospinning for encapsulation and controlled release of fragile water-soluble bioactive agents. *J. Control. Release* **2014**, *193*, 296–303. [CrossRef]

42. Cherwin, A.; Namen, S.; Rapacz, J.; Kusik, G.; Anderson, A.; Wang, Y.; Kaltchev, M.; Schroeder, R.; O'Connell, K.; Stephens, S.; et al. Design of a Novel Oxygen Therapeutic Using Polymeric Hydrogel Microcapsules Mimicking Red Blood Cells. *Pharmaceutics* **2019**, *11*, 583. [CrossRef] [PubMed]

43. Geng, Y.; Zhou, F.; Williams, G.R. Developing and scaling up fast-dissolving electrospun formulations based on poly(vinylpyrrolidone) and ketoprofen. *J. Drug Deliv. Sci. Technol.* **2021**, *61*, 102138. [CrossRef]

44. Bruni, G.; Maggi, L.; Tammaro, L.; Di Lorenzo, R.; Friuli, V.; D'Aniello, S.; Maietta, M.; Berbenni, V.; Milanese, C.; Girella, A.; et al. Electrospun fibers as potential carrier systems for enhanced drug release of perphenazine. *Int. J. Pharm.* **2016**, *511*, 190–197. [CrossRef]

45. Islam, S.; Ang, B.C.; Andriyana, A.; Afifi, A.M. A review on fabrication of nanofibers via electrospinning and their applications. *SN Appl. Sci.* **2019**, *1*, 1248. [CrossRef]

46. Zhang, Y.Z.; Venugopal, J.; Huang, Z.-M.; Lim, C.T.; Ramakrishna, S. Characterization of the Surface Biocompatibility of the Electrospun PCL-Collagen Nanofibers Using Fibroblasts. *Biomacromolecules* **2005**, *6*, 2583–2589. [CrossRef]

47. Khalf, A.; Madihally, S.V. Modeling the permeability of multiaxial electrospun poly(ε-caprolactone)-gelatin hybrid fibers for controlled doxycycline release. *Mater. Sci. Eng. C* **2017**, *76*, 161–170. [CrossRef]

48. Lee, H.; Xu, G.; Kharaghani, D.; Nishino, M.; Song, K.H.; Lee, J.S.; Kim, I.S. Electrospun tri-layered zein/PVP-GO/zein nanofiber mats for providing biphasic drug release profiles. *Int. J. Pharm.* **2017**, *531*, 101–107. [CrossRef]

49. Qian, W.; Yu, D.-G.; Li, Y.; Liao, Y.-Z.; Wang, X.; Wang, L. Dual Drug Release Electrospun Core-Shell Nanofibers with Tunable Dose in the Second Phase. *Int. J. Mol. Sci.* **2014**, *15*, 774–786. [CrossRef]

50. Kostakova, E.K.; Meszaros, L.; Maskova, G.; Blazkova, L.; Turcsan, T.; Lukas, D. Crystallinity of Electrospun and Centrifugal Spun Polycaprolactone Fibers: A Comparative Study. *J. Nanomater.* **2017**, *2017*, 1–9. [CrossRef]

51. Wang, X.; Hsiao, B.S. Electrospun nanofiber membranes. *Curr. Opin. Chem. Eng.* **2016**, *12*, 62–81. [CrossRef]

52. Vass, P.; Hirsch, E.; Kóczián, R.; Démuth, B.; Farkas, A.; Fehér, C.; Szabó, E.; Németh, Á.; Andersen, S.K.; Vigh, T.; et al. Scaled-Up Production and Tableting of Grindable Electrospun Fibers Containing a Protein-Type Drug. *Pharmaceutics* **2019**, *11*, 329. [CrossRef] [PubMed]

53. Pillay, V.; Dott, C.; Choonara, Y.E.; Tyagi, C.; Tomar, L.; Kumar, P.; Du Toit, L.C.; Ndesendo, V.M.K. A Review of the Effect of Processing Variables on the Fabrication of Electrospun Nanofibers for Drug Delivery Applications. *J. Nanomater.* **2013**, *2013*, 1–22. [CrossRef]

54. Farokhi, M.; Mottaghitalab, F.; Reis, R.L.; Ramakrishna, S.; Kundu, S.C. Functionalized silk fibroin nanofibers as drug carriers: Advantages and challenges. *J. Control. Release* **2020**, *321*, 324–347. [CrossRef] [PubMed]

55. Kattamuri, S.B.K.; Potti, L.; Vinukonda, A. Nanofibers in Pharmaceuticals—A Review. *Am. J. Pharmtech. Res.* **2018**, *2*, 188–212.

56. Partheniadis, I.; Nikolakakis, I.; Laidmäe, I.; Heinämäki, J. A Mini-Review: Needleless Electrospinning of Nanofibers for Pharmaceutical and Biomedical Applications. *Processes* **2020**, *8*, 673. [CrossRef]

57. Liu, G.; Gu, Z.; Hong, Y.; Cheng, L.; Li, C. Electrospun starch nanofibers: Recent advances, challenges, and strategies for potential pharmaceutical applications. *J. Control. Release* **2017**, *252*, 95–107. [CrossRef]

58. Ranjbari, E.; Bazgir, S.; Shirazi, M.M.A. Needleless electrospinning of poly(acrylic acid) superabsorbent: Fabrication, characterization and swelling behavior. *Polym. Test.* **2020**, *84*, 106403. [CrossRef]

59. Valipouri, A. Production Scale Up of Nanofibers: A Review. *J. Text. Polym.* **2017**, *5*, 8–16.

60. Wojasiński, M.; Gołiawski, J.; Ciach, T. Blow-assisted multi-jet electrospinning of poly-L-lactic acid nanofibers. *J. Polym. Res.* **2017**, *24*, 975. [CrossRef]

61. Shamshina, J.L.; Zavgorodnya, O.; Bonner, J.R.; Gurau, G.; Di Nardo, T.; Rogers, R.D. "Practical" Electrospinning of Biopolymers in Ionic Liquids. *ChemSusChem* **2017**, *10*, 106–111. [CrossRef]

62. Persano, L.; Camposeo, A.; Tekmen, C.; Pisignano, D. Industrial Upscaling of Electrospinning and Applications of Polymer Nanofibers: A Review. *Macromol. Mater. Eng.* **2013**, *298*, 504–520. [CrossRef]

63. Thakkar, S.; Misra, M. Electrospun polymeric nanofibers: New horizons in drug delivery. *Eur. J. Pharm. Sci.* **2017**, *107*, 148–167. [CrossRef] [PubMed]

64. Asadian, M.; Chan, K.V.; Norouzi, M.; Grande, S.; Cools, P.; Morent, R.; De Geyter, N. Fabrication and Plasma Modification of Nanofibrous Tissue Engineering Scaffolds. *Nanomaterials* **2020**, *10*, 119. [CrossRef] [PubMed]

65. Nayak, R.; Padhye, R.; Kyratzis, I.L.; Truong, Y.B.; Arnold, L. Recent advances in nanofibre fabrication techniques. *Text. Res. J.* **2011**, *82*, 129–147. [CrossRef]

66. Paruchuri, S.; Brenner, M.P. Splitting of a Liquid Jet. *Phys. Rev. Lett.* **2007**, *98*, 134502. [CrossRef]

67. Sureeporn, K.; Wenxia, L.; Darrell, R. Flat polymer ribbons and other shapes by electrospinning. *J. Polym. Sci. Part B Polym. Phys.* **2001**, *39*, 2598–2606. [CrossRef]

68. Theron, S.; Yarin, A.; Zussman, E.; Kroll, E. Multiple jets in electrospinning: Experiment and modeling. *Polymer* **2005**, *46*, 2889–2899. [CrossRef]

69. Niu, H.; Lin, T. Fiber Generators in Needleless Electrospinning. *J. Nanomater.* **2012**, *2012*, 1–13. [CrossRef]

70. Mingjun, C.; Youchen, Z.; Haoyi, L.; Xiangnan, L.; Yumei, D.; Bubakir, M.M.; Weimin, Y. An example of industrialization of melt electrospinning: Polymer melt differential electrospinning. *Adv. Ind. Eng. Polym. Res.* **2019**, *2*, 110–115. [CrossRef]

71. Kurečič, M.; Smole, M.S. Electrospinning: Nanofibre Production Method. *Tekstilec* **2013**, *56*, 4–12. [CrossRef]

72. Zhang, Y.; Cheng, Z.; Han, Z.; Zhao, S.; Zhao, X.; Kang, L. Stable multi-jet electrospinning with high throughput using the bead structure nozzle. *RSC Adv.* **2018**, *8*, 6069–6074. [CrossRef]

73. Jao, P.F.; Fang, S.-P.; David, E.; Kim, K.T.; Yoon, Y.-K. Nanomanufacturing of Large Area Carbon Nanofibers Using Tube Nozzle Electrospinning (TNE), Lithography and Carbonization Processes. In Proceedings of the 2012 IEEE 62nd Electronic Components and Technology Conference, San Diego, CA, USA, 29 May–1 June 2012; IEEE: New York, NY, USA, 2012; pp. 2075–2081. [CrossRef]

74. Yang, Y.; Jia, Z.; Li, Q.; Hou, L.; Liu, J.; Wang, L.; Guan, Z.; Zahn, M. A shield ring enhanced equilateral hexagon distributed multi-needle electrospinning spinneret. *IEEE Trans. Dielectr. Electr. Insul.* **2010**, *17*, 1592–1601. [CrossRef]

75. Jiang, J.; Zheng, G.; Wang, X.; Li, W.; Kang, G.; Chen, H.; Guo, S.; Liu, J. Arced Multi-Nozzle Electrospinning Spinneret for High-Throughput Production of Nanofibers. *Micromachines* **2019**, *11*, 27. [CrossRef] [PubMed]

76. Wu, Y.-K.; Wang, L.; Fan, J.; Shou, W.; Zhou, B.-M.; Liu, Y. Multi-Jet Electrospinning with Auxiliary Electrode: The Influence of Solution Properties. *Polymers* **2018**, *10*, 572. [CrossRef]

77. Holopainen, J.; Penttinen, T.; Santala, E.; Ritala, M. Needleless electrospinning with twisted wire spinneret. *Nanotechnology* **2015**, *26*, 025301. [CrossRef] [PubMed]

78. Jirsak, O.; Sanetrnik, F.; Lukas, D.; Kotek, V.; Martinova, L.; Chaloupek, J. A Method of Nanofibres Production from a Polymer Solution Using Electrostatic Spinning and a Device for Carrying Out the Method. U.S. Patent WO2005024101A1, 8 September 2003.

79. Bazbouz, M.B.; Liang, H.; Tronci, G. A UV-cured nanofibrous membrane of vinylbenzylated gelatin-poly(ε-caprolactone) dimethacrylate co-network by scalable free surface electrospinning. *Mater. Sci. Eng. C* **2018**, *91*, 541–555. [CrossRef] [PubMed]

80. Krogstad, E.A.; Woodrow, K.A. Manufacturing scale-up of electrospun poly(vinyl alcohol) fibers containing tenofovir for vaginal drug delivery. *Int. J. Pharm.* **2014**, *475*, 282–291. [CrossRef]

81. Yarin, A.; Zussman, E. Upward needleless electrospinning of multiple nanofibers. *Polymers* **2004**, *45*, 2977–2980. [CrossRef]

82. He, J.; Qi, K.; Wang, L.; Zhou, Y.; Liu, R.; Cui, S. Combined application of multinozzle air-jet electrospinning and airflow twisting for the efficient preparation of continuous twisted nanofiber yarn. *Fibers Polym.* **2015**, *16*, 1319–1326. [CrossRef]

83. Cengiz-Çallıoğlu, F. Dextran nanofiber production by needleless electrospinning process. *e-Polymers* **2014**, *14*, 5–13. [CrossRef]

84. Manikandan, S.; Divyabharathi, M.; Tomas, K.; Pavel, P.; David, L. Production of poly (ε-caprolactone) Antimicrobial Nanofibers by Needleless Alternating Current Electrospinning. *Mater. Today Proc.* **2019**, *17*, 1100–1104. [CrossRef]

85. Zhou, F.-L.; Gong, R.-H.; Porat, I. Mass production of nanofibre assemblies by electrostatic spinning. *Polym. Int.* **2009**, *58*, 331–342. [CrossRef]

86. Xiong, J.; Liu, Y.; Li, A.; Wei, L.; Wang, L.; Qin, X.; Yu, J. Mass production of high-quality nanofibers via constructing pre-Taylor cones with high curvature on needleless electrospinning. *Mater. Des.* **2021**, *197*, 109247. [CrossRef]

87. Chen, R.; Wu, Y.; Fan, J.; Wang, L.; Su, Z.; Qin, L.; Liang, L.; Li, Y.; Cheng, J.; Liu, Y. Numerical approach to controlling a moving jet's vibration in an electrospinning system: An auxiliary electrode and uniform electric field. *J. Low Freq. Noise Vib. Act. Control.* **2019**, *38*, 1687–1698. [CrossRef]

88. Molnar, K.; Nagy, Z.K. Corona-electrospinning: Needleless method for high-throughput continuous nanofiber production. *Eur. Polym. J.* **2016**, *74*, 279–286. [CrossRef]

89. Valipouri, A.; Hosseini, S.A. Fabrication of Biodegradable PCL Particles as well as PA66 Nanofibers via Air-Sealed Centrifuge Electrospinning. *J. Text. Polym.* **2016**, *4*, 15–19.

90. Balogh, A.; Cselkó, R.; Démuth, B.; Verreck, G.; Mensch, J.; Marosi, G.; Nagy, Z.K. Alternating current electrospinning for preparation of fibrous drug delivery systems. *Int. J. Pharm.* **2015**, *495*, 75–80. [CrossRef] [PubMed]

91. Vysloužilová, L.; Buzgo, M.; Pokorný, P.; Chvojka, J.; Míčková, A.; Rampichová, M.; Kula, J.; Pejchar, K.; Bílek, M.; Lukáš, D.; et al. Needleless coaxial electrospinning: A novel approach to mass production of coaxial nanofibers. *Int. J. Pharm.* **2017**, *516*, 293–300. [CrossRef]

92. Hakkarainen, E.; Kõrkjas, A.; Laidmäe, I.; Lust, A.; Semjonov, K.; Kogermann, K.; Nieminen, H.J.; Salmi, A.; Korhonen, O.; Haeggström, E.; et al. Comparison of Traditional and Ultrasound-Enhanced Electrospinning in Fabricating Nanofibrous Drug Delivery Systems. *Pharmaceutics* **2019**, *11*, 495. [CrossRef] [PubMed]

93. Farkas, B.; Balogh, A.; Cselkó, R.; Molnár, K.; Farkas, A.; Borbás, E.; Marosi, G.; Nagy, Z.K. Corona alternating current electrospinning: A combined approach for increasing the productivity of electrospinning. *Int. J. Pharm.* **2019**, *561*, 219–227. [CrossRef] [PubMed]

94. Valipouri, A.; Ravandi, S.A.H.; Pishevar, A.R. A novel method for manufacturing nanofibers. *Fibers Polym.* **2013**, *14*, 941–949. [CrossRef]

95. Shao, Z.; Yu, L.; Xu, L.; Wang, M. High-Throughput Fabrication of Quality Nanofibers Using a Modified Free Surface Electrospinning. *Nanoscale Res. Lett.* **2017**, *12*, 1–9. [CrossRef] [PubMed]

96. Song, J.; Kim, M.; Lee, H. Recent Advances on Nanofiber Fabrications: Unconventional State-of-the-Art Spinning Techniques. *Polymers* **2020**, *12*, 1386. [CrossRef]

97. Alfaro De Prá, M.A.; Ribeiro-do-Valle, R.M.; Maraschin, M.; Veleirinho, B. Effect of Collector Design on the Morphological Properties of Polycaprolactone Electrospun Fibers. *Mater. Lett.* **2017**, *193*, 154–157. [CrossRef]

98. Electrospinning Device 4SPIN. Available online: https://www.4spin.info/portfolio/4spin-c4s-lab (accessed on 16 January 2021).

99. Electrospinning-Erich Huber GmbH. Available online: https://www.ehuber.de/electrospinning.html (accessed on 16 January 2021).

100. Holmarc. Nano Fiber Electrospinning Unit. Available online: https://www.holmarc.com/nano_fiber_electrospinning_station.php (accessed on 16 January 2021).

101. NaBond Nanofiber Electrospinning Unit. Available online: https://english.keskato.co.jp/archives/products/neu (accessed on 16 January 2021).

102. Nadetech Innovations. ND-ES Lab Electrospinning. Available online: https://nadetech.com/dip-coating-3/ (accessed on 16 January 2021).

103. Physics Eqipment. Available online: http://www.phyeqpt.in/index.html (accessed on 16 January 2021).

104. Spinbox Electrospinning by Bioinicia. Available online: https://www.spinboxsystems.com/electrospinning/ (accessed on 16 January 2021).

105. Bioinicia Electrospinning-Electrospraying. Available online: https://bioinicia.com/electrospinning-electrospraying-lab-equipment/ (accessed on 16 January 2021).

106. Spraybase®Kits for Electrospinning and Electrospraying. Available online: https://www.spraybase.com/kits (accessed on 16 January 2021).

107. Teo, W.-E.; Inai, R.; RamaKrishnaan, S. Technological advances in electrospinning of nanofibers. *Sci. Technol. Adv. Mater.* **2011**, *12*, 013002. [CrossRef] [PubMed]

108. Nanospider Electrospinning Equipment. Available online: https://www.elmarco.com/%0D%0A (accessed on 16 January 2021).

109. Products Fnm Co. Available online: https://fnm.ir/Product (accessed on 16 January 2021).

110. Electrospinning Tong Li Tech. Available online: https://www.electro-spinning.com/ (accessed on 16 January 2021).

111. Inovenso Products. Available online: https://www.inovenso.com/?gclid=EAIaIQobChMImtvekO7i5gIVx-N3Ch2NCgQwEAAY-AiAAEgKt2fD_BwE (accessed on 16 January 2021).

112. Electrospinning Equipments-Linari Nanotech. Available online: https://www.linarinanotech.com/pages/electrospinning-equipments%0D%0A (accessed on 16 January 2021).

113. Nanoflux-Electrospinning Equipments. Available online: http://www.nanoflux.com.sg/en/ (accessed on 16 January 2021).

114. Electrospinning/Electrospray Machines-NC. Available online: http://nanonc.co.kr/wordpress/ (accessed on 16 January 2021).

115. Electrospinning Equipments-Progene Link Sdn Bhd. Available online: http://www.progenelink.com/category/electrospinning-unit/ (accessed on 16 January 2021).

116. Electrospinning System-SKE. Available online: http://www.ske.it/index.php/product-category/electrospinning-systems/%0D%0A (accessed on 16 January 2021).

117. Yflow®Electrospinning Machine. Available online: http://www.yflow.com/electrospinning-machine/ (accessed on 16 January 2021).

118. ANSTCO Electrospinning Machinery. Available online: http://www.anstco.co/anstco/english/p1.html (accessed on 16 January 2021).

119. Pokorny, M.; Řebíček, J.; Novák, J.; Kotzianová, A.; Klemes, J.; Ruzickova, J.; Velebný, V. Produced Nanofibers and Technological Possibilities of Laboratory Apparatus 4SPIN®. In Proceedings of the Fiber Society Spring 2014 Technical Conference: Fibers for Progress, Liberec, Czech Republic, 21–23 May 2014. [CrossRef]

120. Petras, D.; Maly, M.; Kovac, M.; Stromsky, V.; Pozner, J.; Trdlicka, J.; Jakubek, F. Method for spinning a liquid matrix for production of nanofibres through electrostatic spinning of liquid matrix. U.S. Patent 8,231,822, 31 July 2012.

121. Petras, D.; Mares, L.; Stranska, D. Method and device for production of nanofibres from the polymeric solution through electrostatic spinning. U.S. Patent WO 2006131081, 2006.

122. Fotticchia, A.; Demirci, E.; Lenardi, C.; Liu, Y. Cellular Response to Cyclic Compression of Tissue Engineered Intervertebral Disk Constructs Composed of Electrospun Polycaprolactone. *J. Biomech. Eng.* **2018**, *140*, 1–9. [CrossRef] [PubMed]

123. Li, Y.; Meng, Y.; Xiao, M.; Liu, X.; Zhu, F.; Zhang, Y. The surface capacitance behavior and its contribution to the excellent performance of cobalt ferrite/carbon anode in lithium storage. *J. Mater. Sci. Mater. Electron.* **2019**, *30*, 12659–12668. [CrossRef]

124. O'Leary, C.; Soriano, L.; Fagan-Murphy, A.; Ivankovic, I.; Cavanagh, B.; O'Brien, F.J.; Cryan, S.-A. The Fabrication and in vitro Evaluation of Retinoic Acid-Loaded Electrospun Composite Biomaterials for Tracheal Tissue Regeneration. *Front. Bioeng. Biotechnol.* **2020**, *8*, 1–12. [CrossRef] [PubMed]

125. Mahmud, A.; Elumalai, N.K.; Pal, B.; Jose, R.; Upama, M.B.; Wang, D.; Gonçales, V.R.; Xu, C.; Haque, F.; Uddin, A. Electrospun 3D composite nano-flowers for high performance triple-cation perovskite solar cells. *Electrochim. Acta* **2018**, *289*, 459–473. [CrossRef]

126. Electrospinning Unit-Super ES-1& Super ES-2. Available online: https://www.espinnanotech.com/ (accessed on 16 January 2021).

127. Malik, A.; Magisetty, R.; Kumar, V.; Shukla, A.; Kandasubramanian, B. Dielectric and conductivity investigation of polycarbonate-copper phthalocyanine electrospun nonwoven fibres for electrical and electronic application. *Polym. Technol. Mater.* **2019**, *59*, 154–168. [CrossRef]

128. Gläser, S.; Mede, R.; Görls, H.; Seupel, S.; Bohlender, C.; Wyrwa, R.; Schirmer, S.; Dochow, S.; Reddy, G.U.; Popp, J.; et al. Remote-controlled delivery of CO via photoactive CO-releasing materials on a fiber optical device. *Dalton Trans.* **2016**, *45*, 13222–13233. [CrossRef]

129. Bayat, S.; Amiri, N.; Pishavar, E.; Kalalinia, F.; Movaffagh, J.; Hashemi, M. Bromelain-loaded chitosan nanofibers prepared by electrospinning method for burn wound healing in animal models. *Life Sci.* **2019**, *229*, 57–66. [CrossRef]

130. Ghosal, K.; Manakhov, A.; Zajíčková, L.; Thomas, S. Structural and Surface Compatibility Study of Modified Electrospun Poly(ε-caprolactone) (PCL) Composites for Skin Tissue Engineering. *AAPS PharmSciTech* **2017**, *18*, 72–81. [CrossRef]

131. Okutan, N.; Terzi, P.; Altay, F. Affecting parameters on electrospinning process and characterization of electrospun gelatin nanofibers. *Food Hydrocoll.* **2014**, *39*, 19–26. [CrossRef]

132. Modafferi, V.; Panzera, G.; Donato, A.; Antonucci, P.; Cannilla, C.; Donato, N.; Spadaro, D.; Neri, G. Highly sensitive ammonia resistive sensor based on electrospun V2O5 fibers. *Sens. Actuat. B Chem.* **2012**, *163*, 61–68. [CrossRef]

133. MECC CO., LTD. Nanofiber Division. Available online: https://www.mecc-nano.com (accessed on 16 January 2021).

134. Yano, T.; Higaki, Y.; Tao, D.; Murakami, D.; Kobayashi, M.; Ohta, N.; Koike, J.-I.; Horigome, M.; Masunaga, H.; Ogawa, H.; et al. Orientation of poly(vinyl alcohol) nanofiber and crystallites in non-woven electrospun nanofiber mats under uniaxial stretching. *Polymers* **2012**, *53*, 4702–4708. [CrossRef]

135. Corres, J.M.; Arregui, F.J.; Matias, I.R.; Rodriguez, Y. High Sensitivity Optical Fiber pH Sensor Using Poly(acrylic acid) Nanofibers. In Proceedings of the 2013 IEEE SENSORS, Baltimore, MD, USA, 3–6 November 2013; IEEE: New York, NY, USA, 2013; pp. 1–4. [CrossRef]

136. Ang, H.Y.; Irvine, S.A.; Avrahami, R.; Sarig, U.; Bronshtein, T.; Zussman, E.; Boey, F.Y.C.; Machluf, M.; Venkatraman, S.S. Characterization of a bioactive fiber scaffold with entrapped HUVECs in coaxial electrospun core-shell fiber. *Biomatter* **2014**, *4*, e28238. [CrossRef]

137. Heo, Y.-J.; Lee, H.I.; Lee, J.W.; Park, M.; Rhee, K.Y.; Park, S.-J. Optimization of the pore structure of PAN-based carbon fibers for enhanced supercapacitor performances via electrospinning. *Compos. Part B Eng.* **2019**, *161*, 10–17. [CrossRef]

138. Kolathodi, M.S.; Palei, M. MnO 2 Encapsulated Electrospun TiO 2 Nano Fi Bers as Electrodes for Asymmetric Supercapacitors. *Nanotechnology* **2020**, *31*, 125401. [CrossRef] [PubMed]

139. Mani, M.P.; Jaganathan, S.K.; Supriyanto, E. Enriched Mechanical Strength and Bone Mineralisation of Electrospun Biomimetic Scaffold Laden with Ylang Ylang Oil and Zinc Nitrate for Bone Tissue Engineering. *Polymers* **2019**, *11*, 1323. [CrossRef] [PubMed]

140. Products-SPINBOW. Available online: http://www.spinbow.it/en/product-en/ (accessed on 16 January 2021).

141. Sensini, A.; Gotti, C.; Belcari, J.; Zucchelli, A.; Focarete, M.L.; Gualandi, C.; Todaro, I.; Kao, A.P.; Tozzi, G.; Cristofolini, L. Morphologically bioinspired hierarchical nylon 6,6 electrospun assembly recreating the structure and performance of tendons and ligaments. *Med. Eng. Phys.* **2019**, *71*, 79–90. [CrossRef]

142. Aznar-Cervantes, S.; Roca, M.I.; Martinez, J.G.; Meseguer-Olmo, L.; Cenis, J.L.; Moraleda, J.M.; Otero, T.F. Fabrication of conductive electrospun silk fibroin scaffolds by coating with polypyrrole for biomedical applications. *Bioelectrochemistry* **2012**, *85*, 36–43. [CrossRef]

143. Hosie, I. Turning Nanofibre into Products. *NSTI Adv. Mater. TechConnect Briefs* **2015**, *4*, 1–4.

144. Neotherix- Regenerative Scaffold for Tissue Repair. Available online: http://www.neotherix.com/technology.php (accessed on 16 January 2021).

145. Drug Loading-Biosurface. Available online: https://www.biosurfaces.us/drug-loading-1 (accessed on 16 January 2021).

146. Brand and Product Concepts. Available online: http://nask.hk/ (accessed on 16 January 2021).
147. Kaist News Center. Available online: http://news.kaist.ac.kr/newsen/html/news/?mode=V&mng_no=6530 (accessed on 16 January 2021).
148. Seta Filter Media- Revolution Fibres. Available online: https://www.revolutionfibres.com/seta/ (accessed on 16 January 2021).
149. Products-OrthoRebirth. Available online: https://orthorebirth.com/?page_id=338 (accessed on 16 January 2021).
150. BiowebTM E-Spun. Available online: https://www.zeusinc.com/products/biomaterials/bioweb-composites (accessed on 16 January 2021).
151. Polyremedy Personalized Dressings. Available online: https://polyremedy.com/polyremedy-launches-healsmart-hyaluronic-acid-dressing-enhancement/ (accessed on 16 January 2021).
152. SWASA-Breathe Clean Air. Available online: https://swasa.in/ (accessed on 16 January 2021).
153. Product Description- Nicast. Available online: http://nicast.com/avflo/product-description/ (accessed on 16 January 2021).
154. PK Papyrus®. Available online: https://www.biotronik.com/en-de/products/coronary/pk-papyrus (accessed on 16 January 2021).
155. SurgiCLOT®-St Reresa Medical. Available online: https://stteresamedical.com/technology/surgiclot (accessed on 16 January 2021).
156. Zhang, S.; Gelain, F.; Zhao, X. Designer self-assembling peptide nanofiber scaffolds for 3D tissue cell cultures. *Semin. Cancer Biol.* **2005**, *15*, 413–420. [CrossRef] [PubMed]
157. Kim, Y.-J.; Bae, H.-I.; Kwon, O.K.; Choi, M.-S. Three-dimensional gastric cancer cell culture using nanofiber scaffold for chemosensitivity test. *Int. J. Biol. Macromol.* **2009**, *45*, 65–71. [CrossRef]
158. Biopaper- Dipole Materials. Available online: https://www.dipolematerials.com/biopapers/ (accessed on 16 January 2021).
159. 3D-Culture Archives-Nanofiber Solutions. Available online: https://nanofibersolutions.com/product-category/3d-cell-culture/ (accessed on 16 January 2021).
160. Veterinary Products Archives- Nanofiber Solutions. Available online: https://nanofibersolutions.com/product-category/veterinary/ (accessed on 16 January 2021).
161. RenovoDerm-Phoenix Wound Matrix. Available online: https://www.renovoderm.tech (accessed on 16 January 2021).
162. Medprin Biotech. Available online: http://www.medprin.com/home/product/productdetails.html?id=12 (accessed on 16 January 2021).
163. 3D Insert-PCL: Zen Cart, the ARt of E-Commerce. Available online: http://www.3dbiotekstore.com/index.php?main_page=index&cPath=10 (accessed on 16 January 2021).
164. Clinical Trial for the Treatment of Diabetic Foot Ulcers Using a Nitric Oxide Releasing Patch: PATHON. Available online: https://clinicaltrials.gov/ct2/show/record/NCT00428727 (accessed on 16 January 2021).
165. Bioinicia Gmp Certification for Electrospun Nanofibers. Available online: https://bioinicia.com/bioinicia-gmp-certification-for-electrospun-nanofibers/ (accessed on 16 January 2021).
166. Shah, V.P.; Amidon, G.L. G.L. Amidon, H. Lennernas, V.P. Shah, and J.R. Crison. A Theoretical Basis for a Biopharmaceutic Drug Classification: The Correlation of In Vitro Drug Product Dissolution and In Vivo Bioavailability, Pharm Res 12, 413–420, 1995—Backstory of BCS. *AAPS J.* **2014**, *16*, 894–898. [CrossRef] [PubMed]
167. Sebe, I.; Kallai-Szabo, B.; Zelko, R.; Szabo, D. Polymers and formulation strategies of nanofibrous systems for drug delivery application and tissue engineering. *Curr. Med. Chem.* **2015**, *22*, 604–617. [CrossRef]
168. Walsh, T.; Karperien, L.; Dabiri, S.M.H.; Akbari, M. Fiber-based microphysiological systems: A powerful tool for high throughput drug screening. *Microphysiological Syst.* **2019**, *3*, 3. [CrossRef]
169. Azari, P.; Luan, N.S.; Gan, S.N.; Yahya, R.; Wong, C.S.; Chua, K.H.; Pingguan-Murphy, B. Electrospun Biopolyesters as Drug Screening Platforms for Corneal Keratocytes. *Int. J. Mater. Polym. BioMater.* **2015**, *64*, 785–791. [CrossRef]
170. Lakshman, J.P.; Cao, Y.; Kowalski, J.; Serajuddin, A.T.M. Application of Melt Extrusion in the Development of a Physically and Chemically Stable High-Energy Amorphous Solid Dispersion of a Poorly Water-Soluble Drug. *Mol. Pharm.* **2008**, *5*, 994–1002. [CrossRef] [PubMed]
171. Chiou, W.L.; Riegelman, S. Pharmaceutical Applications of Solid Dispersion Systems. *J. Pharm. Sci.* **1971**, *60*, 1281–1302. [CrossRef] [PubMed]
172. Van Den Mooter, G. The use of amorphous solid dispersions: A formulation strategy to overcome poor solubility and dissolution rate. *Drug Discov. Today Technol.* **2012**, *9*, e79–e85. [CrossRef] [PubMed]
173. Murugan, R.; Ramakrishna, S. Design Strategies of Tissue Engineering Scaffolds with Controlled Fiber Orientation. *Tissue Eng.* **2007**, *13*, 1845–1866. [CrossRef]
174. Freed, L.E.; Vunjak-novakovic, G.; Biron, R.J.; Eagles, D.B.; Lesnoy, D.C.; Barlow, S.K.; Langer, R. Biodegradable polymer scaffolds for tissue engineering. *Bio/technology* **1994**, *12*, 689–693. [CrossRef]
175. Pham, Q.P.; Sharma, U.; Mikos, A.G. Pham2006. *Tissue Eng.* **2006**, *12*, 1197–1211. [CrossRef]
176. Li, M.; Mondrinos, M.J.; Chen, X.; Gandhi, M.R.; Ko, F.K.; Lelkes, P.I. Co-electrospun poly(lactide-co-glycolide), gelatin, and elastin blends for tissue engineering scaffolds. *J. Biomed. Mater. Res. Part A* **2006**, *79*, 963–973. [CrossRef]
177. Chandrasekaran, A.R.; Venugopal, J.; Sundarrajan, S.; Ramakrishna, S. Fabrication of a nanofibrous scaffold with improved bioactivity for culture of human dermal fibroblasts for skin regeneration. *Biomed. Mater.* **2011**, *6*, 015001. [CrossRef] [PubMed]

Review

A Systematic Review of Drug-Loaded Electrospun Nanofiber-Based Ophthalmic Inserts

Safaa Omer and Romána Zelkó * (ID)

University Pharmacy Department of Pharmacy Administration, Semmelweis University,
1092 Budapest, Hungary; safaa.omer@phd.semmelweis.hu
* Correspondence: zelko.romana@pharma.semmelweis-univ.hu; Tel.: +36-1-217-0927

Abstract: Currently, ocular inserts and nanoparticles have received much attention due to the limited bioavailability of conventional eye preparations and the toxicity problems of systemic drug administration. The current systematic review aims to present recent studies on the use of electrospun nanofiber-based ocular inserts to improve the bioavailability of drugs used for different ophthalmic diseases. A systematic search was performed in PubMed, Ovid Medline, Web of Science, ScienceDirect, Scopus, Reaxys, Google Scholar, and Google Patents/Espacenet taking "drug-loaded", "nanofibers", and "ophthalmic inserts" and their equivalent terms as keywords. The search was limited to original and peer-reviewed studies published in 2011–2021 in English language. Only 13 out of 795 articles and 15 out of 197 patents were included. All results revealed the success of nanofiber-based ocular inserts in targeting and improved bioavailability. Ocular inserts based on nanofibers can be used as safe, efficient carriers for the treatment of anterior and posterior eye diseases.

Keywords: ophthalmic inserts; drug-loaded; nanofibers; electrospinning

1. Introduction

The unique anatomy and physiology of the eye, because of the physical and blood barriers, makes the targeting of ocular diseases a very difficult and challenging process [1,2]. These barriers interfere with drug absorption and diminish the drug concentration in the eye due to dilution and early drainage through lacrimation and poor permeation due to the effect of blood-retinal and blood-aqueous barriers [3–5]. Drugs used for the treatment of ocular disorders are administered via different routes (Figure 1): systemic, topical, subconjunctival, intrastromal, intracameral, intrascleral, intravitreal, suprachoroidal, and subretinal [6,7]. Oral administration of most drugs is subjected to kidney clearance, hepatic clearance, and failure of absorption due to physical and blood barriers. Likewise, absorption of drugs with the use of parenteral administration may subjected to retardation by blood-aqueous and blood-retinal barriers [8,9]. The most frequently used method is administration of drugs through the conventional topical route, which is characterized by being non-invasive, easy to self-administer, and more acceptable to patients. Nevertheless, it can only be used for the treatment of diseases affecting the surface and anterior segment of the eye, because it has poor bioavailability (less than about 5% of the drug is retained on the ocular surface). In addition, this method is not suitable for hydrophobic drugs or drugs that are unstable at a pH level tolerable to the eye and require frequent administration in order to overcome the barriers and nasolacrimal duct drainage [10,11]. Suitable for administration of up to 500 µL and relatively less invasive, subconjunctival administration is a highly convenient route and can be successfully used for targeting anterior or posterior segments [6,7]. Direct administration of the drug to the site of action with lower bioavailability can be done invasively based on intraocular routes [6], with intravitreal injection being the most promising for targeting posterior diseases, but it can be accompanied by retinal detachment, increased intraocular pressure, intravitreal hemorrhage, cataract, or endophthalmitis, which results in poor patient adherence [2,12].
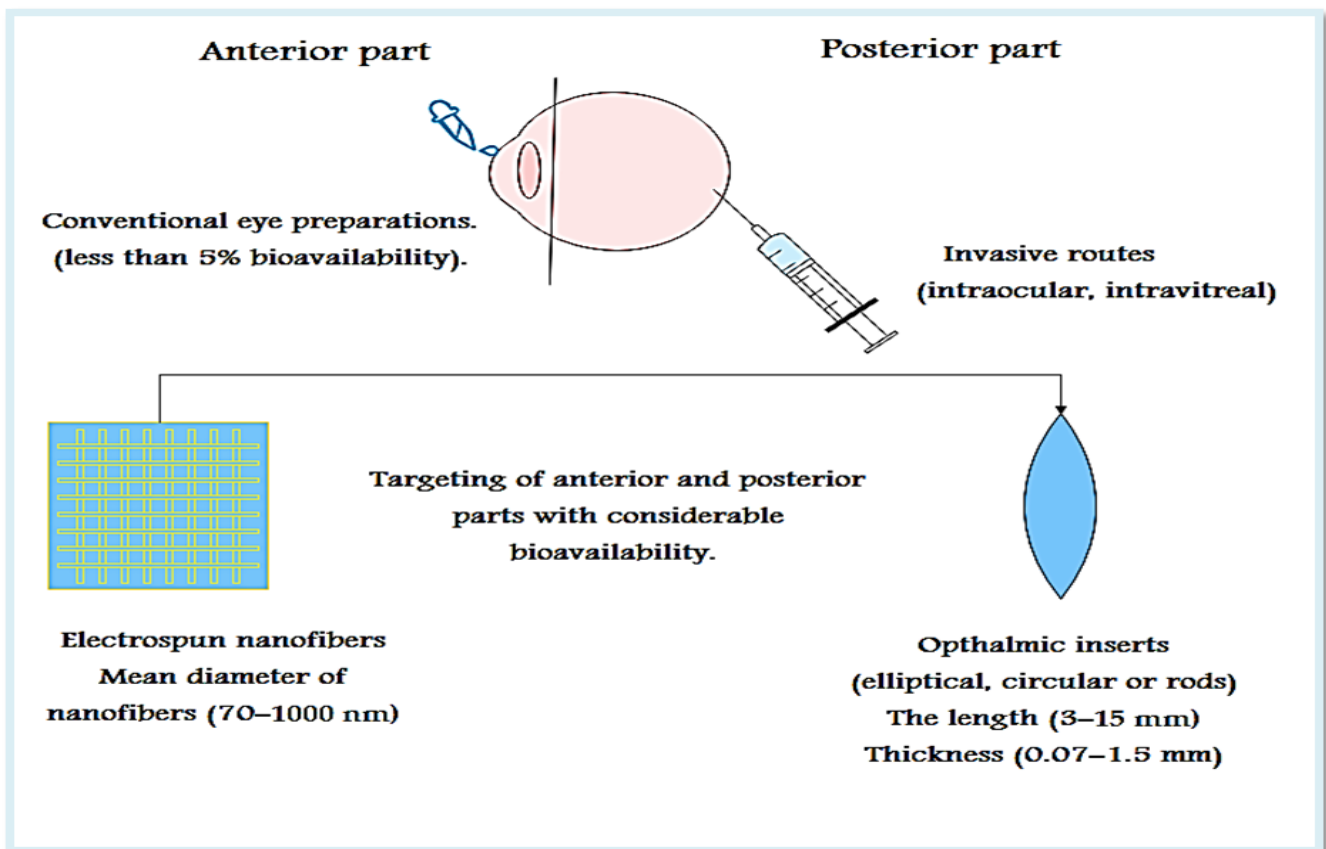
**Figure 1.** The most common routes of targeting different parts of the eye.

Apart from the conventional and parenteral routes, many alternatives, such as permeation enhancers, viscosity modifiers, pro-drug strategies, nanoparticles, long-term or permanent punctal inserts, corneal shields, contact lenses, mini-tablets, disposable lenses, biodegradable polymer systems, hydrogels, implants, and inserts, have been investigated to overcome the ocular barrier problem and increase bioavailability [12–16]. They act by increasing the contact time and slowing down the elimination of the drug from the eye [14]. A very promising approach for ocular targeting is the use of novel drug delivery systems based on nanotechnology; consisting of colloidal particles with sizes ranging from 1–1000 nm [17], nano-carrier drug delivery systems easily penetrate different barriers and have a lower chance of causing eye irritation. Moreover, they offer targeted and sustained release effects [18,19]. They include, but are not limited to, nanocapsules, liposomes, nanomicelles, lipid nanoparticles, niosomes, dendrimers, nanosuspensions, nanoemulsions, and nanocrystals [20,21].

Among the novel alternative approaches, ophthalmic inserts are sterile solid or semi-solid devices consisting of polymeric material with or without medicament, whose suitable size and shape are designed to be placed into the conjunctival sac [22]. Ocular inserts have received attention, as they increase the residence time of the drug on the eye surface, allow slow and controlled drug release, and reduce the overall dose and dose frequency. Moreover, they are stable and eliminate the need for preservatives, thereby reducing the possible side effects and increasing the shelf life of the drug compared to liquid formulations. They are classified into soluble, insoluble, and bio-erodible inserts. Soluble and erodible inserts undergo slow dissolution and do not need to be removed, and insoluble inserts should be removed from the eye when they are free of drugs [23].

Drug release from ocular inserts takes place by three mechanisms: diffusion, osmosis, and erosion. Ocular inserts are prepared using solvent casting, glass substrate, and melt extrusion [24] techniques, and electrospinning (Figure 2) has been used as a simple, ver-

satile technique for the production of nanofibrous film with unique properties [25]. The process of electrospinning is highly flexible and provides the chance to fabricate a wide range of natural and synthetic polymers or drugs; the technique relies on the application of a high voltage between the metallic needle and a grounded collector [26,27]. When the applied voltage exceeds certain critical value, the liquid is ejected from the needle, forming a conical droplet known as Taylor's cone, followed by elongation, thinning and precipitation on the surface of the collector [27]. The resulted fibers are randomly deposited, but for more structured and aligned fibers rotating mandrel or a wheel-like collector are used [28]. The electrospun nanofibers with diameters of 100 nm [29] are constructed from a wide range of biodegradable and biocompatible polymers. The process is carried out simply by applying a high voltage to a drug or mixture of a drug and polymer solution or melts. The drugs can be incorporated through different methods such as blending, surface immobilization, and emulsion [28]. A wide range of drug materials can be encapsulated ranging from small inorganic molecule to large molecules of biological drugs such as protein and nucleic acids. In addition, the technique enables delivery of more than one drug in one step. The produced fibers have unique properties making them a suitable candidate for variety of pharmaceutical and biomedical [26,28,30]. Their large surface area enables ease of surface engineering and modification using different materials, such as permeation enhancers and mucoadhesive agents, and with the proper polymer selection, systems with controlled, sustained, and targeted release can be produced [31–33]. Furthermore, the produced fibers are homogeneous and highly reproducible [34], and due to their characteristic size and texture, they also represent good candidates for tissue reconstitution and promotion of human astrocytoma cell growth [35] and cell migration and proliferation [36]. A wide range of polymers are used for the fabrication of nanofibers for ocular uses, they are classified as natural, semisynthetic, and synthetic [37]. The final properties and quality of fibers are determined by many factors of which the type and concentration of polymers are of paramount importance. Some of the suitable polymers for the electro-spinning technique include polyesters (e.g., poly-glycolic acid- (PGA), poly-lactic acid- (PLA), polycaprolactone- (PCL)) [33]. These polymers are characterized by possessing sufficient mechanical strength to be electrospun, biocompatible, and useful for cell adhesion [34]. In some cases, a blend of the polymers is used together to control the drug release. Other cases include surface modification such as coating with mucoadhesive polymers or complexation with solubility or permeability enhancers [33]. According to the general rule, like dissolves like, hydrophilic polymers are a suitable candidate to encapsulate hydrophilic drugs without sustaining the release, while hydrophobic polymers can modulate sustained effects [37]. Natural polymers are widely used for biomedical applications [38], but synthetic polymers are used to fabricate products with superior quality; therefore, a combination of polymers from different origins is more advantageous for added functional properties [37]. Chitosan is a polysaccharide with a cationic amino group with wide pharmaceutical and biomedical applications [39]. The presence of an amino group leads to extensive protonation in aqueous media due to electrostatic interaction with a solvent molecule, which alters the solubility, viscosity, and mucoadhesive properties of the polymer [40]. Chitosan has gained significant attention in ophthalmic formulations due to its mucoadhesive properties, biocompatibility, and biodegradability and can increase drug permeability [19,41,42]. Nevertheless, it has several limitations include low stability in acidic media and poor mechanical strength. Complexation with cyclodextrins has been developed to strengthen the chitosan structure [43]. Another polymer relatively similar to chitosan is hyaluronic acid; it is a mucoadhesive polymer, forming a hydrogen bond with mucin; hence, it can successfully be used to prolong the drug release rate [37]. Gelatin as biopolymer is a natural protein of an animal origin that contains arginine-glycine-aspartic acids and metalloproteinase residues. Being widely available with lower antigenicity, possessing good bioadhesive properties, and promoting tissue regeneration renders it a good candidate for several biomedical and drug delivery applications. However, it has poor aqueous stability and low mechanical strength [44]. Integration of carbon nan-

otubes, graphene oxide, and carbon nano-onion into gelatin base improves mechanical strength and enables surface modification [45]. The drug loading and release kinetics are affected by molecular weight and cross-linking of the gelatin [46]. Poly-caprolactone (PCL) is a semi-crystalline hydrophobic biopolymer characterized by being biocompatible, possess significant toughness, soluble in most organic solvents; therefore, it is suitable for biomedical and drug delivery purposes [33]. In addition, it has a slow degradation rate, thereby can extend the drug release [25]. However, PCL has some limitations, such as insufficient strength, which necessitates additional reinforcement, such as integrating carbon nano-onions [47,48]. Bovine serum albumin (BSA) can be used as a nanocarrier for various drug molecules, incorporated through electrostatic interactions and covalent or non-covalent conjugation. It has many advantages, including being affordable, producing no immunogenic response, biodegradable, and modulating for different release patterns. Although it is very difficult to produce electrospun nanofibers from BSA alone, they can be combined with other polymers such as polyvinyl alcohol (PVA) and polyethylene oxide (PEO) [49]. Zein is a water-insoluble plant protein that has been used in drug delivery and coating. It requires physical and chemical treatment to improve its low mechanical strength and increase its water stability. Poly 4-mercaptophenyl methacrylate-carbon nano-onions can be incorporated within zein for enforcement of the mechanical strength [50].
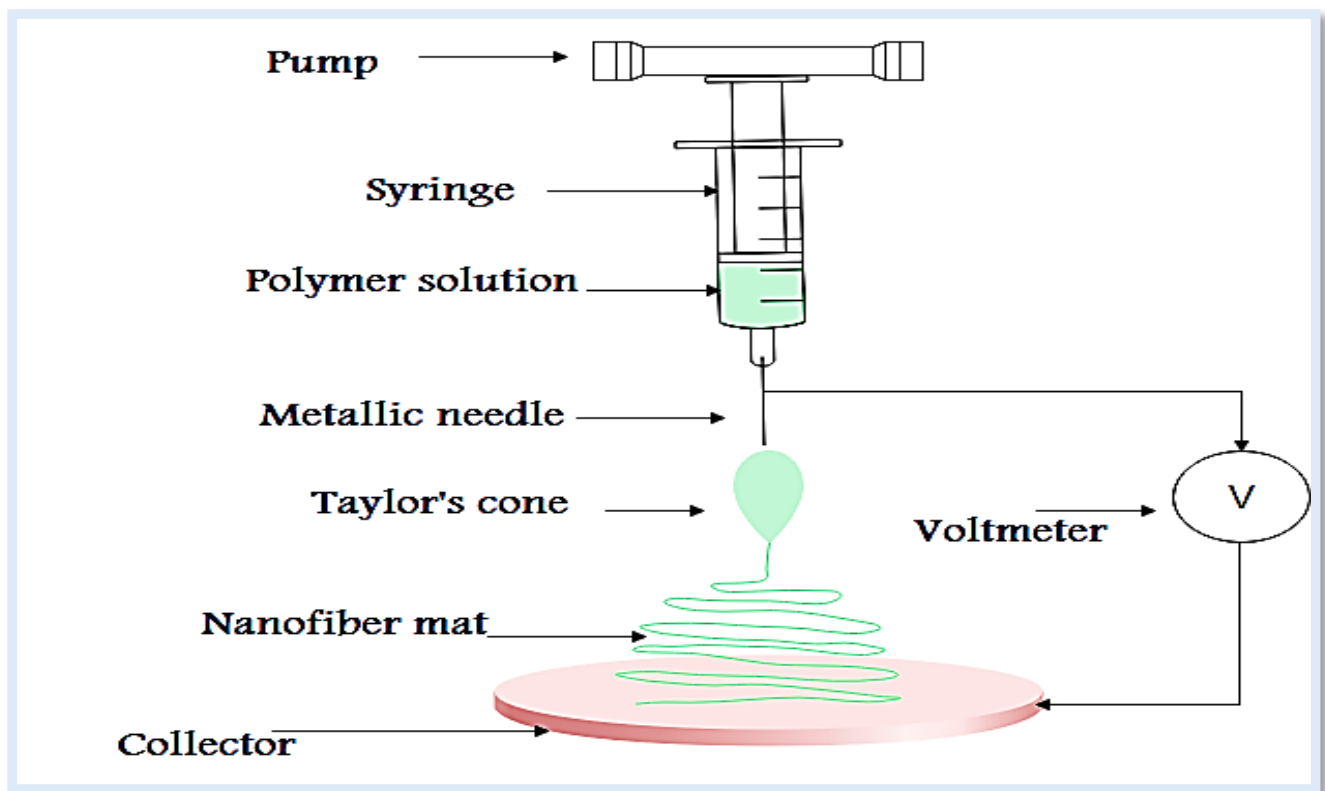
Figure 2. Schematic diagram of electrospinning process.

Although there are many published reviews describing ocular inserts, few of them cover the formulation of ocular inserts based on nanofibers; therefore, the current systematic review aims to describe the use of ocular inserts in the treatment of various eye diseases by shedding light on nanofiber-based ocular inserts as a promising, non-invasive method for targeting the posterior segment of the eye and improving bioavailability.

2. Materials and Methods

Preferred Reporting Items for Systematic Reviews and Meta-Analyses (PRISMA 2020) guidelines were followed to search for the relevant studies and report construction.

2.1. Eligibility Criteria

The following criteria were set for articles to be eligible for inclusion in this systematic review: Original research studies published in peer-reviewed journals and published patents were included, while review articles, conference papers, editorials, and commentaries were not. The study was limited to articles published in 2011–2021 in the English language. In addition, only ocular inserts or products to be placed in the conjunctival sac or cul-de-sac were considered, and all other dosage forms, including contact lenses and ocular implants, were excluded. The study included only nanofibrous ocular inserts fabricated via electrospinning technique; other techniques for fiber production were not considered. No clinical trial limits were set, and all in vitro and in vivo studies were eligible. Studies comparing electrospinning with other techniques were also included.

2.2. Search Strategy

To find the relevant articles and patents of drug-loaded electrospun nanofibrous ocular inserts, a systematized search was performed in PubMed, Ovid Medline, Web of Science, ScienceDirect, Scopus, Reaxys, Google Scholar, Google Patents, and Espacenet using the specified keywords together with their equivalent synonyms. We built up our search queries as: (Drug-loaded) AND (electrospinning) AND (Nanofibers OR nanofibrous) AND (ocular inserts OR ophthalmic inserts). The results were synthesized and tabulated accordingly.

2.3. Data Collection and Extraction

We used a PRISMA 2020 flow diagram to extract the most relevant data essential for synthesizing the results. First, all results obtained from all databases were exported to the Mendeley reference manager, and duplicate studies were removed. The rest of the articles underwent two successive screening processes: Irrelevant articles based on title were immediately excluded, then the abstracts and full texts of eligible articles were reviewed and analyzed. The relevant articles were double-checked by the reviewers based on the inclusion criteria, and the required information was extracted and tabulated into the following variables: polymer base, loaded drug/concentration, dimensions of inserts used in the study, diameter of nanofibers, in vivo animal model, and effects/properties of presented system.

3. Results

3.1. Database Search and Included Studies

A total of 795 articles and 197 patents were obtained from all database searches, among which 594 were from Science Direct, 47 from PubMed, 42 from Web of Science, 39 from Scopus, 31 from Reaxys, 24 from Google Scholar, and 18 from Ovid Medline. Of the total patents obtained, 118 were from Google Patents, 34 from Espacenet, and 45 from Reaxys. Only 13 articles and 15 patents were included in the review, and they were selected based on the specified inclusion criteria. The process of identification and screening is presented in Figure 3.

3.2. Results of Studies

According to the specified criteria, all relevant articles were thoroughly reviewed, and are summarized in Table 1. According to the extracted relevant information, New Zealand albino rabbits and some in vitro models are used to study eye toxicity, and the results revealed no or lower eye toxicity. The main focus was on increased residence time and bioavailability. The results showed the possibility of modulating the drug release from a few minutes up to a month based on the polymer base used and the properties of nanofibers, and the majority of studies showed controlled drug release. The formulations were compatible with the eye and the particle size showed no signs of ocular irritation.
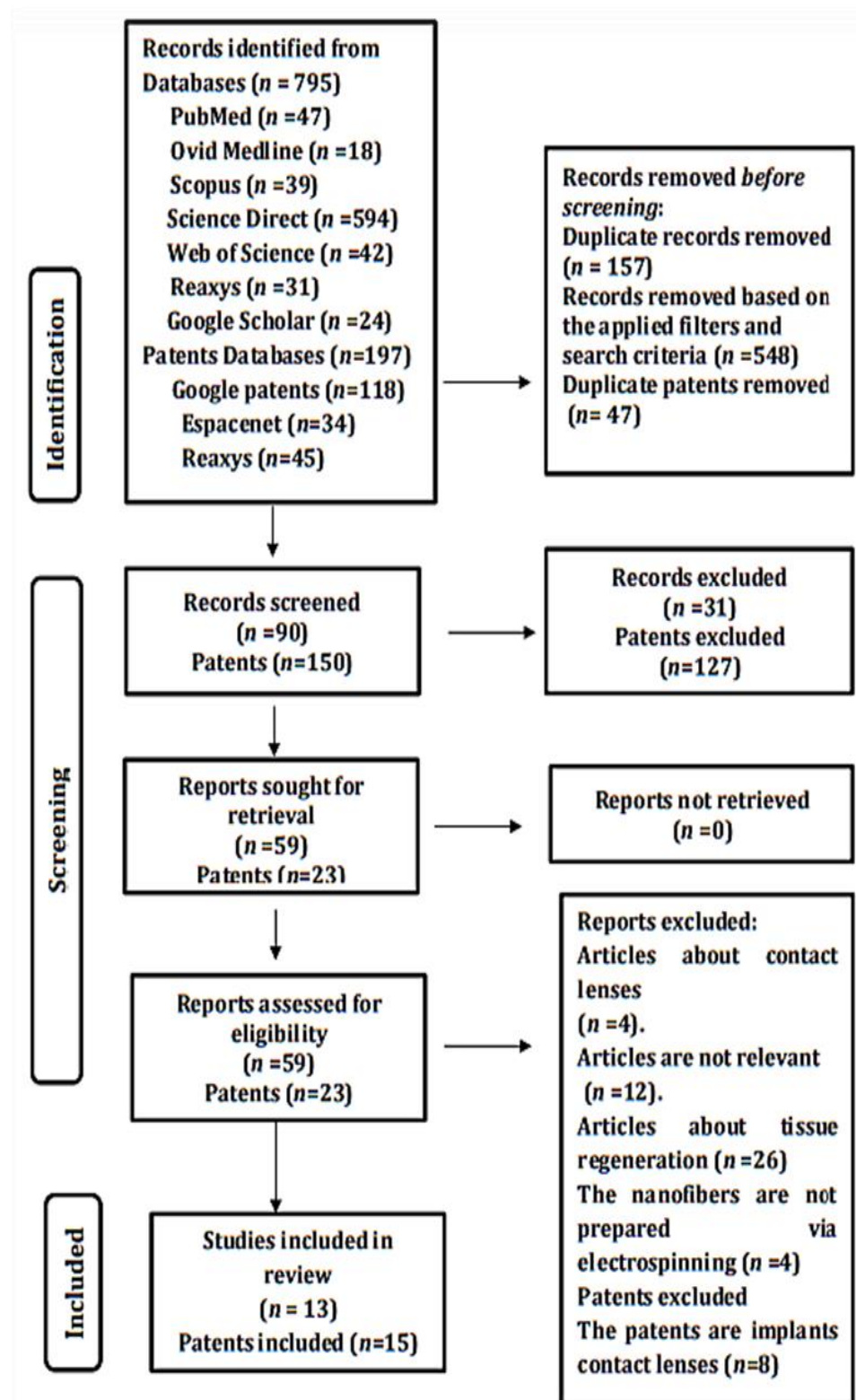
Figure 3. PRISMA-2020 flow diagram showing relevant articles and patents included in the study.

Here is a summary of the published studies based on the use of electrospinning technology for the fabrication of nanofiber-based ocular inserts and formulations designed to be used in the cul-de-sac: Besifloxacin HCl loaded inserts were prepared by electrospinning and investigated in in vitro, ex vivo, and in vivo studies as a potential alternative to commercial formulations. The formulations were subjected to modification with the addition of mucoadhesive polymer (sodium alginate (SA) or thiolated sodium alginate (TSA) as

coating material) or corneal permeation enhancer (HP-β-CD) to the base polymer system of poly-caprolactone (PCL) and polyethylene glycol (PEG) in a 2:1 ratio of PCL/PEG. The in vitro studies, including thickness, diameter, degradation, and encapsulation, were within acceptable limits. The studies showed that the formulations produced no cytotoxic effect, with notable activity against bacteria. Corneal keratitis was significantly reduced by treatment with TSA-coated and HP-β-CD drug complex inserts [33].

Core-shell electrospinning was successfully used to fabricate a nanofibrous mat of pirfenidone-PLGA/moxifloxacin-PVP for the treatment of corneal abrasion. The results showed non-porous and smooth fibers with a diameter of 630 ± 220 nm that were capable of sustaining the release of both drugs and suitable for once-daily use [36]. The same results from pharmacokinetics studies showed the possibility of extended release over 24 h, while a Draize test showed mild irritation to the eye. Furthermore, antimicrobial and anti-scarring effects obtained were comparable to those of free solution [51].

Electrospun nanofiber inserts were fabricated and compared to inserts prepared by solvent casting employing poly-lactic acid (PLA) and poly-vinyl alcohol (PVA) as the polymeric system. The results showed thin, uniform inserts of nanometer size. In addition, the drug content was found to be more uniform in the inserts prepared by electrospinning, and it was concluded that electrospun nanofiber inserts could be a potential alternative to conventional eye drops [52]. Electrospun nanofibers loaded with gentamicin and methylprednisolone were prepared in different structures (single-jet electrospinning, sandwich structure using single-jet electrospinning, and core-shell electrospinning). All formulations were evaluated for physicochemical and antibacterial properties against *S. aureus*. The formulations showed acceptable mechanical and antimicrobial activity, with diameters of 70–350 nm, and the core-shell preparation showed the best drug release [53].

New nanofiber-based ocular inserts were prepared using hyaluronan (HA) and polyvinylpyrrolidone (PVP) for dual delivery of ferulic acid (FA) as antioxidant and ε-polylysine (ε-PL), an antimicrobial peptide. Two series of inserts were prepared, blank, and FA-loaded. The prepared inserts were subjected to physical, morphological, compatibility, release, and antimicrobial studies. The results showed acceptable thickness of 270 ± 21 μm to 273 ± 41 μm with fiber diameter of approx. 100 nm to 1 μm; in addition, they demonstrated adequate drug release, with antimicrobial activity against *Pseudomonas aeruginosa* and *Staphylococcus aureus* [54].

Ocular polymeric inserts loaded with triamcinolone acetonide (TA) have been developed in two steps: electrospinning of a solution of poly-butylene succinate (PBS), followed by surface modification through plasma activation and reaction with inulin, heparin, and α,β-poly(*N*-2-hydroxyethyl)-D,L-aspartamide. The morphological results showed a flexible non-porous scaffold with fibers ranging from 1 to 3 μm in diameter. The surface modification allowed stable, non-erodible, mucoadhesive, and highly loaded inserts that were compatible with human cells; it also allowed extended drug release for up to 30 days [34]. Nanofiber inserts loaded with azithromycin were prepared using a mixture of chitosan, polyvinyl alcohol, and polyvinyl pyrrolidone via electrospinning. The formulated inserts were subjected to physicochemical, morphological, in vitro, and in vivo release, antibacterial activity, cytotoxicity, and ocular irritation evaluation. The results showed acceptable hardness and uniform weight and thickness, with fiber diameter ranging from 119 ± 29 to 171 ± 39 nm. The inserts were also found to be nontoxic and non-irritating to the rabbits' eyes. The drug release was extended up to 6–8 days [55].

In an attempt to target retinal inflammatory disease, nanofibrous ocular inserts loaded with fluocinolone acetonide were prepared and evaluated for permeability, in vivo pharmacokinetic, and in vivo release as well as other mechanical and chemical characteristics. Preclinical results revealed the possibility of retinal delivery with no cytotoxicity. The obtained fibers were smooth, non-woven, and homogeneous. Degradation and release studies confirmed extended drug release up to 12 days [25].

Nanoparticles loaded with azithromycin were incorporated into electrospun nanofibers to obtain ocular inserts that were mucoadhesive and biodegradable. The formulations were

characterized in vitro, ex vivo, and in vivo. The results showed improved bioavailability, low risk of toxicity, and prolonged drug release over 10 days [56]. Two polymer series, polycaprolactone (PCL) and polyvinyl alcohol (PVA), were used to formulate biodegradable polymeric patches containing timolol maleate and dorzolamide hydrochloride for cul-de-sac insertion. The formulations were characterized in terms of morphology, folding endurance, drug release, ocular irritation, and in vivo efficacy. The fibers were uniform and smooth with sufficient mechanical strength. An in vitro release study for up to 24 h confirmed a single daily dose. Ocular irritation results showed minor irritation with PCL formulation and no comparable effect with PVA patches. The products successfully reduced the induced intraocular pressure and maintained for up to 72 h [57].

An internal layer of hydrophilic chitosan/polyvinyl alcohol (CS/PVA) and an outer layer of hydrophobic Eudragit RL100 were used in the fabrication of ocular inserts for delivery of ofloxacin (OFX) to increase the residence time on the eye. All parameters related to strength, thickness, and morphology were within acceptable limits. The formulations showed significant in vitro antimicrobial activity against *S. aureus* and *E. coli.* The formulations allowed prolonged release for up to 95 h with no signs of ocular irritation as demonstrated by in vivo studies [58]. Four formulations were used to prepare nanofibrous ocular inserts; three of them were chitosan-based and the fourth was composed of Eudragit S100 and Zein for sustained delivery of triamcinolone acetonide. All fibers were smooth and fibrous except the formulation containing a mixture of PVP, PVA, and chitosan. In vitro release studies demonstrated sustained drug release (zero-order rate), and no in vivo studies have been done [38].

Based on the results summarized in Table 1, it is obvious that the formulation of these ocular inserts depends on the use of natural and/or synthetic polymers. These polymers are involved in determining the final quality of products. The most widely used polymers include polyglycolic acid (PGA), polylactic acid (PLA), polycaprolactone (PCL), polyvinyl alcohol (PVA), polyacrylic acid (PAA), polyvinyl pyrrolidone, hyaluronic acid, chitosan (CS), polyethylene oxide (PEO), polymethacrylate, and cellulose derivates [25,33,37,41]. The majority of these polymers are biodegradable and classified as being soluble, insoluble, or bioerodible. With the proper base selection, a wide range of ocular inserts with different forms of drug release and targeting can be obtained. The results of many studies based on polymer type are given in Table 2.

Table 1. Summary of nanofiber-based ocular insert studies.

No	Polymer Base	Loaded Drug/Concentration	Dimensions of Inserts Used	Diameter of Nanofibers	In Vivo/Animal Model	Effects/Properties	References
1	Polycaprolactone (PCL), polyethylene glycol (PEG), sodium alginate (SA), thiolated sodium alginate (TSA)	Besiloxacin HCl (BH) (40 µg per 1 cm^2)	3.5 mm^2 (thickness: 0.66 ± 0.004; diameter: 6.7 ± 0.012)	Less than 1057 nm	Yes, New Zealand albino rabbits	• Besifloxacin HCl loaded inserts were developed and investigated in vitro, ex vivo, and in vivo for treatment of bacterial keratitis • SA and TSA increased bioadhesion of formulations • Inserts showed burst release in first 2 days, followed by slow-release profile	[33]
2	Poly-lactic-co-glycolic acid (PLGA), polyvinylpyrrolidone (PVP)	Moxifloxacin HCl (1% *w/v*) pirfenidone (2% *w/v*)	0.5 cm × 0.5 cm	Drug-loaded fibers were 630 ± 300 nm	Yes, New Zealand male albino rabbits,	• Step 1: Successful fiber preparation with encapsulation of two drugs and sustained drug release • Step 2: In vivo pharmacokinetic, antimicrobial, and scar healing properties; release rate over 24 h	[36,51]
3	Polylactic acid (PLA), poly(vinyl alcohol) (PVA)	Dexamethasone (1, 5, and 10% *w/w*)	Thickness of fibers ranged from 50 to 93 µm	Within nanometer size	No in vivo studies have been done	• Electrospun nanofibrous inserts were fabricated and compared to solvent casting ocular inserts • Electrospun nanofibrous inserts showed first-order release rate • Results revealed superiority of electrospun nanofibrous inserts over solvent cast inserts	[52]
4	Polycaprolactone, poly (lactic-co-glycolic acid), polyvinyl alcohol	Gentamicin (GNT) (10% *w/w*), methylprednisolone (MP) (6% *w/w*)	NA	Mean range was 70–650 nm	No in vivo studies have been done	• Simple, sandwich, and core-shell nanofibers were prepared and evaluated for dual sustained delivery of gentamicin (GNT) and methylprednisolone (MP) • Core-shell formulation showed best release profile	[53]
5	Hyaluronan (HA), polyvinylpyrrolidone (PVP)	Ferulic acid (FA) (5.7 ± 0.2% *w/w*)	Mean thickness of 270 ± 21 µm	Approx. 100 nm to 1 µm	No in vivo studies have been done	• Development and evaluation of nanofiber inserts for dual release of ferulic acid and ε-polylysine (ε-PL) • Blank inserts released ε-PL within 30 min and FA-loaded inserts completely released antioxidant within 20 min • All formulations were effective against Pseudomonas aeruginosa and S. aureus	[54]

Table 1. *Cont.*

No	Polymer Base	Loaded Drug/Concentration	Dimensions of Inserts Used	Diameter of Nanofibers	In Vivo/Animal Model	Effects/Properties	References
6	Poly(1,4-butylene succinate) (PBS)	Triamcinolone acetonide (TA) (2 mg/cm^2)	Scaffold disk: 0.4 cm diameter	Range of 1–3 μm	No in vivo studies have been done	• Preparation of novel inserts loaded with triamcinolone acetonide • Further modification through plasma-induced chemical functionalization • Formulation resulted in sustained drug release (up to 30 days, Higuchi model) with good compatibility with human cells	[34]
7	Chitosan/polyvinyl alcohol/polyvinyl pyrrolidone (CS/PVA-PVP)	Azithromycin (AZM)(10% *w/w*)	Diameter: 6 mm; thickness: 0.108 ± 0.012 to 0.121 ± 0.002 mm	Mean range of 119.01 ± 29.77 to 171.61 ± 39.40 nm	Yes, New Zealand rabbits	• Nanofiber inserts loaded with azithromycin were prepared • Stable • Uniform weight and thickness • Non-irritating and non-toxic • Cross-linked nanofibers enabled more controlled drug release than non-cross-linked	[55]
8	Polycaprolactone (PCL)	Fluocinolone acetonide (1–5% *w/w*)	2 cm^2	Average range of 350–400 nm	Yes, New Zealand white rabbits	• Development and characterization of preservative-free nanofibrous ocular inserts • Homogeneous, non-woven nanofibers • Burst drug release phase followed by a steady release rate up to 11 days • High drug permeation to retina • No ocular irritation	[25]
9	Poly(lactic-co-glycolic acid) copolymer/pluronic polyvinylpyrrolidone	Azithromycin (10 m/1 cm^2)	1 cm^2	Range of 200–550 nm	Yes, albino rabbits	• High bioavailability • Highly biodegradable and biocompatible • Drug release over 10 days	[56]
10	Polycaprolactone (PCL),polyvinyl alcohol (PVA)	Timolol maleate (0.5% *w/v*), and dorzolamide hydrochloride (0.2% *w/v*)	1 × 1 cm^2	Range of 200–400 nm	Yes, New Zealand white albino rabbits	• Development of nanofibrous patch for insertion into cul-de-sac for treatment of glaucoma • Fibers were uniform and smooth • Results showed significant bioadhesion with sustained drug release up to 24 h • No ocular irritation with PVA; mild irritation with PLC formulation • Significant reduction of intraocular pressure	[57]

Table 1. *Cont.*

No	Polymer Base	Loaded Drug/Concentration	Dimensions of Inserts Used	Diameter of Nanofibers	In Vivo/Animal Model	Effects/Properties	References
11	Chitosan/polyvinyl alcohol (CS/PVA), Eudragit RL100	Ofloxacin (OFX) (0.6% *w/v*)	Thickness range: 0.075 ± 0.002 to 0.095 ± 0.002 mm	Average 123 ± 23 to 159 ± 30 nm	Yes, New Zealand white albino rabbits	• Two-layer ocular inserts for enhancement of residence time were developed • Acceptable morphological and mechanical parameters • Release up to 95 h • In vivo studies revealed no ocular irritation	[58]
12	Chitosan, polyvinyl alcohol (PVA), polyvinyl pyrrolidone (PVP), Eudragit S100,Zein	Triamcinolone acetonide (1% *w/v*)	NA	Range of 120 ± 30 to 172 ± 48 nm	No in vivo studies have been done	• Development and evaluation of chitosan-based ocular inserts for sustained drug release • Prolonged release was obtained (zero-order kinetics)	[38]

Table 2. Ocular inserts formulations and base types.

Drug (Concentration)	Applied Polymer Base	Type of Base (Soluble/Insoluble/Erodible)	Effect/Aim	References
Azithromycin (20% *w/w*)	Hydroxypropylmethyl cellulose (HPMC) and Eudragit RL100	Erodible	• To prolong release and improve ocular availability • Release: over 12 h	[10]
Triamcinolone acetonide (0.5% *w/w*)	Poly(1,4-butylene succinate) extended with 1,6-diisocyanatohexane (PBS)	Insoluble	• Non-erodible mucoadhesive to sustain release • Release of active for 30 days	[34]
Azithromycin (10% *w/w*)	Hydroxypropyl methylcellulose (HPMC) or hydroxyethyl cellulose (HEC).	Soluble and erodible	• Polymeric inserts to sustain drug release • Significantly prolonged release of AZM in rabbit eyes (121 h)	[59]
Cetirizine (7.5% *w/v*)	Hydroxypropyl methylcellulose (HPMC) and polyvinyl alcohol (PVA)	Soluble and erodible	• To ensure sustained drug release and increased residence time • 210 min	[60]
Ofloxacin (1.5 and 6% *w/w*)	Poly(ethylene oxide) (PEO 400 or PEO 900)	Erodible	• To be able to release different drugs of interest in ophthalmology	[61]
Besifloxacin HCl (40 μg/cm^2)	Poly(caprolactone)/polyethylene glycol (PLC/PEG) (2:1)	Erodible	• To reduce application frequency and increase patient compliance • 7 days	[33]

Table 2. *Cont.*

Drug (Concentration)	Applied Polymer Base	Type of Base (Soluble/Insoluble/Erodible)	Effect/Aim	References
Dorzolamide HCl (0.37% *w/v*)	Polyvinyl alcohol, poloxamer 407	Soluble	• Comparative result shows that dorzolamide HCL soluble insert was more effective than marketed formulation	[62]
Timolol maleate (TM) (0.5% *w/v*)	Hyaluronic acid (HA) and hydroxypropyl methylcellulose (HPMC)	Erodible	• To enhance drug retention on ocular surface and potentially improve bioavailability	[63]
Moxifloxacin hydrochloride (5% *w/w*)	Eudragit™ FS-100 (FS) and propylene glycol (PG)	Soluble	• To provide a once-a-day application as an alternative delivery system in management of bacterial infections	[64]
Gatifloxacin (2.4 mg/78.5 mm^2)	Thiolated sodium alginate (TSA), sodium alginate (SA), and acrylates: ERL:ERS (75:25)	Erodible	• Inserts for twice-a-day therapy with gatifloxacin	[65]
Dexamethasone (1%, 5% and 10% *w/w*)	Polylactic acid (PLA) and poly-vinyl alcohol (PVA)	Erodible	• Nanofibrous inserts were better than solvent cast inserts and could be utilized as a potential delivery system for treating anterior segment ocular diseases	[52]
Curcumin (1% *w/w*)	Carboxymethylcellulose (CMC), polyvinyl alcohol, hydroxypropyl methylcellulose	Soluble	• Developed inserts demonstrated acceptable ocular tolerability, enhanced corneal permeability, and sustained release	[66]
Lysozyme (3% *w/w*)	Hydroxypropyl methylcellulose (HPMC)	Erodible	• Novel drug delivery system (DDS) with sustained release properties was developed to allow ocular protein delivery	[67]
Gentamicin sulfate (25.0% *w/w*)	Mixture of hydroxypropyl cellulose, ethyl cellulose, poly(acrylic) acid	Soluble	• Inserts ensured effective gentamicin levels over 72 h	[68]
Indomethacin (IN; 10% *w/w*), prednisolone sodium phosphate (PSP; 10% *w/w*), ciprofloxacin hydrochloride (CIP; 10% *w/w*)	Polyethylene oxide (PEO) N10	Erodible	• Noninvasive ocular inserts for posterior segment • Trans-membrane flux of IN, prednisolone sodium phosphate, and ciprofloxacin hydrochloride was enhanced by ~3.5, ~3.6, and ~2.9-fold, respectively • Ocular inserts generated significantly higher drug levels in all ocular tissues, including retina-choroid, compared with control formulations	[69]

Table 2. *Cont.*

Drug (Concentration)	Applied Polymer Base	Type of Base (Soluble/Insoluble/Erodible)	Effect/Aim	References
Valacyclovir HCl (20% *w/w*)	HPC and HPMC	Soluble and erodible	• Ocular inserts showed improved flux compared with control formulation • Ocular inserts dissolved completely within 8 h	[70]
Fluorescein (3% *w/w*), lysozyme (3% *w/w*), albumin (3% *w/w*)	HPMC	Erodible	• Ophthalmic inserts with sustained release properties as carriers for thermo-labile therapeutics	[71]
Gentamicin sulfate (25.0% *w/w*), dexamethasone phosphate (5.0 and 25% *w/w*)	Hydroxypropyl cellulose (HPC)	Soluble	• New system ensures concomitant release of drugs during first 10 h of treatment, followed by adequate concentration of gentamicin sulfate	[72]
Ketorolac tromethamine (KT; 1% *w/v*)	Eudragit S100 and Zein	Erodible	• Ocular delivery system using electrospun nanofibers as candidate insert for delivery of triamcinolone acetonide • To improve bioavailability	[38]
Ofloxacin (3–9% *w/w*)	Chitosan/polyvinyl alcohol (CS/PVA), Eudragit RL100.	Erodible	• To enhance ocular residence time of ofloxacin • Sustained release pattern up to 96 h	[58]
Brimonidine tartrate (≈10–30% *w/w*)	PEO with Eudragit (RL 100/RS 100)	Erodible	• To design mucoadhesive and extended release ocular inserts; up to 24 h	[73]
Linezolid (LNZ; 0.2% *w/v*)	Modified sodium alginate-grafted poly (butyl methacrylate) and sodium alginate-grafted poly (lauryl methacrylate)	Erodible	• Polymeric thin films with increased ocular residence time and sustained drug release capacity	[74]

3.3. Ocular Insert Patents Studies (2011–2021)

Ocular inserts have recently received attention and many patents have been published demonstrating conventional and nanofiber-based formulations. Some examples of interesting and promising systems are presented here along with summaries, shown in Table 3. An Australian patent describes a nanostructured biocompatible wafer for placement in the conjunctival cul-de-sac. The wafer contains a tissue-reactive mucoadhesive polymer, and provides a method for treating glaucoma or infection on the eye surface. The thickness of the wafer is between 0.05 and 0.5 mm, preferably between 0.05 and 0.1 mm, but it is not limited to hydrophobic polymers or any combination of biodegradable polymers, with the polymers available commercially and approved for human use being the best choice [75].

Another patent describes an ocular delivery system that consists of a nanofibrous matrix containing drug-loaded nanoparticles as a candidate for ocular inserts. In addition, the method of preparation (electrospinning) and medical uses of the nanofibrous ocular system are demonstrated, which include anti-microbial, anti-glaucoma, anti-inflammatory, analgesic, anesthetic, or combined effects. Biodegradable hydrophobic polymer and/or biodegradable amphiphilic polymer can be used. The system can also contain a mucoadhesive polymer to provide controlled release of drug over a period of at least 3 days [76].

Another patent describes various shapes of ocular inserts together with methods of preparation and potential uses. Hydrophilic polymers with biodegradable, bioabsorbable, or bioerodible properties are used. In addition to active ingredients, it may contain dyes, lubricant, emollient, and jelling agent. The system can be loaded with thermo-labile, poorly soluble, soluble, micronized, and nanoparticle substances. The pharmaceutically active agents include anti-bacterial, steroidal and non-steroidal anti-inflammatory, anti-allergy, anti-viral, anti-cholinergic, and mydriatic drugs, or any suitable combination [77]. Another patent discusses the bimatoprost composition, preparation, and devices comprising these compositions. These formulations are responsible for sustained release of bimatoprost to the eye. The composition of this invention comprises stable amorphous bimatoprost with a thermoplastic polymer matrix, such as acrylonitrile butadiene styrene (ABS), celluloid, cellulose acetate, ethylene-vinyl acetate (EVA), ethylene vinyl alcohol (EVOH), polyacrylate (acrylic), or polyacrylonitrile (PAN or acrylonitrile). It may contain thermosetting polymers. This medical device can serve as an ocular insert with a ring shape (ring diameter can be about 10 to 40 mm or about 20 to 30 mm) [78].

A patent describes a method for preparing rifampicin film to overcome uneven drug content by using poly-vinyl alcohol (PVA) via a simple method with temperature, pressure, and time control [79]. The patent pertains to ocular inserts for sustained release of steroids to the eye. The steroids are considered as articles from D1-L-D2 (A-I), where D1 and D2 are steroid radicals and L is linker that is covalent to D1 and D2. The article can be fiber, fiber mesh, nanoparticles, microparticles, or woven or non-woven fabric. The linker can be carbonate or carbamate ester [80].

Another patent describes soft polymeric hydrogel ocular inserts that are readily available and comfortable for use to release drug and lubricant to the anterior and posterior segments of the eye in a controlled manner. The hydrogel material is derived from at least one arylborono-containing hydrophilic copolymer and at least one mucoadhesive polymer, and cyclic boronic ester. The patent also describes the method for preparation [81]. Another patent describes atropine sulfate ocular inserts and the method of preparation to enhance stability and bioavailability by utilizing hydroxypropyl methylcellulose, polyvinylpyrrolidone, sodium carboxymethyl cellulose, and gelatin or any suitable combination [82]. Another patent describes the delivery of at least one drug to the desired site of action of the human or animal eye. The system contains at least two polymers, preferably from the class of polyethylene oxide block copolymers and cellulose derived polymers, such as hydroxpropyl cellulose. It may also contain an anti-collapsing agent, such as amino acid. The active ingredients include prostaglandin, beta blockers, alpha agonists, carbonic anhydrous inhibitors, or any suitable combination [83].

Another patent describes polymeric ocular inserts composed of a pharmaceutically active semi-crystalline or crystalline agent dispersed in a polymer matrix in order to provide a formulation that is more stable and has fewer impurities. The method of preparation is also described. The composition includes for example, bimatoprost as a pharmaceutically active ingredient, a polymeric matrix, which is a thermoplastic polymer such as acrylonitrile butadiene styrene, and a thermosetting polymer such as silicone and polyesters [84].

Another patent describes an ocular insert that is considered as a new biocompatible polymer-based controlled drug delivery system for the release of suitable drug to the eye for up to 300 days. The inserts are prepared with different shapes and are suitable for self-administration, and can be inserted in the lower or upper fornix conjunctiva. At least one drug can be incorporated, including antibiotics, antibacterials such as sulfonamides, antivirals, anti-allergy, anti-inflammatories such as hydrocortisone or hydrocortisone acetate, decongestants such as tetrahydrozoline, miotics and anticholinesterase, sympathomimetics such as epinephrine, immunological drugs such as vaccines and immune stimulants, hormonal agents, growth factors, or carbonic anhydrase inhibitors. The polymers used are polycaprolactone (PCL), polyethylene glycol (PEG), or co-polymers PEG-PCL, or a mixture of these [85].

Another intervention aims to provide voriconazole-loaded ocular film for continuous release of the drug. The ocular film consists of nanopolymer fiber and film-forming and other excipients. Electrospinning is used to prepare the film in order to obtain nanopolymer fibers with uniform morphology. Polyvinyl alcohol, acrylic resin, polyvinylpyrrolidone, polyvinylpyrrolidone derivative, cellulose, cellulose derivative, and chitosan individually or in combination are considered to be the best materials for film preparation [86]. Another patent describes dissolvable polymeric eye inserts with a biodegradable polymer for sustained release of drugs and lubricants to the anterior and posterior segments of the eye. They provide a way to treat different eye disorders by incorporating different active pharmaceutical ingredients. The inserts are comfortable for patients and the thickness of the film ranges from 50–250 μm, and preferably from 70–150 μm. The polymers used include hyaluronic acid, hydroxypropyl guar (HP guar), and a plasticizer, such as polyethylene glycol (PEG). The inserts are suitable for insertion in the lower eyelid. The composition is rapidly wetted by tears to release the lubricant. The active ingredients may be added to the same polymeric base [87–89].

Table 3. Summary of ocular insert patents studies (2011–2021).

Insert Base	Targeted Diseases	Model Drug Used for Study	Applicant /Manufacturer/Assignee	Patent Number	Publication Date	Reference
Biodegradable, hydrophobic polymer	Tissue regeneration, glaucoma, infections on eye surface (all are possible)	Travoprost	Integral Biosystems LLC	AU 2019250153 A1	31 October 2019	[75]
Biodegradable, hydrophobic, and/or amphiphilic polymer	Eye infections	Azithromycin	Zewail City of Science and Technology, Egypt	GB 2570113 A	17 July 2019	[76]
Hydrophilic, biodegradable, bioabsorbable, or bioerodible polymer	Glaucoma	Timolol maleate	Valeant International (Barbados) SRL	US2012215184A1	23 August 2012	[77]
Thermoplastic polymer such as acrylonitrile butadiene styrene and ethylene-vinyl acetate	Glaucoma	Bimatoprost	ForSight VISION5 Inc. (US)	US2016022695A1	28 January 2016	[78]
Polyvinyl-alcohol (PVA)	Bacterial infections (tuberculosis (TB))	Rifampicin	Tongling Wutongshu Agricultural Dev. Co. Ltd.	CN104116722A	29 October 2014	[79]
Polymer such as poly-lactic/glycolic acid	Ocular inflammation associated with inflammatory diseases or following ocular surgery	Steroids	Interface Biologics Inc. (CA)	WO2019148291A1	08 August 2019	[80]
Arylborono-containing hydrophilic copolymer	Anterior and posterior segment diseases	Optional	Alcon Inc. (CH)	US2021077385A1	18 March 2021	[81]
Hydroxypropyl methylcellulose, polyvinylpyrrolidone, sodium carboxymethyl cellulose, and gelatin	Myopia	Atropine sulfate	Univ. Shenyang Pharmaceutical	CN111358771A	07 July 2020	[82]
Hydroxypropylcellulose and polyethylene oxide block copolymer	Glaucoma	Timolol maleate	Univ. Witwatersrand JHB (ZA)	WO2014041485A1	20 March 2014	[83]
Thermoplastic polymer such as acrylonitrile butadiene styrene and thermosetting polymer such as silicone and polyesters	Glaucoma	Bimatoprost	ForSight VISION5 Inc. (US)	US2016296532A1	13 October 2016	[84]
Polycaprolactone/polyethelyneglycol	Bacterial infections	Moxifloxacin	Univ. De Coimbra (PT)	WO2017137934A1	17 August 2017	[85]
Poly-vinyl-alcohol	Fungal infections	Voriconazole	Univ. Zhejiang	CN105726517A	06 July 2016	[86]
Hyaluronic acid, polyvinyl-pyrrolidone, hydroxypropyl guar, and polyethyleneglycol	Dry eye	-	Alcon Inc. (CH)	WO2021116907A1 WO2020222195A1 US2021169781A1	17 June 2021 05 November 2020 10 June 2021	[87–89]

4. Discussion

It is a very difficult process to deliver drugs to the eye, especially the posterior segment, due to the presence of physical barriers as well as blood retinal barriers, particularly when using conventional topical formulations. Therefore, scientists have performed many studies on eye diseases in an attempt to deliver drugs to the target site of action with sufficient bioavailability. Nanotechnology-based drug carriers have been investigated for their potential technological and therapeutic advantages for ocular delivery. Nanocarriers are used to deliver drugs for local or systemic effect by being localized to a specific site in the eye and releasing the required drug concentration through diffusion or as a response to external stimuli [18,90]. They offer numerous advantages; for example, the surface of the nanocarrier can be modified using different polymers for different purposes, such as mucoadhesive properties, by increasing the residence time, thus tailoring the drug release to reach controlled or sustained delivery. Furthermore, enhanced bioavailability with a lower risk of adverse effects and eye irritation can be obtained to increase patients' adherence to medications [28,91–95].

The current systematic review demonstrates the efficiency and superiority of nanoformulation, particularly nanofibrous webs, as a promising alternative to conventional methods regarding site targeting and improved bioavailability. All toxicity studies proved their safety in animal models and in vitro alternative models. Pharmacokinetic studies have shown sustained drug release through different models such as zero-order and Higuchi models, which allows the possibility for single-dose administration for up to 30 days [34]. Combining the advantages of nanofibers with the advantages of ocular inserts will increase the bioavailability by many times [58] and reduce or even eliminate the disadvantages of using normal macro-size ocular inserts.

5. Future Perspective

Many people have ocular diseases, which interfere with quality of life, and the number is increasing by 7 million per year [96]. Even though many published studies have demonstrated that ocular inserts are a successful and non-invasive method of delivering drugs to the eye, only a small number of ocular inserts are available on the market, for example, Lacrisert®, a topical insert approved by the U.S. Food and Drug Administration [64] and Mydriasert© [97]. A significant amount of research on tailoring the delivery of various drugs to different parts of the eye using ocular inserts has provided very promising results, such as delivery of antimicrobial peptides to the pre-corneal area [98] and ocular inserts for delivery of thermolabile therapeutics [71].

Since nanotechnology has received a great deal of attention in recent years, nanofibers are expected to become an integral part of frequently used dosage forms in the near future, as they are able to penetrate and target different sites, including posterior segments of the eye [38] and the vitreous cavity for the treatment of retinal diseases [99]. From a technical point of view, nanofibers can be used directly as films [58] or after further processing into suitable ocular inserts or other surface modifications [100]. In addition, nanofibers can be formulated using a simple, versatile electrospinning technique [31]. The process enables encapsulation of more than one drug in one step [38], which will result in decreased multiple-drug regimens and increased patient compliance [27,101]. It also enables encapsulation and delivery of macromolecules such as genes and proteins, and this will open the door for research in this area, especially since there are not many studies on macromolecules [102]. In addition it can be scaled up for large-scale production to meet the requirements and sustainability of pharmaceutical companies [103].

Obviously, ocular inserts have also been intensively investigated because of their unique advantages as an alternative way to target eye disease, considering the possibility of fabricating them using different methods and polymeric materials. To meet the needs of the patients and minimize their suffering, a new non-invasive drug delivery system that offers good bioavailability and has the potential to deliver medicaments to posterior parts of the eye is expected to be investigated and introduced to the market in the near future.

As many studies have proven the success of ocular inserts, the application of electrospun nanofibers as film or as part of ocular inserts is expected to result in a great advancement in the targeting of eye diseases, if these studies find a place in human clinical trials to confirm their efficiency and nontoxicity.

6. Conclusions

Eye problems are increasing daily; therefore, a smart approach is needed. It has been proven that drug delivery to the eye involves many problems that result from the barriers present in the eye, including the retinal blood barrier, lacrimation, eye blinking, and dilution, which is eventually reflected in poor drug bioavailability, particularly when using conventional topical drug delivery systems such as eye drops. In order to overcome such barriers, it is important to increase the contact time of the eye formulation to increase absorption and decrease the frequency of drug administration.

Different unconventional approaches are available, but every approach comes with some limitations. Nanofibers have gained attention recently, since they have superior advantages compared to other available systems; they are less irritating to the eye due to their small size and can be fabricated using different polymeric systems, therefore sustained release formulations could be applied, resulting in lower administration frequency. In addition, many studies have demonstrated successful posterior eye targeting.

An interesting characteristic of nanoparticulates is their large surface area, which allows the fabrication of different structures, including ocular inserts. Ocular inserts have been found to have many advantages: they provide increased bioavailability through the prolonged residence time of the drug on the conjunctival surface, can be formulated using different polymeric materials and methods, and allow the preparation of preservative-free formulations, thus resulting in lower eye sensitivity or even no sensitivity or irritation. In the light of the advantages of nanofibers and ocular inserts, a synergistic effect could be obtained by formulating ocular inserts with a nanofibrous architecture. Many published studies confirm the possibility of using such systems as an alternative to conventional topical formulations with better results.

Author Contributions: Conceptualization, S.O. and R.Z.; methodology, S.O. and R.Z.; writing—original draft preparation, S.O.; writing—review and editing, R.Z. Both authors have read and agreed to the published version of the manuscript.

Institutional Review Board Statement: Not applicable.

Informed Consent Statement: Not applicable.

Data Availability Statement: Not applicable.

Conflicts of Interest: The authors declare no conflict of interest.

References

1. Mehta, P.; Al-Kinani, A.A.; Arshad, M.S.; Chang, M.W.; Alany, R.G.; Ahmad, Z. Development and Characterisation of Electrospun Timolol Maleate-Loaded Polymeric Contact Lens Coatings Containing Various Permeation Enhancers. *Int. J. Pharm.* **2017**, *532*, 408–420. [CrossRef] [PubMed]
2. Tsai, C.H.; Wang, P.Y.; Lin, I.C.; Huang, H.; Liu, G.S.; Tseng, C.L. Ocular Drug Delivery: Role of Degradable Polymeric Nanocarriers for Ophthalmic Application. *Int. J. Mol. Sci.* **2018**, *19*, 2830. [CrossRef] [PubMed]
3. Maharjan, P.; Cho, K.H.; Maharjan, A.; Shin, M.C.; Moon, C.; Min, K.A. Pharmaceutical Challenges and Perspectives in Developing Ophthalmic Drug Formulations. *J. Pharm. Investig.* **2019**, *49*, 215–228. [CrossRef]
4. Lynch, C.R.; Kondiah, P.P.D.; Choonara, Y.E.; du Toit, L.C.; Ally, N.; Pillay, V. Hydrogel Biomaterials for Application in Ocular Drug Delivery. *Front. Bioeng. Biotechnol.* **2020**, *8*, 1–18. [CrossRef]
5. Agarwal, P.; Scherer, D.; Günther, B.; Rupenthal, I.D. Semifluorinated Alkane Based Systems for Enhanced Corneal Penetration of Poorly Soluble Drugs. *Int. J. Pharm.* **2018**, *538*, 119–129. [CrossRef]
6. Kim, Y.C.; Chiang, B.; Wu, X.; Prausnitz, M.R. Ocular Delivery of Macromolecules. *J. Control Release* **2014**, *190*, 172–181. [CrossRef]
7. Shen, J.; Lu, G.W.; Hughes, P. Targeted Ocular Drug Delivery with Pharmacokinetic/Pharmacodynamic Considerations. *Pharm. Res.* **2018**, *35*, 1–20. [CrossRef]

8. Jervis, L.P. A Summary of Recent Advances in Ocular Inserts and Implants. *J. Bioequiv. Bioavailab.* **2016**, *9*, 320–323. [CrossRef]
9. Gorantla, S.; Rapalli, V.K.; Waghule, T.; Singh, P.P.; Dubey, S.K.; Saha, R.N.; Singhvi, G. Nanocarriers for Ocular Drug Delivery: Current Status and Translational Opportunity. *RSC Adv.* **2020**, *10*, 27835–27855. [CrossRef]
10. Thakur, R.; Swami, G.; Rahman, M. Development and Optimization of Controlled Release Bioerodable Anti Infective Ophthalmic Insert. *Curr. Drug Deliv.* **2014**, *11*, 2–10. [CrossRef]
11. Mudgil, M.; Pawar, P.K. Preparation and In Vitro/Ex Vivo Evaluation of Moxifloxacin-Loaded PLGA Nanosuspensions for Ophthalmic Application. *Sci. Pharm.* **2013**, *81*, 591–606. [CrossRef]
12. Tundisi, L.L.; Mostaço, G.B.; Carricondo, P.C.; Petri, D.F.S. Hydroxypropyl Methylcellulose: Physicochemical Properties and Ocular Drug Delivery Formulations. *Eur. J. Pharm. Sci.* **2021**, *159*, 105736. [CrossRef]
13. Park, C.G.; Kim, Y.K.; Kim, S.N.; Lee, S.H.; Huh, B.K.; Park, M.A.; Won, H.; Park, K.H.; Choy, Y.B. Enhanced Ocular Efficacy of Topically-Delivered Dorzolamide with Nanostructured Mucoadhesive Microparticles. *Int. J. Pharm.* **2017**, *522*, 66–73. [CrossRef] [PubMed]
14. Rahić, O.; Tucak, A.; Omerović, N.; Sirbubalo, M.; Hindija, L.; Hadžiabdić, J.; Vranić, E. Novel Drug Delivery Systems Fighting Glaucoma: Formulation Obstacles and Solutions. *Pharmaceutics* **2021**, *13*, 28. [CrossRef] [PubMed]
15. Xie, J.; Wang, C.; Ning, Q.; Gao, Q.; Gao, C.; Gou, Z.; Ye, J. A New Strategy to Sustained Release of Ocular Drugs by One-Step Drug-Loaded Microcapsule Manufacturing in Hydrogel Punctal Plugs. *Graefes Arch. Clin. Exp. Ophthalmol.* **2017**, *255*, 2173–2184. [CrossRef] [PubMed]
16. Asim, M.H.; Ijaz, M.; Mahmood, A.; Knoll, P.; Jalil, A.; Arshad, S.; Bernkop-Schnürch, A. Thiolated Cyclodextrins: Mucoadhesive and Permeation Enhancing Excipients for Ocular Drug Delivery. *Int. J. Pharm.* **2021**, *599*, 120451. [CrossRef]
17. Khames, A.; Khaleel, M.A.; El-Badawy, M.F.; El-Nezhawy, A.O.H. Natamycin Solid Lipid Nanoparticles-Sustained Ocular Delivery System of Higher Corneal Penetration against Deep Fungal Keratitis: Preparation and Optimization. *Int. J. Nanomed.* **2019**, *14*, 2515–2531. [CrossRef]
18. Barar, J.; Aghanejad, A.; Fathi, M.; Omidi, Y. Advanced Drug Delivery and Targeting Technologies for the Ocular Diseases. *BioImpacts* **2016**, *6*, 49–67. [CrossRef]
19. Taghe, S.; Mirzaeei, S. Preparation and Characterization of Novel, Mucoadhesive of Loxacin Nanoparticles for Ocular Drug Delivery. *Brazilian J. Pharm. Sci.* **2019**, *55*, 1–12. [CrossRef]
20. Omerovi, N.; Vrani, E. Application of Nanoparticles in Ocular Drug Delivery Systems. *Health Technol.* **2020**, *10*, 61–78. [CrossRef]
21. Chetoni, P.; Burgalassi, S.; Monti, D.; Tampucci, S.; Tullio, V.; Cuffini, A.M.; Muntoni, E.; Spagnolo, R.; Zara, G.P.; Cavalli, R. Solid Lipid Nanoparticles as Promising Tool for Intraocular Tobramycin Delivery: Pharmacokinetic Studies on Rabbits. *Eur. J. Pharm. Biopharm.* **2016**, *109*, 214–223. [CrossRef]
22. Kaul, S.; Kumar, G.; Kothiyal, P. An Insight into Ocular Insert. *Int. J. Pharm. Sci. Res.* **2012**, *3*, 1905–1912.
23. Rozi, M.F.; Mohmad Sabere, A.S. Review on Conventional and Novel Topical Ocular Drug Delivery System. *J. Pharm.* **2021**, *1*, 19–26. [CrossRef]
24. Dabral, K.; Uniyal, Y. Ocular Inserts: Novel Approach for Drug Delivery into Eyes. *GSC Biol. Pharm. Sci.* **2019**, *7*, 001–007. [CrossRef]
25. Singla, J.; Bajaj, T.; Goyal, A.K.; Rath, G. Development of Nanofibrous Ocular Insert for Retinal Delivery of Fluocinolone Acetonide. *Curr. Eye Res.* **2019**, *44*, 541–550. [CrossRef] [PubMed]
26. Sofi, H.S.; Abdal-hay, A.; Ivanovski, S.; Zhang, Y.S.; Sheikh, F.A. Electrospun Nanofibers for the Delivery of Active Drugs through Nasal, Oral and Vaginal Mucosa: Current Status and Future Perspectives. *Mater. Sci. Eng. C* **2020**, *111*, 110756. [CrossRef] [PubMed]
27. Krstić, M.; Radojević, M.; Stojanović, D.; Radojević, V.; Uskoković, P.; Ibrić, S. Formulation and Characterization of Nanofibers and Films with Carvedilol Prepared by Electrospinning and Solution Casting Method. *Eur. J. Pharm. Sci.* **2017**, *101*, 160–166. [CrossRef]
28. Luraghi, A.; Peri, F.; Moroni, L. Electrospinning for Drug Delivery Applications: A Review. *J. Control Release* **2021**, *334*, 463–484. [CrossRef]
29. Fadil, F.; Affandi, N.D.N.; Misnon, M.I.; Bonnia, N.N.; Harun, A.M.; Alam, M.K. Review on Electrospun Nanofiber-Applied Products. *Polymers* **2021**, *13*, 2087. [CrossRef]
30. Vass, P.; Szabó, E.; Domokos, A.; Hirsch, E.; Galata, D.; Farkas, B.; Démuth, B.; Andersen, S.K.; Vigh, T.; Verreck, G.; et al. Scale-up of Electrospinning Technology: Applications in the Pharmaceutical Industry. *Wiley Interdiscip. Rev. Nanomed. Nanobiotechnol.* **2020**, *12*, 1–24. [CrossRef] [PubMed]
31. Arthanari, S.; Mani, G.; Jang, J.H.; Choi, J.O.; Cho, Y.H.; Lee, J.H.; Cha, S.E.; Oh, H.S.; Kwon, D.H.; Jang, H.T. Preparation and Characterization of Gatifloxacin-Loaded Alginate/Poly (Vinyl Alcohol) Electrospun Nanofibers. *Artif. Cells Nanomed. Biotechnol.* **2016**, *44*, 847–852. [CrossRef]
32. Dadashi, S.; Boddohi, S.; Soleimani, N. Preparation, Characterization, and Antibacterial Effect of Doxycycline Loaded Kefiran Nanofibers. *J. Drug Deliv. Sci. Technol.* **2019**, *52*, 979–985. [CrossRef]
33. Polat, H.K.; Bozdağ Pehlivan, S.; Özkul, C.; Çalamak, S.; Öztürk, N.; Aytekin, E.; Fırat, A.; Ulubayram, K.; Kocabeyoğlu, S.; İrkeç, M.; et al. Development of Besifloxacin HCl Loaded Nanofibrous Ocular Inserts for the Treatment of Bacterial Keratitis: In Vitro, Ex Vivo and In Vivo Evaluation. *Int. J. Pharm.* **2020**, *585*, 119552. [CrossRef] [PubMed]

34. Di Prima, G.; Licciardi, M.; Carfì Pavia, F.; Lo Monte, A.I.; Cavallaro, G.; Giammona, G. Microfibrillar Polymeric Ocular Inserts for Triamcinolone Acetonide Delivery. *Int. J. Pharm.* **2019**, *567*, 118459. [CrossRef]

35. Chou, S.F.; Luo, L.J.; Lai, J.Y.; Ma, D.H.K. Role of Solvent-Mediated Carbodiimide Cross-Linking in Fabrication of Electrospun Gelatin Nanofibrous Membranes as Ophthalmic Biomaterials. *Mater. Sci. Eng. C* **2017**, *71*, 1145–1155. [CrossRef] [PubMed]

36. Tawfik, E.A.; Craig, D.Q.M.; Barker, S.A. Dual Drug-Loaded Coaxial Nanofibers for the Treatment of Corneal Abrasion. *Int. J. Pharm.* **2020**, *581*, 119296. [CrossRef]

37. Imperiale, J.C.; Acosta, G.B.; Sosnik, A. Polymer-Based Carriers for Ophthalmic Drug Delivery. *J. Control Release* **2018**, *285*, 106–141. [CrossRef]

38. Mirzaeei, S.; Berenjian, K.; Khazaei, R. Preparation of the Potential Ocular Inserts by Electrospinning Method to Achieve the Prolong Release Profile of Triamcinolone Acetonide. *Adv. Pharm. Bull.* **2018**, *8*, 21–27. [CrossRef]

39. Ashri, L.Y.; Abou El Ela, A.E.S.F.; Ibrahim, M.A.; Alshora, D.H.; Naguib, M.J. Optimization and Evaluation of Chitosan Buccal Films Containing Tenoxicam for Treating Chronic Periodontitis: In Vitro and In Vivo Studies. *J. Drug Deliv. Sci. Technol.* **2020**, *57*, 101720. [CrossRef]

40. Wani, T.U.; Pandith, A.H.; Sheikh, F.A. Polyelectrolytic Nature of Chitosan: Influence on Physicochemical Properties and Synthesis of Nanoparticles. *J. Drug Deliv. Sci. Technol.* **2021**, *65*, 102730. [CrossRef]

41. Almeida, H.; Amaral, M.H.; Lobão, P.; Lobo, J.M.S. In Situ Gelling Systems: A Strategy to Improve the Bioavailability of Ophthalmic Pharmaceutical Formulations. *Drug Discov. Today* **2014**, *19*, 400–412. [CrossRef]

42. Mehta, P.; Al-Kinani, A.A.; Arshad, M.S.; Singh, N.; van der Merwe, S.M.; Chang, M.W.; Alany, R.G.; Ahmad, Z. Engineering and Development of Chitosan-Based Nanocoatings for Ocular Contact Lenses. *J. Pharm. Sci.* **2019**, *108*, 1540–1551. [CrossRef]

43. Mamidi, N.; Delgadillo, R.M.V. Design, Fabrication and Drug Release Potential of Dual Stimuli-Responsive Composite Hydrogel Nanoparticle Interfaces. *Colloids Surf. B Biointerfaces* **2021**, *204*, 111819. [CrossRef] [PubMed]

44. Mamidi, N.; Villela Castrejón, J.; González-Ortiz, A. Rational Design and Engineering of Carbon Nano-Onions Reinforced Natural Protein Nanocomposite Hydrogels for Biomedical Applications. *J. Mech. Behav. Biomed. Mater.* **2020**, *104*, 103696. [CrossRef]

45. Mamidi, N.; Velasco Delgadillo, R.M.; Barrera, E.V. Covalently Functionalized Carbon Nano-Onions Integrated Gelatin Methacryloyl Nanocomposite Hydrogel Containing γ-Cyclodextrin as Drug Carrier for High-Performance Ph-Triggered Drug Release. *Pharmaceuticals* **2021**, *14*, 291. [CrossRef] [PubMed]

46. Ahmady, A.; Abu Samah, N.H. A Review: Gelatine as a Bioadhesive Material for Medical and Pharmaceutical Applications. *Int. J. Pharm.* **2021**, *608*, 121037. [CrossRef] [PubMed]

47. Mamidi, N.; Zuníga, A.E.; Villela-Castrejón, J. Engineering and Evaluation of Forcespun Functionalized Carbon Nano-Onions Reinforced Poly (ε-Caprolactone) Composite Nanofibers for PH-Responsive Drug Release. *Mater. Sci. Eng. C* **2020**, *112*, 110928. [CrossRef]

48. Mahmoud Salehi, A.O.; Heidari Keshel, S.; Sefat, F.; Tayebi, L. Use of Polycaprolactone in Corneal Tissue Engineering: A Review. *Mater. Today Commun.* **2021**, *27*, 102402. [CrossRef]

49. Mamidi, N.; Delgadillo, R.M.V.; González-Ortiz, A. Engineering of Carbon Nano-Onion Bioconjugates for Biomedical Applications. *Mater. Sci. Eng. C* **2021**, *120*, 111698. [CrossRef]

50. Mamidi, N.; González-Ortiz, A.; Romo, I.L.; Barrera, E.V. Development of Functionalized Carbon Nano-Onions Reinforced Zein Protein Hydrogel Interfaces for Controlled Drug Release. *Pharmaceutics* **2019**, *11*, 621. [CrossRef]

51. Tawfik, E.A.; Alshamsan, A.; Abul Kalam, M.; Raish, M.; Alkholief, M.; Stapleton, P.; Harvey, K.; Craig, D.Q.M.; Barker, S.A. In Vitro and In Vivo Biological Assessment of Dual Drug-Loaded Coaxial Nanofibers for the Treatment of Corneal Abrasion. *Int. J. Pharm.* **2021**, *604*, 120732. [CrossRef] [PubMed]

52. Bhattarai, R.S.; Das, A.; Alzhrani, R.M.; Kang, D.; Bhaduri, S.B.; Boddu, S.H.S. Comparison of Electrospun and Solvent Cast Polylactic Acid (PLA)/Poly(Vinyl Alcohol) (PVA) Inserts as Potential Ocular Drug Delivery Vehicles. *Mater. Sci. Eng. C* **2017**, *77*, 895–903. [CrossRef] [PubMed]

53. Mirzaeei, S.; Barfar, D. Design and Development of Antibacterial/Anti-Inflammatory Dual Drug-Loaded Nanofibrous Inserts for Ophthalmic Sustained Delivery of Gentamicin and Methylprednisolone: In Vitro Bioassay, Solvent, and Method Effects' Evaluation. *Adv. Pharm. Bull.* **2021**, in press. [CrossRef]

54. Grimaudo, M.A.; Concheiro, A.; Alvarez-Lorenzo, C. Crosslinked Hyaluronan Electrospun Nanofibers for Ferulic Acid Ocular Delivery. *Pharmaceutics* **2020**, *12*, 274. [CrossRef]

55. Taghe, S.H.; Mehrandish, S.; Mirzaeei, S. Preparation of Azithromycin Nanofibers as Controlled Release Ophthalmic Drug Carriers Using Electrospinning Technique: In- Vitro and In- Vivo Characterization. *Adv. Pharm. Bull.* **2021**. [CrossRef]

56. Khalil, I.A.; Ali, I.H.; El-sherbiny, I.M. Noninvasive Biodegradable Nanoparticles-in-Nanofibers Single-Dose Ocular Insert: In Vitro, Ex Vivo and In Vivo Evaluation. *Nanomedicine* **2018**, *14*, 33–55. [CrossRef]

57. Gagandeep; Garg, T.; Malik, B.; Rath, G.; Goyal, A.K. Development and Characterization of Nano-Fiber Patch for the Treatment of Glaucoma. *Eur. J. Pharm. Sci.* **2014**, *53*, 10–16. [CrossRef]

58. Mirzaeei, S.; Taghe, S.; Asare-Addo, K.; Nokhodchi, A. Polyvinyl Alcohol/Chitosan Single-Layered and Polyvinyl Alcohol/Chitosan/Eudragit RL100 Multi-Layered Electrospun Nanofibers as an Ocular Matrix for the Controlled Release of Ofloxacin: An In Vitro and In Vivo Evaluation. *AAPS PharmSciTech* **2021**, *22*, 1–13. [CrossRef]

59. Taghe, S.; Mirzaeei, S.; Alany, R.G.; Nokhodchi, A. Polymeric Inserts Containing Eudragit® L100 Nanoparticle for Improved Ocular Delivery of Azithromycin. *Biomedicines* **2020**, *8*, 466. [CrossRef] [PubMed]

60. Shah, S.N.H.; Nawaz, A.; Javed, H.; Rafiq, M.; Riaz, R.; Sadaquat, H.; Akhtar, M. Preparation and In Vitro/In Vivo Evaluation of Antihistaminic Ocular Inserts. *Pharm. Chem. J.* **2018**, *52*, 615–622. [CrossRef]
61. Di Colo, G.; Zambito, Y. A Study of Release Mechanisms of Different Ophthalmic Drugs from Erodible Ocular Inserts Based on Poly(Ethylene Oxide). *Eur. J. Pharm. Biopharm.* **2002**, *54*, 193–199. [CrossRef]
62. Patil, S.S.; Bade, A.; Tagalpallewar, A. Design, Optimization and Pharmacodynamic Comparison of Dorzolamide Hydrochloride Soluble Ocular Drug Insert Prepared by Using 32 Factorial Design. *J. Drug Deliv. Sci. Technol.* **2018**, *46*, 138–147. [CrossRef]
63. Tighsazzadeh, M.; Mitchell, J.C.; Boateng, J.S. Development and Evaluation of Performance Characteristics of Timolol-Loaded Composite Ocular Films as Potential Delivery Platforms for Treatment of Glaucoma. *Int. J. Pharm.* **2019**, *566*, 111–125. [CrossRef] [PubMed]
64. Thakkar, R.; Komanduri, N.; Dudhipala, N.; Tripathi, S.; Repka, M.A.; Majumdar, S. Development and Optimization of Hot-Melt Extruded Moxifloxacin Hydrochloride Inserts, for Ocular Applications, Using the Design of Experiments. *Int. J. Pharm.* **2021**, *603*, 120676. [CrossRef] [PubMed]
65. Aher, N.D.; Nair, H.A. Bilayered Films Based on Novel Polymer Derivative for Improved Ocular Therapy of Gatifloxacin. *Sci. World J.* **2014**, *2014*. [CrossRef] [PubMed]
66. Abdelkader, H.; Wertheim, D.; Pierscionek, B.; Alany, R.G. Curcumin in Situ Gelling Polymeric Insert with Enhanced Ocular Performance. *Pharmaceutics* **2020**, *12*, 1158. [CrossRef]
67. Everaert, A.; Broeckx, G.; Fransen, E.; Ludwig, A.; Kiekens, F.; Weyenberg, W. Evaluation of a Newly Developed HPMC Ophthalmic Insert with Sustained Release Properties as a Carrier for Thermolabile Therapeutics. *Int. J. Pharm.* **2015**, *481*, 37–46. [CrossRef]
68. Gurtler, F.; Kaltsatos, V.; Boisramé, B.; Gurny, R. Long-Acting Soluble Bioadhesive Ophthalmic Drug Insert (BODI) Containing Gentamicin for Veterinary Use: Optimization and Clinical Investigation. *J. Control Release* **1995**, *33*, 231–236. [CrossRef]
69. Balguri, S.P.; Adelli, G.R.; Tatke, A.; Janga, K.Y.; Bhagav, P.; Majumdar, S. Melt-Cast Noninvasive Ocular Inserts for Posterior Segment Drug Delivery. *J. Pharm. Sci.* **2017**, *106*, 3515–3523. [CrossRef]
70. Shadambikar, G.; Marathe, S.; Patil, A.; Joshi, R.; Bandari, S.; Majumdar, S.; Repka, M. Novel Application of Hot Melt Extrusion Technology for Preparation and Evaluation of Valacyclovir Hydrochloride Ocular Inserts. *AAPS PharmSciTech* **2021**, *22*, 1–7. [CrossRef]
71. Everaert, A.; Wouters, Y.; Melsbach, E.; Zakaria, N.; Ludwig, A.; Kiekens, F.; Weyenberg, W. Optimisation of HPMC Ophthalmic Inserts with Sustained Release Properties as a Carrier for Thermolabile Therapeutics. *Int. J. Pharm.* **2017**, *528*, 395–405. [CrossRef] [PubMed]
72. Baeyens, V.; Kaltsatos, V.; Boisramé, B.; Varesio, E.; Veuthey, J.L.; Fathi, M.; Balant, L.P.; Gex-Fabry, M.; Gurny, R. Optimized Release of Dexamethasone and Gentamicin from a Soluble Ocular Insert for the Treatment of External Ophthalmic Infections. *J. Control Release* **1998**, *52*, 215–220. [CrossRef]
73. Bhagav, P.; Trivedi, V.; Shah, D.; Chandran, S. Sustained Release Ocular Inserts of Brimonidine Tartrate for Better Treatment in Open-Angle Glaucoma. *Drug Deliv. Transl. Res.* **2011**, *1*, 161–174. [CrossRef]
74. Sadeghi, A.M.; Farjadian, F.; Alipour, S. Sustained Release of Linezolid in Ocular Insert Based on Lipophilic Modified Structure of Sodium Alginate. *Iran. J. Basic Med. Sci.* **2021**, *24*, 331–340. [CrossRef]
75. Barman, S.P.; Liu, M.; Barman, K.; Ward, K.L.; Hackett, B. Methods and Biocompatible Compositions to Achieve Sustained Drug Release in the Eye. Patent Application No. AU 2019250153 A1, 16 October 2019.
76. El-Sherbiny, I.M.; Ali, I.H.; Khalil, I.A. Ocular Drug Delivery System. Patent Application No. GB 2570113 A, 17 July 2019.
77. Johnson LIM, Edison, N. (US). Cylndrical Ocular Inserts. Patent Application No. US2012215184A1, 23 August 2012.
78. Reich, C.; Schuler, C.; Ye, Q.; Stark, L.; Jain, R. Bimatoprost Ocular Silicone Inserts and Methods of Use Thereof. Patent Application No. US2016022695A1, 28 January 2016.
79. Hongzhen, F. Method for Preparing Rifampicin Ocular Inserts. Patent Application No. CN104116722A, 29 October 2014.
80. Parrag, I.C.; Statham, M.A.J.; Battiston, K.; Naimark, W.A.; Fischer, H.C. Ocular Inserts Comprising A Covalently Linked Steroid Dimer. Patent Application No. WO2019148291A1, 8 August 2019.
81. Ge, J.; Zhang, S.Y.; Wu, D.; Cheng, J. Wet-Packed Soft Hydrogel Ocular Inserts. Patent Application No. US2021077385A1, 25 March 2021.
82. Jingxin, G.; Haibing, H.; Muse, J.; Xing, T.; Tian, Y.; Yu, Z. Atropine Sulfate Ocular Inserts and Preparation Method Thereof. Patent Application No. CN111358771A, 7 July 2020.
83. Choonara, Y.E.; Du Toit, L.C.; Kumar, P.; Pillay, V.; Moosa, R.M.; Jhetam, R. Fast Dissolving Ocular Insert. Patent Application No. WO2014041485A1, 20 March 2014.
84. Stark, L.; Jain, R.; Srinivasan, R.; Reich, C.J.; Schuler, C. Ocular Insert Composition of a Sem-Crystalline or Crystalline Pharmaceutically Active Agent. Patent Application No. US2016296532A1, 20 October 2016.
85. Mota Leite Machado Mariz, M.J.; Nunes Ferreira Calvinho, P.C.; Mendes Gil, M.H.; Neto Murta, J.C. Non-Invasive Ocular Drug Delivery Insert Technology. Patent Application No. WO2017137934A1, 17 August 2017.
86. Xiaoyi, S.; Lingyan, Y.; Zhenwei, Y. Ocular Insert Containing Voriconazole. Patent Application No. CN105726517A, 6 July 2016.
87. Allen, K.H.; Rekha, R. Dissolvable Polymeric Eye Inserts with A Biodegradable Polymer. Patent Application No. WO2021116907A1, 17 June 2021.

88. Ketelson, H.A.; Rangarajan, R.; Laredo, W.R.; John, C.S. Dissolvable Polymeric Eye Inserts and Method of Using Same. Patent Application No. WO2020222195A1, 5 November 2020.

89. Ketelson, H.A.; Rangarajan, R. Dissolvable Polymeric Eye Inserts with a Biodegradable Polymer and Method of Using Same. Patent Application No. US2021169781A1, 10 June 2021.

90. Fang, G.; Yang, X.; Wang, Q.; Zhang, A.; Tang, B. Hydrogels-Based Ophthalmic Drug Delivery Systems for Treatment of Ocular Diseases. *Mater. Sci. Eng. C* **2021**, *127*, 112212. [CrossRef]

91. Brahamdutt, M.C.; Kumar, S.; Bhatia, M.; Budhwar, V. Formulation and In-Vitro Evaluation of Sustained Release Tropicamide Loaded Chitosan Nanoparticles for Ocular Drug Delivery. *Int. Res. J. Pharm.* **2016**, *7*, 27–35. [CrossRef]

92. Bachu, R.D.; Chowdhury, P.; Al-Saedi, Z.H.F.; Karla, P.K.; Boddu, S.H.S. Ocular Drug Delivery Barriers—Role of Nanocarriers in the Treatment of Anterior Segment Ocular Diseases. *Pharmaceutics* **2018**, *10*, 28. [CrossRef]

93. Chen, H.; Jin, Y.; Sun, L.; Li, X.; Nan, K.; Liu, H.; Zheng, Q.; Wang, B. Recent Developments in Ophthalmic Drug Delivery Systems for Therapy of Both Anterior and Posterior Segment Diseases. *Colloids Interface Sci. Commun.* **2018**, *24*, 54–61. [CrossRef]

94. El Hoffy, N.M.; Abdel Azim, E.A.; Hathout, R.M.; Fouly, M.A.; Elkheshen, S.A. Glaucoma: Management and Future Perspectives for Nanotechnology-Based Treatment Modalities. *Eur. J. Pharm. Sci.* **2021**, *158*, 105648. [CrossRef]

95. Mahaling, B.; Katti, D.S. Physicochemical Properties of Core-Shell Type Nanoparticles Govern Their Spatiotemporal Biodistribution in the Eye. *Nanomed. Nanotechnol. Biol. Med.* **2016**, *12*, 2149–2160. [CrossRef] [PubMed]

96. Pascolini, D.; Mariotti, S.P. Global Estimates of Visual Impairment: 2010. *Br. J. Ophthalmol.* **2012**, *96*, 614–618. [CrossRef] [PubMed]

97. Bertens, C.J.F.; Gijs, M.; van den Biggelaar, F.J.H.M.; Nuijts, R.M.M.A. Topical Drug Delivery Devices: A Review. *Exp. Eye Res.* **2018**, *168*, 149–160. [CrossRef] [PubMed]

98. Terreni, E.; Burgalassi, S.; Chetoni, P.; Tampucci, S.; Zucchetti, E.; Fais, R.; Ghelardi, E.; Lupetti, A.; Monti, D. Development and Characterization of a Novel Peptide-Loaded Antimicrobial Ocular Insert. *Biomolecules* **2020**, *10*, 664. [CrossRef] [PubMed]

99. Da Silva, G.R.; Lima, T.H.; Fernandes-Cunha, G.M.; Oréfice, R.L.; Da Silva-Cunha, A.; Zhao, M.; Behar-Cohen, F. Ocular Biocompatibility of Dexamethasone Acetate Loaded Poly(ε-Caprolactone) Nanofibers. *Eur. J. Pharm. Biopharm.* **2019**, *142*, 20–30. [CrossRef]

100. Yan, D.; Yao, Q.; Yu, F.; Chen, L.; Zhang, S.; Sun, H.; Lin, J.; Fu, Y. Surface Modified Electrospun Poly(Lactic Acid) Fibrous Scaffold with Cellulose Nanofibrils and Ag Nanoparticles for Ocular Cell Proliferation and Antimicrobial Application. *Mater. Sci. Eng. C* **2020**, *111*, 110767. [CrossRef]

101. Baskakova, A.; Awwad, S.; Jiménez, J.Q.; Gill, H.; Novikov, O.; Khaw, P.T.; Brocchini, S.; Zhilyakova, E.; Williams, G.R. Electrospun Formulations of Acyclovir, Ciprofloxacin and Cyanocobalamin for Ocular Drug Delivery. *Int. J. Pharm.* **2016**, *502*, 208–218. [CrossRef]

102. Wen, P.; Zong, M.H.; Linhardt, R.J.; Feng, K.; Wu, H. Electrospinning: A Novel Nano-Encapsulation Approach for Bioactive Compounds. *Trends Food Sci. Technol.* **2017**, *70*, 56–68. [CrossRef]

103. Omer, S.; Forgách, L.; Zelkó, R.; Sebe, I. Scale-up of Electrospinning: Market Overview of Products and Devices for Pharmaceutical and Biomedical Purposes. *Pharmaceutics* **2021**, *13*, 286. [CrossRef]

Development of innovative electrospun nepafenac-loaded nanofibers-based ophthalmic inserts

Safaa Omer [a], Nándor Nagy [b], Emőke Szőcs [b], Szabina Kádár [c,d], Gergely Völgyi [d], Balázs Pinke [e], László Mészáros [e], Gábor Katona [f], Anna Vincze [g], Péter Dormán [h], Zoltán Zs. Nagy [h], György T. Balogh [d], Adrienn Kazsoki [a,*], Romána Zelkó [a,*]

[a] University Pharmacy Department of Pharmacy Administration, Semmelweis University, Hőgyes Endre Street 7-9, H-1092 Budapest, Hungary
[b] Department of Anatomy, Histology and Embryology Semmelweis University, Tűzoltó Street 58, H-1094 Budapest, Hungary
[c] Department of Organic Chemistry and Technology, Faculty of Chemical Technology and Biotechnology, Budapest University of Technology and Economics, Műegyetem Rkp. 3, H-1111 Budapest, Hungary
[d] Department of Pharmaceutical Chemistry, Semmelweis University, Hőgyes Endre Street 9, H-1092 Budapest, Hungary
[e] Department of Polymer Engineering, Faculty of Mechanical Engineering, Budapest University of Technology and Economics, Műegyetem Rkp. 3, H-1111 Budapest, Hungary
[f] Institute of Pharmaceutical Technology and Regulatory Affairs, University of Szeged, Eötvös u. 6, H-6720 Szeged, Hungary
[g] Department of Chemical and Environmental Process Engineering, Budapest University of Technology and Economics, Műegyetem Rkp. 3, H-1111 Budapest, Hungary
[h] Department of Ophthalmology, Semmelweis University, Má´ria Street 39, 1085 Budapest, Hungary

ARTICLE INFO

ABSTRACT

Electrospun nanofibers can be utilized to develop patient-centric ophthalmic formulations with reasonable bioavailability at the targeted site. The current study aimed to develop 0.1 % w/w of nepafenac-loaded electrospun nanofibrous webs as potential candidates for ocular delivery of nepafenac with improved solubility and stability. Nine different formulations were prepared by electrospinning and investigated for morphology, physicochemical properties, drug release, cytocompatibility, and in vitro and ex vivo permeability. The scanning electron microscopy images showed fibrous samples. Fourier transform infrared spectroscopy and X-ray diffraction confirmed the polymer cross-linking and the formation of amorphous solid dispersion. All formulations showed complete and fast release of nepafenac ($\leq$60 min), and the release followed first-order kinetics (β values for all formulations were $<$ 1). The formulations (F3, F6, and F9) showed considerable in vitro and ex vivo permeability. The Raman studies revealed comparable corneal distributions of F3 and the commercial Nevanac® suspension at 60 min (p value = 0.6433). The fibrous composition remains stable under stress conditions (40 $\pm$ 2 °C, 75 $\pm$ 5 % relative humidity). The formulation composition showed good cytocompatibility with hen eggs tested on the chorioallantoic membrane of chick embryos. The developed nanofiber webs could be a promising candidate for nepafenac-loaded ophthalmic inserts.

1. Introduction

Delivery of the drug to the eye is a complex process due to its unique structure. This unique structure consists of different anatomical and physiological layers and barriers that protect the eye from invasion by foreign objects and interfere with drug permeation (Chen et al., 2018; Maharjan et al., 2019; Mehta et al., 2017). The ever-increasing number of eye diseases can lead to socioeconomic difficulties and interfere with individuals' quality of life (Pascolini & Mariotti, 2012). Untreated patients may develop serious symptoms involving both the anterior and posterior segments; consequently, glaucoma, vision impairment, or even blindness can occur (Kaur et al., 2021; Liang et al., 2021; Pinxten et al., 2017).

Treatment of different ocular diseases is based on the utilization of conventional topical formulations. Eye drops are most popular among physicians and patients due to their convenient way of self-administration. However, because of the limitations of premature loss of the drug and limited bioavailability (less than 5 %) from such formulations, the therapeutic goal is only achieved through frequent administration (Maharjan et al., 2019). The intravitreal injection can be

used successfully for site targeting, yet it is considered an invasive method, requires a skilled ophthalmologist, and may expose the individual to serious complications such as severe hemorrhage, retinal detachment, and blindness (Singla et al., 2019). Novel drug delivery systems comprise a successful and promising alternative to conventional formulations for site targeting. They are designed to increase the residence of the drug and/or improve drug permeation (Barse et al., 2017; Lakhani et al., 2020). These novel formulations include, but are not limited to, hydrogels, liposomes, nanoparticles, ophthalmic inserts, implants, contact lenses, nanosuspensions, and in situ gels (Tighsazzadeh et al., 2019).

Ophthalmic inserts (OIs) have received a great deal of attention due to their numerous advantages. They are fabricated from a wide range of polymers and excipients that can be utilized to increase the residence time, sustain the drug release, enhance transcorneal absorption, and consequently improve bioavailability. Because OIs are solid preparations, they are more stable compared to liquid formulations and eliminate the need for preservatives, thereby reducing the side effects and irritation arising from different preservatives (Di Prima et al., 2019; Polat et al., 2020a; Thakkar et al., 2021).

Electrospinning is one of the novel and promising methods that are used for the fabrication of ophthalmic inserts (Polat et al., 2020b). The method enables the encapsulation of one or more drugs and/or excipients in a single compartment. A more complex nanofibrous structure can be prepared and utilized to deliver incompatible and large drug molecules, including proteins and nucleic acids. The process enables easy surface engineering and modification using different materials such as permeation enhancers, solubility modifiers, and mucoadhesive polymers (Singla et al., 2019).

Polyvinyl alcohol (PVA) is a synthetic polymer that is widely used in the electrospinning process due to its desirable properties such as mechanical strength and biodegradability (Fan et al., 2019; Meireles et al., 2018). Poloxamers are tri-block copolymers consisting of repeated units of terminal hydrophilic ethylene oxide (EO) and central hydrophobic propylene oxide (PO) (Dumortier et al., 2006). They are considered a unique class of polymers due to their thermoreversible phenomenon and amphiphilic features that enable micelle formation and encapsulation of hydrophobic drugs while using an aqueous platform. Poloxamer 407 (Pluronic F127) is widely used in ophthalmic formulations to solubilize drugs and impart adhesiveness to the formulation (Dumortier et al., 2006; Galgatte & Chaudhari, 2014; Russo & Villa, 2019).

Cyclodextrins (CD) are a family of cyclic oligosaccharides with a hydrophobic core and hydrophilic shell. They can be used to form inclusion complexes with hydrophobic compounds to improve water solubility and stability (Grimaudo et al., 2018; MacHín et al., 2012; Miranda et al., 2021).Hydroxypropyl-β-cyclodextrin (HPβCD) is frequently utilized in ophthalmic formulations due to its low tendency to precipitate eye irritation (He et al., 2011).

Inflammatory eye diseases have a high incidence rate and affect both the anterior and posterior parts. Failure of the treatment can lead to visual impairment and blindness. Nepafenac is a non-steroidal anti-inflammatory drug approved by the FDA for the topical treatment of allergic conjunctivitis as well as post-operative pain and inflammation (Lorenzo-Veiga et al., 2020). It is a crystalline powder with low water solubility and low permeability (class IV) (Lorenzo-Veiga et al., 2019). Nepafenac is stable in solid form, while it tends to form degradation products in liquid formulations (Aleo et al., 2020). Nepafenac is normally used as a suspension because of its low water solubility. The suspensions have many limitations, such as irritation and unpleasant sensations that can lead to excessive loss of the drug through lacrimation; hence, frequent dosing is required, which can result in patient noncompliance and treatment failure that might eventually lead to blindness and social difficulties. To avoid these limitations, there is a need for topical formulations that have more tolerability and the ability to overcome the inherently defensive mechanisms of the eye layers (Di Prima et al., 2019; Polat et al., 2020a; Thakkar et al., 2021).

The current study aimed to develop and formulate electrospun nanofiber-based ophthalmic inserts for the delivery of nepafenac to find a stable, solid preservative-free formulation that can overcome premature drainage and increase patients' acceptability. The formulation uses PVA as a matrix-forming polymer, Poloxamer 407 to impart adhesiveness and form in situ gel, and HPβCD as a solubilizer and stabilizer.

2. Material and methods

2.1. Materials

Nepafenac (NEPA, a product of TCI Ltd. (Tokyo, Japan)). polyvinyl alcohol (PVA, Mowiol® 18–88 with an average molecular weight Mw ∼ 130 kDa), poloxamer 407 (average molecular weight, Mw ∼ 12.6 kDa), chloroform (anhydrous, ≥ 99 %), hexane (anhydrous, 95 %), dodecane (anhydrous, ≥ 99 %) and methanol (anhydrous, 99.8 %) were obtained from Merck Ltd. (Budapest, Hungary). L-α-phosphatidylcholine was purchased from Merck KGaA (Darmstadt, Germany). Hydroxypropyl-β-cyclodextrin (HPβCD) (average degree of substitution (n): 4.5, average molecular weight: $1135.0 + n \times 58.1$ g mol^{-1}) was purchased from Cyclolab Ltd. (Budapest, Hungary). Sodium chloride, sodium hydrogen carbonate, calcium chloride hexahydrate and Ethylenediaminetetraacetic acid (EDTA) were purchased from Molar Chemicals Ltd (Budapest, Hungary). Pharmacopeial-grade distilled water was used as solvent for precursor solution preparation. For the permeation experiments, distilled water was purified by the Millipore Milli-Q® 140 Gradient Water Purification System. For the ex vivo experiments, porcine eyes were obtained from a local slaughterhouse (Porció-ÉK Ltd., Albertirsa, Hungary). Physiological salt solution (PSS) contained 0.9 % NaCl (Hungaropharma Plc., Budapest, Hungary). All materials were used without further purification.

2.2. Methods

2.2.1. Preparation of Nepafenac/ HPβCD solution in water

The solubility of nepafenac in water in the presence of HPβCD has been conducted based on the results of the published report (Lorenzo-Veiga et al., 2019). 1 mg of nepafenac was added to 50 mM HPβCD aqueous solutions and subjected to heating in sealed vials at 60 °C for 60 min. The concentrations of resultant solutions were determined by measuring the absorbance at λ_{max} 238 nm by Jasco 530 UV–VIS spectrophotometer coupled with inline probe. The experiments were carried out in triplicate and the average amounts were determined based on the previously constructed calibration curve. The method of analysis was validated according to the reported work (Rajput et al., 2015; Wagh et al., 2017).

2.2.2. Preparation of electrospinning solutions

Variable amounts of HPβCD and PVA/poloxamer 407 were used to prepare nine different solutions of nepafenac (Table 1). The precursor solutions containing HPβCD to improve NEPA solubility; PVA as fiber

Table 1
Composition of nepafenac (NEPA)/hydroxypropyl-beta-cyclodextrin (HPβCD), loaded in different ratios of polyvinyl alcohol (PVA): Poloxamer 407.

Formulation Code	NEPA (% w/w)	HPβCD (mM)	PVA: Poloxamer 407 (m:m)
F1	0.1	50	100:00
F2	0.1	50	85:15
F3	0.1	50	80:20
F4	0.1	100	100:00
F5	0.1	100	85:15
F6	0.1	100	80:20
F7	0.1	150	100:00
F8	0.1	150	85:15
F9	0.1	150	80:20

forming polymer; and poloxamer 407 to impart the bio-adhesiveness. The individual solutions were prepared using appropriate amounts of polymers and distilled water. PVA solutions were prepared by dispersing the polymers in the distilled water, followed by stirring under heating until clear solutions were obtained. Poloxamer 407 solutions were prepared by dissolving the required amounts in cold water. PVA/poloxamer 407 solutions were prepared by adding poloxamer 407 solutions to the PVA solutions and stirred at room temperature until complete homogenization. NEPA/ HPβCD was added either to the PVA or PVA/poloxamer 407 solutions and subjected to stirring at 60 °C for 60 min followed by stirring at room temperature for 2 h until complete solubility of nepafenac.

2.2.3. Electrospinning of the solutions

The fiber formation was conducted using laboratory scale electrospinning equipment (SpinSplit Ltd., Budapest, Hungary). A plastic syringe (Luer lock syringe, Merck Ltd., Budapest, Hungary) of 1 mL volume was filled with the precursor solution and connected to conventional needle (22G) through a Teflon tube. The filled syringe was then placed on the pump to ensure persistent solution flow. Several preliminary experiments have been conducted to optimize the process parameters. The electrospinning process was set at flow rate of (0.08–0.1 μL/sec); the applied voltage was in a range of (10–20 kV); and the effective distance between the needle tip and the grounded collector was maintained at (10 cm, 12.5 cm, and 15 cm). An aluminum foil wrapped on the surface of the grounded plate collector was used to collect each individual sample. The samples were then stored in desiccator for subsequent analysis. Parameter combinations that provided the best sample morphology were used for further sample preparation. The process was conducted at ambient conditions of 22 ± 1 °C room temperature and 40 ± 5 % relative humidity.

2.2.4. Morphological characterization

Electrospun samples were subjected to morphological characterization using the scanning electron microscope (SEM) type JEOL JSM-6380LA. Samples were initially fixed to the copper ingots with double-sided carbon adhesive and coated with gold under vacuum. Images were captured at 3500 and 5000 magnifications at 10 mm distance and an acceleration voltage of 15 kV. Images taken were evaluated in terms of fibrous and beads containing samples. For all fibrous samples, the diameters of 100 randomly selected individual fibers (n = 100) were measured from two different images using ImageJ software (US National Institutes of Health, 138 Bethesda, MD, USA). The average fiber diameters and the standard deviations for all sample measurements were calculated using Excel 2010. The histograms and fitting to the gaussian (normal) distribution were conducted using OriginPro 2018 software (v9.5.1, OriginLab Corporation, Northampton, MA, USA). For assessing the normality of fiber diameter distribution, skewness and kurtosis have been calculated using Microsoft Excel 2010 functions based on the Equations (1) and (2):

$$Skew = \frac{n}{(n-1)(n-2)}\Sigma(\frac{xi-x}{s})^2 \tag{1}$$

$$Curtosis = \frac{n}{(n-1)(n-2)(n-3)}\Sigma\left(\frac{xi-x}{s}\right)^4\} - \frac{3(n-1)^2}{(n-2)(n-3)} \tag{2}$$

2.2.5. Solid state characterization

2.2.5.1. Fourier transform infrared spectroscopy.
Fourier transform infrared spectroscopy (FTIR) was used to investigate the physicochemical properties, compatibility, and interactions between polymers and other excipients using the Jasco FT/IR-4200 spectrophotometer (Jasco Inc., Easton, MD, USA). The analysis was performed for the physical forms of the individual components and the fibrous mixtures. The measurement was conducted in the 400–4000 cm^{-1} range at a resolution of 4 cm^{-1} at ambient temperature in an average of 100 scans.

2.2.5.2. X-ray diffraction (XRD).
Diffraction patterns were measured on PANalytical X'Pert3 Powder diffractometer (Malvern Panalytical B.V., The Netherlands) using Cu Kα radiation with 45 kV accelerating voltage and 40 mA anode current over the range of 4–38 ° 2 θ with 0.0080 ° step size and 99.695 s times per step in reflection mode, spinning the sample holder by 1 s^{-1}. Incident beam optics were as following: Programmable divergence slit with 15 mm constant irradiated length, anti-scatter slit at fixed 2 °. Diffracted beam optics consisted of X'Celerator Scientific ultrafast line detector with 0.02 soller slit and programmable anti-scatter slit with 15 mm constant observed length. Data were collected by PANalytical Data Collector Application, version 5.5.0.505 (Malvern Panalytical B.V., The Netherlands).

2.2.6. Determination of the drug content

The nepafenac content of different fibers was determined by dissolving the amount required to produce a final concentration of 10 μg/mL in 10 mL phosphate-buffered saline (PBS) at pH 7.4 and stirring at ambient conditions for 120 min. The absorbance of the resultant solution was measured at λ$_{max}$ 238 nm by a Jasco 530 UV–VIS spectrophotometer coupled with an inline probe. The experiment was carried out in triplicate and the average amounts were determined based on the previously constructed calibration curve.

2.2.7. In vitro release study and release kinetics

The in vitro release of nepafenac from electrospun nanofibers was studied using a modified method analogous to the basket method reported by Pharmacopoeia Hungarica (Ph.Hg. VIII) (Kazsoki et al., 2021). The method was adjusted to mimic small volume physiological compartments. The process was conducted in a 25-mL beaker. The weighed samples were folded on a dry magnetic bar and fixed inside a steel coil. The folded samples were then inserted inside the 25-mL beaker and magnetically stirred at 100 rpm at a temperature of 37 ± 0.5 °C. An inline probe of a spectrophotometer (Jasco-V-750 UV–VIS spectrophotometer) was immersed in the beaker for continuous measurement of the absorbance of the released nepafenac. 10 mL of pre-warmed phosphate buffer pH 7.4 (to 37 °C) was added to the sample (dissolution media), and the absorbances were measured at a predetermined time interval (5 s) at λ$_{max}$ 238 nm. The amounts of the drug released were determined based on the previously constructed calibration curve by measuring the absorbance every 5 s until the complete dissolution of the fibrous samples. The dissolution was conducted in triplicate, and the nepafenac release curve was built from the average value of the three measurements. The kinetics of the nepafenac release from nanofibers were then evaluated using Weibull model based on the Equation (3):

$$M_t = M_\infty\left(1 - e^{-\frac{(t-t_0)^\beta}{\tau_d}}\right) \tag{3}$$

where M_t is the nepafenac release at (t) time, while M_∞ is the maximum amount of the released nepafenac. The parameters t_0 and τ_d are the lag time and average dissolution time, respectively. The shape of the release curve is specified by the β parameter ($\beta = 1$ denotes first-order kinetics, $\beta > 1$ indicates a slow onset followed by an accelerated release, and $\beta < 1$ indicates a fast onset followed by a slow release) (Kazsoki et al., 2022; Pourtalebi Jahromi et al., 2020).

2.2.8. Permeability studies

2.2.8.1. In vitro corneal-PAMPA assay.
Right before the experiment, electrospun samples were dissolved in PBS to create solutions with 1 mg/ml concentration, then the samples were diluted 20-fold to mimic tear production. Nevanac® (1 mg/mL) was diluted 20-fold with PBS. In the case of the test formulations, each matching well of the acceptor plate (Multiscreen Acceptor Plate, MSSACCEPTOR; Millipore) were

filled with HPßCD solution to reduce the reverse sink effect (containing 10 % HPßCD of the diluted electrospun-samples) whereas in the case of Nevanac® the acceptor wells were filled with PBS. Each sample were measured in six replicates. The artificial membrane was fabricated by dissolving 16 mg phosphatidylcholine in a solvent mixture of dodecane, hexane and chloroform (25:70:5 v/v) and coating each well of the donor plate (MultiscreenTM-IP, MAIPN4510, pore size 0.45 mm; Millipore) with 5 μL of the lipid solution (Dargó et al., 2019).After that, the donor plate was filled with 150 μL sample solutions. Finally, the sandwich plate was assembled and covered with a wet sheet of paper and a plate lid to avoid evaporation. The system was incubated for 4 h at 35 °C (Heidolph Titramax 1000, Heidolph Instruments, Swabach, Germany). After that, initial, donor and acceptor samples were collected and analysed by HPLC-DAD. Effective permeability was calculated using the Eqs. (4) and (5):

$$P_e = \frac{-2.303}{A \bullet (t - \tau_{ss})} \bullet \left(\frac{1}{1 + r_v}\right) \bullet \lg\left[-r_v + \left(\frac{1 + r_v}{1 - MR}\right) \bullet \frac{c_D(t)}{c_D(0)}\right] \quad (4)$$

$$MR = 1 - \frac{c_D(t)}{c_D(0)} - \frac{V_A c_A(t)}{V_D c_D(0)} \quad (5)$$

where A is the filter area (0.3 cm^2), V_D and V_A are the volumes in the donor (0.15 cm^3) and acceptor phase (0.3 cm^3), t is the incubation time (s), τ_{SS} is the time to reach steady-state (s), $c_D(t)$ is the concentration of the compound in the donor phase at time point t (mol/cm^3), $c_D(0)$ is the concentration of the compound in the donor phase at time point zero (mol/cm^3), $c_A(t)$ is the concentration of the compound in the acceptor phase at time point t (mol/cm^3), r_v is the aqueous compartment volume ratio (V_D/V_A). For the comparison, the same experiment was repeated with omitting the effect of HPβCD.

2.2.8.2. Ex vivo corneal permeability studies on porcine eyes. For the ex vivo assay, electrospun samples were dissolved in PSS right before the experiment. Freshly donated porcine eyes obtained from the slaughterhouse were placed on a sterile cotton wool bed moistened with physiological saline solution and kept in a refrigerator box during transportation. The porcine eyes were first placed into PTFE inserts, where the cornea was uncovered and surrounded by a PTFE ring to prevent the flow of eye drops (Vincze et al., 2023). The orifice above the corneal surface was first washed with PSS, and then the devices were pre-incubated at 35 °C in a water bath for 5 min. After that, PSS was removed from the corneal surface, and 100 μL of the undiluted formulations were pipetted on each cornea using 3 eyes for each formulation, then the devices were incubated for 1 min. After that, the samples on the eye surface were diluted by adding PSS to the device's orifice to reach a 20-fold diluted concentration of the original dose (~0.05 mg/mL), and the eyes were incubated with these diluted formulations for another 14, 29, or 59 min. At these endpoints, diluted formulations were removed from the precorneal area, the devices were disassembled, then aqueous humor was drained using a 26G needle, and finally the cornea was excised and NEP was extracted with 2 mL of AcN:water 50:50 (v/v) using an orbital shaker (Heidolph Titramax 100, Heidolph Instruments, Swabach, Germany) for 60 min at 450 rpm. Samples of precorneal fluid, aqueous humor, and corneal extract were analyzed by HPLC-DAD, and the nepafenac concentration was calculated using a calibration curve. The corneal retention (CR) of nepafenac, the apparent permeability (P_{app}C) of nepafenac into the cornea, and the apparent permeability (P_{app}Aq) of nepafenac into the aqueous humor were calculated using Equations (6)–(8), respectively.

$$CR = 1 - \frac{c_{CS}(t)}{c_{CS}(0)} - \frac{V_{AC} c_C(t)}{V_{CS} c_{CS}(0)} \quad (6)$$

$$P_{app}C(cm/s) = \frac{\Delta[C]_C \times V_{AC}}{A \times [C]_{CS} \times \Delta t} \quad (7)$$

$$P_{app}Aq(cm/s) = \frac{\Delta[C]_{Aq} \times V_{AC}}{A \times [C]_{CS} \times \Delta t} \quad (8)$$

where $c_{CS}(t)$ is the concentration of the compound on the corneal surface at time point t (mol/cm^3), $c_{CS}(0)$ is the concentration of the compound on the corneal surface at time point zero (mol/cm^3), $c_C(t)$ is the concentration of the compound in the cornea at time point t (mol/cm^3), and V_{AC} and V_{CS} are the volumes in the anterior chamber (0.25 cm^3) and on the corneal surface (0.75 cm^3).

P_{app}C was calculated from the concentration difference of NEP in the aqueous humor ($\Delta[C]_C$) after treatment, the initial concentration of the compound on the corneal surface at time point zero ($c_{CS}(0)$), the volume on the corneal surface V_{CS} (0.75 cm^3), A is the surface area available for permeability (1.77 cm^2), and t is the incubation time (s). P_{app}Aq was calculated from the concentration difference of NEP in the cornea ($\Delta[C]_{Aq}$) after treatment, the initial concentration of the compound on the corneal surface at time point zero ($c_{CS}(0)$), the volume on the corneal surface V_{CS} (0.75 cm^3), A is the surface area available for permeability (1.77 cm^2), and t is the incubation time (s).

2.2.8.3. Ex vivo cornea Raman mapping. Parallel with the corneal permeability determined with HPLC, the distribution of NEP (nepafenac) in the excised cornea was also investigated with Raman mapping after 15-, 30-, and 60-minute treatment. The cornea was frozen after the treatment and divided into cross sections (15 μm thick) with a Leica CM1950 Cryostat (Leica Biosystems GmbH, Wetzlar, Germany). The selected specimens were mounted on aluminum-coated slides before the experiment. Raman spectroscopic analysis was performed with a Thermo Fisher DXR Dispersive Raman Spectrometer (Thermo Fisher Scientific Inc., Waltham, MA, USA) equipped with a CCD camera and a diode laser with a wavelength of 780 nm. For marking the corneal area for investigation, an objective with 50x magnification was used. For the measurements, a laser power of 24 mW was used, and a slit aperture with a 50 μm size was applied. Raman maps were captured from an area of 150 × 1000 μm, with a step size of 50 μm vertically and horizontally. The OMNIC for Dispersive Raman 8.2 software (Thermo Fisher Scientific) was used for chemical evaluation. The individual spectrum of unformulated NEP was used as a reference when profiling the chemical map.

2.2.9. Hen's egg test on chorioallantoic membrane (HET-CAM)

The HET-CAM test was performed to evaluate the biocompatibility of the developed formulations by observing if hyperemia, hemorrhage, and coagulation were induced after direct application of the ocular films on the chorioallantoic membrane (CAM) of 9-day-old chicken embryos. The test has been conducted based on the reported work (Luepke, 1985). Fertilized White Leghorn chicken (*Gallus gallus domesticus*) eggs were obtained from commercial breeders (Prophyl-BIOVO Hungary Ltd., Mohacs) and maintained at a temperature of 37.5 °C ± 0.5 °C in a humidified HEKA 1 + egg incubator (Rietberg, Germany). On the 9th day of incubation, a small hole was created using fine forceps at the blunt end of the eggs, then the hole on the hard eggshell was expanded to about 2 cm with ophthalmic surgical scissors, followed by careful removal of the inner membrane to expose the vascularized CAM. On the surface of the vascularized CAM, plain and nepafenac-loaded nanofiber mats were placed and evaluated against phosphate-buffered saline (PBS) pH 7.4 and 0.1 N NaOH solution as negative and positive controls, respectively. After 20 s of applying the tested materials, the vascular CAM was irrigated with 5 mL of PBS and evaluated for irritation effects. Images were captured at 0.5, 2, and 5 min using a Nikon SMZ25 stereomicroscope (Unicam Ltd., Hungary). Image processing was conducted using Nikon's proprietary software, QCapture Pro. Each sample was given a score based on the numerical time-dependent scores for hyperemia, hemorrhage, and coagulation (Andreadis et al., 2022; Luepke, 1985).

2.2.10. Accelerated stability study

For the accelerated stability study, the nepafenac-loaded electrospun samples were collected in aluminum foils and packed into hermetic bags with zip closures. The samples were stored in a stability chamber (Sanyo type 022, Leicestershire, UK) for 4 weeks under controlled conditions (40 ± 2 °C, 75 ± 5 % relative humidity). The samples were subjected to SEM and FTIR evaluations in 0, 1, 2, 3, and 4 weeks to study the effect of applying elevated levels of temperature, humidity, and pressure on the morphology and solid-state characters of the NEPA-loaded electrospun nanofibers.

2.2.11. Statistical analysis

The statistical analysis and figures were prepared using OriginPro 2018 software (v9.5.1., OriginLab Corporation, Northampton, MA, USA). ANOVA tests were used to assess the difference between the data. A p-value of less than 0.05 was considered statistically significant. For assessing the normality of fiber diameters distribution, skewness and curtosis have been calculated by using Microsoft Excel 2010 functions.

3. Results and discussion

3.1. Solution of NEPA/ HPβCD in water

The solution of nepafenac in water has been prepared based on a published work (Lorenzo-Veiga et al., 2019), and it has been confirmed that each 1 mg/mL (3.9 mM) of nepafenac can be dissolved by adding approximately 0.069 g (50 mM) of HPβCD to produce a clear yellow solution. The amount of the dissolved nepafenac was successfully determined and confirmed according to a previously constructed calibration curve.

3.2. Morphological evaluation

The morphological features of the electrospun samples were studied using a scanning electron microscope (SEM). The SEM images and corresponding fiber diameter distributions are displayed in Figs. 1 and 2, respectively.

The images show bead-free, randomly oriented fiber depositions and no gel droplets on the fibers' surfaces, with fiber diameters ranging from 124 ± 20 nm to 464 ± 49 nm. The results reflect that the selected polymers (PVA/Poloxamer 407) and the drug complex (NEPA/HPβCD) are appropriate for fiber formation within the designated drug-to-polymer ratios. It has been observed that increasing the HPβCD amount results in a better fiber's surface with more clear, smoother, and more uniform fibers. This enhancement in the fiber structure might be attributed to the unique physicochemical properties of HPβCD and its ability to form self-assembling aggregates that enhance the intermolecular interactions of the components of the electrospinning solution (Dodero et al., 2021).

Although there was no significant difference between average fiber
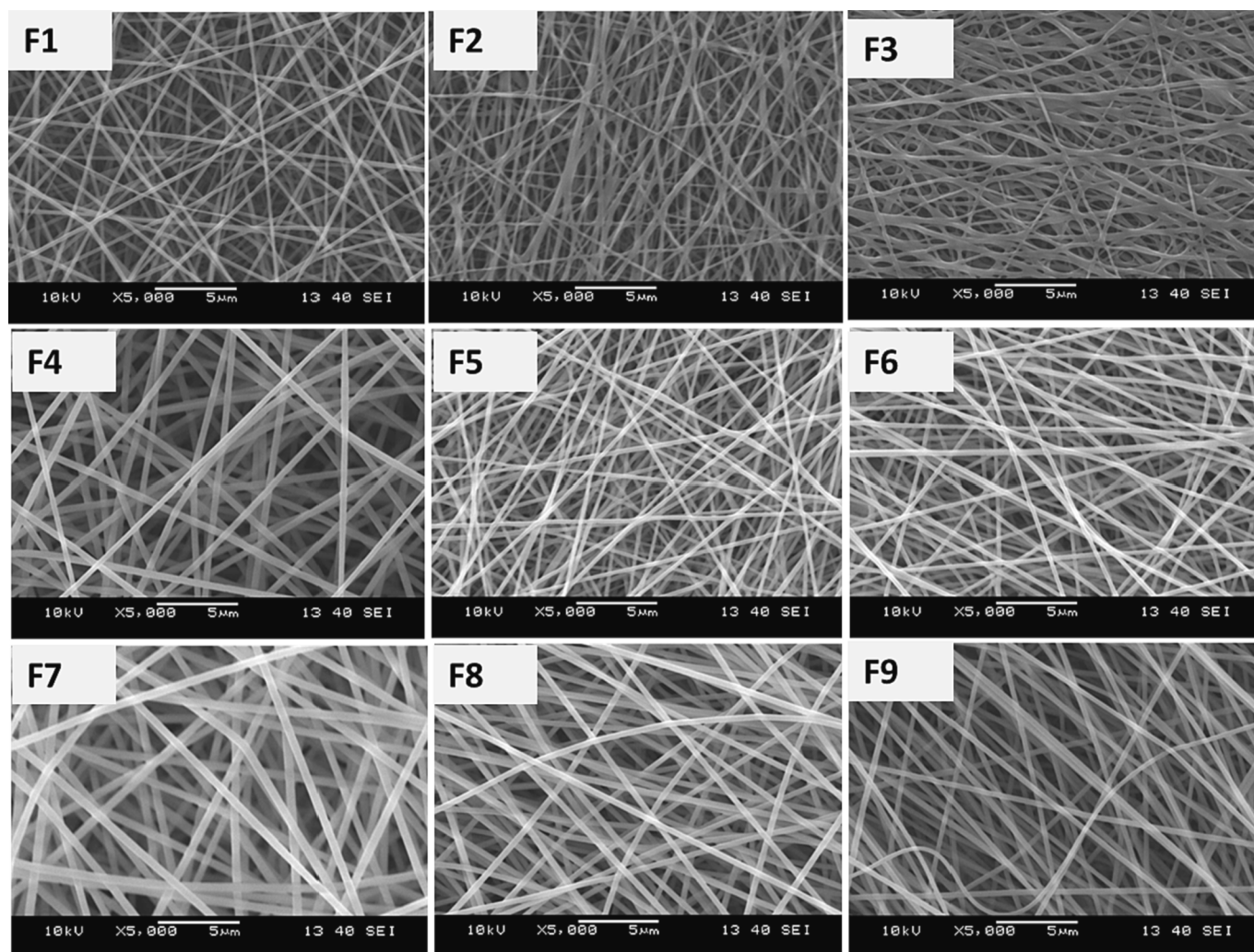
Fig. 1. Scanning Electron Microscope (SEM) images of Nepafenac-loaded electrospun samples prepared from nepafenac/ hydroxypropyl-beta-cyclodextrin/polyvinyl alcohol (NEPA/HPβCD/PVA) (F1, F4, and F7); and NEPA/ HPβCD/PVA/Poloxamer 407 (F2, F3, F5, F6, F8, and F9) (magnification: 5000×).
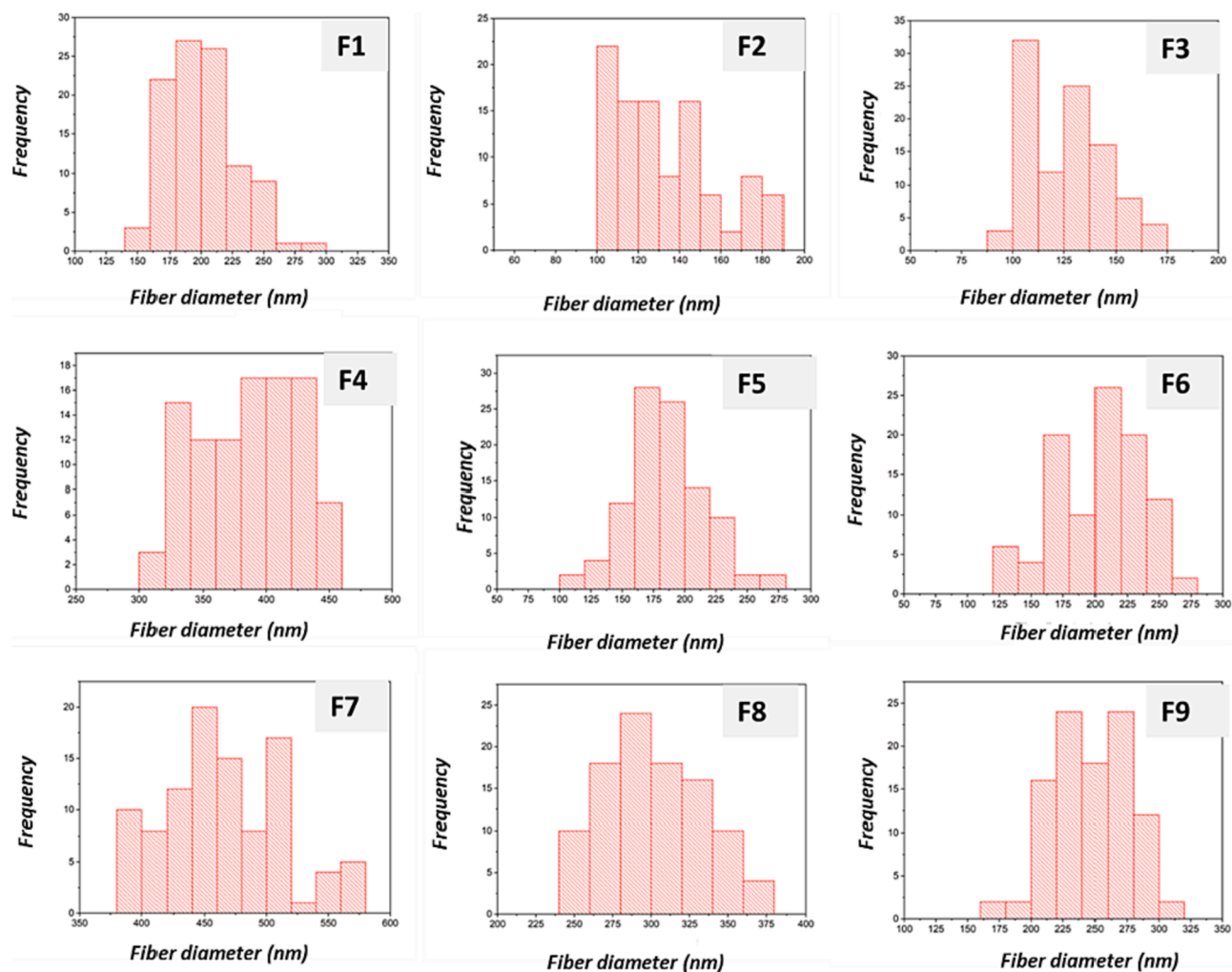
Fig. 2. Fiber diameter distributions of Nepafenac-loaded electrospun samples prepared from nepafenac/ hydroxypropyl-beta-cyclodextrin/polyvinyl alcohol (NEPA/ HPβCD/PVA) (F1, F4, and F7); and NEPA/ HPβCD/PVA/Poloxamer 407 (F2, F3, F5, F6, F8, and F9).

diameters at p-value < 0.05 ($p = 0.16921$), the histograms showed different diameter distributions (Fig. 2). The presence of HPβCD in low amounts (F2 and F3) resulted in a lower average fiber diameter when compared to the double and triple the amount in the formulations (F5 and F6) and (F8 and F9), respectively. This effect can be attributed to the increased solution viscosity (Haider et al., 2018) and/or the presence of HPβCD in higher amounts. The latter may interfere with the surface active effect of poloxamer 407 (thinning effect) and increase the solution entanglement and intermolecular interactions (Dodero et al., 2021; Haider et al., 2018).

3.3. Effect of poloxamer 407 and HPβCD on the diameter distribution

Based on the morphological results, there is great diversity among different formulations. The calculated average fiber diameters, skewness, and kurtosis values are shown in Table S1. Most formulations containing HPβCD have skewness values within an acceptable range, and the distribution curves are symmetric (the absolute skewness values lie between -0.5 and $+0.5$). The exceptions are F1 and F2, which showed moderate skewness values lying between $+0.5$ and $+1$. Results revealed no definite relationship between HPβCD content and histograms or skewness values. The fiber distribution curves showed variable behavior (Figure S1). This ununified behavior can be justified by the fact that electrospun nanofibers are not only evaluated by the SEM images, but further analyses to be conducted to evaluate and characterize

normally distributed curves from compound distribution curves. This fiber's behavior proves that many factors overlap during electrospinning including, for instance, the precursor solution composition as well as the process parameters. The kurtosis values for the fiber distribution showed no very sharp peak or too flat curve (k values between $+1$ and -1). Some formulations showed good fit ($R^2 \geq 0.95$) to the normal distribution, while the rest did not fit. These results are in accordance with skewness calculations (distribution curves are of symmetric and moderately skewness types).

3.4. FTIR analysis

FTIR analysis was conducted to study the structural changes in the components of NEPA-loaded electrospun nanofibers. The spectra of all individual components, including NEPA, PVA, poloxamer 407, and HPβCD and the spectra of electrospun fibrous samples are presented in Fig. 3. The spectra of nepafenac powder showed the following distinctive peaks: medium absorption bands at 3317.92 cm^{-1} and 3326.6 cm^{-1} confirmed N-H$_2$ stretching; a peak appeared at 1676 cm^{-1} is attributed to C $=$ C stretching; N–H bending appeared at 1554 cm^{-1}; a peak at1283 cm^{-1} is attributed to stretching of aromatic amine; an absorption peak at 1236 cm^{-1} is due to stretching of aliphatic amine (Lorenzo-Veiga et al., 2019; Mecozzi & Sturchio, 2017; Shelley et al., 2018).

The spectra of HPβCD showed the most important peaks as follows: a broad band at 3200 cm^{-1}–3485 cm^{-1} characteristic of O–H stretching
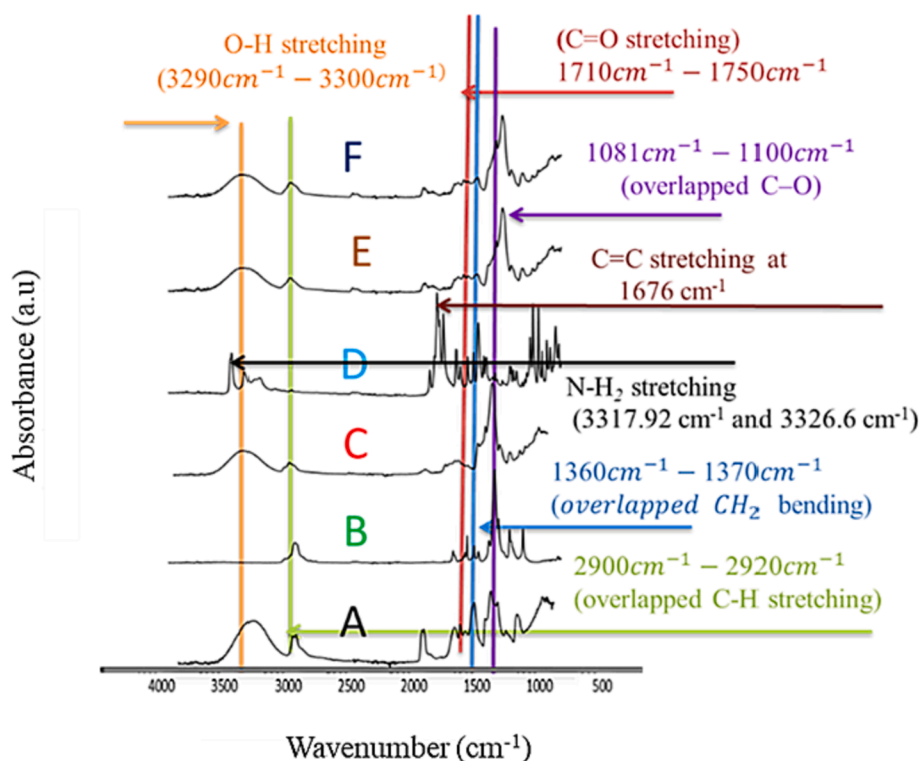
Fig. 3. Fourier transform infrared (FTIR) spectra of: (A): polyvinyl alcohol (PVA) (physical form); (B): Poloxamer 407 (physical form); (C): Hydroxypropyl-β-cyclodextrin (HPβCD); (D): Nepafenac (NEPA) (physical form); (E): Electrospun nanofibers of NEPA/HPβCD/PVA (F1, F4, and F7); and (F): Electrospun nanofibers of NEPA/ HPβCD/PVA/Poloxamer 407 (F2, F3, F5, F6, F8, and F9). The PVA grade used was intermediate molecular weight (Mw ~ 130 kDa).

arising from the intermolecular and intra-molecular hydrogen bonds; an absorption band at 2912 cm^{-1}–2986 cm^{-1} characteristic of C–H stretching; a peak at 1670 cm^{-1} is attributed to C $=$ C stretching; a strong, sharp peak at 1024.9 cm^{-1} is related to C-O stretching (Mecozzi & Sturchio, 2017; Topal et al., 2015).

The PVA spectra showed the following important peaks: a broad band at 3282 cm^{-1}–3300 cm^{-1} characteristic for O–H stretching arising from the intermolecular and intra-molecular hydrogen bonds; the band at 2910 cm^{-1}–2920 cm^{-1} is related to C–H stretching from alkyl group; the band at 1710 cm^{-1}–1750 cm^{-1} is attributed to carbonyl (C $=$ O stretching); the band at 1400 cm^{-1}–1420 cm^{-1} is due to bending stretching of CH_2; the band at 1345 cm^{-1}–1370 cm^{-1} resulting from C-H vibration; the band at 1080 cm^{-1}–1090 cm^{-1} is related to C-O stretching of acetyl groups; and the band at 830 cm^{-1}–840 cm^{-1} is attributed to C–C stretching vibration (Bhat et al., 2005; García-Millán et al., 2017; Kharazmi et al., 2015; Mansur et al., 2008).

Regarding poloxamer 407 spectra, the absorption peak at 2939 cm^{-1} is related to CH_3 stretching; the peak at 2872 cm^{-1} is due to CH_2 stretching; absorption bands at 1095 cm^{-1} and 1340 cm^{-1} are attributed to C-O stretching and O–H bending, respectively (Ellakwa et al., 2017; Laurano et al., 2020; Yasser et al., 2019). The spectra of the nanofiber blends (PVA/poloxamer 407/nepafenac/HPβCD) display the presence of the main distinctive peaks of PVA, Poloxamer 407, and HPβCD: An overlapped absorption band ranging at 3118.3 cm^{-1}–3598.5 cm^{-1} (overlapped band of N-H_2 stretching from nepafenac and O–H stretching from PVA and HPβCD); an overlapped absorption peak at 2823.2 cm^{-1}–2995.8 cm^{-1} (overlapped band of C–H stretching from PVA, Poloxamer 407 and HPβCD); absorption band at 1704 cm^{-1}–1744 cm^{-1} related to carbonyl (C $=$ O stretching of PVA); an overlapped absorption band appeared at 1670 cm^{-1}–1674 cm^{-1} (is attributed to C $=$ C stretching); absorption peak at 1360 cm^{-1}–1370 cm^{-1} indicating overlapped CH_2 bending stretching from PVA and O–H bending from poloxamer 407; a strong sharp peak at 1024.9 cm^{-1} is related to that arising from C-O stretching of HPβCD; absorption peak at 1081

cm^{-1}–1100 cm^{-1} indicating overlapped peak due to C–O stretching from (PVA, poloxamer 407); and peak at 828 cm^{-1}– 840 cm^{-1} is related to C–C stretching vibration of PVA. The O–H absorption of nanofibers blends (PVA/poloxamer 407/nepafenac/HPβCD) was lower than that of individual PVA and HPβCD. This may be due to the incorporation of nepafenac into HPβCD via inclusion complex and interaction of the resulting complex with O–H of the PVA.

3.4.1. X-ray diffraction (XRD)

The R-ray diffraction patterns of the NEPA, physical mixture, F3, F6, and F9 are displayed in Figure S3. The presence of sharp peaks confirmed the crystallinity of the NEPA in its pure state. The intensities of the peaks have decreased upon mixing the NEPA with HPCD, PVA, or polymer 407. The complete disappearance of these peaks from the nanofibers (F3, F6, and F9) confirms the formation of amorphous solid dispersion from crystalline nepafenac through electrospinning of NEPA, HPβCD, PVA, and Poloxamer 407.

3.5. Determination of the drug content

The drug content of all formulations (F1–F9) of nepafenac-loaded nanofibers ranged from 100.01 (% w/w) $\pm$ 0.03 to 101.05 (% w/w) $\pm$ 0.02. The results show uniform drug content throughout the PVA/poloxamer 407 fiber structure. This reflects the complete dissolution of the nepafenac through complexation with HPβCD during the solution preparation. During electrospinning, a homogenous precipitation of the drug/polymer blend occurred after solvent evaporation. Therefore, any deviation from the theoretically stated amounts might be attributed to errors that can occur during solution preparation or during fibers' weighing.

3.6. In vitro drug release and release kinetics

In vitro dissolution profiles of the NEPA/ HPβCD-loaded nanofibers

(0.1 % w/w) conducted in phosphate buffered solution (pH 7.4) at 37 °C are displayed in Fig. 4. All formulations (F1-F9) showed complete release of nepafenac in less than 60 min (16.5—40 min). The fast release of the drug from nanofibers can be explained by the formation of amorphous solid dispersion. All formulations completely dissolved within 5 s, forming a viscous gel when placed on the surface of filter paper wetted with a phosphate buffered solution (pH 7.4), as shown in Table S2, which are in good agreement with the previously published work (Pandit et al., 2023). Regardless of HPβCD amount, all formulations containing poloxamer 407 (F2, F3, F5, F6, F8, and F9) released the nepafenac at a faster rate compared to the formulations without poloxamer 407. This can be attributed to the surface-active effects of poloxamer 407, resulting in faster disintegration and dissolution of the formulations. Some variations were observed in the dissolution profiles with varying the HPβCD and poloxamer 407 amounts. Higher HPβCD levels resulted in a longer drug release, while higher poloxamer 407 levels resulted in a faster release ($p = 0.03253$ at p-value < 0.05). In a conclusion, there was no significant difference in the overall release of the nine formulations. Since each drug-loaded fiber formulation is within the nanometer scale, it is straightforward that there is no great difference in the surface and the consequent release among the different formulations. Therefore, factors other than the diameter of the fibers were considered. The formulations F3, F6, and F9 (with different ratios of HPβCD) were chosen for further permeability studies. Based on published works HPβCD resulted in enhancing the ophthalmic permeability of dexamethasone from hydrogel system (Kesavan et al., 2011), and in some cases, it can decrease permeability (Loftsson et al., 2007).

The release kinetics of nepafenac from nanofibrous matrix was studied using Weibull distribution due to the flexibility of the model in dealing with diverse release patterns. The release parameters including M_∞, β, τ_d and R^2 are summarized in Table 2. All formulations (F1-F9) were successfully fitted to the Weibull model and R^2 values were greater than 0.9 indicating linear regression. The shape of the release curve was found to follow first-order release (β values for all formulation were < 1) with good correlation.
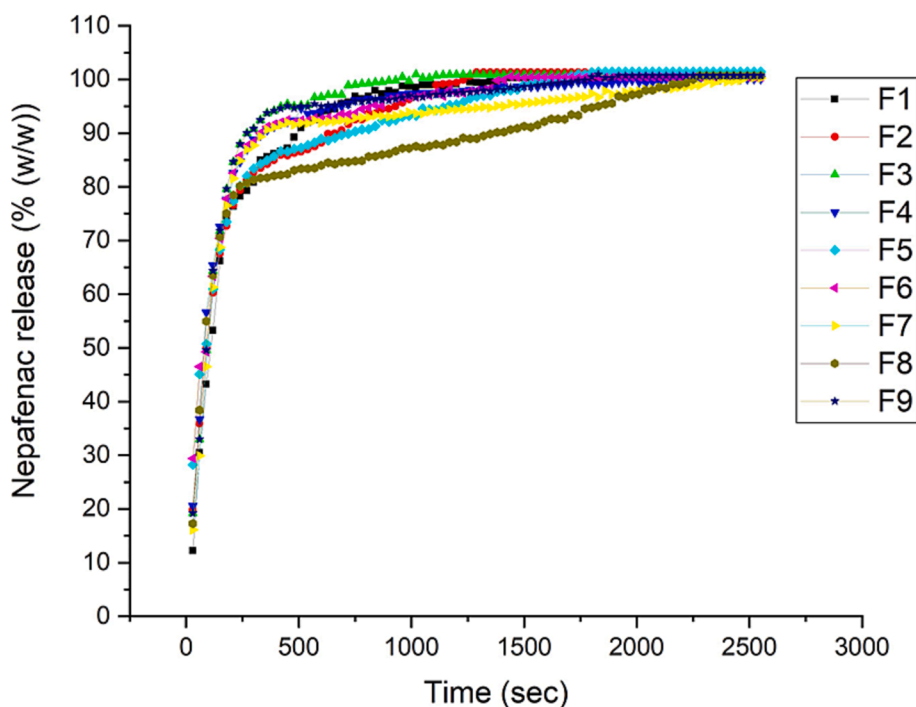
Table 2
Dissolution kinetic parameters of Nepafenac (NEPA) (0.1%w/w)/Hydroxypropyl-β-cyclodextrin (HPβCD) loaded in polyvinyl alcohol/poloxamer 407 nanofibers.

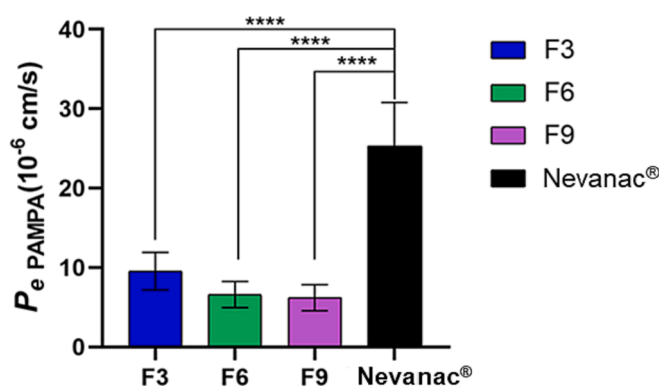| Formulation code	M_∞ (min)	β Parameter	τ_d (min)	Correlation Coefficient (R^2)
F1	100.3	0.6838	128.7	0.9929
F2	102.3	0.5154	121.4	0.9858
F3	100.4	0.8466	105.7	0.9909
F4	99.0	0.6501	88.4	0.9896
F5	103.5	0.4222	110.3	0.9824
F6	100.1	0.5807	92.7	0.9751
F7	96.2	0.8506	103.3	0.9681
F8	119.2	0.2479	259.1	0.9397
F9	98.6	0.9268	104.9	0.9812

Fig. 5. In vitro Corneal-PAMPA studies for the formulation F3, F6 and F9. Using nepafenac commercial product Nevanac®).

Fig. 4. In vitro dissolution profiles of Nepafenac (NEPA)/ Hydroxypropyl-β-cyclodextrin (HPβCD) (0.1 %w/w) loaded in polyvinyl alcohol (PVA)/poloxamer 407 nanofibers. The dissolution was conducted in phosphate buffered solution (pH 7.4) at 37 °C.

3.7. Permeability studies

3.7.1. In vitro corneal-PAMPA assay

PAMPA permeability assay results are presented in Fig. 5. Results from experiment showed no significant difference between the 3 formulations (F3, F6 and F9) regardless of the HPβCD content per formulation (50 mM, 100 mM and 150 mM for F3, F6 and F9 respectively). However, their permeability values were significantly lower than the value measured for Nevanac® ($p < 0.05$). In the case of the PAMPA system where only passive diffusion occurs through the artificially fabricated lipid membrane, a reverse sink is created as the donor compartment contains HPβCD (in high amount) as solubilizing agent. To mitigate this reverse sink effect, 10 % of the donor's HPβCD content was added to the acceptor wells to create a more desirable environment for the poorly soluble nepafenac molecules. Unfortunately, in this case corneal-PAMPA could not make a difference between the three formulations. The experiments conducted using PBS acceptor media resulted different tendencies within the samples containing various amounts of HPβCD. The increase in HPβCD amount among the 3 formulations resulted in an increased flux of nepafenac to the acceptor compartment. The average permeabilities ± SD (10–6/cm) for the F3, F6, and F9 formulations were 11.9 ± 2.21, 13.8 ± 1.59, and 21.6 ± 2.968 respectively. However, F3 is a good choice as it contains the least amount of CD and shows similar average permeability values independently the applied models. The lower amount of CD can be physiologically favorable for the penetration process (Loftsson et al., 2007). Therefore, F3 was chosen for the ex vivo study. Moreover, conducting the experiment in only phosphate-buffered media, omitting the reverse sink effect of HPβCD, the same permeability value was obtained in the case of F3.

3.7.2. Ex vivo corneal permeability studies on porcine eyes

The concentration of the NEPA for the F3 in precorneal area, cornea, and aqueous humor has been determined at 15, 30, and 60 min. The results of Fig. 6 show that F3 has a significantly higher concentration than Nevanac® in precorneal area, and this can be attributed to the complete dissolution of the NEPA-loaded nanofibers, as shown in Fig. 6A. The values for the concentrations of nepafenac in precorneal fluid for F3 and commercial Nevanac® at 15, 30 and 60 min were found to be 0.0269, 0.0013 and < 0.0001 respectively. The highest dissolution was attained at 60 min, which means the F3 had sufficient time to release more NEPA from the formulation. Regarding the cornea, although there is a slight increase in the Nevanac® compared to F3 formulation, it is only a numerical difference without statistical significance (Fig. 6B). The NEPA concentrations in the aqueous humor were not significantly different at 15 and 30 min (Fig. 6C). At 60 min Nevanac® had a significantly higher concentration than F3 formulation, with *p value* at 0.05 level of confidence being 0.0242. By compiling all these

findings, it can be concluded that bioequivalent drug concentrations might be obtained if the study is conducted in vivo.

3.7.3. Ex vivo cornea Raman mapping

The NEPA distribution within corneal tissues has been studied using Raman mapping. The F3 exposed porcine corneal tissues are presented in Fig. 7. Based on the intensity scale, the high concentration of NEPA is reflected by the red color, the green color reflects lower concentration, whereas the blue color represents the area of the map where spectral resolution specify the untreated corneal tissue. The results show that in both cases NEPA distribution at 15 min was restricted to outer layers of the cornea, but it distributed to the inner most layer (stroma) at 30 and 60 min with more homogenous feature. In conclusion, there results support our finding that F3 could be bioequivalent to Nevanac® in vivo.

3.8. Hen's egg test on chorioallantoic membrane (HET-CAM)

All applied samples, including plain fibers, nepafenac-loaded fibers, and negative controls, have not resulted in any noticeable irritation on the CAM surface when compared to the positive control (0.1 N NaCl). The results suggest the cytocompatibility of the formulation components. The HET-CAM results are displayed in Fig. 8. These results confirm that the ingredients of the formulation are well tolerated. Despite its simplicity, the HET-CAM method can be utilized as a surrogate for the Draize test. The increasing research in ocular formulations dictates less animal-intensive experimental methods; therefore, a method that mimics the in vivo Draize test should be a valid alternative to comply with the global 3R's requirements. This test falls on the borderline between in vitro and in vivo, which means reduction and/or elimination of pain and injuries when performing the experiments on whole animals, in addition to the accurate results demonstrated by this model.

3.9. Accelerated stability study

The scanning electron microscope images of the nepafenac-loaded electrospun nanofibers for the freshly prepared samples and samples stored under stressful conditions are illustrated in Fig. 9. It can be observed that samples retained their morphological features despite exposure to elevated levels of temperature, humidity, and pressure. Stability under these stressful conditions could be taken to indicate the long-term stability under ambient conditions. The fibrous structures have been maintained throughout the whole period of study (4 weeks). No considerable morphological changes were observed, and the sample remained fibrous during the whole period of study.

The time dependent changes in physicochemical characteristics of the Nepafenac-loaded nanofibers exposed to stressful conditions have
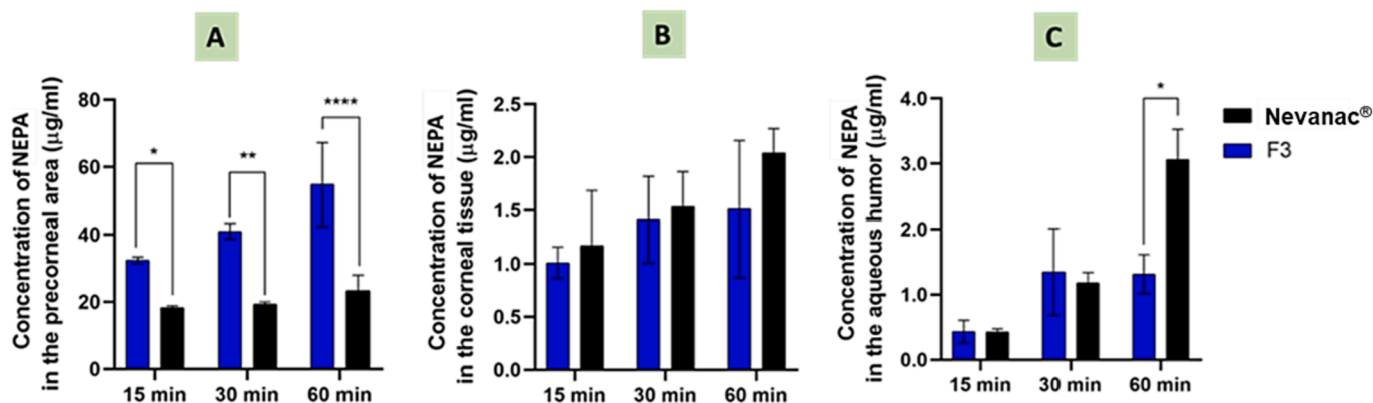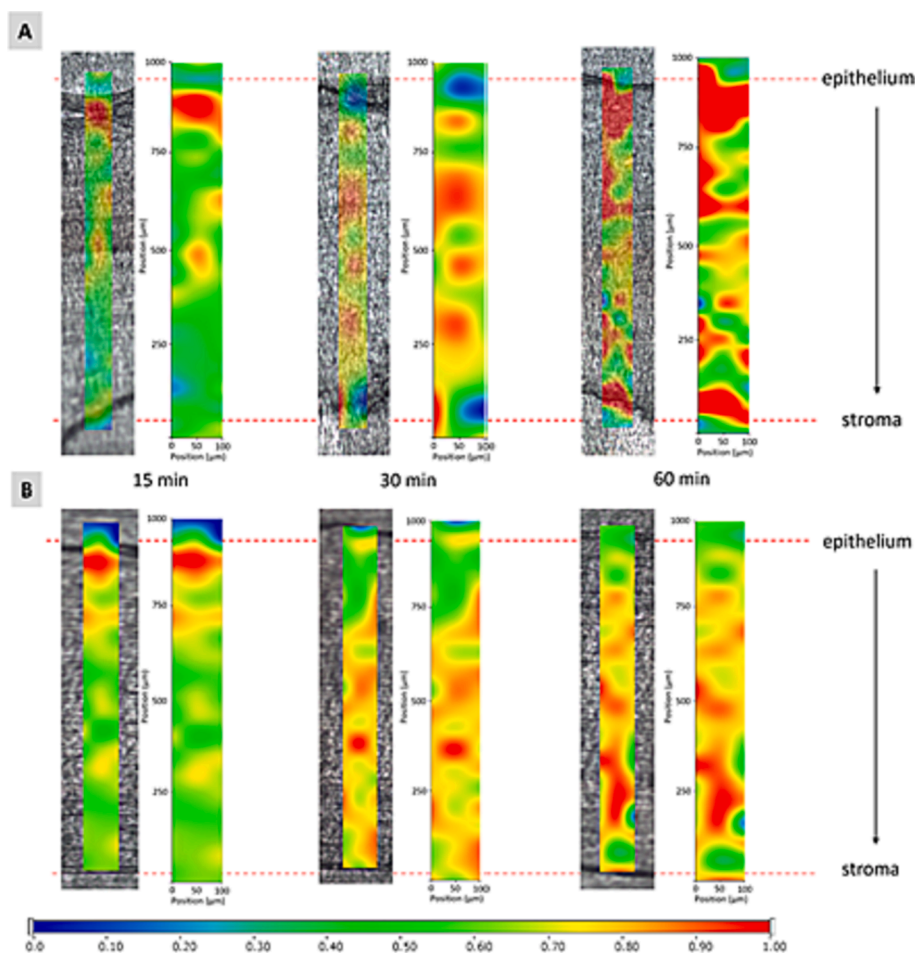

Fig. 6. Nepafenac concentration of F3 for ex vivo experiment on porcine eye measured at (A): precorneal area; (B): cornea; and (C): aqueous humor, using Nevanac® as reference.

Fig. 7. The Raman mapping of the distribution nepafenac in the excised porcine cornea for F3 formulation (A) and Nevanac® (B). The high concentration of NEPA is reflected by the red color, the green color reflects lower concentration, whereas the blue color represents the area of the map where spectral resolution specify the untreated corneal tissue. (For interpretation of the references to color in this figure legend, the reader is referred to the web version of this article.)
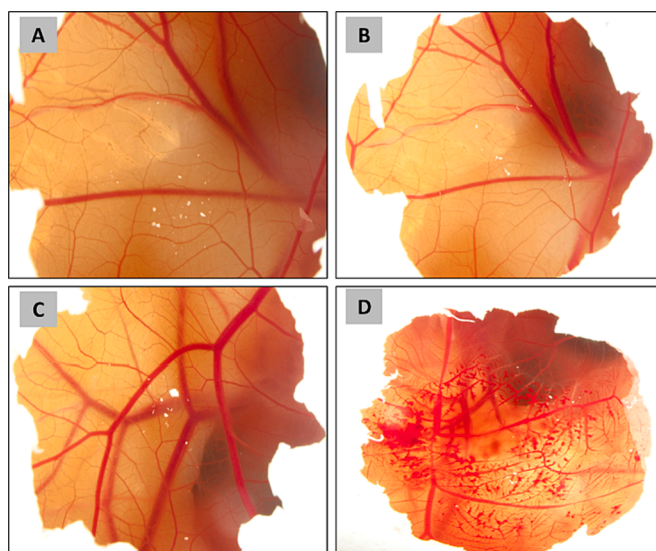
Fig. 8. Representative images of Hen's Egg Test on Chorioallantoic Membrane (HET-CAM) conducted for a period of 5 min. (A): PBS (negative control); (B): Empty fibers polyvinyl alcohol (PVA)/ Hydroxypropyl-β-cyclodextrin (HPβCD)/ poloxamer 407; (C): Nepafenac-loaded fibers; (D): 0.1 N NaOH (positive control).

been displayed in Fig. 10. Elevated temperature and humidity have no substantial effects on the essential functional groups of the fibrous samples during the period of study. These results come along with morphological studies. In conclusion, this short-term stability test under stressful conditions suggests that a stable, solid nanofibrous formulation could be successfully obtained using preservative-free components.

4. Conclusion

Nanofibrous webs can be utilized as potential candidates regarding novel technologies for targeting ophthalmic diseases. Because of their advantages compared to conventional topical formulations, they can deliver myriad number of drugs including water soluble, water insoluble, genes and proteins as well as agents for corneal regeneration and cell proliferation. On the other hand, it can be a suitable candidate to overcome the inherited ocular barriers including anatomical, physiological as well as biochemistry barriers. Therefore, it can be considered as a smart platform for current and future issues. The HPβCD not only improved the solubility of NEPA through inclusion complex formation, but also enhanced the spinnability of the precursor solution. SEM results showed that smooth fibers can be obtained. FTIR spectra confirmed the compatibility of the matrix formers with the active. Formation of amorphous solid dispersion was confirmed by FTIR spectra and XRD analysis. The release and in vitro kinetics studies showed immediate release of the drug, which was characterized by the model-independent Weibull distribution. The porous feature of nanofiber webs, along with their high surface-to-volume ratio, resulted in rapid dissolution of the
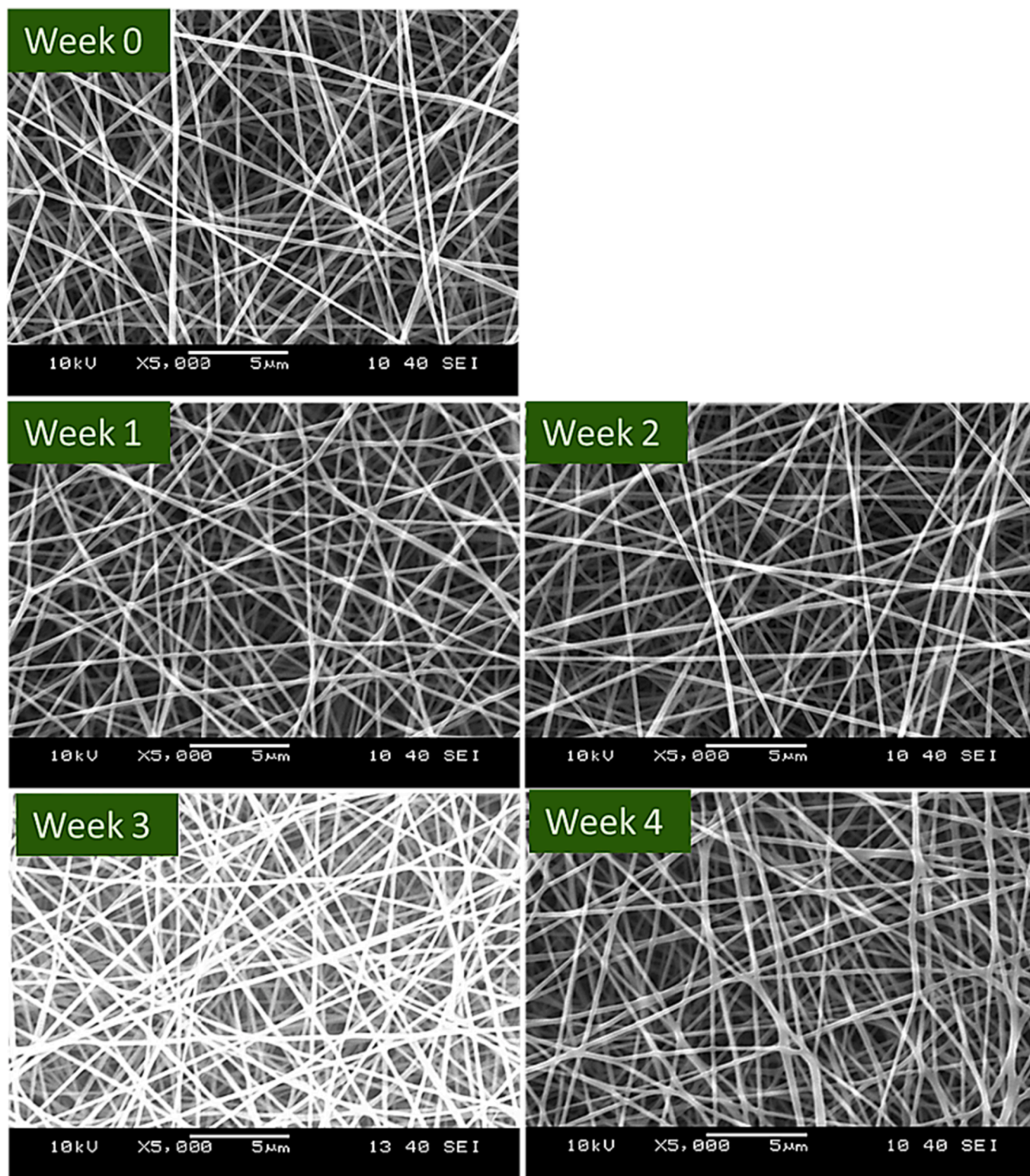
Fig. 9. Scanning electron microscopic (SEM) images of the Nepafenac-loaded fibers at 0, 1, 2, 3, and 4 weeks storage under stress conditions (40 ± 2 ∘C, 75 ± 5 % relative humidity). (magnification: 5000×).

proposed ophthalmic inserts upon contact with the phosphate buffer solution. The permeability results showed a good penetration of the developed formulation to the corneal layers and the component of the developed polymeric matrix displayed a good compatibility with HET_CAM of fertilized chicken embryos. In conclusion, the obtained results reflect that the electrospun NEPA-loaded nanofibers-based ocular inserts could be a promising alternative to conventional systems with better bioavailability and stability.
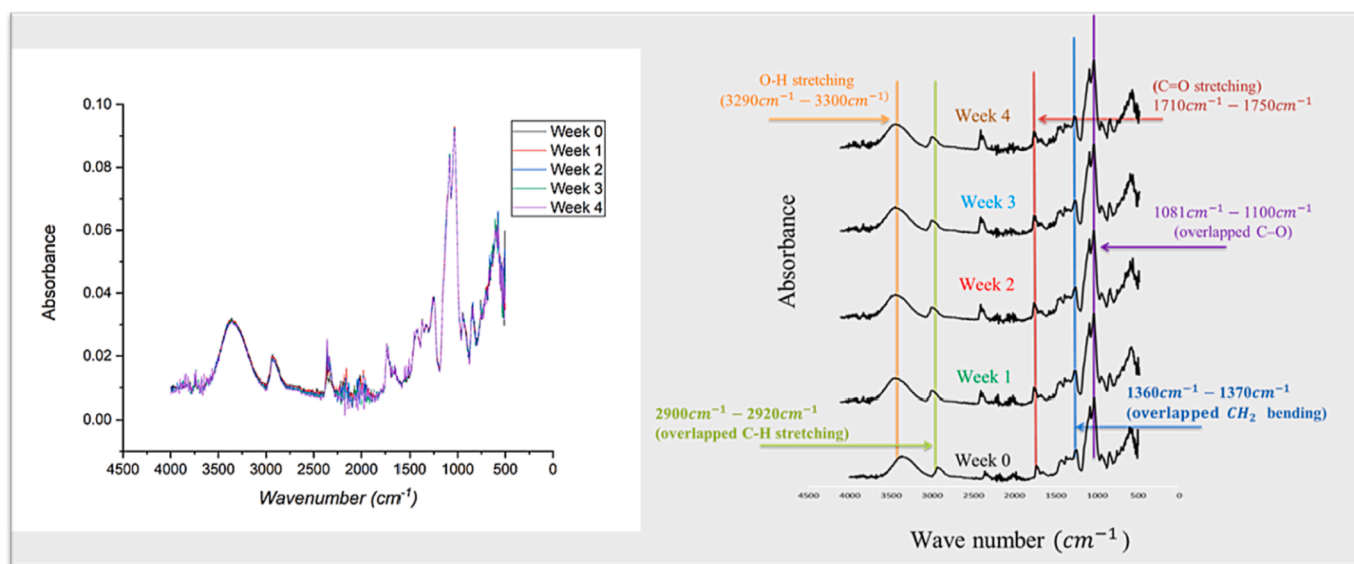
Fig. 10. Fourier transform infrared (FTIR) spectra of the Nepafenac-loaded fibers at 0, 1, 2, 3, and 4 weeks storage under stress conditions (40 $\pm$ 2 $\circ$C, 75 $\pm$ 5 % relative humidity).

CRediT authorship contribution statement

Safaa Omer: Conceptualization, Methodology, Formal analysis, Investigation, Data curation, Writing – original draft. **Nándor Nagy:** Methodology, Investigation, Writing – review & editing. **Emőke Szőcs:** Methodology, Investigation. **Szabina Kádár:** Methodology, Formal analysis, Investigation. **Gergely Völgyi:** Methodology, Formal analysis, Investigation. **Balázs Pinke:** Investigation, Visualization. **László Mészáros:** Investigation, Visualization. **Gábor Katona:** Methodology, Formal analysis, Investigation. **Anna Vincze:** Methodology, Formal analysis, Investigation. **Péter Dormán:** Methodology, Investigation. **Zoltán Zs. Nagy:** Methodology. **György T. Balogh:** Methodology, Formal analysis, Investigation, Writing – review & editing. **Adrienn Kazsoki:** Writing – review & editing, Supervision. **Romána Zelkó:** Writing – review & editing, Supervision.

Declaration of Competing Interest

The authors declare that they have no known competing financial interests or personal relationships that could have appeared to influence the work reported in this paper.

Data availability

Data will be made available on request.

Acknowledgments

Appendix A. Supplementary material

Supplementary data to this article can be found online at https://doi.org/10.1016/j.ijpharm.2023.123554.

References

Aleo, D., Saita, M.G., Spitaleri, F., Sanfilippo, C., Patti, A., 2020. Degradation profile of nepafenac in aqueous solution and structural characterization of a novel degradation product. J. Pharm. Biomed. Anal. 189, 113432 https://doi.org/10.1016/j.jpba.2020.113432.

Andreadis, I.I., Karavasili, C., Thomas, A., Komnenou, A., Tzimtzimis, M., Tzetzis, D., Andreadis, D., Bouropoulos, N., Fatouros, D.G., 2022. In Situ Gelling Electrospun Ocular Films Sustain the Intraocular Pressure-Lowering Effect of Timolol Maleate. In Vitro, Ex Vivo, and Pharmacodynamic Assessment. Mol. Pharm. 19 (1), 274–286. https://doi.org/10.1021/acs.molpharmaceut.1c00766.

Barse, R.K., Tagalpallewar, A.A., Kokare, C.R., Sharma, J.P., Sharma, P.K., 2017. Formulation and ex vivo- in vivo evaluation of pH triggered brimonidine tartrate in situ gel for the glaucoma treatment using application of 32 factorial design. Drug Dev. Ind. Pharm. 000. https://doi.org/10.1080/03639045.2017.1414229.

Bhat, N.V., Nate, M.M., Kurup, M.B., Bambole, V.A., Sabharwal, S., 2005. Effect of γ-radiation on the structure and morphology of polyvinyl alcohol films. Nucl. Instrum. Methods Phys. Res., Sect. B 237 (3–4), 585–592. https://doi.org/10.1016/j.nimb.2005.04.058.

Chen, H., Jin, Y., Sun, L., Li, X., Nan, K., Liu, H., Zheng, Q., Wang, B., 2018. Recent Developments in Ophthalmic Drug Delivery Systems for Therapy of Both Anterior and Posterior Segment Diseases. Colloids Interface Sci. Commun. 24 (April), 54–61. https://doi.org/10.1016/j.colcom.2018.03.008.

Dargó, G., Vincze, A., Müller, J., Kiss, H.J., Zsolt, Z., 2019. European Journal of Pharmaceutical Sciences Corneal-PAMPA : A novel, non-cell-based assay for prediction of corneal drug permeability. Eur. J. Pharm. Sci. 128 (November 2018), 232–239. https://doi.org/10.1016/j.ejps.2018.12.012.

Di Prima, G., Licciardi, M., Carfi Pavia, F., Lo Monte, A.I., Cavallaro, G., Giammona, G., 2019. Microfibrillar polymeric ocular inserts for triamcinolone acetonide delivery. Int. J. Pharm. 567 (June), 118459 https://doi.org/10.1016/j.ijpharm.2019.118459.

Dodero, A., Schlatter, G., Hébraud, A., Vicini, S., Castellano, M., 2021. Polymer-free cyclodextrin and natural polymer-cyclodextrin electrospun nanofibers: A comprehensive review on current applications and future perspectives. Carbohydr. Polym. 264 (April) https://doi.org/10.1016/j.carbpol.2021.118042.

Dumortier, G., Grossiord, J.L., Agnely, F., Chaumeil, J.C., 2006. A review of poloxamer 407 pharmaceutical and pharmacological characteristics. Pharm. Res. 23 (12), 2709–2728. https://doi.org/10.1007/s11095-006-9104-4.

Ellakwa, T.E., Fahmy, A., Ellakwa, D.E., 2017. Influence of poloxmer on the dissolution properties of mosapride and its pharmaceutical tablet formulation. Egypt. J. Chem. 60 (3), 443–451. https://doi.org/10.21608/EJCHEM.2017.3685.

Fan, J., Li, G., Deng, S., Wang, Z., 2019. Mechanical properties and microstructure of polyvinyl alcohol (PVA) modified cement mortar. Applied Sciences (switzerland) 9 (11). https://doi.org/10.3390/app9112178.

Galgatte, U.C., Chaudhari, P.D., 2014. Preformulation study of poloxamer 407 gels: Effect of additives. Int J Pharm Pharm Sci 6 (1), 130–133.

García-Millán, E., Quintáns-Carballo, M., Otero-Espinar, F.J., 2017. Solid-state characterization of triamcinolone acetonide nanosuspensions by X-ray spectroscopy, ATR Fourier transforms infrared spectroscopy and differential scanning calorimetry analysis. Data Brief 15, 133–137. https://doi.org/10.1016/j.dib.2017.09.002.

Grimaudo, M.A., Nicoli, S., Santi, P., Concheiro, A., Alvarez-Lorenzo, C., 2018. Cyclosporine-loaded cross-linked inserts of sodium hyaluronan and hydroxypropyl-β-cyclodextrin for ocular administration. Carbohydr. Polym. 201 (August), 308–316. https://doi.org/10.1016/j.carbpol.2018.08.073.

Haider, A., Haider, S., Kang, I.K., 2018. A comprehensive review summarizing the effect of electrospinning parameters and potential applications of nanofibers in biomedical and biotechnology. Arab. J. Chem. 11 (8), 1165–1188. https://doi.org/10.1016/j.arabjc.2015.11.015.

He, Z., Wang, Z., Zhang, H., Pan, X., Su, W., Liang, D., Wu, C., 2011. Doxycycline and hydroxypropyl-β-cyclodextrin complex in poloxamer thermal sensitive hydrogel for ophthalmic delivery. Acta Pharm. Sin. B 1 (4), 254–260. https://doi.org/10.1016/j.apsb.2011.10.004.

Kaur, S., Sarma, P., Kaur, H., Prajapat, M., Shekhar, N., Bhattacharyya, J., Kaur, H., Kumar, S., Medhi, B., Ram, J., Das, D., Avti, P., Prakash, A., Singh, R., Bhattacharyya, A., 2021. Efficacy and Safety of Topical Cysteamine in Corneal Cystinosis: A Systematic Review and Meta-Analysis. Am. J. Ophthalmol. 223, 275–285. https://doi.org/10.1016/j.ajo.2020.07.052.

Kazsoki, A., Palcsó, B., Omer, S. M., Kovacs, Z., & Zelkó R (2022). Formulation of Levocetirizine-Loaded Core – Shell Type Nanofibrous Orally Dissolving Webs as a Potential Alternative for Immediate Release Dosage Forms. *Pharmaceutics*. https://www.mdpi.com/1999-4923/14/7/1442.

Kazsoki, A., Palcsó, B., Alpár, A., Snoeck, R., Andrei, G., Zelkó, R., 2021. Formulation of acyclovir (core)-dexpanthenol (sheath) nanofibrous patches for the treatment of herpes labialis. Int. J. Pharm. 611 https://doi.org/10.1016/j.ijpharm.2021.121354.

Kesavan, K., Kant, S., Singh, P.N., Pandit, J.K., 2011. Effect of hydroxypropyl-β-cyclodextrin on the ocular bioavailability of dexamethasone from a pH-induced mucoadhesive hydrogel. Curr. Eye Res. 36 (10), 918–929. https://doi.org/10.3109/02713683.2011.593728.

Kharazmi, A., Faraji, N., Hussin, R.M., Saion, E., Yunus, W.M.M., Behzad, K., 2015. Structural, optical, opto-thermal and thermal properties of ZnS-PVA nanofluids synthesized through a radiolytic approach. Beilstein J. Nanotechnol. 6 (1), 529–536. https://doi.org/10.3762/bjnano.6.55.

Lakhani, P., Patil, A., Taskar, P., Ashour, E., Majumdar, S., 2020. Curcumin-loaded Nanostructured Lipid Carriers for Ocular Drug Delivery: Design Optimization and Characterization. J Drug Deliv Sci Technol. 662, 159–166. https://doi.org/10.1016/j.jddst.2018.07.010.Curcumin-loaded.

Laurano, R., Abrami, M., Grassi, M., Ciardelli, G., Boffito, M., Chiono, V., 2020. Using Poloxamer® 407 as Building Block of Amphiphilic Poly(ether urethane)s: Effect of its Molecular Weight Distribution on Thermo-Sensitive Hydrogel Performances in the Perspective of Their Biomedical Application. Front. Mater. 7 (November), 1–15. https://doi.org/10.3389/fmats.2020.594515.

Liang, H., Labbé, A., Baudouin, C., Plisson, C., Giordano, V., 2021. Long-term follow-up of cystinosis patients treated with 0.55% cysteamine hydrochloride. Br. J. Ophthalmol. 105 (5), 608–613. https://doi.org/10.1136/bjophthalmol-2020-316450.

Loftsson, T., Vogensen, S.B., Brewster, M.E., 2007. Effects of Cyclodextrins on Drug Delivery Through Biological Membranes. J. Pharm. Sci. 96 (10), 2532–2546. https://doi.org/10.1002/jps.

Lorenzo-Veiga, B., Sigurdsson, H.H., Loftsson, T., 2019. Nepafenac-loaded cyclodextrin/polymer nanoaggregates: A new approach to eye drop formulation. Materials 12 (2). https://doi.org/10.3390/ma12020229.

Lorenzo-Veiga, B., Diaz-Rodriguez, P., Alvarez-Lorenzo, C., Loftsson, T., Sigurdsson, H.H., 2020. In Vitro and Ex Vivo Evaluation of Nepafenac-Based Cyclodextrin Microparticles for Treatment of Eye Inflammation. Nanomaterials 10 (4). https://doi.org/10.3390/nano10040709.

Luepke, N.P., 1985. Hen's egg chorioallantoic membrane test for irritation potential. Food Chem. Toxicol. 23 (2), 287–291. https://doi.org/10.1016/0278-6915(85)90030-4.

MacHín, R., Isasi, J.R., Vélaz, I., 2012. β-Cyclodextrin hydrogels as potential drug delivery systems. Carbohydr. Polym. 87 (3), 2024–2030. https://doi.org/10.1016/j.carbpol.2011.10.024.

Maharjan, P., Cho, K.H., Maharjan, A., Shin, M.C., Moon, C., Min, K.A., 2019. Pharmaceutical challenges and perspectives in developing ophthalmic drug formulations. J. Pharm. Investig. 49 (2), 215–228. https://doi.org/10.1007/s40005-018-0404-6.

Mansur, H.S., Sadahira, C.M., Souza, A.N., Mansur, A.A.P., 2008. FTIR spectroscopy characterization of poly (vinyl alcohol) hydrogel with different hydrolysis degree and chemically crosslinked with glutaraldehyde. Mater. Sci. Eng. C 28 (4), 539–548. https://doi.org/10.1016/j.msec.2007.10.088.

Mecozzi, M., Sturchio, E., 2017. Computer assisted examination of infrared and near infrared spectra to assess structural and molecular changes in biological samples exposed to pollutants: A case of study. *Journal of*. Imaging 3 (1). https://doi.org/10.3390/jimaging3010011.

Mehta, P., Al-Kinani, A.A., Arshad, M.S., Chang, M.W., Alany, R.G., Ahmad, Z., 2017. Development and characterisation of electrospun timolol maleate-loaded polymeric contact lens coatings containing various permeation enhancers. Int. J. Pharm. 532 (1), 408–420. https://doi.org/10.1016/j.ijpharm.2017.09.029.

Meireles, A.B., Corrêa, D.K., da Silveira, J.V.W., Millás, A.L.G., Bittencourt, E., de Brito-Melo, G.E.A., González-Torres, L.A., 2018. Trends in polymeric electrospun fibers and their use as oral biomaterials. In. Exp. Biol. Med. Vol. 243(8, 665–676. https://doi.org/10.1177/1535370218770404.

Miranda, G.M., Santos, R.E., V. O., Bessa, J. R., Teles, Y. C. F., Yahouédéhou, S. C. M. A., Goncalves, M. S., & Ribeiro-Filho, J., 2021. Inclusion complexes of non-steroidal anti-inflammatory drugs with cyclodextrins: A systematic review. Biomolecules 11 (3), 1–24. https://doi.org/10.3390/biom11030361.

Pandit, J., Chaudhary, N., Emad, N.A., Ahmad, S., Solanki, P., Aqil, M., Sultana, Y., Solanki, P., 2023. Fenofibrate loaded nanofibers based thermo-responsive gel for ocular delivery: Formulation development, characterization and in vitro toxicity study. J. Drug Delivery Sci. Technol. 89 (July), 104935 https://doi.org/10.1016/j.jddst.2023.104935.

Pascolini, D., Mariotti, S.P., 2012. Global estimates of visual impairment: 2010. Br. J. Ophthalmol. 96 (5), 614–618. https://doi.org/10.1136/bjophthalmol-2011-300539.

Pinxten, A.M., Hua, M.T., Simpson, J., Hohenfellner, K., Levtchenko, E., Casteels, I., 2017. Clinical Practice: A Proposed Standardized Ophthalmological Assessment for Patients with Cystinosis. Ophthalmol Therapy 6 (1), 93–104. https://doi.org/10.1007/s40123-017-0089-3.

Polat, H.K., Bozdağ Pehlivan, S., Özkul, C., Çalamak, S., Öztürk, N., Aytekin, E., Fırat, A., Ulubayram, K., Kocabeyoğlu, S., İrkeç, M., Çalış, S., 2020a. Development of besifloxacin HCl loaded nanofibrous ocular inserts for the treatment of bacterial keratitis: In vitro, ex vivo and in vivo evaluation. Int. J. Pharm. 585 (April) https://doi.org/10.1016/j.ijpharm.2020.119552.

Polat, H.K., Bozdağ Pehlivan, S., Özkul, C., Çalamak, S., Öztürk, N., Aytekin, E., Fırat, A., Ulubayram, K., Kocabeyoğlu, S., İrkeç, M., Çalış, S., 2020b. Development of besifloxacin HCl loaded nanofibrous ocular inserts for the treatment of bacterial keratitis: In vitro, ex vivo and in vivo evaluation. Int. J. Pharm. 585 (June) https://doi.org/10.1016/j.ijpharm.2020.119552.

Pourtalebi Jahromi, L., Ghazali, M., Ashrafi, H., Azadi, A., 2020. A comparison of models for the analysis of the kinetics of drug release from PLGA-based nanoparticles. Heliyon 6 (2). https://doi.org/10.1016/j.heliyon.2020.e03451.

Rajput, S., Shrimali, C., Baghel, M., 2015. Development and validation of UV and RP-HPLC method for estimation of Nepafenac in bulk drug and opthalmic formulation. Journal of Advanced Pharmacy Education & Research 5 (1), 1–20.

Russo, E., Villa, C., 2019. Poloxamer hydrogels for biomedical applications. Pharmaceutics 11 (12). https://doi.org/10.3390/pharmaceutics11120671.

Shelley, H., Grant, M., Smith, F.T., Abarca, E.M., Jayachandra Babu, R., 2018. Improved Ocular Delivery of Nepafenac by Cyclodextrin Complexation. AAPS PharmSciTech 19 (6), 2554–2563. https://doi.org/10.1208/s12249-018-1094-0.

Singla, J., Bajaj, T., Goyal, A.K., Rath, G., 2019. Development of Nanofibrous Ocular Insert for Retinal Delivery of Fluocinolone Acetonide. Curr. Eye Res. 44 (5), 541–550. https://doi.org/10.1080/02713683.2018.1563196.

Thakkar, R., Komanduri, N., Dudhipala, N., Tripathi, S., Repka, M.A., Majumdar, S., 2021. Development and optimization of hot-melt extruded moxifloxacin hydrochloride inserts, for ocular applications, using the design of experiments. Int. J. Pharm. 603 (January), 120676 https://doi.org/10.1016/j.ijpharm.2021.120676.

Tighsazzadeh, M., Mitchell, J.C., Boateng, J.S., 2019. Development and evaluation of performance characteristics of timolol- loaded composite ocular fi lms as potential delivery platforms for treatment of glaucoma. Int. J. Pharm. 566 (May), 111–125. https://doi.org/10.1016/j.ijpharm.2019.05.059.

Topal, B., Çetin Altindal, D., Gümüsderelioglu, M., 2015. Melatonin/HPβCD complex: Microwave synthesis, integration with chitosan scaffolds and inhibitory effects on MG-63CELLS. Int. J. Pharm. 496 (2), 801–811. https://doi.org/10.1016/j.ijpharm.2015.11.028.

Vincze, A., Facskó, R., Budai-Szűcs, M., Katona, G., Gyarmati, B., Csorba, A., Zelkó, R., Nagy, Z.Z., Szente, L., Balogh, G.T., 2023. Cyclodextrin-enabled nepafenac eye drops with improved absorption open a new therapeutic window. Carbohydr. Polym. 310 (February) https://doi.org/10.1016/j.carbpol.2023.120717.

Wagh, D., Shahi, S.R., Dabir, P.D., Deore, W., 2017. Spectrophotometric Method for the Determination of Nepafenac in Ophthalmic Formulation. World J. Pharm. Res. 6 (6), 623–630. https://doi.org/10.20959/wjpr20176-8410.

Yasser, M., Teaima, M., El-Nabarawi, M., El-Monem, R.A., 2019. Cubosomal based oral tablet for controlled drug delivery of telmisartan: formulation, in-vitro evaluation and in-vivo comparative pharmacokinetic study in rabbits. Drug Dev. Ind. Pharm. 45 (6), 981–994. https://doi.org/10.1080/03639045.2019.1590392.